DEFORMATION BEHAVIOUR OF GRADIENT MATERIALS BASED ON Al-Al$_2$O$_3$ PARTICULATE COMPOSITE

A THESIS

Submitted in partial fulfilment of the
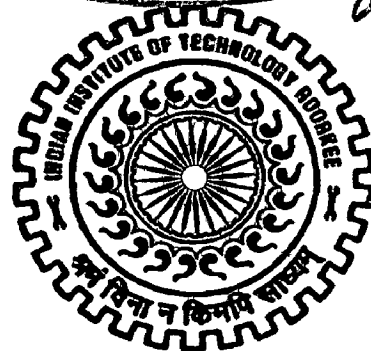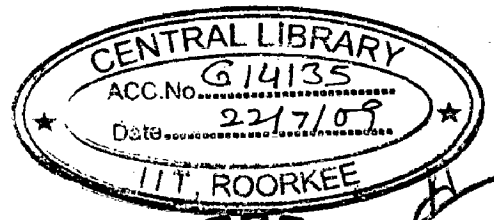*requirements for the award of the degree*
of

DOCTOR OF PHILOSOPHY

in

METALLURGICAL AND MATERIALS ENGINEERING

By

K. K. S. MER

DEPARTMENT OF METALLURGICAL AND MATERIALS ENGINEERING
INDIAN INSTITUTE OF TECHNOLOGY ROORKEE
ROORKEE-247 667 (INDIA)
AUGUST, 2007

INDIAN INSTITUTE OF TECHNOLOGY ROORKEE
ROORKEE

CANDIDATE'S DECLARATION

I hereby certify that the work which is being presented in the thesis entitled **DEFORMATION BEHAVIOUR OF GRADIENT MATERIALS BASED ON Al-Al$_2$O$_3$ PARTICULATE COMPOSITE** in partial fulfilment of the requirements for the award of degree of Doctor of Philosophy, submitted in the Department of Metallurgical and Materials Engineering, Indian Institute of Technology Roorkee, Roorkee is an authentic record of my own work carried out during a period from July 2003 to August 2007 under the supervision of Dr. Subrata Ray, Professor, Department of Metallurgical and Materials Engineering and Dr. B. K. Mishra, Professor, Department of Mechanical and Industrial Engineering, Indian Institute of Technology Roorkee, Roorkee... The matter embodied in this thesis has not been submitted by me for the award of any other degree of this or any other Institute.

(K.K.S.MER)

This is to certify that the above statement made by the candidate is correct to the best of our knowledge.
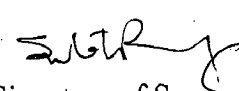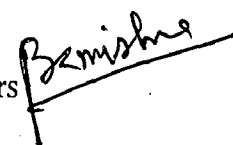
(B. K. Mishra)
Supervisor

(Subrata Ray)
Supervisor

Date: 30-8-2007

The Ph.D. Viva-Voce Examination of **Mr. K. K. S. Mer**, Research Scholar, has been held on ..10...4...2008...

Signature of Supervisors

Signature of External Examiner

ABSTRACT

A Functionally Graded Material (FGM, or sometimes also called "gradient material") is characterized by a gradual change of material properties with position. The property gradient in the material is caused by a position-dependent variation of constituents, microstructure and consequently, the mechanical properties. Functionally graded materials based on composites are a special class distinct from the normal composites, which have properties uniform along the dimensions while the FGMs have properties tailored to vary with position depending on the needs of a particular application. A unique example is that of ceramic tiles used as thermal barrier on the outer surface of space vehicles presently where the temperature reaches up to 2100 K. Because of the difference of thermal expansion coefficients of the inner shell of metal and the ceramic at the surface, there is a steep change in the thermal stresses at the surface of contact. Such thermal stresses cause the ceramic tiles to peel off or crack with disastrous consequences. The ceramic materials cannot be used alone because of its low toughness and strength and the metal alone cannot be used as it cannot withstand high temperatures. The best replacement for these ceramic tiles may be the functionally graded metal-ceramic composite, with outer layer made of ceramic entirely and the volume fraction of ceramic decreases continuously till the all metal layer starts. Since there is no sharp interface between metal and ceramic and there is a gradual change in the coefficient of thermal expansion, no steep change in thermal stresses will set in to cause delamination. Thus the FGMs are the new class of composite materials being researched and developed for such critical applications where gradient in properties is a requirement. Gradient in properties is important in several other applications also, as in the case of automobile cylinder and piston, better tribological properties are required at one surface, while better toughness is required on the other.

In order to make good use of engineering materials, it is required to understand their behaviour sufficiently well to be able to predict their performance. For composites, this means developing models which represent reasonably closely the known experimental response of real composites to applied stresses and environmental conditions. For structural applications, the prediction of the mechanical behaviour of any given composite

accurately with the help of modelling is important for designing and developing composites in order to ensure the material designed is likely to meet the service requirements of the application concerned. The solidification processing of metal or alloy based gradient materials results in porosity which affects the mechanical behaviour of the material adversely and so, the modelling of such gradient material will be unrealistic unless porosity is taken into account. Although, it is generally accepted that tensile properties decrease with an increase in porosity content but the effect of other porosity parameters like shape, size and distribution on the mechanical properties are yet to be investigated.

The application of any material is dictated by its suitability for the given application, cost of production and reliability of knowledge about its behaviour. To popularize the use of FGMs, cheaper manufacturing processes for the mass production of FGMs are required. These manufacturing processes should be reproducible, reliable and cost effective. Presently, there are no reliable and inexpensive ways of fabricating FGMs that also allows for bulk production of large parts. Current methods of fabrication include solidification processing, chemical vapor deposition, spray atomization and codeposition and powder metallurgy techniques (Gao and Wang, 2000). Amongst these various techniques, the most economical and attractive processing route is offered by solidification processing. The process involves the addition of reinforcing particle phase to molten metal or alloy and mixing them uniformly, followed by application of suitable differential forces to cause segregation of particles required for the desired gradient in the particle concentration for a given application. The preservation of the spatially graded distribution through solidification is the final step. Chapter-1 of the thesis provides the general context of the present investigation.

The detailed literature review given in chapter-2, indicates that although the processing of FGMs in the laboratory scale has reached considerable level of maturity, there is still a need for developing a reliable, reproducible and cost effective manufacturing process for the bulk production of the FGMs. The literature available on modelling the properties of Particle Reinforced Metal Matrix Composites (PMMCs) and Functionally Graded Materials (FGMs) has instances of application of a number of mathematical and finite element models for estimating the properties of PMMCs and FGMs, but there is need to proceed further in view of certain deficiencies.

The simplest models available for the elastic properties of composites are rules of mixture, Halpin–Tsai equations, Hashim Shtrikman bounds etc. These models estimate the upper and lower bounds for the modulus of elasticity, modulus of rigidity and Poisson's ratio. The Finite Element Method (FEM) models available for estimating the elastic properties are mostly based on the unit cell. In the unit cell models the composite is modelled as a unit cell or periodic array of identical unit cells, each containing a reinforcement particle dimensioned to represent the overall reinforcement volume fraction. In practice however particulate reinforced metal matrix composites have highly heterogeneous microstructures. Porosity is one of the most important parameter affecting the deformation behaviour of composites. The formation of porosity and its effect on the mechanical properties of PMMCs have been the subject of several experimental studies. It is generally accepted that tensile properties decrease with increasing porosity content. However, the effect of parameters such as shape, size and distribution of porosity on mechanical properties of a composite is still not well understood.

Although the properties of FGMs are being investigated experimentally as well as by the modelling techniques, the estimation of local as well as global properties of FGMs is still a challenge. A reliable estimation of elastic as well as nonlinear properties of FGMs is important to make these materials acceptable for industrial use. FGMs have also been modelled in the past using the unit cell models like those developed for uniform composites. The current modelling strategies often do not explicitly couple the heterogeneous microstructure with the structural global analysis. FGMs were originally conceived for super heat resistant applications involving severe thermo-mechanical loading, such as the outer wall and the engine parts of the future spacecrafts. Conventional super heat resistant materials, such as those found in the exterior of space shuttles, consist of heat resistant ceramic tiles bonded to metal structures. In view of this it is felt that a model which is capable of estimating thermal stress distribution inside the FGM should also be investigated. In the context of the gaps in literature review, the present study has been formulated with the following objectives:

1. To develop a simple and practical modelling technique capable of describing the heterogeneous microstructure of PMMCs more faithfully with flexibility to distribute a given volume fraction of the particles of different shapes and sizes, randomly in the matrix and estimate the elastic as well as nonlinear

deformation behaviour on the basis of the behaviour of the constituent materials.

2. To incorporate in the model the effect of volume fraction of porosity and also, their shapes, sizes and orientations relative to the direction of loading for a given volume fraction and study their effect on the mechanical properties.

3. To study through the same model the deformation behaviour, both local and global, of gradient materials and uniform composites by distributing the particles with some desired gradation in volume fraction or uniformly so that the properties as determined through the same model could be compared between different types of particle distribution.

4. To estimate and study the temperature distribution and thermal stresses as encountered in certain applications under thermo-mechanical loading.

5. To develop FGM based on Al-Al_2O_3 by centrifugal casting technique and determine the particle distribution in order to model this composite and compare the hardness behaviour with the local yield stress in order to judge the capability of the model to predict deformation behaviour of real life composites.

Chapter-3 describes the experimental work on fabrication of set-up for centrifugal casting and synthesis of gradient materials from aluminium based composite containing alumina particles with the assistance of differential of centrifugal force field operating on particles and the surrounding molten metal. In the present work, solid cylindrical ingots of FGMs have been cast in a rotating mold solidifying the melt-particle slurry. FGM ingots with different alumina mass percentages have been synthesized and their transverse and horizontal sections have been prepared for metallographic studies to study the distribution of particles under optical and scanning electron microscope. Hardness measurements have been conducted on the FGM samples using Vickers hardness testing machine to characterize local mechanical properties. Aluminium alloy is selected for use as the matrix materials due to its (a) low density, (b) low melting point, (c) reasonably high thermal conductivity, (d) good processing flexibility, (e) easy availability, (f) low cost, (g) high toughness and (h) good malleability. Alumina is selected as reinforcement material due to high thermal and wear resistance, chemical inertness, high hardness and availability at reasonable price.

Chapter-4 describes modelling of MMCs by finite element method as followed in this study. First the metal matrix composite with uniformly distributed particles has been modelled by two dimensional Finite Element Method (FEM) using FEM tool ANSYS 5.4. In the present modelling effort, plane stress condition is assumed. For the modelling of MMCs with uniform random distribution of particles, a square area consisting of 10000 elements (plane42, four-node) having the same size as that of particle (average particle size) is considered. Out of these 10000 elements, $10000*V_f$ (V_f is the average particle volume fraction) elements are randomly selected with the help of a FORTRAN programme in such a way that these elements are uniformly distributed over the whole matrix. These elements are assigned the properties corresponding to the reinforcement. Remaining elements are assigned the properties of the matrix material. One of the most important features of the present modelling technique is the random distribution of the particles in the matrix. Randomness in the distribution of particles produces a near realistic distribution of the particles in the matrix. The effect of randomness on the material properties has also been established in the present study. It has been found that the random distribution of particles has negligible effect on the mechanical properties on the global scale, although it may affect the local behaviour of the composites.

The properties of the uniform composites with different particle volume fractions and with different shapes and sizes of particles have been investigated. The present model is used to estimate the elastic properties of particle reinforced metal matrix composites with uniformly distributed particles for different average particle contents. The results from the present model for elastic behaviour are verified with the existing results for elastic properties of composites for the same average particle volume fractions. The present model has also been used to estimate the nonlinear behaviour of the particle reinforced metal matrix composites with uniform random distribution of particles. The results from the present model for the nonlinear behaviour have also been compared with the results of existing models for uniform composites with different average particle contents. The present work is concerned with uniaxial stress-strain behaviour of the composites with elastically deforming particles reinforced in ductile matrix. The stress-strain behaviour of the matrix is characterized by elastic-perfectly plastic behaviour.

In the present work the same model which has been used to estimate the elastic as well as non linear behaviour of uniform composites is further modified to make it suitable

for FGMs. In the case of model for uniform composite the element size particles are uniformly and randomly distributed over the whole matrix. In the case of FGMs the particle distribution is still random locally but follows a prescribed distribution so as to mimic the FGM. This has been achieved with the help of a FORTRAN program which generates the required variation in the particle concentration over the matrix. Elastic as well as nonlinear behaviour of FGM models with variation of particle volume fraction from one end to the other for different average particle contents have been investigated in the present work. FGMs having different average particle contents and tailored variation in particle concentration in one direction have been investigated. The response of FGM models with variation in particle concentration in both the directions has also been investigated. Polynomial and linear distributions are used for modelling the variation in particle concentration in the FGM models. The local variation in the FGM properties has also been investigated with the help of the present model. FGM models with constant average particle content and with different types of variations in particle concentration have also been investigated.

It has been found that during the manufacturing of particle reinforced metal matrix composites (PMMCs) using the processing route, such as melt-stirring or powder metallurgy, some defects occur in the resulting material. These defects lower quality and the performance characteristics of the composites. One of the most important defects is the porosity which affects the mechanical properties of the composites adversely. The presence of porosity within a component leads to the reduction in the load bearing area of the material as well as inhomogeneity is stress distribution and hence is observed to reduce both Young's modulus and strength. It is generally accepted that tensile properties decrease with increasing porosity content. However, the effect of parameters, such as shape, size, distribution and volume fraction of porosity on the mechanical properties and fracture behaviour is not yet well understood. In the present work, the present modelling technique has also been used to create pores with different shapes and sizes, uniformly distributed with random distribution in the whole matrix. Uniform composite models as well as FGM models with different average porosity contents and different average particle contents have been investigated for elastic as well as nonlinear behaviour. The effects of pore size on the elastic as well as nonlinear behaviour have also been studied. The results of the present model are compared with the existing models and experimental results.

In gradient materials based on composites containing metal and ceramics, the difference in thermal expansion coefficients between the constituents causes steep change in thermal stresses at the contact surface. It is necessary to examine whether the thermal stresses generated may cause the ceramic to de-bond and peel off or crack from the metal as it happens in case of ceramic tiles attached on the surface of metal shell. It has been claimed that FGMs should reduce such thermal stresses and resist super high temperatures but it is necessary to develop modelling techniques to determine the thermo-mechanical stresses due to thermal or/and mechanical loads. The objective is to find out a continuous material distribution which minimizes the thermal stresses under the required conditions. The present model may also be used to determine the thermal stresses in metal matrix composites when subjected to temperature gradients. The distribution of thermal stresses in uniform composite models, layered composites and functionally graded material models as estimated through the model described above, have been compared.

The results and discussion are given in two chapters, 5 and 6. Chapter-5 describes the results on fabrication of gradient composites and characterization of their local mechanical behaviour through measurement of hardness. Al-Al$_2$O$_3$ based FGM ingots with average weight percentage of alumina particles of 10%, 20% and 30% have been successfully synthesized by using centrifugal casting method. Alumina content decreases gradually in the radial direction from the centre towards the outer radius of the circular section of the cast ingots at any height below the shrinkage cavity. Alumina content also decreases gradually in the axial direction from the top to the bottom of the cast ingots. The decrease in alumina content from the centre towards the outer wall is not in agreement with the theory that the higher centrifugal force acting on relatively denser alumina particles during rotation will force them relatively towards the outer wall because of higher density, leaving behind the relatively lighter aluminium melt. The decreasing alumina content from the top to the bottom of cast ingots is also surprising in view of higher density of alumina particles relative to the melt.

The fact that a larger amount of alumina particles is observed at higher heights from the bottom and towards the inner side along the radius is due to the flotation of the bubble-particle combine due to their lower combined density. Clusters of particles are not commonly observed in the cast FGM ingots synthesized in this study, as evident from optical micrographs. It is possible that centrifugal force acting on the bubble-particle

combinations has helped to keep these combined entities separate from each other on the basis of their density. However, the centrifugal force at the rotational speed used does not appear adequate to detach particles from bubbles. Vickers hardness distribution of the cast ingot follows the particle distribution but there are sometimes some abrupt changes locally in the hardness distribution, which has been attributed to inhomogeneous cast structure of the matrix in cast FGM ingots. Annealing of the cast FGM ingots results in the elimination of inhomogeneous cast structure and the radial hardness distributions become relatively smooth in FGM ingots.

In Chapter-6, the results of 2-D FEM model on the mechanical properties of particle reinforced composites are given. The model is based on the random distribution of particles, which produces a realistic distribution. Uniform composite models with randomly distributed particles containing particle vol% from 10% to 90% in a step of 10% are obtained. The effect of random distribution of particles on the modulus of elasticity for uniform composite has been investigated through this model with a domain size of 5 mm x 5 mm. It has been concluded that though there may be variation in material properties at the micro level due to random distribution of particles, the properties at the global level remain unchanged for a given average particle volume fraction for uniform distribution of particles. It is also concluded the use of a domain size of 5 mm x 5 mm is adequate. For composite samples of the size taken in the present study or bigger, random distribution of particles produces the same macroscopic properties irrespective of the local variation in particle positions in different composite models due to the random distribution of particles.

The results for modulus of elasticity of the present modelling technique for uniform composite are compared with the well established rule of mixture (ROM) and inverse rule of mixture (IROM). ROM and IROM may be assumed as the most conservative upper and lower bounds for the modulus of elasticity of uniform composite. It was observed that the results of the present modelling technique are well within the bounds given by the rule of mixture and the inverse rule of mixture. The results predicted by the present model for modulus of elasticity are also compared with the well known Hashim-Shtrikman (1963) bounds. The results from the present modelling technique are found to be well within the Hashim-Shtrikman bounds. The present model results for modulus of elasticity are also compared with those given by Halpin–Tsai (1968) equation. It has been concluded that the present model results are in good agreement with the

Halpin-Tsai equation with the parameter $\zeta = 2$. From the results of the present modelling technique a simple equation for estimating modulus of elasticity has been suggested. The results for modulus of rigidity for the uniform composites with different average particle contents have also been obtained through the model. It has been concluded that the results for the modulus of rigidity with the present modelling technique are well within the bounds of rule of mixture and inverse rule of mixture and also within the bounds given by Hashim-Shtrikman (1963).

Non linear analysis has been carried out with the present model to predict nonlinear behaviour of the uniform composites with different average particle contents. It has been concluded that the strain required for a composite to undergo transition from elastic to plastic behaviour decreases as the level of reinforcement increases. These results are similar to those obtained by Bao and coworkers (1991) with their unit cell model. Yield stress is estimated for different average particle contents by the crossover method. An empirical relation showing the dependence of yield stress on the particle content has been obtained from the results of the model by curve fitting. The relation between the particle content and the ratio of flow stress of a composite (σ_{oc}) to that of the matrix (σ_o) has been obtained under the plane strain conditions for different shapes and orientation of particles by Bao and coworkers (1991) for their unit cell model. It is observed that for lower particle contents their results compare quite well with those obtained in the present study. For higher particle contents, the result of the present model gives higher value for the flow stress ratio. The present model may have resulted into clustering of the particles at higher particle contents and contributed to the difference in results with unit cell model. The clustering of the particles causes a rapid increase in flow stress ratio of the composites at higher particle content. The effect of the shape of the particles on the uniform composite has also been investigated. It is concluded that the shape of the particles affect both the modulus of elasticity and yield stress and the particles elongated in the direction of loading results in higher modulus of elasticity and yield strength.

Numerical results have been obtained for the variation of modulus of elasticity of uniform composites with increasing particle vol% from 0 to 100, with three different porosity contents of 2.5, 5.0 and 7.5 vol%. It is concluded that porosity lowers the Young's modulus of the composites. The results of the present model for modulus of elasticity have been compared with Sprigg's equation. Nonlinear analysis has also been carried out to predict the effect of porosity on the yield strength using four different types

of pores represented by *1*1*, *1*4*, *2*2* and *4*1*. The notation *m*n* represents the pore introduced by the removal of $m \times n$ elements where *m* represents the length of *m* grid elements along the direction perpendicular to that of loading (x-axis) and *n* represents the length of *n* grid elements in the direction of loading (y-axis). These results indicate that for 7.5 vol% of porosity, the yield strength of a composite containing 30 vol% of particle decreases from 77 MPa to 47.8 MPa when the pore type changes from *1*4* to *4*1*, which are the least and most damaging pore types considered in the present work. Thus, there could be 38% reduction in the yield strength depending on the shape, size and orientation of pores for the same porosity content. Similarly, for the elastic modulus, there is 33% reduction when the pore type changes from *1*4* to *4*1* for 7.5 vol% of porosity. These results also show that for the same porosity type (type *1*4*) the reduction in the modulus of elasticity is only 5.3% when the porosity content increases from 2.5 to 5 vol%. Also the results for yield strength show that there is only 9% reduction in the yield stress for the same porosity type (type *1*4*) when the porosity content increases from 2.5 to 5 vol%. These results clearly indicate the dominance of the porosity type on the mechanical properties of the composites. Thus, the average porosity content is not a reliable parameter to predict the mechanical properties as the shape and orientation of pores are also important in determining the damage. The existence of large pores perpendicular to the loading direction is more damaging than the overall porosity content. It has been observed that the ratio of yield stresses with and without porosity decreases with the level of reinforcement. The results of the present model for the effect of porosity on the mechanical properties have been compared with those given by Tekmen and coworkers (2003) and Ghosh (1986). The results of the present model are found to be well in agreement with these experimental results.

FGM models with variation of particle concentration in the direction of x-axis from 0 vol% at one end and 100 vol% at the other end following a polynomial distribution have been investigated. It has been observed that the global average values of modulus of elasticity in the gradation direction (x-axis direction) are lower than that in the uniform composite for the same average particle content. While in the perpendicular direction (y-axis) these values are higher than that in the corresponding uniform composite. FGM models with gradation in both x-axis and y-axis directions have also been studied. It has been observed that the global average values of modulus of elasticity for the FGM models with gradation in both directions are almost equal to that obtained for uniform composites with the same average particle vol%.

Nonlinear analysis has been performed on FGM models with gradation in x-direction. In the y-direction FGM models exhibit better yield properties in comparison to those in uniform composite with the same average particle contents. It is observed that in the x-direction FGM models show the same yield stress as that of the matrix up to almost 70 vol% of particle content. In the x-direction the modulus of elasticity of the FGM models is also lower than that of the uniform composites for the same average particle contents. Variation in local values of modulus of elasticity has also been obtained for the FGM models for different amount of average particle contents. It is found that the variation in modulus of elasticity within the model follows closely the variation in particle concentration. FGM models with average particle content of 30 vol% but following different types of polynomial and linear gradation have also been investigated.

Thermal analysis has also been performed in the present study. Three different types of materials combinations are considered in the present analysis. In the first case a layered composite plate of alumina and aluminium is considered. In the second case a uniform composite with particle content of 30 vol% has been studied. In the third case, FGM model with variation in particle concentration from 0 vol% at one end to 100 vol% at the other end and with 30 vol% average particle content has been considered. It is concluded that in the case of uniform composite and FGM, there is smooth change in the temperature and thermal stresses. In the case of layered composite there is steep change in the thermal stresses at the metal ceramic interface. FGM with 100 vol% ceramic at one side may, thus, be used for high temperature applications to smoothen the thermal stress distribution.

The FGM samples synthesized experimentally in the present study have also been modelled in the present study. The results for modulus of elasticity and yield stress have been obtained at different layers below the shrinkage cavity perpendicular and along the gradation direction. In the cast composites particles are generally associated with porosity. Higher particle concentration is associated with higher porosity. The effect of the gradation of porosity on the FGM samples has also been investigated. It is observed that the linear variation in porosity does not affect the properties of FGMs significantly. The hardness distributions at different height have been compared with the local yield stresses determined from the model.

Chapter-7 outlines the conclusions drawn from the present investigation.

ACKNOWLEDGEMENTS

(K. K. S. Mer)

CONTENTS

LIST OF FIGURES

LIST OF TABLES

NOMENCLATURE

α	Coefficient of thermal expansion
b	Sprigg's constant
$c(x)$	Particle content at location x for 1-D variation
$c(xy)$	Particle content at location (x, y) for 2-D variation
$\mathbf{D}$	Material matrix
$\det \mathbf{J}$	Determinant of Jacobian matrix
E	Modulus of elasticity
E_f	Modulus of elasticity for the reinforcement
E_{irom}	Modulus of elasticity from inverse rule of mixture
E_m	Modulus elasticity for of the matrix
E_{rom}	Modulus of elasticity from rule of mixture
ε	Strain
ε_y	Yield strain
ε_{xx}	Normal strain in x-axis direction
ε_{yy}	Normal strain in y-axis direction
$\mathbf{F}^e$	Load matrix of the element
FGM	Functionally Graded Material
FMMC	Fiber Reinforced Metal Matrix Composite
G, μ	Modulus of rigidity or shear modulus
h	Convection coefficient
H	Tangent modulus
η	A function of E_f/E_m used in Halpin-Tsai equation
IROM	Inverse Rule of Mixture
$\mathbf{J}$	Jacobian matrix
$\mathbf{k}^e$	Element stiffness matrix
K	Bulk modulus
k	Restraint coefficient

MA	Mechanical Alloying
MMC	Metal Matrix Composite
ν	Poisson's ratio
N	Shape function
p	Average particle content in vol%
PM	Powder Metallurgy
PMMC	Particle Reinforced Metal Matrix Composite
Π	Potential energy
q	Ratio of stress-to-strain transfer
$\mathbf{q}$	Element displacement vector
ROM	Rule of Mixture
SEM	Scanning Electron Microscope
σ	Stress
σ_{oc}	Flow stress for the composite
σ_o	Flow stress for the matrix.
σ_{vm}	Von Mises stress
σ_{xx}	Normal stress in x-axis direction
σ_{yy}	Normal stress in y-axis direction
σ_y	Yield stress
T	Temperature in K
$\mathbf{T}$	Traction vector
T_f	Fluid temperature in K
T_w	Wall temperature in K
$\mathbf{u}$	Displacement
U	Strain energy
V	Volume fraction
V_f	Volume fraction of the reinforcement
V_{fp}	Volume fraction of porosity
V_m	Volume fraction of the matrix
X	Mechanical property with porosity
X_0	Mechanical property with zero porosity

Y_c	Yield stress of the composite
Y_f	Yield stress of the FGM
Y_m	Yield stress of the matrix.
Y_p	Yield stress with porosity
Y_0	Yield stress without porosity
ζ	Factor used in Halpin -Tsai equation

In many demanding applications such as aviation, spacecraft, automobile, electronics and cutting tools, there are often contradictory property requirements in components like very high hardness, heat resistance and high wear resistance along with fairly good ductility and toughness. Homogenous materials like monolithic alloys may not be suitable because different properties may be required in different locations in the components. For example, wear resistance is required in the surface region which may require high hardness but if the same hardness is there even in the bulk the toughness and ductility may be seriously impaired. Thus, surface modification or coating evolved for imparting the required properties at the surface, distinctly different from that of the bulk. But this type of combination of surface and bulk often has different deformation characteristics resulting in development of intense shear stress leading to failure. The recent catastrophe in the space shuttle Columbia due to detachment of ceramic tiles reminds us of danger of combining two materials of dissimilar thermal and mechanical characteristics.

Composite materials may alleviate the situation in certain circumstances by combining dissimilar materials in the bulk and not along a specific interface in order to synergize them to obtain unique combination of properties while compensating the deficiencies of one another. This process of material optimization can release a designer from the constraints associated with the conventional materials. One can make use of tougher and lighter materials, with properties that can be tailored to suit particular design requirements. Complex shapes can also be manufactured easily using composite materials. Hence a complete rethinking of an established design in terms of composites can often lead to both cheaper and better solutions.

The basic attributes of metals reinforced with hard ceramic particles (Particle Reinforced Metal Matrix composites or PMMCs) or fibers (Fiber Reinforced Metal Matrix Composites or FMMCs) are improved strength and stiffness, improved creep and fatigue resistance, increased hardness, better wear and abrasion resistance and higher operating

temperatures. The increasing interest for research in the area of aluminium and magnesium based metal matrix composites (MMCs) is due to the increasing demand of lightweight components from aerospace, automobile and other industries. In automobile industries, the potential application of MMCs and its benefits have been demonstrated in cast engine blocks, cylinder liners, pistons, valves and other components. Some automobile components are already being manufactured using MMCs. The aluminium and magnesium based MMCs lead to lightweight components and there is, consequently, weight savings and lower consumption of fuel, the price of which has escalated sharply over the past few years.

Normal composite materials consist of a continuous phase, which forms the matrix, where one or more phases called dispersoids are uniformly distributed or dispersed over the entire body of the composite. However, by intentionally distributing the dispersoids selectively in a component at locations where it is required from application standpoint, it is possible to save costly dispersoids and at the same time not affecting the properties elsewhere. Thus, it allows one to create a tailored material having functions usually not found in the common composites. Functionally Graded Materials (FGMs) are developed based on the concept of tailored distribution of second phase to achieve the required properties in different locations in a component as required. In its simplest form, it could consist of one material on the outer surface side, a second material on the inner surface side, and an intermediate layer whose structure, composition and morphology vary smoothly from one material to the other at microscopic level. This variation of microstructure distinguishes FGMs from conventional composite materials and the compositional variation across the cross-section results in unique physical properties. These characteristic microstructures make the thermal stress distribution relatively smooth in contrast to sharp change across the interface joining dissimilar materials, thus developing the required thermal shock resistance properties in FGM.

The concept of FGMs was proposed in 1984 by the material scientists in the Sendai area in Japan as a means of preparing thermal barrier material (Koizumi, 1997). Although FGMs attracted scientific interest only towards the end of the twentieth century, these materials are not new. In fact, spatial variations in the microstructure of materials have been exploited for millions of years by living organisms. In many structures found in plants, microstructural gradients have so evolved in order to produce optimum structure

2

required for functional performance with minimum material use. An example is the culm of bamboo, which consists of high-strength natural fibers embedded in a matrix of ordinary cells. The fiber content is not homogeneous over the entire cross-section of the culm but decreases from outside to inside. This gradation in fiber content is a natural adaptation of the plant to flexural loads; the fiber content is high only in those sections where the highest stresses occur (Neubrand, 2001).

The use of FGMs is important in context of application in aerospace industry. The outer surface temperature of the space vehicles is estimated to reach 2100 K while the inner surface is to be maintained at normal temperature for personnel, machines and storage of fuel inside. The outer surface of these space vehicles is exposed to very high temperature due to friction with air while moving through earth's atmosphere. To withstand this high temperature, these vehicles are covered with heat resistant ceramic tiles. These ceramic tiles are bonded to the metal surface with some adhesives. Thus the layered composites are being used in these space vehicles to withstand high temperatures. Due to the high temperature gradients, very high thermal stresses develop in the outer shell of these space vehicles. Due to mismatch in the properties of the metal and ceramic, there is a steep change in the thermal stresses at the metal ceramic contact surface and due to this steep change in the thermal stresses, the outer ceramic tiles become prone to delamination or cracking. Gradient in properties is important in several other applications also, as in the case of automobile cylinder and piston where better tribological properties are required at one surface, while in the bulk inside better toughness is required.

Functionally graded metal-ceramic metal matrix composites or functionally graded materials (FGMs), selectively reinforced at one surface by ceramic particles are a promising response to these specific application requirements. FGMs provided with heat-resistance and hard ceramics on the high-temperature side and tough metals with high thermal conductivity on the low-temperature side and gradual change from ceramic to metal in between, are capable of withstanding severe thermo-mechanical loadings. Weight saving is another prime requirement in the aerospace applications. Functionally graded aluminium-ceramic MMCs may be the appropriate materials for these requirements.

The use of material is dictated by the cost of production and reliability of knowledge about the behaviour of material under different conditions. To popularize the use of FGMs, cheaper manufacturing processes for the mass production of FGMs are

required. These manufacturing processes must be repeatable, reliable and cost effective. Presently, there is no inexpensive way of fabricating FGMs that allows for bulk production of large parts. Most of the presently used methods are expensive. Aerospace industry can probably afford these methods for the required quality but certainly not the automobile industry. Current methods of fabrication include solidification processing, chemical vapour deposition, spray atomization, codeposition and powder metallurgy techniques. Amongst these various techniques, the most economical and attractive processing route affordable for many applications is offered by solidification processing. This process involves the addition of reinforcing particles to a liquid metal matrix and mixing them uniformly, followed by segregation of particles and liquid under some forces in order to create the desired gradient in the particle concentration. The preservation of the spatially graded structure by solidification is the final step. The forces creating gradient in particle content could be gravitational force, centrifugal force or similar forces, which act differently on the particles and the melt.

An understanding of the common types of failures is important in good design because it is always necessary to relate the loads and dimensions of a member to some significant material parameter which limits the load carrying capacity of the member. Excessive elastic deformation of a machine part can mean failure of the machine, even if the part is not fractured. Yielding, or excessive plastic deformation, occurs when the elastic limit of the metal has been exceeded. The permanent change of shape prevents the part from functioning properly any longer. In order to make good use of engineering materials, it is required to understand their behaviour sufficiently well to be able to predict their performance. For composites, this means developing models which represent reasonably closely the known experimental response of real composites to applied stresses and environmental conditions. If we can predict the behaviour of any given composite accurately with the help of modelling techniques, then we can have the confidence that the material we have designed will meet the service requirements of the application concerned.

Theories of elastic behaviour of composite materials are well developed and predictions of elastic response for composite materials are often very satisfactory. Nonlinear behaviour of metal matrix composites (MMCs) has also been extensively investigated by using the unit cell models. In the unit cell models the composite is

4

modelled as a unit cell or periodic array of identical unit cells, each containing a reinforcement particle dimensioned to represent the overall reinforcement volume fraction. The unit cell model creates an artificial distribution of particles non-representative of reality, particularly at higher concentration of dispersoïds. In practice, however, particulate reinforced metal matrix composites have highly heterogeneous microstructures. Particles are distributed more or less randomly in the metal matrix.

The shape, size and orientation of particles are important in determining the deformation behaviour of particle reinforced MMCs. The elastic behaviour may be understood in terms of bounds given by the rule of mixture and the inverse rule of mixture corresponding to iso-stress and iso-strain conditions respectively. The rule of mixture which gives the upper bounds for modules of elasticity is originally developed for determining the modulus of elasticity for fiber reinforced composites with the fibers oriented along the loading direction. The inverse rule of mixture which gives the lower bounds for the modulus of elasticity is for determining the modulus of elasticity for the fiber reinforced composites with fibers oriented transverse to the loading direction. Thus it may be said that the particles elongated in the direction of loading will attribute to higher values of modulus of elasticity, while the particles elongated transverse to the direction of loading will attribute to lower values of modulus of elasticity in comparison to that in isotropic composites reinforced by spherical particles with unit aspect ratio. Thus, it is important to establish the effect of shape, orientation and aspect ratio of particles on the deformation behaviour of composites.

It has been observed in the past that during the manufacturing of particle reinforced metal matrix composites (PMMCs) using the processing techniques, such as melt-stirring or powder metallurgy, some defects like pores or voids occur in the microstructure. These defects alter the deformation behaviour and the performance of the composites. The defects like pores or voids cause reduction in mechanical properties of the composites. The presence of porosity or voids within a component leads to the reduction in the load bearing area of the material and also, stress concentration around. Therefore, it is expected to result in the reduction in both Young's modulus and strength. It is generally accepted that tensile properties decrease with an increase in porosity content. However, the effect of parameters related to porosity such as size, shape and distribution, on the mechanical properties and fracture behaviour is yet to be adequately studied.

The properties of FGMs are being investigated experimentally as well as by the modelling techniques in the recent past. The estimation of local as well as global properties of FGMs with the help of a simple model is still a challenge. A reliable estimation of deformation behaviour of FGMs is important to make these materials popular for industrial use. FGMs have also been modelled in the past using the unit cell models, originally developed for the uniform composites. FGMs also have more or less random microstructure at the local scale like uniform composites. Particles are distributed randomly on the local scale. It has been observed in the past that in the cast composites particles are generally associated with porosity. Higher particle concentration is associated with higher porosity content. Thus, in the case of functionally graded cast materials there is gradation of porosity as well along with the gradation of particles. It is, therefore, important to study the effect of gradation in porosity on the deformation behaviour of FGMs. The type of gradation in the particle content is also important in context to FGMs. The global as well as local behaviour of FGMs should depend on the type of gradation in FGMs. In this context it is important to investigate the deformation behaviour of FGMs with different types of profiles for variation in particle concentrations.

As already discussed, FGMs are special class of composite materials which are being researched and developed mainly for applications under severe thermo-mechanical loading, such as the outer wall and the engine parts of the future spacecrafts. Conventional super heat resistant materials, such as those found in the exterior of space shuttles, consist of heat resistant ceramic tiles bonded to metallic structures. Because of the difference of thermal expansion coefficients between ceramic and metal, there is steep change in thermal stresses at the contact surface of ceramic and metal. These thermal stresses cause the ceramic tiles to peel off or crack from the metal structure. FGMs have been developed to reduce such thermal stresses and to resist super high temperatures. To reduce the thermal stresses, FGMs need to have continuous transition from metal at low temperature surfaces to ceramic at high temperature surfaces. To determine the optimum variation in particle concentration in FGMs, it is necessary to develop modelling techniques to determine the thermo-mechanical stresses due to thermal or/and mechanical loads.

In the present work, MMCs have been modelled with the help of finite element modelling technique where particles are distributed randomly in a matrix in order to get a more realistic model compared to those based on unit cell. The effect of different random

distribution of particles on the mechanical properties of the composites at the global as well as the local scale has also been investigated. The properties of the uniform composites with different particle volume fractions and with different shapes and orientations of particles have been investigated within the framework of the present model in the context of elastic as well as non-linear deformation behaviour in terms of stress-strain behaviour under uniaxial loading. The composites are assumed to consist of elastically deforming particles reinforced in elastic-perfectly plastic matrix. In the study on FGMs the particle distribution is still random locally but follows a prescribed distribution so as to mimic FGM with variation in particle concentration from one end to other end for different average particle contents. The deformation behaviour of FGMs with variation in particle concentration in both the directions has also been investigated. Polynomial as well as linear variations have been used for modelling the particle distribution in the FGMs. FGMs with the same average particle content but with different types of gradations in particle concentration have also been investigated to study the effect of particle gradation on deformation behaviour.

In the present work, the models of uniform composite have been extended to include pores or voids distributed in it along with particles. A given volume fraction of pores with different shapes, sizes, and orientation with respect to the loading direction, have been uniformly distributed randomly in the matrix and the influence of pore characteristics on the deformation behaviour has been determined. Uniform composites as well as FGMs with different average porosity contents and different average particle contents have been investigated for elastic as well as nonlinear behaviour.

The present work also involves development of FGM based on Al-Al$_2$O$_3$ by solidification processing. The slurry of alumina particles in molten aluminium has been cast in a rotating mold to get particle gradient under the action of centrifugal force. The particle distribution as determined under optical and scanning electron microscope has been used for modelling the FGM with and without porosity and its local and global properties have been studied. The variation of local yield stress has been compared with the hardness distribution to judge the ability of the model to determine deformation of the FGM.

LITERATURE REVIEW

2.1 COMPOSITES : PARTICLE REINFORCED METAL MATRIX COMPOSITES

A composite is a mixture of two or more different constituents or phases. Composites are produced when two or more different materials are combined at macroscopic level to give a combination of properties that cannot be attained in the original materials. Composites can be broadly classified into three categories-particulate composites, fiber composites and laminar composites. This classification is based on the shapes of the reinforcement materials. Concrete, a mixture of cement and gravel, is a particulate composite; fiber-glass, containing glass fibers embedded in a polymer, is a fiber-reinforced composite; and plywood, having alternating layers of wood veneer, is a laminar composite. In composites, materials are combined in such a way so as to enable us to make better use of their properties while minimizing to some extent the effects of their deficiencies. This process of material optimization can release a designer from the constraints associated with the conventional materials. One can make use of tougher and lighter materials, with properties that can be tailored to suit particular design requirements. Complex shapes can be manufactured easily using composite materials. Hence a complete rethinking of an established design in terms of composites can often lead to both cheaper and better solutions.

The concept of composites is not a human invention. Nature is replete with very fine examples of natural composites. Wood is a natural composite material consisting of one species of polymer, cellulose fibers with good strength and stiffness, in a resinous matrix of another polymer, the polysaccharide lignin. Nature makes a much better job of design and manufacture than we do. Although we have been able to recognize the ways of overcoming two major disadvantages of natural wood, that of size (a tree has a limited transverse dimension), and that of anisotropy (properties are markedly different in the axial and radial directions). The resulting solution is a composite material called plywood. Bone, teeth and mollusc shells are other natural composites, combining hard ceramic reinforcing phases in natural organic polymer matrices.

Particle-Reinforced Metal Matrix Composites (PMMCs) are a special category of practically isotropic composites, which have either hard or soft particles, or their mixtures embedded in a ductile metal or alloy matrix. Therefore, PMMCs combine metallic properties (ductility and toughness) with the characteristics of reinforcement particles, often leading to greater strength, higher wear resistance and better properties at elevated temperature depending on the nature of particles. These properties offer potential for exploitation in a range of pump and engine applications, including compressor bodies, vanes and rotors, piston sleeves and inserts, connecting rods, and so forth. The PMMCs are of particular interest due to their ease of fabrication by conventional methods at lower costs (Ray, 1993).

2.1.1 Synthesis of PMMCs

The synthesis methods of PMMCs can be divided into two categories; the phase-joining (*ex-situ*) method and the phase-separating (*in-situ*) method. For the composites obtained by *in-situ* methods the size of a dispersoid may be of the order of nanometer.

2.1.1.1 Ex-situ method

Traditionally, PMMCs have been produced by several processing routes such as powder metallurgy (PM), spray deposition, mechanical alloying (MA) and various casting techniques, i.e. gravity casting, squeeze casting, rheocasting and compocasting. All these techniques are based on external addition of reinforcement particles to the matrix materials, which may be in molten or semi-solid or powder form. For the conventional PMMCs, the reinforcing phases are prepared separately prior to the composite fabrication. Thus, conventional PMMCs may be viewed as *ex-situ* PMMCs. In this case, the scale of the reinforcing phase is limited by the starting powder size, which is typically of the order of microns to tens of microns and rarely below one micron. Other drawbacks that have to be overcome are the interfacial reactions between the reinforcement particles and the matrix, which lead to brittle reaction products and a poor wettability between the reinforcements and the matrix due to surface contamination of the reinforcement particles.

2.1.1.2 In-situ method

It is widely suggested by fundamental considerations as well as experimental studies that the size and volume fractions of reinforcements as well as the nature of the

matrix reinforcement interfaces control the properties of PMMCs. An optimum set of properties may be achieved when fine and thermally stable reinforcements are dispersed uniformly in metal matrix. During the past two decades, considerable research efforts have been directed towards the production of *in-situ* PMMCs, in which the reinforcements are formed *in-situ* in the metallic matrix by chemical reaction between the constituents during the composite fabrication. Using this approach, PMMCs with a wide range of matrix materials (including aluminium, titanium, copper, nickel and iron), and second phase particles (including borides, carbides, nitrides, oxides, silicides and their mixtures) have been synthesized.

Compared to conventional *ex-situ* PMMCs, the *in-situ* PMMCs exhibit the following advantages: (i) the *in-situ* formed reinforcements are thermodynamically stable and do not dissolve at higher temperature or do not have a reaction layer, thereby leading to less degradation during elevated-temperature services; (ii) the *in-situ* generated reinforcements are finer in size and their distribution in the matrix is relatively more uniform, which may lead to better mechanical properties; and (iii) the reinforcement-matrix interfaces are clean and uncontaminated which improve wettability and may result in excellent interfacial strength, leading to higher ductility and toughness.

2.1.2 Porosity in PMMCs

During the manufacturing of particle reinforced metal matrix composites (PMMCs) using the processing techniques, such as melt-stirring or powder metallurgy, some defects occur in the cast microstructure. These defects lower the casting quality and performance characteristics of the composites. One of the most important defects is the porosity which causes the reduction in the mechanical properties of the composites. Porosity formation may be attributed to the factors as shrinkage during solidification and evolution of hydrogen gas bubbles due to a sudden decrease in hydrogen solubility during solidification. The solubility is a function of temperature, pressure and alloy composition. After solidification is complete, these bubbles become micro pores. Once porosity forms, the pores grow until they achieve equilibrium with the forces acting on them. Also, it has been observed that reinforcement particles have a tendency to associate themselves with porosity, thereby giving rise to particle porosity clusters.

The presence of porosity within a component leads to the reduction in the load

bearing area of the material and hence can be expected to lead the reduction in both Young's modulus and strength (Dorey and coworkers, 2002). A number of empirical and semi-empirical models have been proposed to describe the manner in which the mechanical properties vary with the level of porosity. One of the most commonly used forms of equation describes the effect of porosity on mechanical property as

$$X = X_0 \exp(-b \times V_{fp})$$
(2.1)

In the Eq. 2.1, X is a particular mechanical property, V_{fp} is the volume fraction of porosity, b is an empirical constant and the subscript 0 indicates zero porosity. The above equation was originally proposed by Duckworth (1953) to describe the effect of porosity on strength following the experimental work by Rysckewitch (1953). It was later adopted by Sprigg (1961) for use in describing the effect of porosity on the Young's modulus and is better known as the Sprigg's equation.

It is generally accepted that the tensile properties decrease with an increase in porosity content. However, the understandings of the effects of parameters, such as porosity type, porosity volume fraction, porosity size and porosity distribution on the mechanical properties and fracture behaviour are still incomplete. Tekmen and coworkers (2003) in their work have studied the effect of porosity on the mechanical properties and fracture behaviour in composites of Al-Si matrix alloy reinforced with SiC particles in the as-cast state and after extrusion process. They have concluded that the existence of large pores controls the fracture behaviour of these components.

Dorey and coworkers (2002) in their work have shown that the reduction in strength and Young's modulus with increased amounts of discrete pores is frequently greater than that predicted by models based on a homogeneous pore distribution. They examined the effect of pore distribution by producing samples containing a non-homogeneous distribution of pores and compared the results with data reported for samples containing homogeneously distributed pores. Young's modulus and, to a greater extent, strength were shown to have stronger dependencies on the porosity than predicted for homogeneous samples. Ghosh and Ray (1986) have studied the effect of porosity on the mechanical behaviour of Al-Al$_2$O$_3$ metal matrix composites. Their experimental results show that the rate of reduction in yield stress with increasing porosity is higher in the particle reinforced MMCs with lower particle contents.

2.1.3 Properties of Composites

Mechanical properties of composites have been investigated extensively in the past by different researchers. It has been observed by fundamental considerations as well as experimental studies that the size and volume fractions of reinforcements as well as the nature of the matrix reinforcement interfaces control the properties of PMMCs. Agarwal and Narang (1977) studied the behaviour of specimens of glass fibre-reinforced epoxy with various fibre orientations under tensile and impact loads. Pillai and coworkers (1987) investigated the effect of volume fraction and size of graphite particulates on fracture behaviour of Al-graphite composites. Majumdar and coworkers (1984) investigated the strength and fracture behaviour of metal matrix particulate composites prepared by a liquid metallurgy technique.

2.1.3.1 Properties of ex-situ PMMCs

The mechanical properties of the particulate composites depend upon the type, the size, the volume fraction and the distribution of particles inside the composites. The characteristics of particle-matrix interface also play an important role in controlling mechanical properties of the composites. Asthana (1998) studied the dynamic wetting effects (effects arise when an imposed velocity distorts the contact angle) during infiltration of metals of porous bodies to fabricate multi-phase materials. The particle matrix interface is governed by the wettability of reinforced particles in the melt. The addition of hard ceramic particles to the matrix alloy results in an increase in the hardness and wear resistance of the composite. However, an addition of soft particles like graphite may work as a solid lubricant supplied by the composite itself.

In particle reinforced metal matrix composites (PMMCs), the matrix and the dispersed particles both share the load. The strength of a particle reinforced composite is governed by (i) the deformation characteristics of the matrix, particle and their interface, (ii) shape, size, amount and distribution of particles in the matrix and (iii) the interaction between the particles and the flaws like porosity and voids in the matrix. The tensile properties of a composite depend on the mechanical behaviour of its components under a given condition of loading. In the initial stage of loading of a two phase composite both the phases deform elastically. Law of mixture has been used to estimate the theoretical tensile strength of composite materials, when tensile strength values and volume fractions

12

of composite's constituent phases are known. However, this approach gives limited success because in the calculations only volume fraction of the constituent phases are taken into account and not their shape or size or other microstructural scale. The strength of a composite depends on the plastic behaviour of its phases also. The strength of a particulate composite should be considered from two different angles such as the composite having deformable or nondeformable particles in the matrix (Ghosh and Ray, 1986). In the presence of deformable particles the composite may under go an extensive plastic deformation.

2.1.3.2 Properties of in-situ PMMCs

The homogeneity of composite materials is of prime importance for high performance engineering applications such as in the automotive and aircraft industries. A uniform distribution of reinforcement particles in MMCs is essential to achieve effective load-bearing capacity of the reinforcement. Non-uniform distribution of the reinforcement could lead to lower ductility, strength and toughness of the MMCs. Conventional fabrication of ex-situ MMCs involves the incorporation of the reinforcing phase into the matrices via casting or powder metallurgy routes. The homogeneity of the reinforcing particles in ex-situ MMCs is relatively poor. On the other hand, fine in-situ formed reinforcing particles are dispersed more uniformly in the matrices of in-situ composites, leading to significant improvements in the strength, stiffness, creep and wear resistance of the composites.

The mechanical properties of in-situ particulate composites have been evaluated by several workers. The superior mechanical properties of in-situ composites were first reported by Westwood and Winzer (1987). Kuruvilla and coworkers (1990) compared the tensile properties of in-situ TiB_2/Al composites with those of the ex-situ composites containing the same amount of reinforcing phase. They found that the elastic modulus, tensile strength and hardness of the in-situ composite are comparatively higher than those of ex-situ composite.

2.1.4 Models Available for Properties of Composites

In particle reinforced metal matrix composites, both the matrix and the dispersoid particles are load bearing constituents. Many factors contribute to the strength of a particulate composite - (a) the deformation characteristics of the matrix, the particle and

their interface (b) amount, distribution, shape and size of particles in the matrix and (c) the interaction between the particles and the flaws like porosity and voids in the matrix. The tensile properties of a composite depend on the mechanical behaviour of its constituents. At the initial stage of loading of a composite containing two constituents, the matrix and the dispersoid, both the constituents deform elastically. The limits of elastic properties of such a composite could be estimated following two simple models resulting in two rules of mixtures (Broutman and Krock, 1967). The first one represents the iso-strain condition of the two constituent phases and predicts the upper limit estimate of the Young's modulus of the composite, E_{rom}, which is written as

$$E_{rom} = E_f V_f + E_m V_m \qquad (2.2)$$

where, E_f and E_m are respectively the Young's moduli of the reinforcement and the matrix. V_f and V_m are respectively the volume fractions of the reinforcement and the matrix. The other limiting model represents the iso-stress condition of the two constituent phases and predicts the lower limit estimate of the Young's modulus of the composite, E_{irom}, which is written as

$$\frac{1}{E_{irom}} = \frac{V_f}{E_f} + \frac{V_m}{E_m} \qquad (2.3)$$

The rule of mixture expressions have been found most appropriate for the composites with continuous reinforcement. The models discussed above are simple models, although, if treated with care, they can still give useful approximations to the behaviour of many composites.

There are many more formal treatments based on more realistic models of distribution of reinforcement, which yield results with varying degrees of complexity. These more rigorous approaches may give predictions of elastic properties that are closer to experimentally observed values than the simple models, but they are seldom easy to use in practice. For design purposes it is more useful to have simple and rapid computational procedures for estimating properties rather than more exact but intractable solutions. Convenient interpolation procedures have been developed by Halpin and Tsai (1969) who showed that many of the more rigorous mathematical models could be reduced to a group of approximate relationships of the form

14

$$E_l = E_f V_f + E_m (1 - V_f) \qquad (2.4)$$

and

$$E_2 = \frac{\left(1 + \zeta\eta V_f\right)}{\left(1 - \eta V_f\right)} E_m \qquad (2.5)$$

The Eq. 2.4 is the same rule of mixture that has already been discussed. In the second equation, ζ is a factor, specific to a given material, is determined by the shape and distribution of the reinforcement (i.e. whether they are fibers, particles, etc.), the packing geometry and by the nature of loading. The parameter η is a function of the ratio of the fiber and matrix moduli (E_f/E_m) and of the reinforcement factor ζ and is given as

$$\eta = \frac{\left(\dfrac{E_f}{E_m} - 1\right)}{\left(\dfrac{E_f}{E_m} + \zeta\right)} \qquad (2.6)$$

The parameter ζ is the only unknown, and its value is obtained empirically for a given composite material. A number of analyses have been carried out to compare the predictions of above equations with the theory of elasticity calculations, often with a great degree of success, and it is frequently quoted from the early work of Halpin and Tsai that for practical materials the reasonable value of ζ is 2.

The research to find the effective elastic modulus of particulate composites is continuing. A number of mathematical and finite element models have been presented by different researchers in the recent past. On the basis of all these models it may be said that the elastic properties of the composites may be predicted quite accurately with the help of all these existing models. To predict the nonlinear properties of the composites accurately with the help of simple models is still a challenge. Bao and coworkers (1991) carried out a theoretical investigation to determine the role of non-deforming particles in reinforcing ductile matrix materials against plastic flow and creep. The study was carried out within the framework of continuum plasticity theory using cell models to implement most of the calculations. Systematic results were given for the influence of particle volume fraction and shape on the overall behaviour of composites with uniformly distributed, aligned reinforcement particles. The stress-strain behaviour of the matrix material is characterized

by elastic-perfectly plastic behaviour or by power-law hardening behaviour of the Ramberg-Osgood type. Pettermann and Suresh (2000) used a finite element unit cell model for investigation of arbitrary loading conditions for composites with periodic arrangements of continuous aligned fibers. Johannesson and coworkers (2001) studied the effect of reinforcement geometry on matrix stresses in three different aluminium metal matrix composite systems. They have shown that the reinforcement aspect ratio strongly affects the relaxation mechanism in the composites.

Marur (2004) proposed a simple approach to compare the effective elastic moduli of two phase particulate composites. He computed the bulk modulus of composites using the three phase spherical model. The Poisson's ratio was obtained using the rule of mixture. His results for modulus of elasticity were found to be in good agreement with the available computational models and experimental data. Pal (2005) developed four models for relative Young's modulus of concentrated particulate composites using a differential scheme along with the solution of an infinitely dilute dispersion of particles in a solid matrix. He evaluated his proposed models using seven sets of experimental data on Young's modulus of concentrated particulate composites. One of his models was found to be capable of predicting the effect of particle size distribution on Young's modulus of concentrated particulate composites.

In the past, investigators have also proposed numerical analysis approaches for the prediction of behaviour of particulate composites, utilizing finite element models. Agarwal and coworkers (1974) studied the elastic-plastic response of aligned short fibre composites using finite element method. Agarwal and Broutman (1974) used a three dimensional finite element analysis to determine the internal stresses in an ordered spherical particle composite. They determined the stresses for various volume fractions of particles and calculated the Young's modulus from the knowledge of stresses and the applied deformation. Agarwal and Bansal (1977) investigated the influence of fibre interactions on the load transfer mechanism, failure at the fibre matrix interface and stress-strain behaviour of a composite using an elastic-plastic finite element analysis for discontinuous fibre composites.

Dong and Schmauder (1996) investigated the limit flow stress for transverse loading of metal matrix composites reinforced with continuous fibers and for uniaxial loading of spherical particle reinforced metal matrix composites by embedded cell models

in conjunction with the finite element method. Leggoe and coworkers (1998) modelled the deformation in particulate reinforced metal matrix composites with locally varying reinforcement volume fraction using a two scale finite element approach. The responses of axisymmetric unit cell models were used to define the constitutive response of mesoscale regions possessing varying volume fractions. Macroscale response was investigated using two and three dimensional random arrays of finite elements in which element properties were randomly assigned in line with a Gaussian distribution. Chakraborti and coworkers (2001) modelled the mold region of the continuous caster; the most widely used casting device used by the steel industry has been through a combination of a steady-state heat transfer approach and a recently developed Pareto-Converging Genetic Algorithm (PCGA).

Yang and coworkers (2003) evaluated the effective material properties of composites using a two dimensional (2D) finite element method (FEM) and the concept of equivalent homogeneous materials. They demonstrated as well as validated their model with the help of numerical results. Kenesei and coworkers (2004) have given the elastic-plastic response of metal matrix composites (MMCs) consisting of AA6061-T6 aluminium matrix reinforced with 20 vol% Al_2O_3 particles using the finite element method. Aradhya and Surappa (1991) investigated the mechanical properties of 6061 Al-SiC$_p$ composites using finite element method. They compared their results for modulus of elasticity with experimentally determined and theoretically predicted values. They found their experimental values in good agreement with the values calculated using the Halpin-Tsai equation. Although the values estimated by the FEM model were slightly lower than the experimentally measured values.

2.2 FUNCTIONALLY GRADED MATERIALS

The future advancement in science and technology will rely heavily upon the development of new material systems that safely withstand the ever-increasing performance demands imposed upon them. Functionally Graded Materials (FGMs) hold promise for applications requiring ultrahigh material performance such as thermal barrier coatings, bone and dental implants, piezoelectric and thermoelectric devices, optical materials with graded reflective indices and high-performance space flight structures (including engines). New applications are continuously being envisaged.

2.2.1 History and Definitions of FGMs

FGMs are characterized by spatially varied microstructures created by non uniform distributions of the reinforcement phases with different properties, sizes and shapes. This new concept of engineering the microstructure of the material marks the beginning of a paradigm shift in the way we think about materials and structures. The concept of functionally graded materials (FGMs) was proposed in 1984 by materials scientists in the Sendai area in Japan as a means of preparing thermal barrier material. Continuous change in composition microstructure, porosity, etc. of these materials results in gradients in properties such as mechanical strength and thermal conductivity. A functionally graded material (FGM, or sometimes also called "gradient material") is characterized by a gradual change of material properties with position. The property gradient in the material is caused by a position-dependent chemical composition, microstructure, or atomic order. The spatial extension of the gradient may differ: in a bulk FGM the property variation extends over a large part of the material, whereas in a graded coating or joint it is restricted to the surface of the material or a small interfacial region.

Although FGMs attracted scientific interest only towards the end of the twentieth century, these materials are not new. In fact, spatial variations in the microstructure of materials have been exploited for millions of years by living organisms (Neubrand, 2001). In many structures found in plants, micro structural gradients are formed in order to produce optimum structural and functional performance with minimum material use. An example is the culm of bamboo, which consists of high-strength natural fibers embedded in a matrix of ordinary cells (Fig. 2.1(a)). The fiber content is not homogeneous over the entire cross-section of the culm but decreases from outside to inside (Fig. 2.1(b)). This gradation in fiber content is a natural adaptation of the plant to flexural loads–the fiber content is high only in those sections where highest stresses occur. There are also some examples of materials taking advantage of property gradients such as case-hardened steels in which a hard surface is combined with a tough interior.

The vast majority of FGMs are composite materials with a macroscopic microstructural gradient. For example, the composite may contain a spatially varying volume fraction of one of the phases (Fig. 2.2(a)). However, a composition gradient is not inherent to all FGMs. Microstructural gradients may also be obtained in composites by changing the shape (Fig. 2.2(b)), orientation (Fig. 2.2(c)), or size (Fig. 2.2(d)) of the

18

dispersed phase (Neubrand, 2001). FGMs may be characterized by a continuously changing property from one surface, X of the material to the other surface, Y as shown in Fig. 2.3.

According to Gasik (2003) there is still no clear, internationally accepted definition of FGM (there are still different opinions about what does the "FGM" stands for). The concept of the FGM seems to be self-explanatory. One of the possible definitions of an FGM might be expressed as follows "A functionally graded material, an FGM, is a material with engineered gradients of composition, structure and/or specific properties aiming to become superior over the homogenous materials composed of the same or similar constituents". It is a must for a FGM to be a competitive material as compared to other alternatives to become economically and technically feasible.

2.2.2 Processing Techniques of FGMs and their Characteristics

The manufacturing process of FGMs can usually be divided in building the spatially inhomogeneous structure ("gradation") and transformation of this structure into a bulk material ("consolidation"). Gradation processes can be classified into constitutive, homogenizing and segregating processes. Constitutive processes are based on a stepwise build-up of the graded structure from precursor materials or powders. Advances in automation technology during the last few decades have rendered constitutive gradation processes technologically and economically viable. In homogenizing processes, a sharp interface between two materials is converted into a gradient by material transport. Segregating processes start with a macroscopically homogeneous material, which is converted into a graded material, by material transport caused by an external field (for example a gravitational, centrifugal or electric field). Homogenizing and segregating processes produce continuous gradients, but have limitations concerning the types of gradients, which can be produced. Usually drying and sintering or solidification follows the gradation step. These consolidation processes are chosen in such a way that the gradient is not destroyed or altered in an uncontrolled fashion. Presently there are no inexpensive ways of fabricating FGMs that allows for bulk production of large parts. Current methods of fabrication include solidification processing, chemical vapor deposition, plasma spraying and powder metallurgy techniques.

High fiber density

Low fiber density

Position

(a) Bamboo culm
(Schematic)

(b) Fiber content
(Schematic)
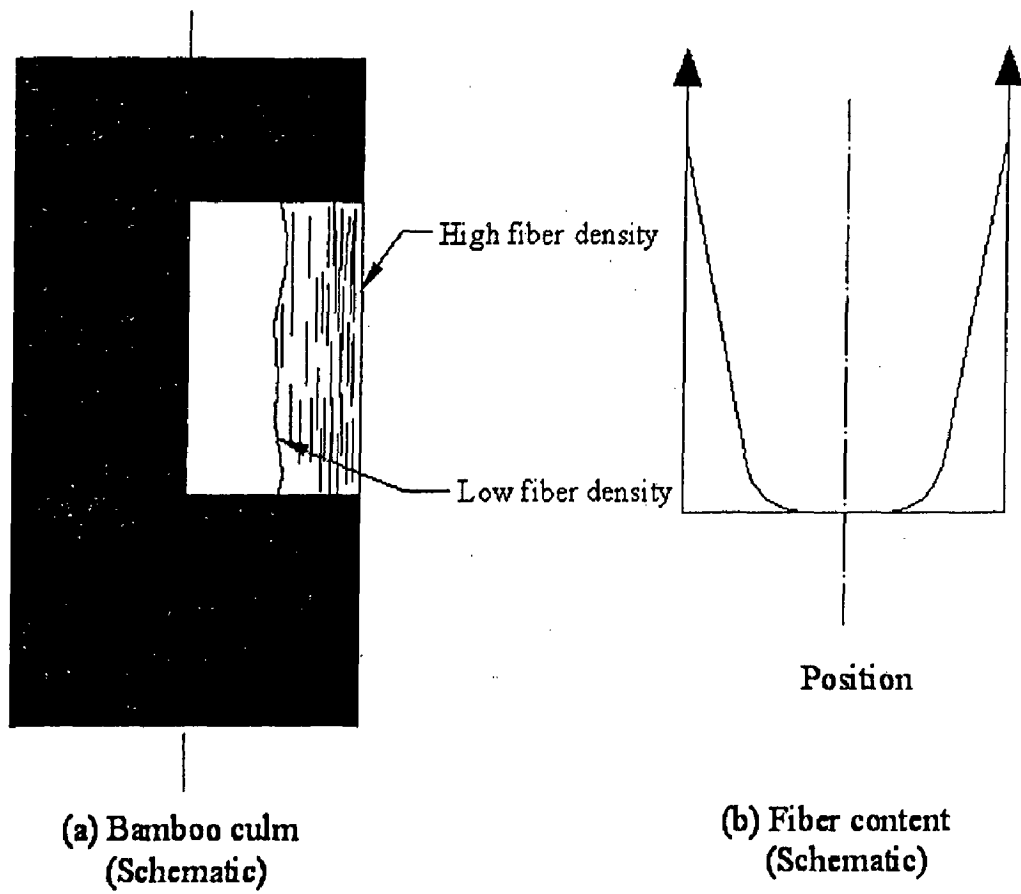
Fig. 2.1 Cross-section of a bamboo culm: (a) cross-section; (b) distribution of fibers across the culm.
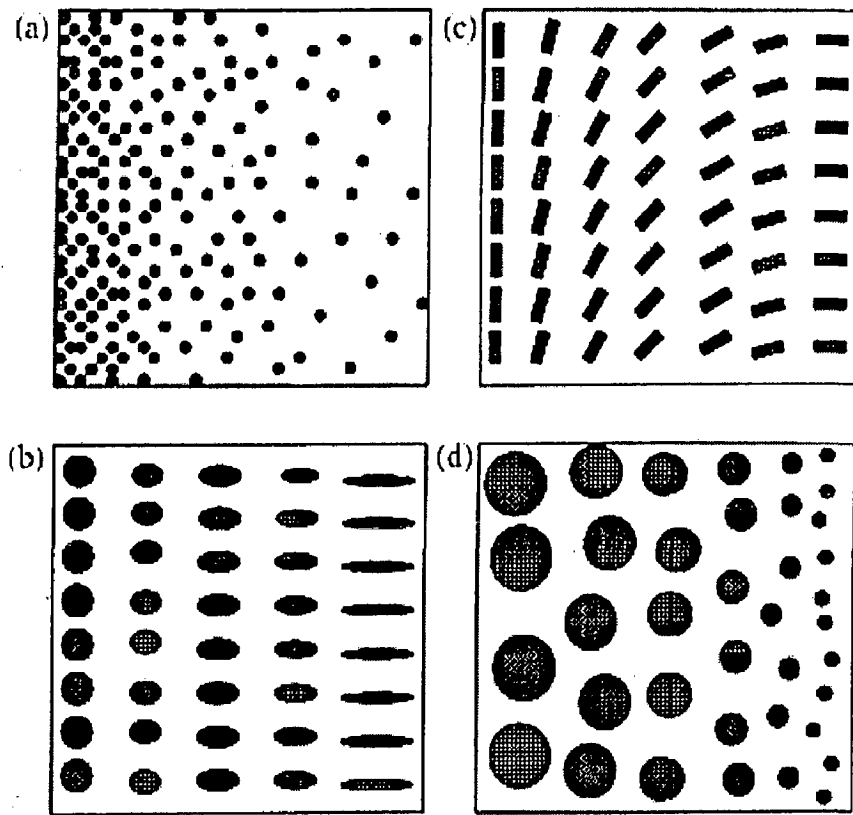
Fig. 2.2 Different types of functionally graded composites with gradient of: (a) volume fraction, (b) shape, (c) orientation, and (d) size of material.
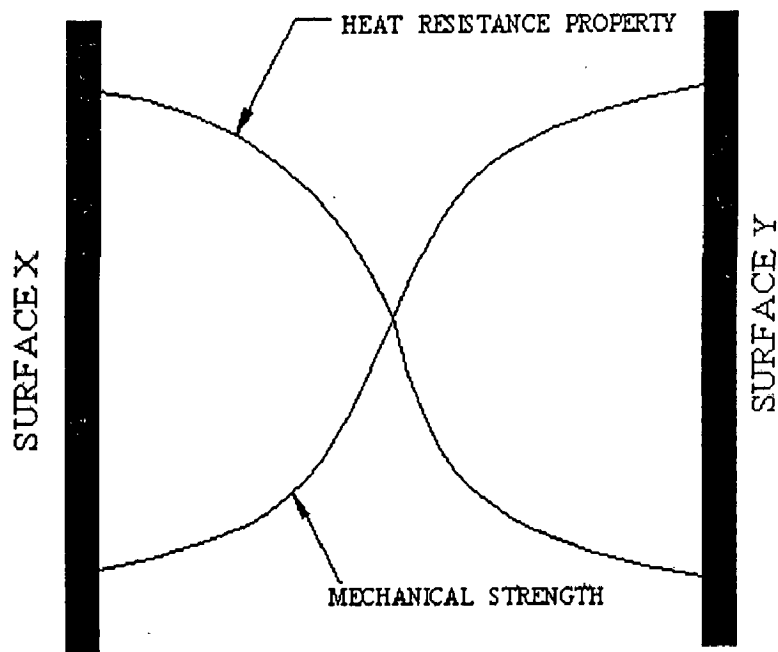
Fig. 2.3 An example of FGM showing the variation in properties along dimensions.

Details of processing technologies are available in the review papers published by Hirari (1996) and Suresh and Mortensen (1998). Some of the processing techniques of FGMs are discussed as follows:

2.2.2.1 Powder metallurgy

The powder metallurgy (PM) for processing of materials and engineering parts includes powder production, powder processing, forming operations and sintering or pressure assisted hot consolidation. Powders of many metals, alloys, compounds and ceramic materials with particle sizes ranging from nanometers to several hundred micrometers are available from industrial sources or may be produced by the methods developed over decades in the field of powder metallurgy or ceramics.

By the powder metallurgy route, the following types of gradients can be processed:

(i)   Porosity and pore-size gradients.

(ii)   Gradients in chemical composition of single-phase materials.

(iii)   Gradients of the volume content of phases and grain size gradients in two or multiphase materials.

2.2.2.2 Melt processing

Gradient formation may be achieved by transport processes in the molten state and subsequent consolidation. Melt processing may be used for the production of FGMs containing a metal as one constituent. The following melt processing techniques may be used for the FGM production.

(i)   Centrifugal casting

In centrifugal casting, particles of a refractory phase are dispersed in a metal melt. These particles may be formed *in-situ* or may be introduced externally in the metal melt. The density difference between particles and the melt leads to the formation of a particle concentration gradient if the melt is cast in a centrifuge (Fig. 2.4). Particles with a lower density or a higher density than the melt are used to prepare functionally graded tubes, which are selectively reinforced at the inner or outer surface of the tube. If platelets are used as particles a gradient in particle orientation may also be produced during the casting process.

(ii)   Sedimentation casting

One-dimensional FGM can be produced by sedimentation of particles.

Sedimentation casting technique results in a high concentration of particulates at a flat surface of the final product.

(iii) Controlled mold filling

The functionally graded material may also be produced by successive casting of two melts (Kieback and coworkers, 2003). In a gravity casting process, the mold is partially filled with the first melt, and in a further step, the second melt is cast on the partially solidified first material (Fig. 2.5). Gradient formation occurs by forced and thermal convection and the width of the graded interface is predominantly controlled by the degree of solidification of the first melt at the time when the second melt is cast. In a modification of this process casting may be carried out in a rotating mold, and components with a cylindrical shape may be obtained.

(iv) Directional Solidification

In this process, the difference between the solidus and liquidus composition during directional solidification of an alloy is used to prepare a FGM (Kieback and coworkers, 2003). In order to avoid solidification under steady state with constant solid concentration, the melt in front of the solidification front must be stirred as effectively as possible. This can be achieved by natural convection in a vertical resistance furnace (Fig. 2.6). A temperature gradient is generated by inserting cooling coils in the top end of the furnace. Samples are melted inside the furnace and then moved toward the chilled zone with a constant velocity. The solidification direction is thus upwards, and for alloying elements with higher density than the matrix element, a solutally and thermally unstable density gradient in the melt is generated.

Rohatgi and coworkers (1991) studied the effects of remelting and isothermal holding, unidirectional solidification, multidirectional solidification and rapid solidification on particle segregation and the dendritic structure of an Al357-15 vol% SiC particle composite. They observed that the segregation of silicon carbide particles occurred owing to settling of the silicon carbide during isothermal hold; countergravity unidirectional solidification led to the SiC particles being pushed by the growing dendrites against gravity. Owing to the pushing of the silicon carbide particles by the growing dendrites, the final distribution of silicon carbide was influenced by the rate of solidification; the best distribution was obtained under fast cooling rates during multidirectional cooling.
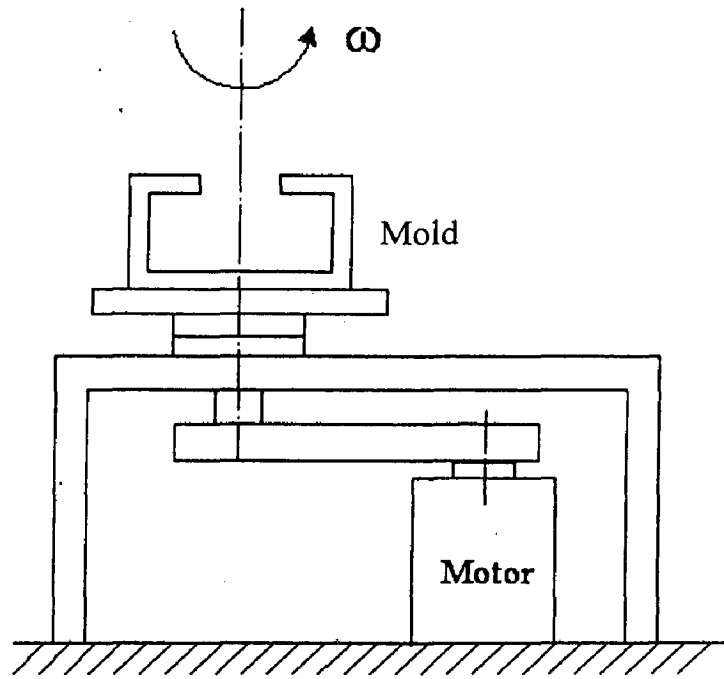
Fig. 2.4 Centrifugal casting of FGM, schematic of the process.
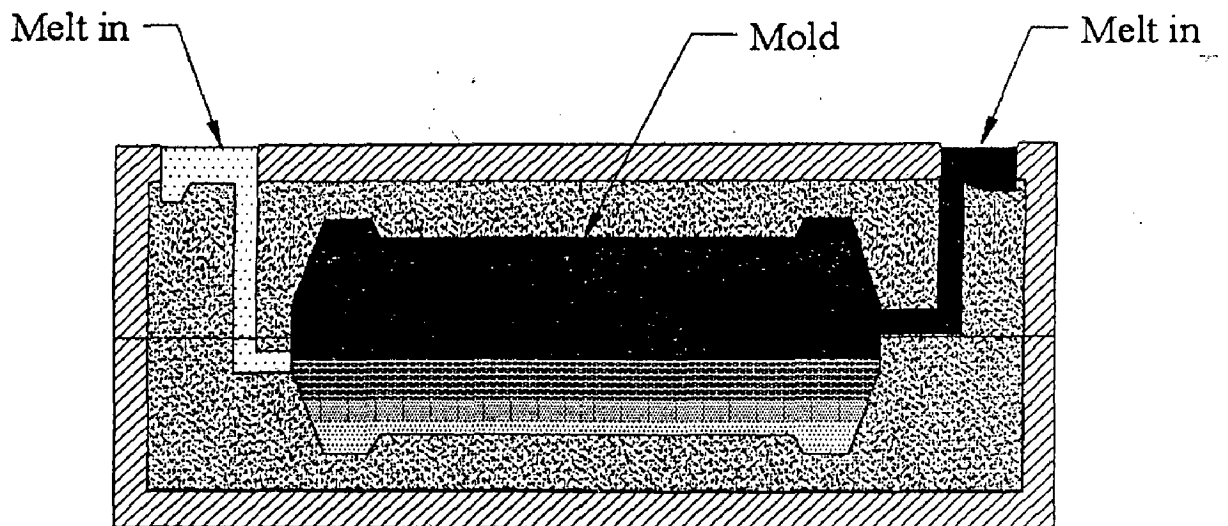
Fig. 2.5 Schematic for multi-alloy gravity casting process.
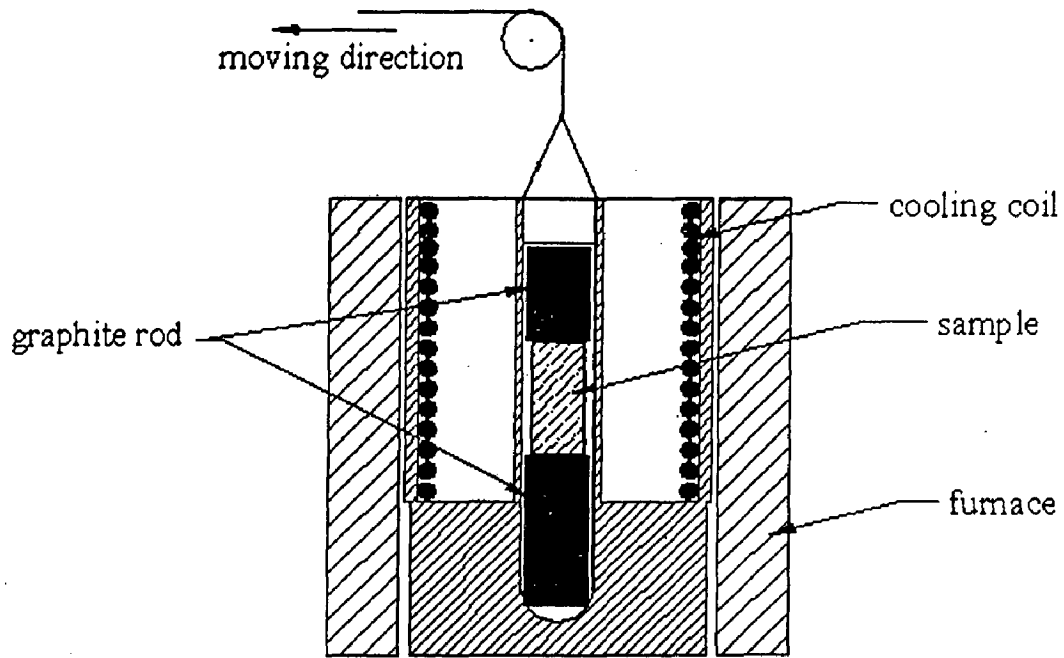
Fig. 2.6 Schematic for directional solidification experiment with natural convection.

Characteristics of different FGM processing techniques

The following table describes the characteristics of different FGM processing methods (Neubrand, 2001):

Table 2.1 Characteristics of different FGM processing techniques

Processing Method Type of FGM processed	Powder Metallurgy	Thermal Spraying	Coating Processes	Melt Processing
Processing of bulk FGMs	Good (very suitable)	Fair (suitable)	Poor (unsuitable)	Good (very suitable)
Processing of graded joints	Fair (suitable)	Poor (unsuitable)	Poor (unsuitable)	Fair (suitable)
Processing of graded coatings	Poor (unsuitable)	Good (very suitable)	Good (very suitable)	Poor (unsuitable)
Variability of transition function	Good (very suitable)	Good (very suitable)	Good (very suitable)	Fair (suitable)
Achievable density	Fair (suitable)	Poor (unsuitable)	Fair (suitable)	Good (very suitable)
Processing of complex shapes	Fair (suitable)	Poor (unsuitable)	Poor (unsuitable)	Good (very suitable)

For the bulk processing, and for the processing of complex shapes, melt processing is the most suitable technique. Of the various melt processing methods available, perhaps the most economical and attractive processing routes are gravity and centrifugal casting. These processes involve the addition of a reinforcing particle phase to a liquid metal matrix and mixing them uniformly, followed by segregation of particles and liquid under gravity or in a centrifugal field to create a desired gradient in the particle concentration and finally preservation of the spatially graded structure by solidification.

Zhang and coworkers (1999) fabricated Al-Mg$_2$Si *in-situ* composite tubes by centrifugal casting process. They also examined the microstructure and tensile strength of the composite tubes revealing an inhomogeneous distribution of Mg$_2$Si particles along the radial direction. Gupta and Loke (2000) successfully synthesized aluminium-silicon carbide based functionally graded material using a new technique termed as gradient slurry disintegration and deposition process to develop gradients of SiC, with particle distribution ranging between 15-20%. The results were confirmed using microstructural characterization techniques and microhardness measurements.

Nai and Gupta (2002) in their work studied the effects of different stirrer geometries on the synthesis of Al/SiC functionally gradient materials (FGMs) by the gradient slurry disintegration and deposition process. Kieback and coworkers (2003) after an overview of the different processing techniques concluded that the processing of FGMs in the laboratory scales has reached a considerable level of maturity and a range of processing methods is available today for almost any material combination. The choice of the most appropriate processing methods depends not only on the materials involved but also on the type of extension of the gradient and geometry of the required component. Despite all these achievements they believe that there will be new challenges in the future when applications for FGMs will evolve. These include,

a) Adaptation of the manufacturing processes to the mass production and upscaling.

b) Repeatability of production processes and reliability of the produced FGMs.

c) Cost effectiveness of production processes.

d) Quality control.

Although the centrifugal method has the advantage of possible application to mass production, accurately controlling and understanding the distribution of particles remains

difficult. Various processing parameters such as crucible furnace temperature, mold heating furnace temperature and velocity of mold rotation significantly influence the composition gradient in FGM. With a similar principle of centrifugal casting technique, Sivakumar and coworkers (2003) developed a new technique named as centrifugal molding technique. In their work they processed and characterized continuous microstructural graded hollow cylinders using centrifugal molding technique.

Mukherjee and Bandyopadhyay (1995), using mechanical smearing and hot isostatic pressing routes, made Fe_3Al-4 vol% Al_2O_3 composite, with very fine size Al_2O_3 particles. They produced compacts with density close to the theoretical density. Vickers' microhardness values of 390 and 500 HV have been achieved for the Fe_3Al and Fe_3Al-Al_2O_3 materials respectively, indicating a strengthening of the matrix in the composite. Scanning electron microscopy and energy-dispersive X-ray analysis studies confirmed the presence of Al_2O_3 as a smeared coating on the Fe_3Al in the composite, and from ultra-microindentation studies the coating thickness was ascertained to be between 0.6 and 1 μm. They observed that the materials exhibited very high mechanical properties, and in particular, the composite compact appeared to possess 50% more strength than, and the same modulus of elasticity as, ultra high strength steels. They observed a functionally graded zone, 0.6-1.0 μm in thickness with hardness varying from 9 GPa at the boundaries to 6 GPa in the interior (Mukherjee and Bandyopadhyay, 1997).

2.2.3 Applications of FGMs

The concept of FGM was developed in the 1990s. The practical use of FGMs is still very limited. There are, however, a few examples of early applications of materials that are FGMs by definition. In the 1960s itself, glass/metal joints with a gradient in thermal expansion coefficient were used to reduce thermal stresses at the interface of the two materials, thus preventing failure of the joint. Glasses with graded refractive index were developed in the early 1970s and were probably the first materials in which a very specific and precise gradation profile was essential for application. A circular plate with a gradient in refractive index can act as a miniature focusing lens with no spherical aberration. Glass rods with a radial index gradient drawn to a fiber are used in wideband optical fiber cables. Another well-established application of FGMs is in polymer skin foams with a dense surface layer and an increasing porosity towards the interior. These

foams can provide high impact strength at low weight in applications such as instrument panels.

All the materials mentioned above are graded glasses or polymers, which are comparatively easy to manufacture. Gradient composite materials consisting of components with widely different properties, i.e., graded ceramic/metal composites, have been manufactured only since the 1990s and tests of graded components from such materials in a real environment are still a rarity. Therefore, they are not being used widely in commercial products. A few promising examples of FGMs for structural applications are given below.

2.2.3.1 Wear protection

The wear resistance of tools can be substantially increased by a hard surface layer in a compressive stress state (Lin and coworkers, 1998). However, if the coating is under compressive stress the risk of delamination is considerable for many material combinations. However in a WC/Co FGM with a gradual variation in cobalt binder contents from the surface to the interior this risk of delamination can be overcome (Neubrand, 2001).

2.2.3.2 Thermal protection systems

One of the earliest applications of the FGM concept was the thermal protection of space vehicles (Neubrand, 2001). A SiC/C FGM nose cone for a space plane was developed at the Japanese National Aerospace Laboratory. A nose cone with a SiC protection layer on a SiC/C composite exposed to a supersonic gas flow at 1900°C deteriorated after the first thermal cycle. In contrast, a nose cone with an additional graded SiC/C interlayer did not show any deterioration even after 10 cycles (Sohda and coworkers, 1993).

2.2.3.3 Medical implants

It is generally acknowledged that a porous surface of a bioactive material such as hydroxyapatite is ideal for rapid bone ingrowths and good mechanical bonding in prosthetic devices. However, for the sake of mechanical stability it is often necessary to use metals as load-carrying materials in implants. As a result, titanium coated with hydroxyapatite is used as an implant material. The adhesion of hydroxyapatite on titanium

is only moderate and failure of the interface may occur after implantation. However, it has been demonstrated that the bonding of certain glasses to titanium is very strong. Therefore, a coating of glass on a Ti-6Al-4V substrate possessing an increasing volume fraction of hydroxyapatite and pores close to its outer surface is an excellent material for cementless artificial joints and dental implants (Neubrand, 2001).

2.2.4 Properties of FGMs

For an FGM component to be commercially viable, the prerequisite is an absence of suitable homogenous materials or composite to be able to provide necessary level of properties for demanding applications (aviation, spacecraft, electronics, tools, etc.). Such an issue eventually has given an impetus to the FGM development, looking for a superior stress relaxation, oxidation resistance, wear and thermal shock resistance as well as fracture toughness properties for spacecraft, gas turbines and other applications. Functionally graded materials are developed for specific requirements. Properly designed property gradients in these materials lead to a performance that cannot be achieved with a homogeneous material or by the joining of two different materials. The gradient can thus be regarded as an additional material design parameter which may be adapted and optimized to meet the requirements of a particular application.

Most of the theoretical researches on FGMs have been devoted to their macroscopic mechanical and thermal behaviour and there has been considerable progress in understanding the effects of gradients on the stress distribution within such materials. A gradation of the elastic modulus and/or of the thermal expansion coefficient changes the stress distribution in a component when it is loaded mechanically or thermally. FGMs are a new generation of engineered materials wherein the microstructural details are spatially varied through non-uniform distribution of the reinforcement phase(s). It is accomplished by using reinforcement with different properties, sizes and shapes, as well as by interchanging the roles of reinforcement and matrix phases in a continuous manner. The result is a microstructure that produces continuously or discretely changing thermal and mechanical properties at the macroscopic or continuum scale. This new concept of engineering the material's microstructure marks the beginning of a revolution both in the materials science and mechanics of materials areas as it allows one, for the first time, to fully integrate the material and structural considerations into the final design of structural components.

Castro and coworkers (2002) in their work investigated the microstructure and mechanical behaviour including tensile and fracture properties of a functionally gradient Al(A359)/SiC$_p$ composite processed by centrifugal casting. The particle volume fraction and, therefore, elasticity modulus was gradually changed in a continuous manner along a certain direction by using centrifugal casting method. The effect of SiC particulate reinforcement on strengthening of A359, Al alloy was experimentally studied by tensile testing with specimens having different SiC contents. There was a continuous increase in tensile and yield strength with increasing SiC volume fractions in the range of 0.20–0.30.

Butcher and coworkers (1999) in their work prepared a functionally graded particulate composite material and measured the spatial gradation of the Young's modulus in the functionally graded material. The optical measurements were used to extract fracture parameters based on the prevailing understanding of the crack tip behaviour in FGMs. The results were also compared with finite element computations, which incorporated measured elastic properties of the FGM. Rooney and Ferrari (2001) examined the tension, bending and flexure of cylinders with functionally graded cross section. They demonstrated that, as the elastic moduli were convex functions of the volume fractions, the effective Young's modulus in simple tension reached its minimum for the homogeneous distribution of the phase. Sankar (2001) in his work obtained an elasticity solution for a functionally graded beam subjected to transverse loads. The Young's modulus of the beam was assumed to vary exponentially through the thickness, and the Poisson's ratio was held constant.

FGMs were originally developed for super heat resistant applications, such as the outer wall and the engine parts of the future space-planes. Conventional super heat resistant materials, such as those found in the exterior of space shuttles, consist of heat resistant ceramic tiles bonded to metal structures. Because of the difference of thermal expansion coefficients, thermal stresses are induced at the contact surface between the ceramic and the metal, when there are temperature gradients. Such thermal stresses cause the ceramic tiles to peel off or crack. Many composite materials also have the same problem at the molecular level.

Functionally graded materials are ideal candidates for applications involving severe thermal gradients, ranging from thermal structures in advanced aircraft and aerospace engines to computer circuit boards. In one such application, a ceramic-rich

region of a functionally graded composite is exposed to hot temperature while a metal-rich region is exposed to cold temperature, with a gradual microstructural transition in the direction of the temperature gradient. By adjusting the microstructural transition appropriately, optimum temperature, deformation and stress distributions can be realized. Thus the thermally induced interlaminar stresses which result from a large property mismatch between the adjacent plies can be reduced by using functionally graded materials. Along the similar lines, joining of dissimilar materials can be made more efficient through the use of functionally graded joints.

Fuchiyama and Noda (1995) developed computer programs for thermal stress analysis of FGMs by Finite Element Method (FEM). These programs can automatically calculate material properties of FGM by using rules of mixture. They have shown that the temperature dependence of material properties has great influence on thermal stress. They have found that the optimization of the material distribution of FGM can reduce the maximum thermal stress. Under the conditions of their study, the maximum stress is lowest when the volumetric ratio is distributed linearly. Ravichandran (1995) presented a one-dimensional calculation of thermal residual stresses, arising from the fabrication of a functionally graded material (FGM) system. His FGM system consists of ceramic (Al_2O_3) and metal (Ni) phases varying with distance in one direction. Several functional forms of gradation of constituents were examined to arrive at the optimum profile giving the minimum residual stress level. A linear variation in composition from fully ceramic to fully metal showed the least residual stress. Residual stresses were found to increase when fully ceramic and/or fully metal regions are included in the structure, adjoining the graded zone. Nemat-Alla (2003) introduced a two-dimensional functionally graded material, 2D-FGM, to withstand super high temperatures and to give reduction in thermal stresses. He compared 2D-FGM and conventional FGM and showed that 2D-FGM has high capability to reduce thermal stresses than the conventional FGM.

2.2.5 Modelling Techniques for FGMs

Various mechanics models are available in the literature to predict the material properties of FGM. From the continuum mechanics point of view FGMs might be viewed as nonhomogeneous materials whose properties like Young's modulus, Poisson's ratio, mass density, yield stress and tangent modulus are functions of spatial position. The

31

material properties of an FGM, such as Young's modulus and Poisson's ratio, most often are evaluated from properties of the constituent materials using micromechanics models (Paulino and coworkers, 2003). Conventional composite models generally apply when the volume fraction of one constituent in the FGM remains much smaller than that of the other (Nemat and Hori, 1993). However, the validity of such models cannot be assured over the entire range of material volume fractions; they rely on the spatial uniformity of constituent distributions and microstructure of the composite. The main feature of FGMs lies in the nonuniform microstructure with continuous change in volume fractions. In fact widely accepted micromechanics models of FGMs remain largely unavailable.

Dvorak and Zuiker (1994) and Reiter and Dvorak (1998) have indicated that, among various micromechanics models for conventional composite materials, Mori–Tanaka and self-consistent models may be used to estimate the effective properties of graded materials with reasonable accuracy. However, a theoretical basis for such applications remains unclear because the concept of a representative volume element cannot be unique for FGMs in the presence of continuously graded properties. To overcome this limitation of standard micromechanics models in FGM applications, Aboudi and coworkers (1999) developed a higher-order micromechanical theory. The fundamental framework of the higher-order theory relies upon volumetric averaging of the various quantities, satisfaction of the field equations in a volumetric sense and imposition in an average sense of boundary and interfacial conditions between the sub volumes to characterize the graded microstructures. Yin and coworkers (2004) developed a micromechanics based elastic model for two-phase functionally graded materials with locally pair-wise interactions between particles. Some of the mathematical models developed for composite materials which may be used for FGMs are discussed in the following sections.

2.2.5.1 Micromechanics models

2.2.5.1.1 Self-consistent model

The self-consistent model was first proposed to estimate the elastic properties of polycrystalline materials which are, in fact, just one phase media (Paulino and coworkers, 2003). When applying the self-consistent method to a two-phase composite, the shear and

bulk moduli μ and K of the composite have the following forms (Hill, 1965)

$$\frac{1}{K+(4/3)\mu} = \frac{V_1}{K_1+(4/3)\mu} + \frac{V_2}{K_2+(4/3)\mu} \qquad (2.7)$$

$$\left(\frac{V_1 K_1}{K_1+(4/3)\mu} + \frac{V_2 K_2}{K_2+(4/3)\mu}\right) + 5\left(\frac{V_1 \mu_2}{\mu-\mu_2} + \frac{V_2 \mu_1}{\mu-\mu_1}\right) + 2 = 0 \qquad (2.8)$$

where, V_1 and V_2 are the volume fractions of phase 1 and phase 2, respectively, μ_1 and μ_2 are the shear moduli of phase 1 and phase 2, respectively, and K_1 and K_2 are the bulk moduli of phase 1 and phase 2, respectively. Once the above nonlinear equations are solved for μ and K, Young's modulus E and Poisson's ratio v of the composite are then determined from the following elasticity relations

$$E = \frac{9\mu K}{\mu+3K}, \qquad v = \frac{3K-2\mu}{2(\mu+3K)} \qquad (2.9a, b)$$

2.2.5.1.2 Mori–Tanaka model

Like the self-consistent method, the Mori–Tanaka method also uses the average local stress and strain fields in the constituents of a composite to estimate the effective material properties of the composite. The Mori–Tanaka method (Mori and Tanaka, 1973), however, involves rather complicated manipulations of the field variables along with the concepts of Eigen strain, back stress, etc. Later, Benveniste (1987) provided a more direct and simplified derivation of the Mori–Tanaka method. The Mori–Tanaka estimates of the effective shear and bulk moduli μ and K of a two-phase composite with spherical inclusion were derived by Benveniste (1987) as follows

$$\mu = \mu_1 + V_2 (\mu_2 - \mu_1) \times \left\{1 + V_1 (\mu_2 - \mu_1)\left[\mu_1 + \frac{\mu_1(9K_1+8\mu_1)}{6(K_1+2\mu_1)}\right]^{-1}\right\} \qquad (2.10)$$

$$K = K_1 + V_2 (K_2 - K_1)\left\{1 + V_1\left[\frac{K_2 - K_1}{K_1+(4/3)\mu_1}\right]\right\}^{-1} \qquad (2.11)$$

Once the above equations are evaluated for μ and K, Young's modulus E and Poisson's ratio v are obtained by Eq. 2.9(a, b).

33

2.2.5.1.3 Tamura–Tomota–Ozawa model

Based on a rule of mixtures, Tamura and coworkers (1973) proposed a simple model (Tamura–Tomota–Ozawa (TTO) model) to describe the stress–strain curves of composite materials. Their model has been employed to study FGMs by Williamson and coworkers (1993), Giannakopoulos and coworkers (1995), and Carpenter and coworkers (1999). The TTO model couples the uniaxial stress (σ) and strain (ε) of the composite to the corresponding average uniaxial stresses and strains of the two constituent materials by

$$\sigma = V_1 \sigma_1 + V_2 \sigma_2, \quad \varepsilon = V_1 \varepsilon_1 + V_2 \varepsilon_2 \qquad (2.12a, b)$$

where, σ_i and ε_i (i = 1, 2) are the average stresses and strains of the constituent phases, respectively, and V_i (i = 1, 2) are the volume fractions. The TTO model introduces an additional parameter, q, to represent the ratio of stress -to- strain transfer

$$q = \frac{\sigma_1 - \sigma_2}{\varepsilon_1 - \varepsilon_2}, \quad 0 < q < \infty \qquad (2.13)$$

q = 0 and q $\rightarrow$ ∞ correspond to property averaging with equal stress and equal strain, respectively. Young's modulus of the composite may be obtained from the above equations as

$$E = \left[V_2 E_2 \frac{q + E_1}{q + E_2} + (1 - V_2) E_1 \right] \times \left[V_2 \frac{q + E_1}{q + E_2} + (1 - V_2) \right]^{-1} \qquad (2.14)$$

where, E_i (i = 1, 2) are Young's moduli of the basic constituent phases. For applications of the TTO model to ceramic/metal (brittle/ductile) composites, the yield stress of the composite, σ_Y, is given by

$$\sigma_Y (V_2) = \sigma_{Y2} \left[V_2 + \frac{(q + E_2) E_1}{(q + E_1) E_2} (1 - V_2) \right] \qquad (2.15)$$

where, σ_{y2} is the yield stress of the metal (phase 2). Idealization of the metal as a bilinear material with a tangent modulus H_2 leads to a bilinear composite with the following tangent modulus H

$$H = \left[V_2 H_2 \frac{q+E_1}{q+H_2} + (1-V_2)E_1 \right] \times \left[V_2 \frac{q+E_1}{q+H_2} + (1-V_2) \right]^{-1}$$

(2.16)

When the metal follows a power-law relation with an exponent n_2, the following nonlinear equations determine the stress–strain curve for the composite

$$\frac{\varepsilon}{\varepsilon_Y} = \frac{V_1 E}{q+E_1} \frac{\sigma_2}{\sigma_Y} + \frac{(q+V_2 E_1)E}{(q+E_1)E_2} \frac{\sigma_{Y2}}{\sigma_Y} \left(\frac{\sigma_2}{\sigma_{Y2}} \right)^{n2}$$

(2.17)

$$\frac{\sigma}{\sigma_Y} = \frac{V_2 q+E_1}{q+E_1} \frac{\sigma}{\sigma_{Y2}} + \frac{V_1 q E_1}{(q+E_1)E_2} \frac{\sigma_{Y2}}{\sigma_Y} \left(\frac{\sigma_2}{\sigma_{Y2}} \right)^{n2}$$

(2.18)

where, $\varepsilon_{Y2} = \frac{\sigma_{Y2}}{E_2}$ and $\varepsilon_Y = \frac{\sigma_Y}{E}$ denote the yield strains of the metal and the composite, respectively. The constant q in the TTO model governs the interaction of the constituents in an FGM. In applications, q may be approximately determined by experimental calibration.

2.2.5.1.4 Hashim–Shtrikman bounds

Effective properties of a composite material are estimated from micromechanics models such as the self-consistent and Mori– Tanaka models discussed above. It is important to provide bounds for these material properties. For a two-phase composite material, Hashim and Shtrikman (1963) derived the following bounds for the effective shear and bulk moduli

$$\mu_1^* = \mu_1 + V_2 \left\{ \frac{1}{\mu_2 - \mu_1} + \frac{6(K_1 + 2\mu_1)V_1}{5\mu_1(3K_1 + 4\mu_1)} \right\}^{-1}$$

(2.19)

$$\mu_2^* = \mu_2 + V_1 \left\{ \frac{1}{\mu_1 - \mu_2} + \frac{6(K_2 + 2\mu_2)V_2}{5\mu_2(3K_2 + 4\mu_2)} \right\}^{-1}$$

(2.20)

$$K_1^* = K_1 + V_2 \left\{ \frac{1}{K_2 - K_1} + \frac{3V_1}{(3K_1 + 4\mu_1)} \right\}^{-1}$$

(2.21)

$$K_2^* = K_2 + V_1 \left\{ \frac{1}{K_1 - K_2} + \frac{3V_2}{(3K_2 + 4\mu_2)} \right\}^{-1}$$

(2.22)

where, μ_1^* and K_1^* are the lower bounds, and μ_2^* and K_2^* are the upper bounds of the shear and bulk moduli, respectively, when $K_2 > K_1$, $\mu_2 > \mu_1$.

2.2.5.2 Aboudi's higher order theory for FGMs

Presently, most computational strategies for the response of FGMs do not explicitly couple the material's heterogeneous microstructure with the structural global analysis. Rather, local effective or macroscopic properties at a given point within the FGM are first obtained through homogenization based on a chosen micromechanics scheme, and subsequently used in a global thermomechanical analysis. In this approach, the local micromechanical analysis is carried out in an independent fashion from the global macromechanical analysis, essentially decoupling the influence of the surrounding spatially inhomogeneous microstructure on the local response of the equivalent (homogenized) continuum point. The exclusion of the possibility of coupling between local and global effects often leads to potentially erroneous results. Perhaps the most important objection to using the standard micromechanics approach based on the concept of a representative volume element (RVE) in the analysis of FGMs is the lack of a theoretical basis for the definition of an RVE, which clearly cannot be unique in the presence of continuously changing properties due to non-uniform inclusion spacing.

As a result of the limitation of the standard micromechanics approaches in FGM applications, a new higher-order micromechanical theory (HOTFGM), which explicitly couples the local (microstructural) and global (macrostructural) effects, has been developed and applied to functionally graded composites by Aboudi and coworkers (1999). The theoretical framework is based on volumetric averaging of the various field quantities, satisfaction of the field equations in a volumetric sense, and imposition in an average sense of the boundary and interfacial conditions between the sub volumes used to characterize the composite's functionally graded microstructure. The need for development of such a theory has been demonstrated by comparison with results obtained using a standard micromechanics approach that neglects the micro-macrostructural coupling effects.

2.2.5.3 Finite element models for FGMs

In the recent past, few investigators have proposed numerical analysis approaches for behaviour prediction of FGMs, utilizing finite element dicretized models. Reiter and coworkers (1997) presented a discrete micromechanics model in which each inclusion is replaced with a planer hexagonal cell and carried out the comparative numerical experiments. Grujicic and Zhang (1998) proposed a numerical analysis technique for determining the accurate effective microstructure dependent elastic properties, by utilizing the Voroni cell finite element method. Cho and Ha (2001) numerically compared the elastic and thermoelastic predictions by three representative averaging approaches, the linear and modified rule of mixture and the Wakashima-Tsukamoto estimate (Wakashima and Tsukamoto, 1991), with those predicted by finite–element discretized models employing rectangular cells.

2.3   SCOPE OF THE PRESENT WORK

After going through the literature available on the Particle Reinforced Metal Matrix Composites (PMMCs) and Functionally Graded Materials (FGMs) in detail, it was found that although a number of mathematical and finite element models are available for estimating the properties of PMMCs and FGMs, there is further need to concentrate on the following points:

1. The simplest models available for the elastic properties of composites are Rules of Mixture, Halpin–Tsai equations, Hashim Shtrikman bounds etc. These models estimate the upper and lower bounds for the modulus of elasticity, modulus of rigidity and Poisson's ratio. The Finite Element Method (FEM) Models available for estimating the elastics properties are mostly based on the unit cell. In the unit cell models the composite is modelled as a unit cell or periodic array of identical unit cells, each containing a reinforcement particle, dimensioned to represent the overall reinforcement volume fraction. In practice however particulate reinforced metal matrix composites have highly heterogeneous microstructures and there is a need to evolve models with better particle distribution.

2. Porosity or voids are inevitable features of composites processed through either solidification or powder metallurgy routes. There are attempts to understand

the effect of porosity on the deformation behaviour of composite experimentally in terms of the broad parameter of volume fraction but there is no effort to incorporate porosity in the model of composite. Further, there is no understanding of the effect of size, shape and orientation of pores on the mechanical properties apart from the broad understanding of shape of voids and stress concentration through models of infinite solids.

3. Although the properties of FGMs are being investigated experimentally as well as by the modelling techniques, the estimation of local as well as global properties of FGMs is still a challenge. A reliable estimation of elastic as well as nonlinear properties of FGMs is important to make these materials acceptable for industrial use. FGMs have also been modelled in the past using the unit cell models like the uniform composite models. The modelling strategies followed so far, often do not explicitly couple the heterogeneous microstructure with the structural global analysis. The exclusion of coupling between local and global effects often leads to potentially erroneous results.

4. FGMs were originally conceived for super heat resistant applications, such as the outer wall and the engine parts of the future spacecrafts. Conventional super heat resistant materials, such as those found in the exterior of space shuttles, consist of heat resistant ceramic tiles bonded to metal structures. In view of this it is felt that a model which is capable of estimating thermal stress distribution inside the FGM should be investigated.

In view of the gaps identified, the scope of the present work was framed in terms of two distinct steps.

In the first step a simple and practical modelling technique has been developed. It was decided to go for a model which is capable of describing the heterogeneous microstructure of PMMCs. The model has the flexibility to distribute a given volume fraction of particles of different shapes and sizes, randomly in the matrix. The model is also capable of determining the elastic as well as nonlinear deformation behaviour of composites under uniaxial loading based on the mechanical behaviour of the constituent materials. The model has the facility to incorporate porosities of different shapes, sizes and volume fraction along with particles and distribute them in the matrix randomly and study their effect on the mechanical properties.

With the help of present modelling method, particles may be distributed uniformly or following some gradation in volume fraction. The modelling technique remains the same for both the uniform composites and FGMs and is capable of estimating the elastic as well as the nonlinear deformation behaviour of FGMs with tailored variation of particle concentration in one or both the directions for a given average particle content. The modelling technique has the flexibility to design the gradation of particles inside the model. The model is capable of estimating the local as well as the global properties of functionally graded materials with or without porosity. The functionally graded materials find applications in space vehicles as a heat resistant material. In view of this, the model has been so developed as to be able to determine the temperature distribution and thermal stresses within the same framework.

In the present work Al/Al$_2$O$_3$ based functionally graded solid cylindrical ingots have been synthesized and its particle distribution has been determined under scanning electron and optical microscope. The particle distributions at different heights of cast FGM ingot have been used as input to the model to determine its elastic and nonlinear deformation behaviour. The hardness distributions at different height have been compared with the local yield stresses determined from the model.

EXPERIMENTAL PROCEDURE

This chapter describes the experimental procedures used in the present work with respect to synthesis and characterization of FGM ingots obtained in the present study.

3.1 COMPOSITION AND CHARACTERISTICS OF STARTING MATERIALS

3.1.1 Aluminium

In the present work, commercially pure aluminium ($\geq$ 99.6 wt. % Al) has been used as the primary constituent of the matrix of the gradient material to be developed due to its (a) low density, (b) low melting point, (c) reasonably high thermal conductivity, (d) good processing flexibility, (e) easy availability, (f) low cost, (g) high toughness and (h) good malleability. It is silver white in colour. The melting point of this is 660 °C and specific gravity is 2.7 gcm^{-3}. Table 3.1 shows the chemical composition of aluminium ingots used for present work.

Table 3.1 Chemical composition of aluminium and magnesium ingots used for present work

Material	Chemical composition, wt%								
	Si	Fe	Zn	Cr	Ni	Mn	Cu	Mg	Al
Al Ingot	0.091	0.202	0.102	0.002	0.006	0.000	0.001	0.001	Bal.
Mg Ingot	0.007	0.021	0.003	0.000	0.002	0.001	0.018	Bal.	0.025

3.1.2 Alumina

In aluminium base composites, alumina has been found to be suitable as reinforcement material since both these materials are physically and chemically compatible at projected service temperature of the resultant composite. High wear resistance, chemical inertness, high strength and availability at reasonable price were the

additional properties, leading to its choice as reinforcement material. LR grade alumina particles of an average size of 50 μm, having melting point 2100°C and density 3.9 gcm^{-3} are used for this work. These particles are approximately round in shape as shown in Fig. 3.1.

3.1.3 Magnesium

Magnesium is used as a surface active agent to promote wetting of alumina by molten aluminium during processing (Pai and coworkers, 1976). The molten aluminium is alloyed by addition of required amount of magnesium (Mg), which is chosen as an alloying element for its significant role in promoting wetting between the molten alloy and the alumina particles in order to retain the particles inside the melt. The presence of magnesium is well known to enhance the wettability of alumina particles in molten aluminium due to a limited chemical reaction at the particle-alloy interface. Magnesium used in this work is cut into small pieces from the cast ingot of silvery white colour. Table 3.1 shows the chemical composition of magnesium ingots used for present work.

3.2   COMPOSITION OF SYNTHESIZED FGM INGOTS

Al-Al$_2$O$_3$ based functionally graded cylindrical ingots were synthesized for three different compositions. These were designated as 10Al/Al$_2$O$_3$, 15Al/Al$_2$O$_3$ and 20Al/Al$_2$O$_3$. The first two digits in the designation indicate the nominal Al$_2$O$_3$ weight percentage added during melt processing of the FGM ingots. The amount of magnesium lump used for FGM ingot preparation was about 5 weight percentage of aluminium used. Table 3.2 gives the nominal weight of the constituents used.

Table 3.2 Nominal composition of cast ingots

Designation	Constituents (in gm)		
	Aluminium	Alumina	Magnesium
10Al/Al$_2$O$_3$	1000	100	50
15Al/Al$_2$O$_3$	1000	150	50
20Al/Al$_2$O$_3$	1000	200	50
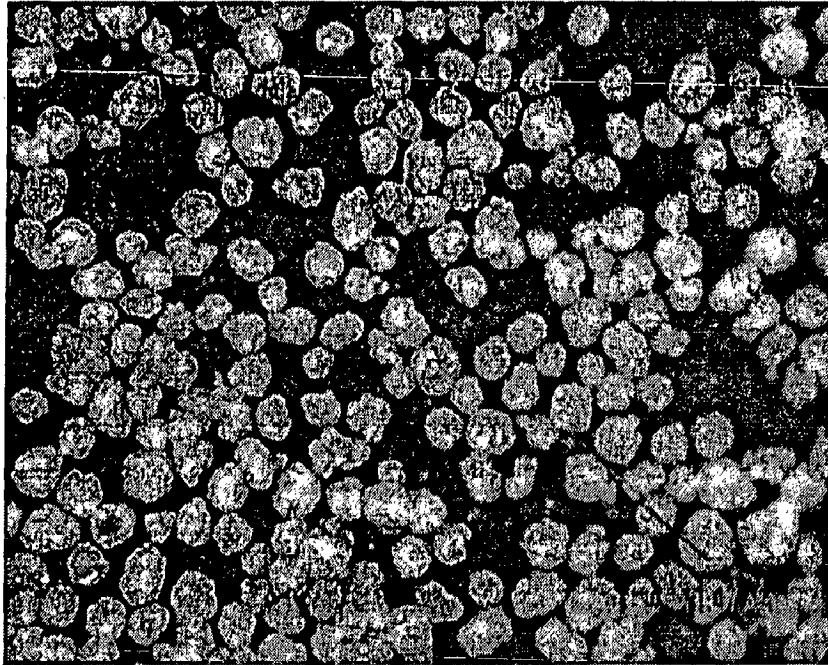
Fig. 3.1 Photomicrograph showing the alumina particles used in this investigation, magnification 100X.

3.3 CONSTRUCTION OF MECHANISM FOR ROTATING MOLD

In order to apply the centrifugal force to the hot melt-particle slurry, a set-up for rotating mold was constructed. As the intention was to construct a robust, safe and economical set-up for the fabrication of FGM, the construction of the set-up was made with the help of easily available components. Fig. 3.2 shows the schematic of the set-up which consists of a table on which the mold was mounted with the help of a holding mechanism. An induction motor was connected with the reduction gear unit using a flexible coupling. This motor and gear unit was firmly clamped on a wooden platform at the base of the steel frame structure. A pulley of diameter 24 cm was attached to the output shaft of the reduction gear unit, which was connected to the second pulley of diameter 6 cm, attached to one end of the horizontal shaft mounted at the top of the table. The horizontal shaft was 40 cm long and of 3 cm diameter. This shaft was used to transmit power from the second pulley to the vertical shaft attached to the mold holder. The horizontal shaft was well supported by two bearings mounted on mild steel stands. A bevel gear unit was used to transmit rotational motion from horizontal shaft to the vertical shaft driving the rotating platform. Vertical shaft was well supported by taper roller bearings. A circular platform having diameter 14 cm, attached to the upper part of the shaft was having a holding mechanism for mounting cylindrical molds of different diameters.

3.4 SET-UP FOR PREPARING METAL CERAMIC SLURRY

The furnace set up for preparing melt-particle slurry consists of a melting unit and a stirring arrangement. The melting unit is a resistance heating vertical muffle furnace constructed by winding 18 SWG kanthal wire over a muffle of 125x125x260 mm^3 size, with a total resistance of 30 ohms. The electrical connection to the furnace has been given from an auto-transformer to control power input to the furnace. A chromel/alumel thermocouple connected to a temperature controller having a range of 0-1200°C and a control accuracy of ±5°C has been placed close to the muffle wall to control the temperature of the furnace at the desired level. A stirrer driven by 1 HP motor having a maximum rated speed of 4000 rpm has been used for stirring the melt. The motor is held rigidly over the furnace with the help of a gripping arrangement fixed with the steel frame structure of the set-up. The stirrer is having an impeller with four blades machined out from a 3 mm thick mild steel sheet, fastened at one end of the stirrer shaft. This impeller is

used for stirring the melt. Fig. 3.3 shows the schematic of furnace for preparing melt particle slurry.

3.5 PROCEDURE FOR SYNTHESIS OF FGM INGOTS

The ingots of commercially pure aluminium alloy ($\geq$99.6 wt % Al) were cut into small pieces (weighing nearly 100 gm) and cleaned by pure water to remove any surface impurities prior to usage. About 1000 gm of cleaned pieces of aluminium were melted in a cylindrical graphite crucible machined from a graphite block. The inner diameter of the crucible was 8 cm and height was 15 cm. This crucible was placed in the furnace of the set-up shown schematically in Fig. 3.3. The temperature of the melt was continuously measured with the help of a chromel/alumel thermocouple having a protective covering, placed inside the melt at a depth of 15-20 mm from the top surface. The temperature of the melt was observed continuously. The temperature was read out directly in centigrade scale on a potentiometer calibrated for measuring temperature.

When the temperature of the melt reached 850°C, 50 gm of magnesium lump covered in an aluminium foil was added to the melt. The stirrer was then introduced into the melt. The stirrer was always kept at the centre of the melt surface. The speed of the stirrer was maintained approximately at 400 rpm. A strobometer was used to measure the stirring speed. The alumina particles preheated to 200°C, were added to the melt. The particles were added at the rate of 2.0-2.5 gm/s with the help of a long narrow steel pipe to form slurry. The melt was continuously stirred during the addition of the particles. The stirring was continued for 5 minutes after the addition of the particles to the melt. The stirring speed was maintained at 400 rpm by regulating the power input to the motor of the stirrer through an auto transformer. Table 3.3 shows the processing conditions used during preparation of melt-particle slurry.

During the mixing of metal melt and particles, the temperature of the melt was maintained approximately at 850°C. After mixing properly, the cylindrical graphite crucible was removed from the furnace and was immediately mounted on the rotating platform shown in Fig. 3.2, with the axis of the cylindrical crucible coinciding with the axis of rotation. The time taken for taking the crucible from the furnace to mounting it on the rotating platform was approximately 10 seconds.
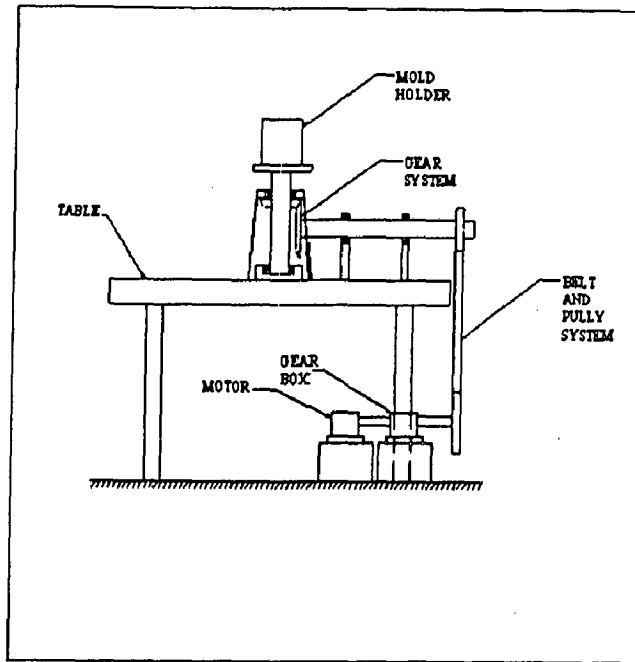
Fig. 3.2   Schematic of mechanism for rotating mold for introducing gradient in particle distribution.
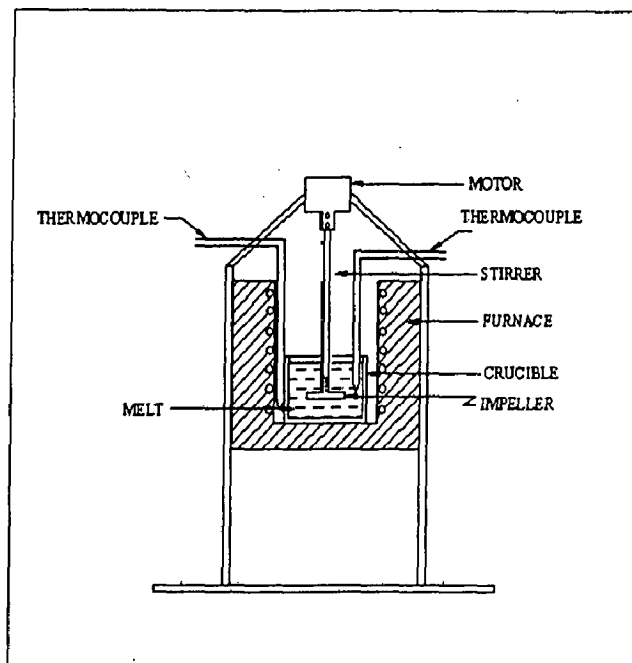
Fig. 3.3   Schematic of furnace for preparing melt-particle slurry.

45

After mounting the crucible properly at the middle of the rotating platform, the motor driving the rotating platform was switched on. It was taking approximately 5 seconds to achieve maximum angular acceleration. The mold was rotated at the speed of 300 rpm. This rotation was continued till the solidification is completed. The different centrifugal forces acting on the particles and the melt due to their different densities resulted in a gradient in the distribution of alumina particles.

Table 3.3 Processing conditions during preparation of melt-particle slurry

Stirring speed	400 rpm
Stirring temperature	850°C
Stirring time (prior to Al_2O_3 addition)	2 minutes
Stirring time (during and after Al_2O_3 addition)	15 minutes
Alumina preheat temperature (prior to mixing in melt)	200°C
Wt.% of Al_2O_3 in melt	10 %, 15%, 20%
Wt. % of Mg in melt	5 % of aluminium

3.6 METALLOGRAPHIC EXAMINATION

3.6.1 Metallographic preparation

The transverse and horizontal sections of cast ingots of FGM were prepared for metallographic studies by following standard metallographic procedures. The specimens were initially polished with various grades of emery papers from coarse to fine grades, mounted on rotating polishing wheels. The specimens were then polished using polishing grade alumina powder on a blazer cloth mounted on a polishing wheel.

3.6.2 Optical Micrography

Microstructural characterization was carried out using an AXIOVERT 200 MAT (ZEISS) optical microscope, on metallographically polished samples to investigate the distribution of Al_2O_3 particles.

3.6.3 Scanning Electron Micrography

Microstructural characterization of the metallographically polished specimens of three FGM ingots was carried out using a LEO 435-25-20 scanning electron microscope (SEM). The objective of SEM is aimed to investigate the distribution of alumina particles at different positions across the section of cast cylindrical FGM ingots and the interfacial continuity between the aluminium matrix and alumina particles.

3.7 HARDNESS MEASUREMENT

Hardness measurements were conducted on the FGM samples using Vickers Hardness Testing Machine. A diamond indenter with a face angle of 136° was used to make indentation. To measure the hardness at a particular location a 5 kg load was employed on the indenter for 10 seconds at a chosen location in the sample. The hardness is proportional to the dimension of the impression made by the indenter at that particular location. The surface of sample was carefully polished before the hardness test to allow for the correct measurements of the impression size. For each sample the indentations were made at different radial locations between the inner and the outer radius. At each location three to five readings were taken in the close vicinity and the average of these values was taken as the hardness at that particular location. The distance between the subsequent indentations was kept at least two times the diameter of the indenter to facilitate free development of the deformation zone under the indenter during indentation.

MODELLING AND FORMULATION

4.1 INTRODUCTION

In order to make good use of materials in engineering structures, an understanding of their deformation behaviour is required so as to predict their performance. For composites, this means developing models which represent reasonably closely the known experimental response of real composites to applied stresses and environmental conditions. Theories for elastic behaviour of composites are well developed and predictions of elastic response are often very satisfactory. Nonlinear behaviour of composites has also been extensively investigated by using unit cell models. In the unit cell models, the composite is modelled as a unit cell or periodic array of identical unit cells, each containing a reinforcement particle dimensioned to represent the overall reinforcement volume fraction. However, particulate reinforced metal matrix composites have highly heterogeneous microstructures. Particles are randomly distributed in the metal matrix. Therefore, the periodic arrangement of particles in unit cell model does not represent the arrangement of particles in composites. Few models are also available for Functionally Graded Materials in the literature. These models are also either based on the unit cell method or on periodic array of particles. Mathematical models available are mostly very difficult to use. There is a need of a simple modelling scheme for uniform composites as well as for Functionally Graded Materials (FGMs) which can predict their mechanical and thermal behaviour quite accurately taking into account the random distribution of particles.

4.2 FEM FORMULATION

Composites are two or more phase materials. In the present work, two phase composites are considered. Finite Element Method (FEM) has been used for modelling the composites. In FEM the whole continuum is divided into an assemblage of a large number of finite elements. In the present work, Rayleigh-Ritz method based on the theory of minimum potential energy is used. Four-node isoparametric quadrilateral element is used

in the present analysis as shown in Fig. 4.1. The local nodes are numbered as 1, 2, 3 and 4 in a counterclockwise fashion as shown, and (x_i, y_i) are the coordinates of node i. The vector $\mathbf{q} = [q_1, q_2, \ldots\ldots, q_8]^T$ denotes the element displacement vector $[u_1, v_1, u_2, v_2, u_3, v_3, u_4, v_4]^T$. The displacement of an interior point P located at (x, y) is represented as $\mathbf{u} = [u(x, y), \ v(x, y)]^T$.

A particular element in global Cartesian coordinate system is mapped in to a master element (Fig. 4.2) in natural coordinate system (ξ, η). This master element is square in shape and has vertices (-1, -1), (1, -1), (1, 1), (-1, 1) in natural coordinate system. The shape functions N_i (ξ, η) where $i = 1, 2, 3, 4$ are defined such that N_i is equal to unity at node i and is zero at other nodes. The shape functions can be written as

$$
\left.
\begin{aligned}
N_1 &= \frac{1}{4}(1 - \xi)(1 - \eta) \\[4pt]
N_2 &= \frac{1}{4}(1 + \xi)(1 - \eta) \\[4pt]
N_3 &= \frac{1}{4}(1 + \xi)(1 + \eta) \\[4pt]
N_4 &= \frac{1}{4}(1 - \xi)(1 + \eta)
\end{aligned}
\right\}
\tag{4.1}
$$

Now, the displacement field within the element in terms of the nodal values is expressed. Thus, if $\mathbf{u} = [u, v]^T$ represents the displacement components of a point located at (ξ, η), and $\mathbf{q}$, dimension (8×1), is the element displacement vector, then

$$
\left.
\begin{aligned}
u &= N_1 q_1 + N_2 q_3 + N_3 q_5 + N_4 q_7 \\[4pt]
v &= N_1 q_2 + N_2 q_4 + N_3 q_6 + N_4 q_8
\end{aligned}
\right\}
\tag{4.2a, b}
$$

This can be written in matrix form as

$$
\mathbf{u} = \mathbf{N}\mathbf{q}
\tag{4.3}
$$

where, $\mathbf{N} = \begin{bmatrix} N_1 & 0 & N_2 & 0 & N_3 & 0 & N_4 & 0 \\ 0 & N_1 & 0 & N_2 & 0 & N_3 & 0 & N_4 \end{bmatrix}$ (4.4)

In the isoparametric formulation, the same shape functions N_i is used to express the coordinates of a point within the element in terms of natural coordinates.
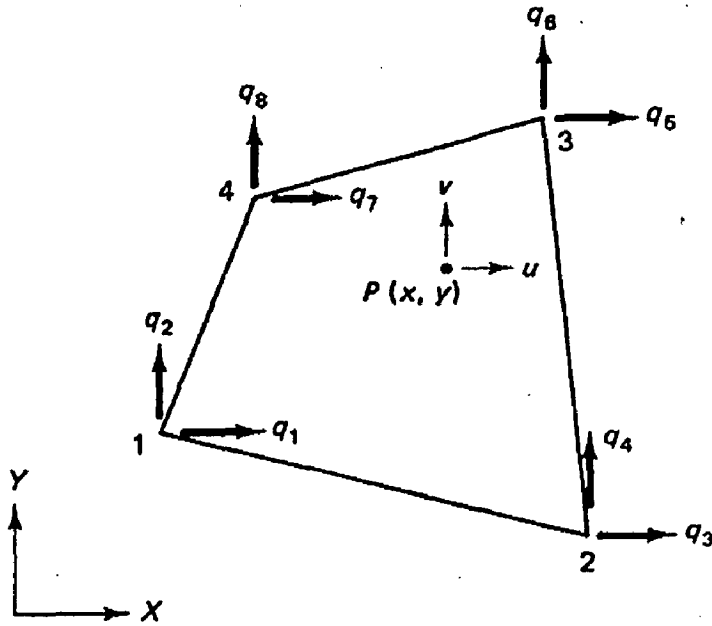
Fig. 4.1 Four-node quadrilateral element.
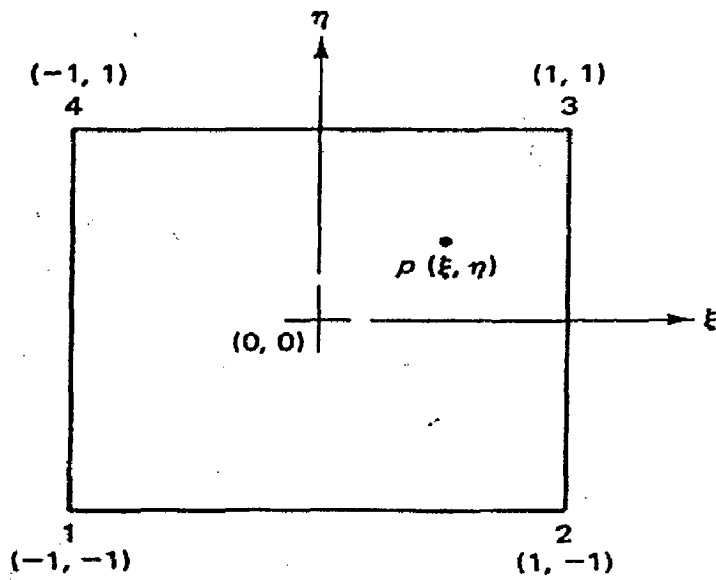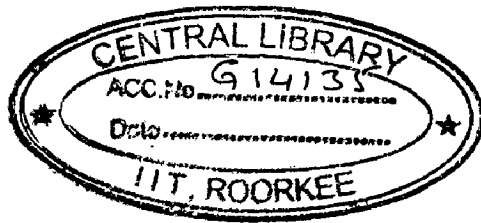
Fig. 4.2 The quadrilateral element in ξ, η *space*.

Thus

$$
\left.\begin{aligned}
x &= N_1 x_1 + N_2 x_2 + N_3 x_3 + N_4 x_4 \\
y &= N_1 y_1 + N_2 y_2 + N_3 y_3 + N_4 y_4
\end{aligned}\right\}
\qquad (4.5a, b)
$$

Using the chain rule of differentiation, one can have

$$
\left.\begin{aligned}
\frac{\partial u}{\partial \xi} &= \frac{\partial u}{\partial x}\frac{\partial x}{\partial \xi} + \frac{\partial u}{\partial y}\frac{\partial y}{\partial \xi} \\
\frac{\partial u}{\partial \eta} &= \frac{\partial u}{\partial x}\frac{\partial x}{\partial \eta} + \frac{\partial u}{\partial y}\frac{\partial y}{\partial \eta}
\end{aligned}\right\}
\qquad (4.6a, b)
$$

or

$$
\left\{\begin{array}{c}\dfrac{\partial u}{\partial \xi} \\[2mm] \dfrac{\partial u}{\partial \eta}\end{array}\right\} = \mathbf{J}\left\{\begin{array}{c}\dfrac{\partial u}{\partial x} \\[2mm] \dfrac{\partial u}{\partial y}\end{array}\right\}
\qquad (4.7)
$$

where, $\mathbf{J}$ is Jacobian matrix given as

$$
\mathbf{J} = \begin{bmatrix} \dfrac{\partial x}{\partial \xi} & \dfrac{\partial y}{\partial \xi} \\[3mm] \dfrac{\partial x}{\partial \eta} & \dfrac{\partial y}{\partial \eta} \end{bmatrix}
\qquad (4.8)
$$

Jacobian matrix $\mathbf{J}$ may be written as

$$
\mathbf{J} = \frac{1}{4}\begin{bmatrix} -(1-\eta)x_1 + (1-\eta)x_2 + (1+\eta)x_3 - (1+\eta)x_4 & -(1-\eta)y_1 + (1-\eta)y_2 + (1+\eta)y_3 - (1+\eta)y_4 \\ -(1-\xi)x_1 - (1+\xi)x_2 + (1+\xi)x_3 + (1-\xi)x_4 & -(1-\xi)y_1 - (1+\xi)y_2 + (1+\xi)y_3 + (1-\xi)y_4 \end{bmatrix}
$$

$$
\equiv \begin{bmatrix} J_{11} & J_{12} \\ J_{21} & J_{22} \end{bmatrix}
\qquad (4.9a, b)
$$

Equation 4.7 can be inverted as

$$
\left\{\begin{array}{c}\dfrac{\partial u}{\partial x} \\[2mm] \dfrac{\partial u}{\partial y}\end{array}\right\} = \mathbf{J}^{-1}\left\{\begin{array}{c}\dfrac{\partial u}{\partial \xi} \\[2mm] \dfrac{\partial u}{\partial \eta}\end{array}\right\}
\qquad (4.10)
$$

or

$$
\left\{\begin{array}{c}\dfrac{\partial u}{\partial x} \\[2mm] \dfrac{\partial u}{\partial y}\end{array}\right\} = \frac{1}{\det \mathbf{J}}\begin{bmatrix} J_{22} & -J_{12} \\ -J_{21} & J_{11} \end{bmatrix}\left\{\begin{array}{c}\dfrac{\partial u}{\partial \xi} \\[2mm] \dfrac{\partial u}{\partial \eta}\end{array}\right\}
\qquad (4.11a)
$$

51

Similarly,

$$\begin{Bmatrix} \dfrac{\partial v}{\partial x} \\ \dfrac{\partial v}{\partial y} \end{Bmatrix} = \dfrac{1}{\det \mathbf{J}} \begin{bmatrix} J_{22} & -J_{12} \\ -J_{21} & -J_{11} \end{bmatrix} \begin{Bmatrix} \dfrac{\partial v}{\partial \xi} \\ \dfrac{\partial v}{\partial \eta} \end{Bmatrix}$$ (4.11b)

These expressions are used in the derivation of the element stiffness matrix. An additional result used for area integration is

$$dx\, dy = \det \mathbf{J}\, d\xi\, d\eta$$ (4.12)

The stiffness matrix for the quadrilateral element can be derived from the strain energy stored in an element, given by

$$U^e = \int_{V_e} \frac{1}{2} \sigma^{\mathrm{T}} \varepsilon\, dV$$ (4.13)

or $$U^e = t_e \int_e \frac{1}{2} \sigma^{\mathrm{T}} \varepsilon\, dA$$ (4.14)

where, t_e is the thickness of the element. The strain-displacement relations are

$$\varepsilon = \begin{Bmatrix} \varepsilon_x \\ \varepsilon_y \\ \varepsilon_z \end{Bmatrix} = \begin{Bmatrix} \dfrac{\partial u}{\partial x} \\ \dfrac{\partial v}{\partial y} \\ \dfrac{\partial u}{\partial y} + \dfrac{\partial v}{\partial x} \end{Bmatrix}$$ (4.15)

Equations 4.11 (a, b) and 4.15 yield

$$\varepsilon = \mathbf{A} \begin{Bmatrix} \dfrac{\partial u}{\partial \xi} \\ \dfrac{\partial u}{\partial \eta} \\ \dfrac{\partial v}{\partial \xi} \\ \dfrac{\partial v}{\partial \eta} \end{Bmatrix}$$ (4.16)

52

where, A is given as

$$A = \frac{1}{\det J} \begin{bmatrix} J_{22} & -J_{12} & 0 & 0 \\ 0 & 0 & -J_{21} & J_{11} \\ -J_{21} & -J_{11} & J_{22} & -J_{12} \end{bmatrix} \qquad (4.17)$$

From Eqs. 4.2(a, b)

$$\begin{Bmatrix} \dfrac{\partial u}{\partial \xi} \\ \dfrac{\partial u}{\partial \eta} \\ \dfrac{\partial v}{\partial \xi} \\ \dfrac{\partial v}{\partial \eta} \end{Bmatrix} = Gq \qquad (4.18)$$

where,

$$G = \frac{1}{4} \begin{bmatrix} -(1-\eta) & 0 & (1-\eta) & 0 & (1+\eta) & 0 & -(1+\eta) & 0 \\ -(1-\xi) & 0 & -(1+\xi) & 0 & (1+\xi) & 0 & (1-\xi) & 0 \\ 0 & -(1-\eta) & 0 & (1-\eta) & 0 & (1+\eta) & 0 & -(1-\eta) \\ 0 & -(1-\xi) & 0 & -(1+\xi) & 0 & (1+\xi) & 0 & (1-\xi) \end{bmatrix} \qquad (4.19)$$

Equations 4.16 and 4.18 now yield

$$\varepsilon = Bq \qquad (4.20)$$

where, $\qquad B = AG \qquad (4.21)$

The strain in the element is expressed in terms of its nodal displacement. The stress is given by

$$\sigma = DBq \qquad (4.22)$$

where, D is a (3 × 3) material matrix. For plane stress conditions D is given as

$$D = \frac{E}{1-v^2} \begin{bmatrix} 1 & v & 0 \\ v & 1 & 0 \\ 0 & 0 & \dfrac{1-v}{2} \end{bmatrix} \qquad (4.23)$$

where, E is the Young's modulus of elasticity and v is the Poisson's ratio for the material.

The strain energy as given in Eq. 4.14 may be expressed as

$$U^e = \frac{1}{2} \mathbf{q}^T t_e \int_{-1}^{1} \int_{-1}^{1} \mathbf{B}^T \mathbf{D} \mathbf{B} \, \det\mathbf{J} \, d\xi \, d\eta \, \mathbf{q} \tag{4.24a}$$

$$= \frac{1}{2} \mathbf{q}^T \mathbf{k}^e \mathbf{q} \tag{4.24b}$$

where, $\qquad \mathbf{k}^e = t_e \int_{-1}^{1} \int_{-1}^{1} \mathbf{B}^T \mathbf{D} \mathbf{B} \, \det\mathbf{J} \, d\xi \, d\eta \tag{4.25}$

is the element stiffness matrix of dimension (8 × 8).

The expression for the potential energy of an element may be written as

$$\Pi^e = U^e - \int_{Le} \mathbf{u}^T \mathbf{T} \, t_e \, dl \tag{4.26}$$

where, L_e is the boundary of the element, and

$$\mathbf{T} = \begin{Bmatrix} t_x \\ t_y \end{Bmatrix} \tag{4.27}$$

is the traction vector. Equation 4.26 may be expressed as

$$\Pi^e = \frac{1}{2} \mathbf{q}^T \mathbf{k}^e \mathbf{q} - \mathbf{q}^T \mathbf{F}^e \tag{4.28}$$

where, $\mathbf{F}^e$ is the load matrix of the element. Using the Rayleigh-Ritz method, the potential energy may be minimized and the resulting equation may be written as

$$\mathbf{k}^e \mathbf{q} = \mathbf{F}^e \tag{4.29}$$

Using usual method of assembly, the element equation may be assembled into a global matrix as

$$[\mathbf{k}] \{\mathbf{q}\} = \{\mathbf{F}\} \tag{4.30}$$

4.3   APPLICATION OF FEM IN THE PRESENT PROBLEM USING ANSYS 5.4

The FEM formulation discussed in the previous section has been applied in the present problem using FEM tool ANSYS 5.4. The present analysis consists of two materials with different properties; hence two different D matrices have been used. In the case of linear analysis, elements having different material properties deform linearly. The stresses and strains of the elements are calculated according to the FEM formulation discussed above with the help of ANSYS 5.4. In the case of nonlinear analysis matrix material is elastic-perfectly plastic while the particles are linear elastic. As unloading is not being considered in the present work, the similar methodology as used for linear analysis is also used for the nonlinear analysis. In the case of nonlinear analysis the load is applied in steps. After each step the stresses and strains for all the elements are calculated. If after a load step the stress in any element is observed to be beyond the elastic limit it stops taking any further load.

Von Mises stress criterion is used for determining yielding in ductile matrix material in the present analysis. This yield criterion states that the von Mises stress σ_{vm} should be less than or equal to the uniaxial yield stress σ_y of the material. The criterion may be put as

$$\sigma_{vm} \leq \sigma_y \tag{4.31}$$

where, $$\sigma_{vm} = \left(I_1^2 - 3I_2 \right)^{1/2} \tag{4.32}$$

I_1 and I_2 are the first two invariants of the stress tensor.

For the state of plane stress

$$I_1 = \sigma_{xx} + \sigma_{yy} \tag{4.33}$$

$$I_2 = \sigma_{xx}\,\sigma_{yy} - \tau_{xy}^{2} \tag{4.34}$$

For the modelling of particle reinforced composites a square domain of size 5 mm x 5 mm under plane stress conditions has been considered. Particle size elements are

generated in the whole model area with the help of ANSYS 5.4. In the present modelling method, particles are randomly distributed inside the matrix material. It produces a realistic distribution of particles in the composite. The objective of the present work is to model functionally graded materials. However, in the first step, the present work is concentrated on the modelling of uniform composites without and with porosity. The idea behind this is to validate this model for the uniform composites by comparing the results with the available results from existing models and experiments, and also to examine the impact of porosity on uniform composites. From the literature review it is realized that models of uniform composites based on realistic distribution of particles are rare. With the help of random distribution of particles, a more realistic composite model can be achieved.

For distributing elements having properties of the particle with random distribution, all the elements in the model are assigned random numbers between zero and one. For modelling a uniform composite with given particle volume fraction, a random number is generated for every element and if this number is lower than or equal to the volume fraction desired, the element is assigned the particle material property. Remaining elements are assigned the matrix material property. In this manner, the resulting model mimics a uniform random distribution of particulate reinforcement corresponding to the required volume fraction of the composite. This assignment of material property to each element has been accomplished with the help of a FORTRAN program. In ANSYS, different material numbers can be assigned to different elements. The particle distribution can be observed in the matrix by assigning different colors to different materials. Randomly distributed pores may also be created with the help of the present modelling scheme to establish the effect of porosity on the mechanical properties of the composites. In the case of Functionally Graded Materials (FGMs) the randomness in particle distribution as well as the variation in particle concentration is achieved with the help of a FORTRAN program.

In the present work, particles are assigned the property of alumina and matrix material is assigned the property of commercial aluminium. For linear analysis particles and matrix are considered linear elastic with modulus of elasticity of 375 GPa and 75 GPa respectively and Poisson's ratios of 0.3 for both. For the nonlinear analysis the particles

are still linear elastic but the matrix is considered elastic-perfectly plastic with yield stress of 90 MPa. In the present work, plane42 elements are used for the structural analysis. For the thermal analysis plane55 elements are used. It is assumed in the present work that the particles are perfectly bonded to the matrix i.e. there is no debonding of the particles from the matrix.

4.3.1 Modelling for Uniform Composites

For modelling the uniform composite, a square area with an edge length 5 mm has been considered. This area is meshed with four-node plane42 elements, with an edge length of 50 μm. Thus the whole model consists of 10000 elements with 50 μm edge length. Out of these elements, $10000*V_f$ elements (V_f is the particle volume fraction in the composite) are randomly selected from the list of elements. These selected elements are assigned particle material properties and remaining elements are assigned matrix material properties. The particle property elements are randomly distributed over the whole matrix, thus producing a realistic distribution of particles in particle reinforced metal matrix composites. Uniform composite models with average particle contents varying from 0 vol% to 100 vol% with an interval of 10 vol% have been investigated. Eleven models of composites have been obtained in this way containing different amount of alumina particles with average particle contents ranging from 0 to 100 vol%. Figure 4.3 shows a uniform composite model with 10 vol% average particle content with particles randomly distributed in the matrix.

The elastic modulus in the loading direction of y-axis is estimated for composites with different average particle contents. To find the modulus of elasticity in the y-axis direction, one end of the model is kept fixed. On the other end, a uniform displacement is imposed. Figure 4.4 shows a model with uniform displacement loading in y-axis direction. To find the global value of modulus of elasticity in y-axis direction for the model, the average of the normal stresses and the normal strains in y-axis direction of all the elements are obtained. The average normal stress σ_{yy} in y-axis direction for the model may be obtained as

$$\sigma_{yy} = \sum_{i=1}^{n} \frac{\sigma_{yyi}}{n} \qquad (4.35)$$

where, σ_{yyi} is the normal stress in y-axis direction for the ith element and n is the number of elements in the model.

The average strain ε_{yy} in y-axis direction for the model is obtained as

$$\varepsilon_{yy} = \sum_{i=1}^{n} \frac{\varepsilon_{yyi}}{n} \qquad (4.36)$$

where, ε_{yyi} is the normal strain in y-axis direction for the ith element and n is the number of elements in the model. The modulus of elasticity in y-axis direction for the model is obtained as the ratio of average stress and average strain for the model in y-axis direction as

$$E = \frac{\sigma_{yy}}{\varepsilon_{yy}} \qquad (4.37)$$

To estimate the nonlinear behaviour of the composite, one end of the model is kept fixed as shown in Fig. 4.4 and on the other end of the model a uniform displacement load is applied. This uniform displacement is applied in 20 equal steps. The average elemental stresses and strains for each step for a given model of composite are plotted in graphical form. This graph, thus, represents the nonlinear deformation behaviour of that particular model of composite. To find the yield stress of the metal matrix composite the crossover method is used. In the crossover method, the stress at the point where the tangent of the elastic line crosses the tangent of the plastic line is taken as the yield stress. The crossover method provides a conservative value for the yield stress.

Modulus of rigidity has also been estimated for the uniform composites. To estimate the modulus of rigidity of a uniform composite, the model is subjected to a shear load as shown in Fig. 4.5. The average of shear stresses and shear strains of all the elements are obtained. The modulus of rigidity of the composite is calculated using the following simple relation.

$$G = \frac{\sigma_{xy}}{\varepsilon_{xy}} \qquad (4.38)$$

where, G is the modulus of rigidity for the composite, σ_{xy} is the average of shear stresses of all the elements and ε_{xy} is the average of shear strains of all the elements.
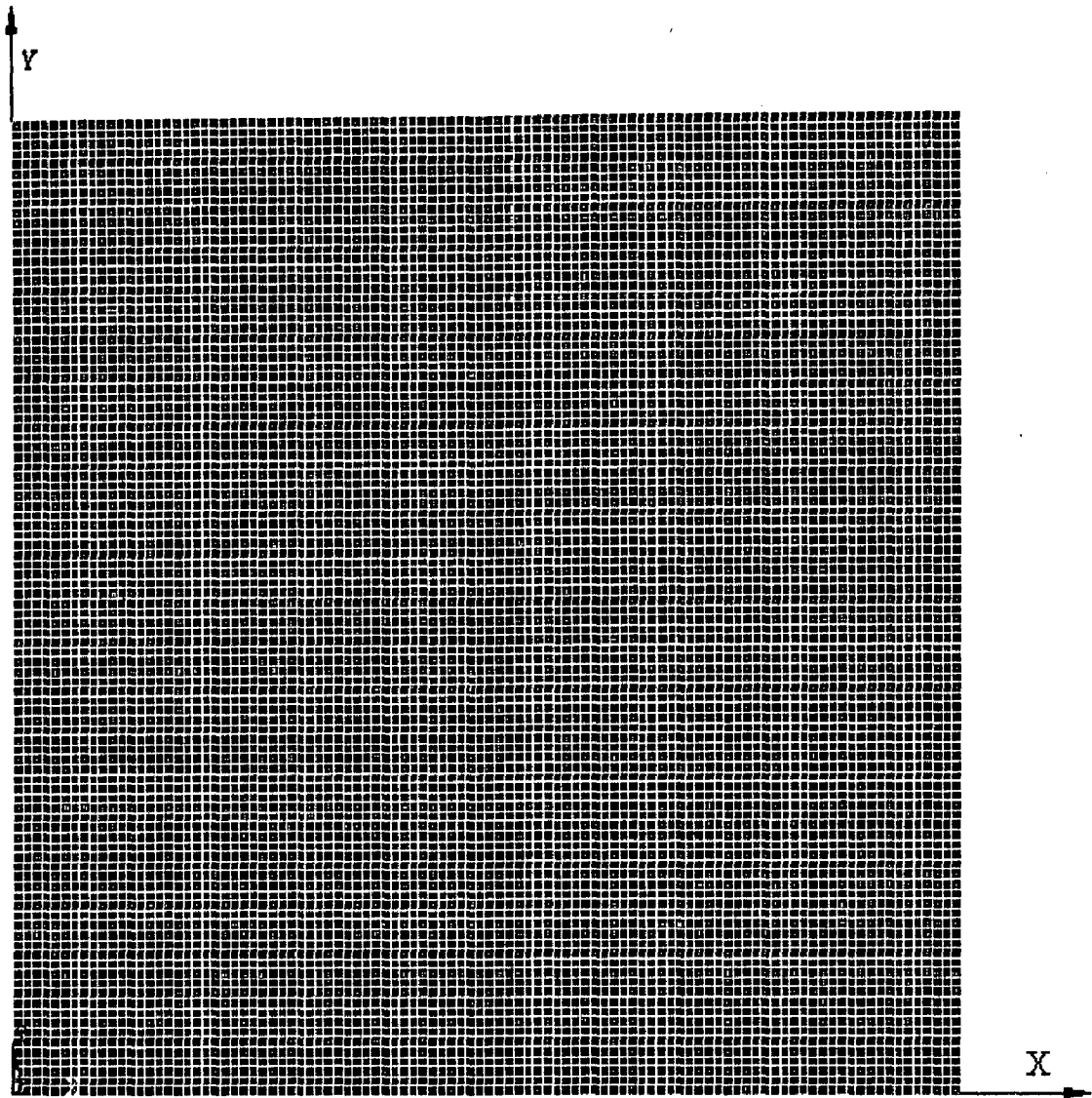
Fig. 4.3 A schematic showing the model of a uniform composite with average particle content of 10 vol%. Particles are randomly distributed over the area. Turquoise colour shows aluminium matrix and dark lavender colour shows alumina particles.

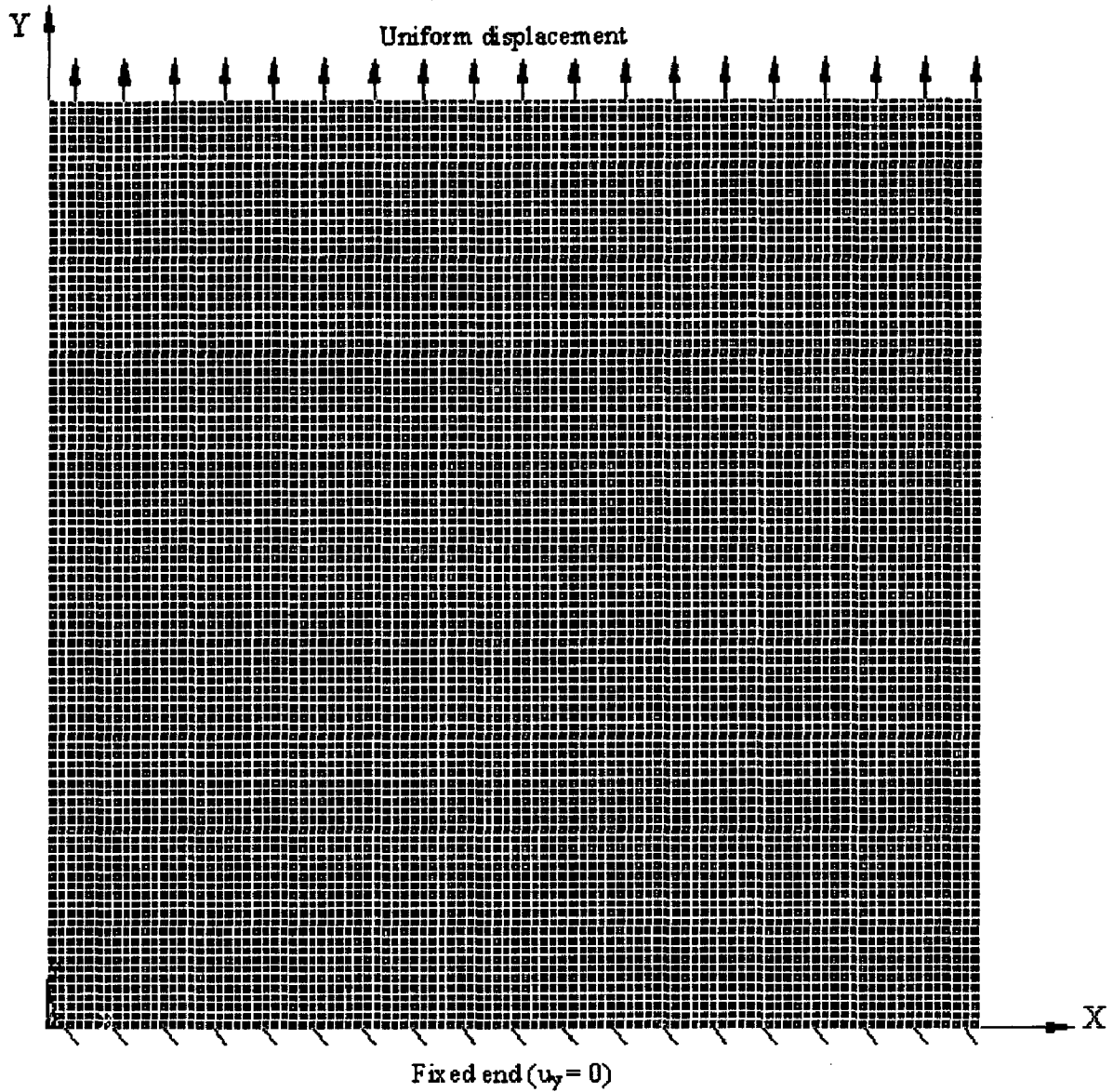**Fig. 4.4** A schematic showing the loading of uniform composite model to find mechanical properties in y-axis direction. Turquoise colour shows aluminium matrix and dark lavender colour shows alumina particles.
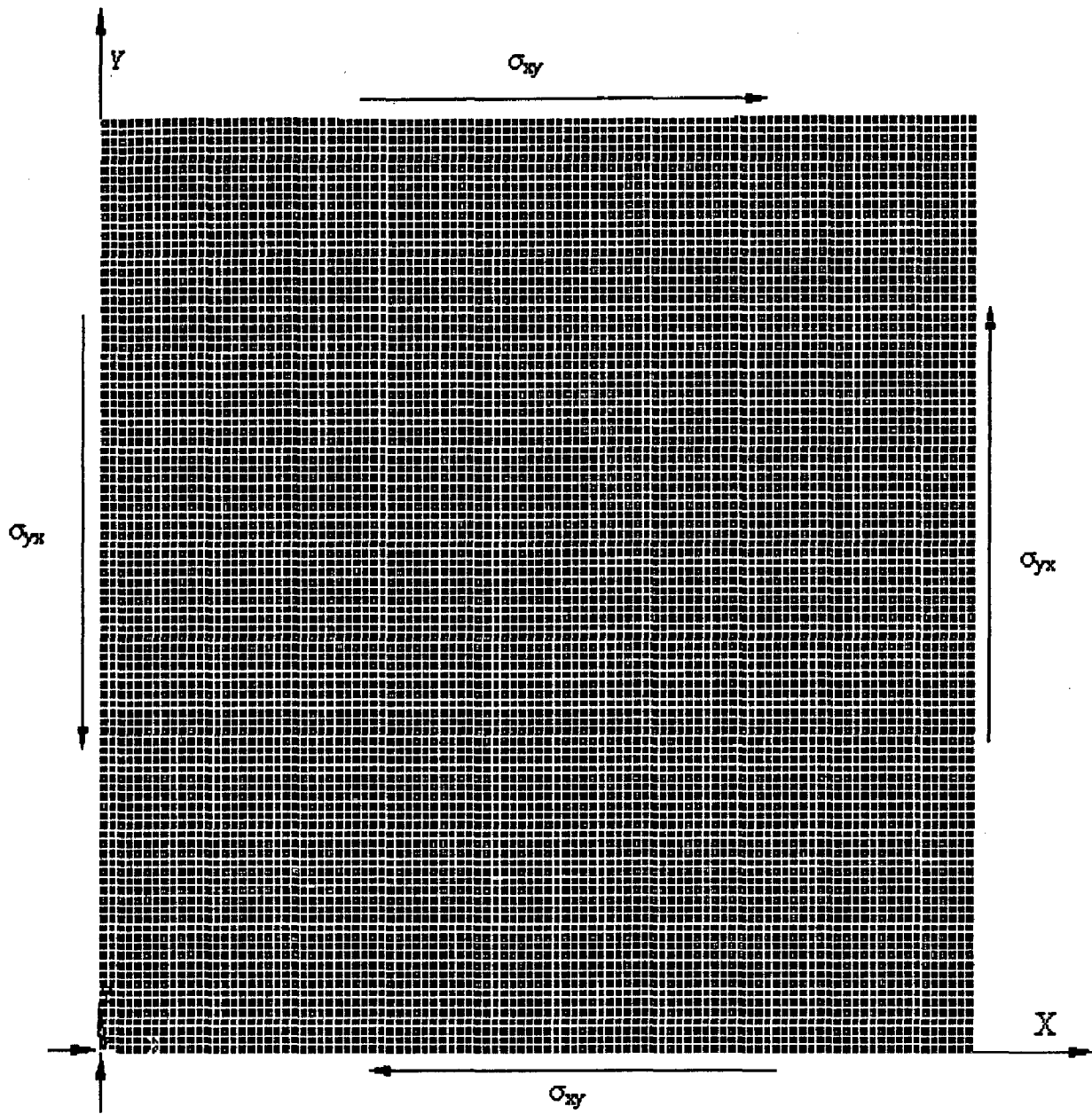
Fig. 4.5 A schematic showing the loading for estimation of modulus of rigidity of the model of a uniform composite. Turquoise colour shows aluminium matrix and dark lavender colour shows alumina particles.

For the application of the shear load as shown by arrows in Fig. 4.5, all the nodes on the particular face are selected and are subjected to uniform shear load.

Uniform composites with different shapes and sizes of particles have also been modelled. The effect of particle shape on the elastic modulus and yield stress of the uniform composites is investigated. For this uniform composite model with 20 vol% average particle content has been modelled. Four different shapes of particles have been investigated for linear and non linear analysis. These particles with different shapes are designated as *1*1*, *1*4*, *2*2* and *4*1*. Particle type *1*4* represents the particle made of four neighbouring elements in y-axis direction. Particle type *4*1* represents the particle made of four neighbouring elements in x-axis direction. Particle type *2*2* represents the four neighbouring elements, two in x-axis direction and two in y-axis direction. For the modelling of particles of shapes *1*4*, *2*2* and *4*1*, first a uniform composite model has been obtained with 5 vol% average particle content with particles of shape *1*1*, distributed randomly over the whole model. After this the neighbouring three other elements of a particle property element are also assigned as particle property according to the final shape of the particle required.

4.3.2 Modelling for Porosities

For the modelling of porosities in composites, the square area with an edge length of 5 mm as previously considered is taken. This area is meshed with plane42, four node elements with an edge length of 50 μm. Thus the whole model consists of 10000 elements. Out of these elements $10000 * V_{fp}$ (V_{fp} is the volume fraction of the porosity) are randomly selected with the help of a FORTRAN program and are removed from the element list. Again $10000(1-V_{fp}) * V_f$ elements are randomly selected from the list of the remaining elements with the help of a FORTRAN program (V_f is the particle volume fraction in the composite) and are assigned particle property. The remaining elements are assigned the matrix material property. The particle property elements are randomly distributed in the matrix for the different models of composites with porosity.

A composite model with 10 vol% average particle content and 2.5 vol% average porosity content is shown in Fig. 4.6. To find the modulus of elasticity in a particular direction the model is kept fixed at one end in that direction. The other end is subjected to

uniform normal displacement. The modulus of elasticity in that direction is obtained from the relation of average elemental stress and strains in that direction as already discussed for uniform composites. Models with 2.5, 5.0 and 7.5 vol% porosity contents are obtained containing different average particle contents. The nonlinear behaviour of the composite models with porosity is found in a manner similar to the one adopted for uniform composites without porosity. The yield stresses of the composites with three different porosity contents, containing different average particle contents have been obtained.

Porosities of different shape and sizes have also been modelled in the present work to find the effect of porosity type on the properties of composites as well as on the FGMs. Four different types of pores (represented by *1*1*, *1*4*, *2*2* and *4*1* in the present work) have been investigated. Porosity type *1*1* represents the pore introduced by the removal of 1 element, *1*4* represents the pore represented by removal of four adjacent elements in the y-axis direction, *2*2* represents the pore introduced by the removal of four adjacent elements in the area of two in y-axis direction and two in x-axis direction and *4*1* represents pore introduced by removal of four adjacent elements in x- axis direction.

To create the porosity of type *1*1* for any given porosity volume fraction V_{fp}, $10000 * V_{fp}$ elements are removed randomly from the model with the help of a FORTRAN program. To create the porosity of type *1*4* for any given porosity volume fraction V_{fp}, in the first step $(10000 * V_{fp})/4$ element are removed from the element list randomly with even distribution over the entire model with the help of FORTRAN program. In the second step three other adjacent elements are also removed from the element list to create porosity type of *1*4*. Similarly the porosities of type *2*2* and *4*1* are created. Porosities are created before creating particles in a composite model. Composite models with four different types of porosities (*1*1*, *1*4*, *2*2*, *4*1*) with porosity contents of 2.5, 5.0 and 7.5 vol% for each type of porosity and average particle content of 30 vol% have been taken to establish the effect of the type of porosity on the mechanical properties of the uniform composites with porosity. The elastic as well as nonlinear properties in y-axis direction of the uniform composites with different types of porosities have been obtained.
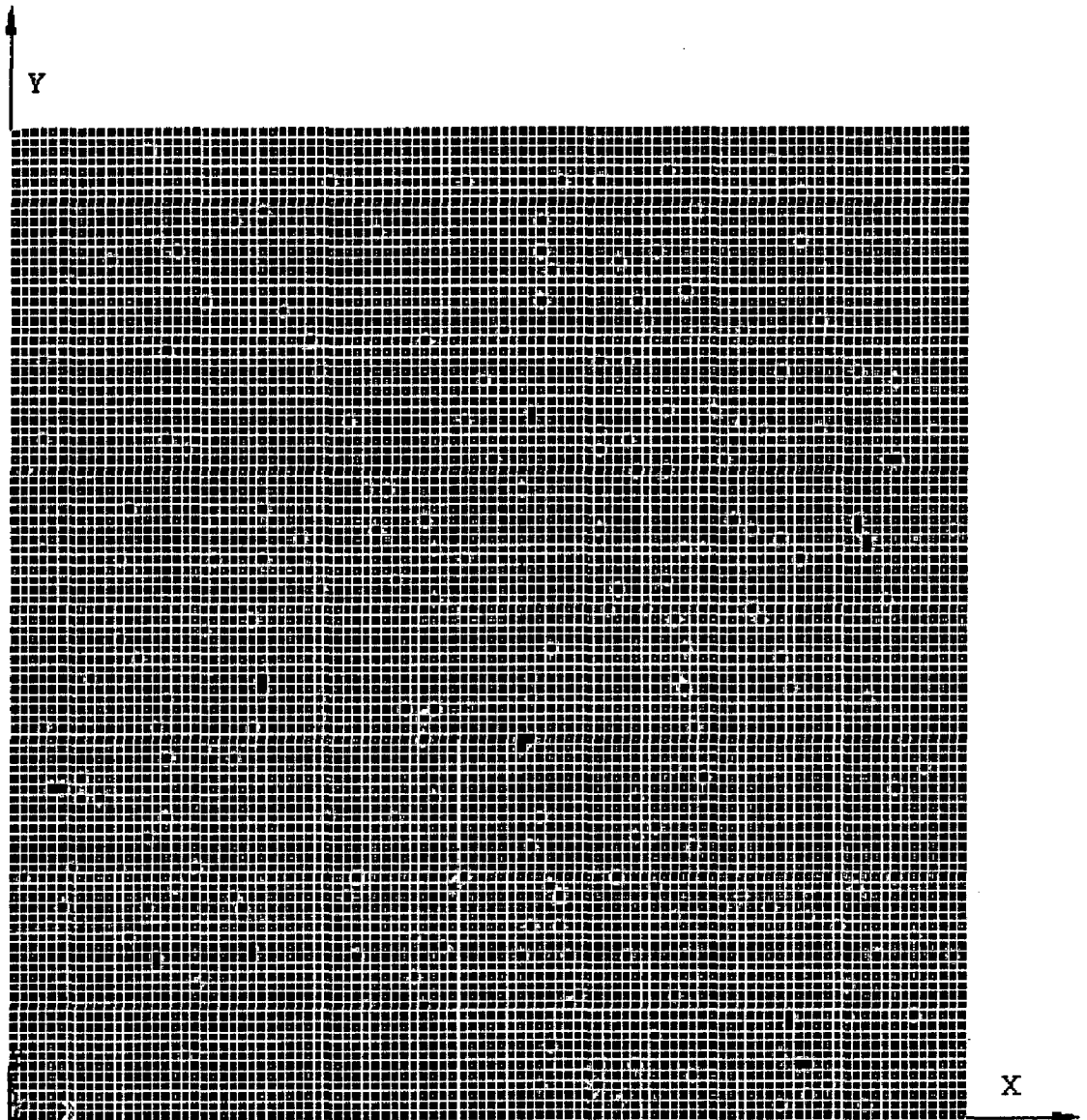
Fig. 4.6 A schematic of the model of uniform composite with randomly distributed particles and pores of 10 and 2.5 vol% respectively. Turquoise colour shows aluminium matrix, dark lavender colour shows alumina particles and black colour shows porosity.

4.3.3 Modelling for Functionally Graded Materials (FGMs)

For modelling the functionally graded materials, again a square area with an edge length 5 mm is considered. This area is meshed with four node plane42 square elements, with an edge length of 50 μm. Thus the whole model consists of 10000 square elements with 50 μm edge length. Out of these elements $10000 * V_f$ elements are randomly selected in a way that the concentration of these elements in the model is as per the gradation of the particles desired. Here, V_f is the average particle volume fraction in the FGM. These selected elements are assigned particle material property and the rest of the elements are assigned the matrix material property.

In the present work a polynomial distribution has been used for modelling the variation in particle concentration in the model. The following equation governs the variation of particle volume fraction in x-axis direction.

$$c(x) = a_1 + (a_2 - a_1)\left(\frac{x}{l}\right)^n \tag{4.39}$$

where

l is the length of the specimen in x-axis direction.

$c(x)$ = local particle content in vol% at a distance x from one end.

a_1 and a_2 are concentration of particles in percentage at $x = 0$ and $x = 1$ respectively.

If the average particle content in the FGM model is p vol% the constant n is given by the equation

$$n = \frac{(a_2 - a_1)}{(p - a_1)} - 1 \tag{4.40}$$

Polynomial variation in particle concentration along both the directions of x-axis and y-axis has been obtained with the help of the following equation

$$c(xy) = a(xy)^n \tag{4.41}$$

with no particles at the corner (0, 0) and similar variation in both x-axis and y-axis directions. With 100% particle concentration at the other corner (l, l) of the square FGM

model with edge length *l*, the equation for particle content at location (x, y) may be simplified as

$$c(xy) = 100 \frac{(xy)^n}{l^{2n}} \qquad (4.42)$$

For an average particle vol% p, the constant n is given by

$$n = \sqrt{\frac{100}{p}} - 1 \qquad (4.43)$$

For modelling a FGM with polynomial distribution of particles, 10000 square elements of size 50 μm x 50 μm are generated as discussed. Corresponding to the location of the element, local volume fraction is obtained using either Eq. 4.39 or Eq. 4.42. Simultaneously a random number between 0 and 1 is generated for each element. If the random number is less than or equal to the local volume fraction at the centroid of the element, then the element is assigned the properties of the reinforcement. Figure 4.7 shows the variation of local vol%, $c(x)$, of particles in x-axis direction from 0% particles at $x = 0$ to 100 % particles at $x = l$ for different average particle contents. Figure 4.8 shows a FGM model with variation in particle content in x-axis direction from 0 vol% of particles at one end to 100 vol% of particles at the other end with an average particle content of 30 vol%. Figure 4.9 shows a FGM model with variation in particle content in both x-axis and y-axis directions but containing an average particle content of 30 vol%.

Models with average particle contents varying between 10 vol% to 90 vol% in steps of 10 vol% have been obtained with the variation of particle content in x-axis direction from 0 vol% at one end to 100 vol% at the other end. Similarly, models for variation of particle content in both the directions have also been obtained with different average particle contents. The global values of the modulus of elasticity in y-axis direction are obtained for the FGMs adopting the similar methodology as explained for uniform composites. To find the global values of modulus of elasticity in x-axis direction the model is kept fixed at one end and the other end is subjected to uniform load by applying uniform displacement. Figure 4.10 shows a FGM model with load arrangement to find the global value of modulus of elasticity in x-axis direction. To find the global value of modulus of elasticity in x-axis direction for the model, the averages of the normal stresses and normal strains in x-axis direction of all the elements are obtained.
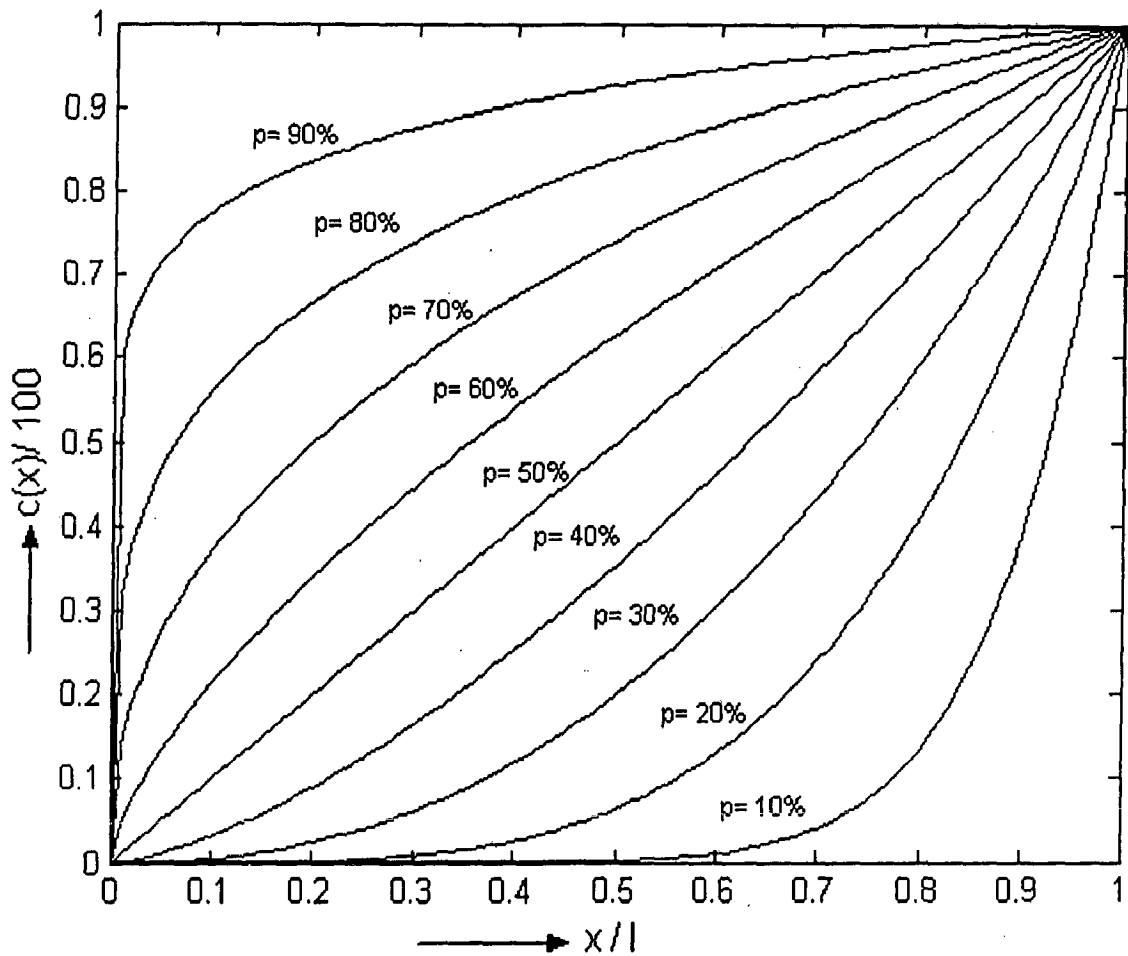
Fig. 4.7 Polynomial variations of local particle content, c(x) in vol %, in x-axis direction from 0 vol% at x = 0 to 100 vol% at x = l for different average particle contents of p vol %.
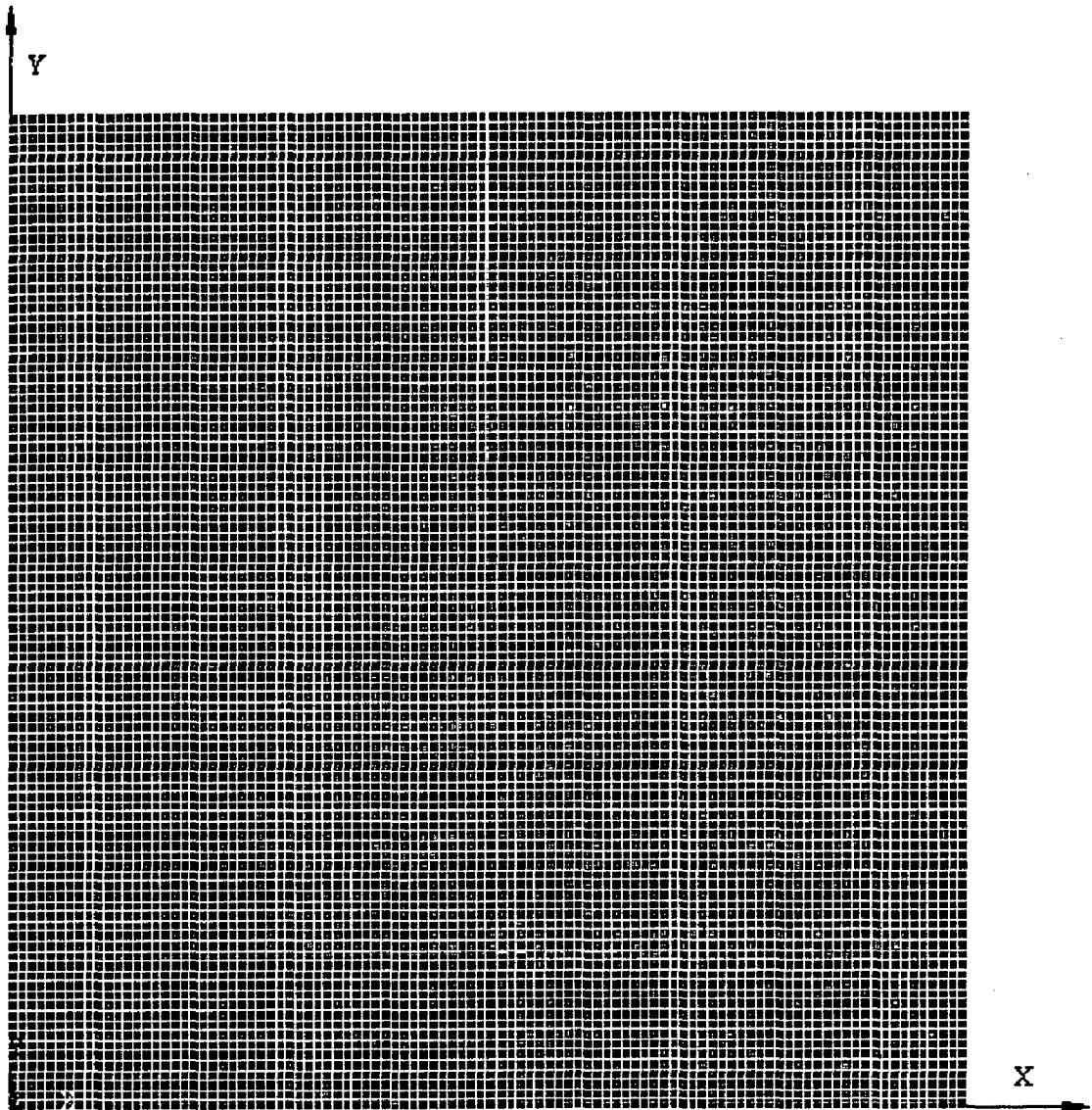
Fig. 4.8 A schematic of FGM model with polynomial variation in particle content in x-axis direction from 0 vol% at one end to 100 vol% at the other end with an average particle content of 30 vol%. Particles are randomly distributed. Turquoise colour shows aluminium matrix and dark lavender colour shows alumina particles.
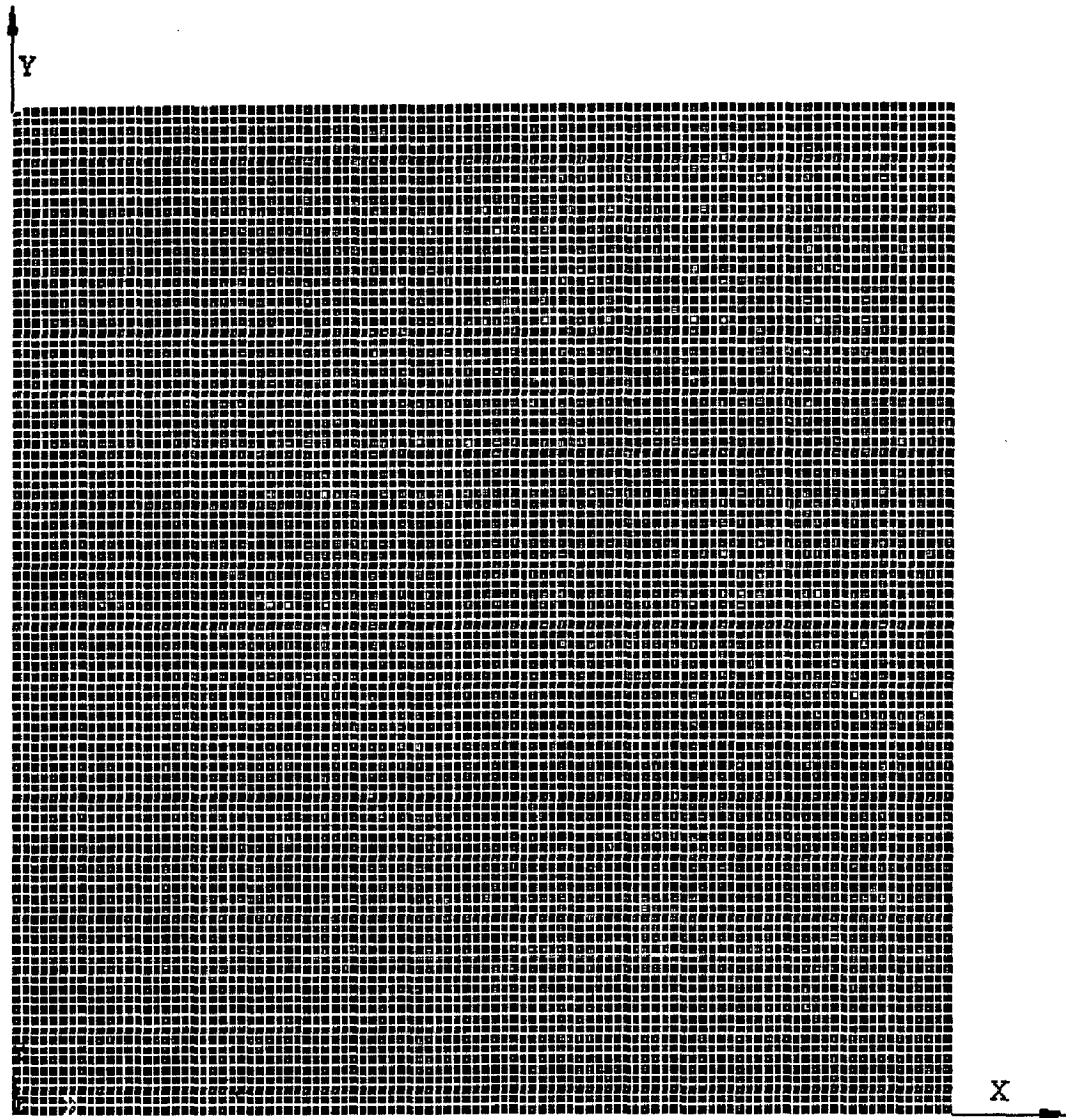
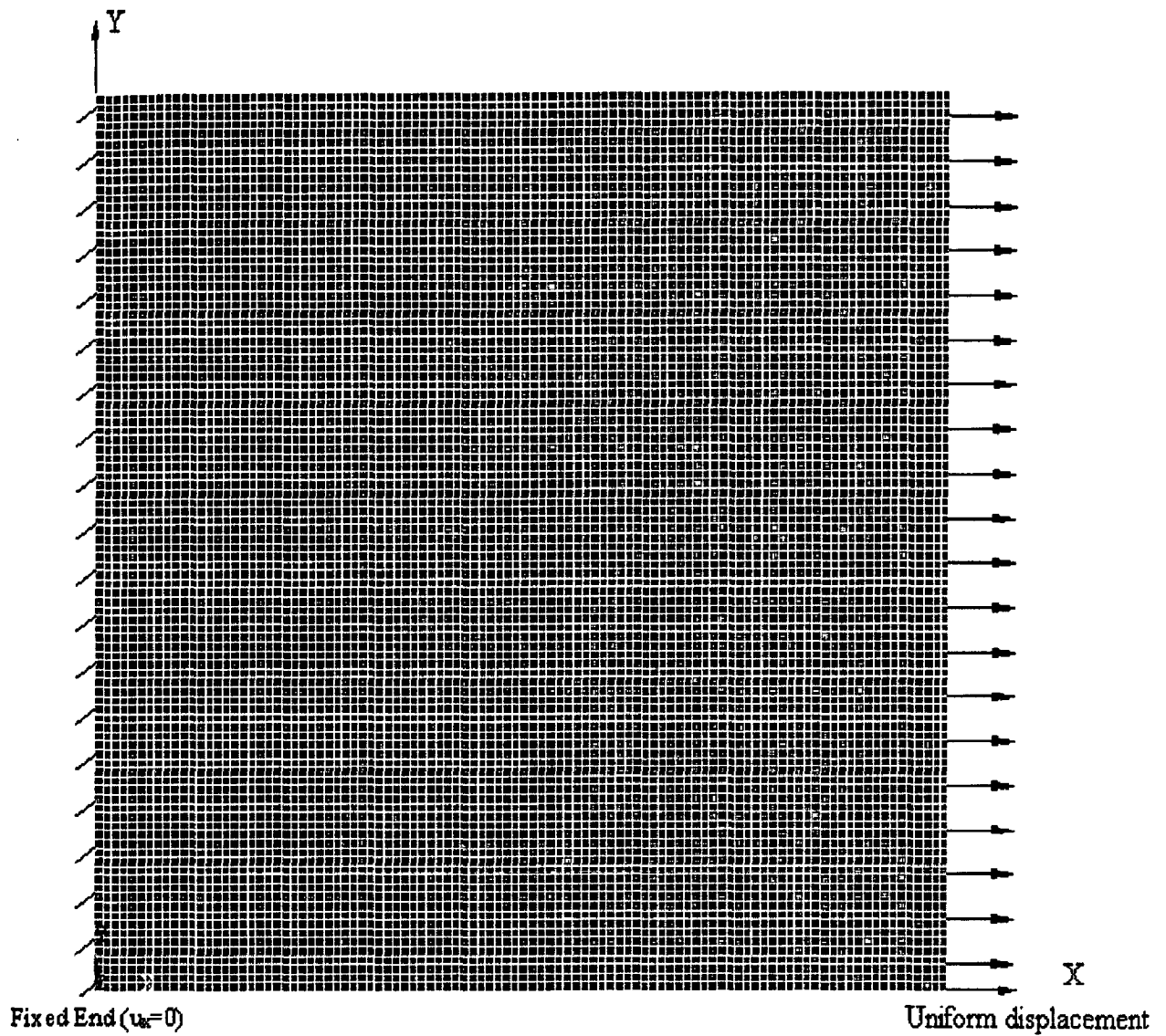**Fig. 4.9** A schematic of FGM model with polynomial variation in particle content in both x-axis and y-axis directions from 0 vol% at one corner (0, 0) to 100 vol% at the other corner (*l, l*) with average particle content of 30 vol%. Particles are randomly distributed over the whole matrix. Turquoise colour shows aluminium matrix and dark lavender colour shows alumina particles.

Fig. 4.10 Schematic of loading of FGM model to find mechanical properties in x-axis direction. Turquoise colour shows aluminium matrix and dark lavender colour shows alumina particles.

The average normal stress σ_{xx} in x-axis direction for the model may be obtained as

$$\sigma_{xx} = \sum_{i=1}^{n} \frac{\sigma_{xxi}}{n} \qquad (4.44)$$

where, σ_{xxi} is the normal stress in x-axis direction for the ith element and n is the total number of elements in the model. The average strain ε_{xx} in x-axis direction for the model is obtained as

$$\varepsilon_{xx} = \sum_{i=1}^{n} \frac{\varepsilon_{xxi}}{n} \qquad (4.45)$$

where, ε_{xxi} is the normal strain in x-axis direction for the ith element and n is the number of elements in the model. The modulus of elasticity in x-axis direction for the model is obtained as the ratio of average stress and average strain for the model in x-axis direction.

$$E = \frac{\sigma_{xx}}{\varepsilon_{xx}} \qquad (4.46)$$

A similar methodology is adopted to estimate the modulus of elasticity in x-axis and y-axis directions for the FGM models with variation in particle contents in both x-axis and y-axis directions.

FGM models with different linear and polynomial variations in particle concentration for constant average particle content have also been obtained. Figure 4.11 shows different polynomial particle concentration variation profiles for FGM models with 30 vol% average particle content. Figure 4.12 shows linear particle concentration variations for FGM models with 30 vol% of average particle content.

Functionally graded materials have continuous variation in the microstructure along a particular direction. This gives a unique feature of continuous variation of the mechanical properties on a local scale. FGMs having different average particle contents with gradation of particles in x-axis direction from 0 vol% of particle concentration at one end to 100 vol% of particle concentration at the other end and having polynomial distribution for variation in particle concentration have been investigated for local variation in the modulus of elasticity. To find the local variation in the modulus of

elasticity inside the FGM model along the gradation direction, the modulus of elasticity is calculated at eleven different locations along the x-axis direction (gradation direction). For this purpose, FGM model is divided in 10 equal parts along the x-axis. To find the values of modulus of elasticity in y-axis direction, the FGM model is kept fixed at y = 0. A uniform normal displacement is applied on the edge y = 5 mm. To determine the modulus of elasticity at a particular location along x-axis, the stresses and strains (y direction component) of all the nodes at a specified x location have been obtained. The average of all the nodal stresses at a particular x location has been taken as the average stress at that location. The average of all the nodal strains at that particular x location is assumed to be the average strain at that location. On the basis of the average stress and average strain at that particular location, the Young's modulus at that particular location has been estimated. The same procedure is repeated for all the eleven locations along the x-axis.

To estimate the global nonlinear behaviour of the FGMs in a particular direction a procedure similar to the one adopted for uniform composites has been used. One end of the model is kept fixed in that direction and on the other end of the model a uniform load is applied by applying a uniform displacement. This load is applied in 20 equal steps. The average elemental stresses and strains for a particular FGM model for each step are plotted in the graphical form. This graph represents the nonlinear deformation behaviour of that particular FGM model. To estimate the yield stress of the FGMs, the crossover method has been used.

4.3.4 Modelling for Thermal Stresses

It is well known that the changes in temperature cause bodies to expand or contract. The change in the length of a uniform bar of length L, when its temperature is raised from T_0 to T, is given by:

$$\Delta L = \alpha \, L (T - T_0)$$
(4.47)

where, α is the coefficient of thermal expansion. If the bar is prevented from expanding in axial direction completely then the average compressive stress induced is given by

$$\sigma = E \left(\frac{\Delta L}{L} \right)$$
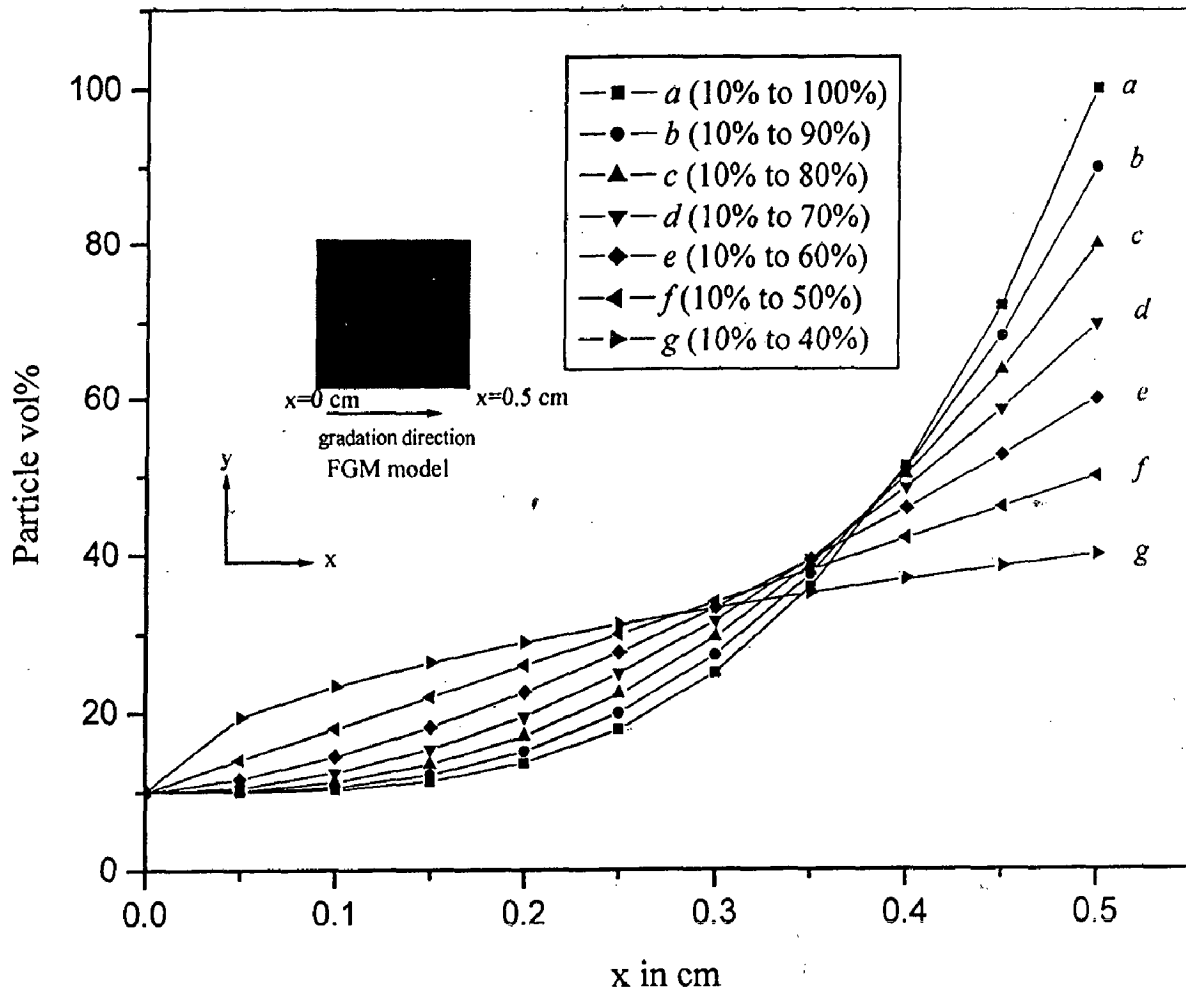(4.48)

where, E is the Young's modulus.

Fig. 4.11 Polynomial variations of particle content in x-axis direction of FGM models from 0 vol% at $x=0$ to different vol% of particles at the boundary $x=l$ but with a fixed average particle content of 30 vol%. Particle gradation is in x-axis direction.
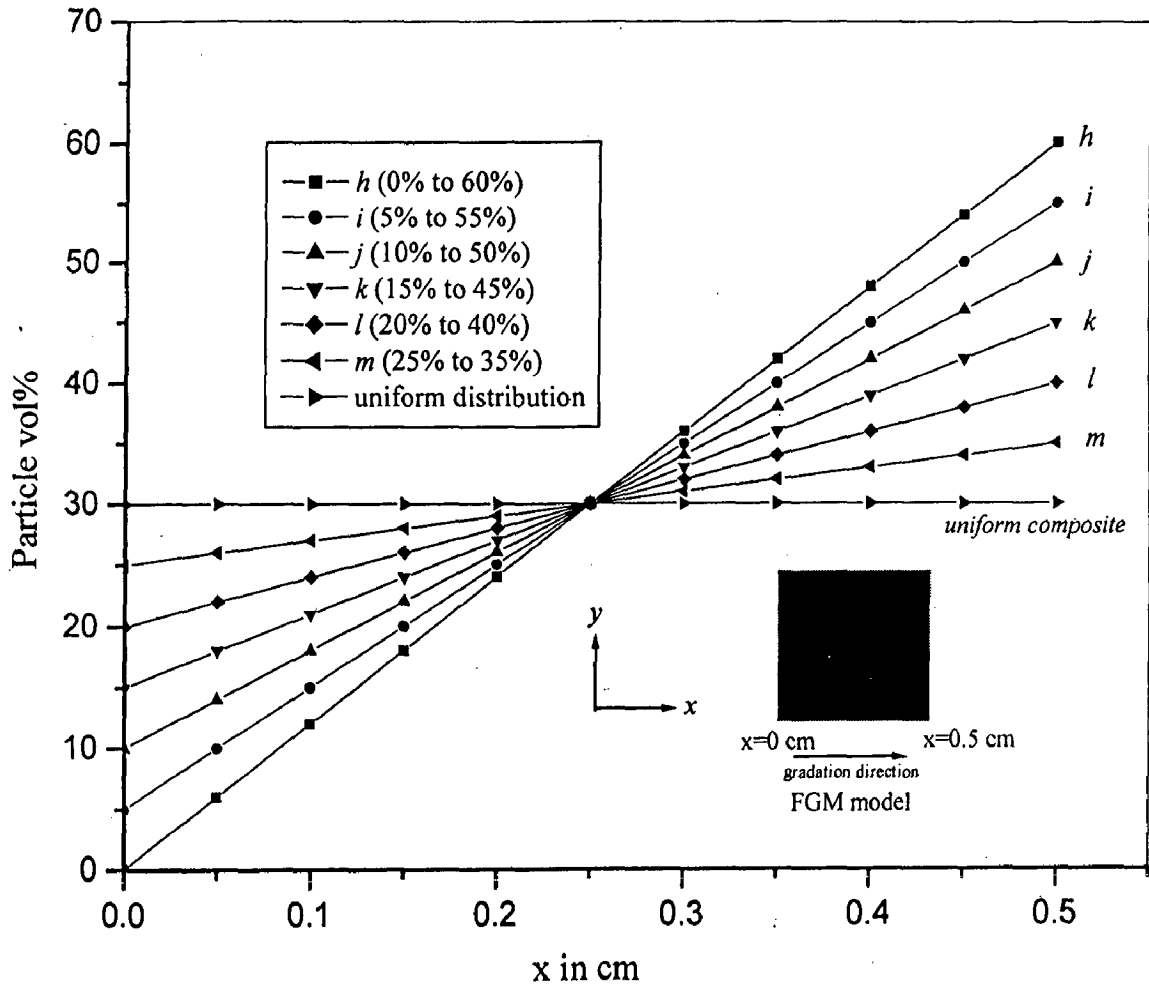
Fig. 4.12 Different types of linear particle variations of FGM models containing an average particle content of 30 vol%. Particle gradation is in x-axis direction.

For complete restraint, the thermal stress is given by

$$\sigma = -\alpha E (T - T_0) \qquad (4.49)$$

where, the negative sign indicates the compressive nature of the stress. If the expansion is prevented only partially, then the stress induced is given by

$$\sigma = -k \alpha E (T - T_0) \qquad (4.50)$$

where, k represents a restraint coefficient.

Thermal analysis has been performed on three different combinations of materials for comparison. In the first case, a uniform composite model with 30 vol% average particle content is considered. In the second case, a FGM model with variation in particle content in x-axis direction from 0 vol% of particle concentration at one end to 100 vol% of particle concentration at the other end and having 30 vol% average particle content is considered. In the third case a layered composite model, as shown in Fig. 4.13 is considered. All the models are subjected to thermal boundary conditions as shown for the layered composite model in Fig. 4.13. In the case of FGM model, the alumina face is subjected to hot fluid conditions with convection heat transfer coefficient h_f and fluid temperature T_f.

As already discussed, the most demanding application of FGMs in the future is as a replacement for the ceramic tiles being used as thermal barrier outer layers in the space vehicles. These ceramic tiles are bonded to the metal surfaces with some adhesive. There are chances of delamination of these ceramic tiles at the metal ceramic interface due to mismatch in the metal ceramic properties at the metal ceramic interface. This is the motivation behind selecting the three different configurations mentioned above.

The material properties considered for the thermal analysis are as follows :

Aluminium

Young's modulus of elasticity	:	75 GPa
Thermal expansion coefficient	:	$23.4 \times 10^{-6} \ K^{-1}$
Thermal conductivity	:	$237 \ W \ m^{-1} \ K^{-1}$

Alumina

Young's modulus of elasticity	:	375 GPa
Thermal expansion coefficient	:	8.4×10^{-6} K^{-1}
Thermal conductivity	:	35 W m^{-1} K^{-1}

One face of the models is subjected to constant wall temperature T_w and the other face is subjected to the hot fluid conditions at temperature T_f. The convection heat transfer coefficient between the model and the hot fluid is h_f. The wall temperature and the fluid conditions taken in the present work are as follows.

Fluid temperature $T_f = 1000$ K

Wall temperature $T_w = 300$ K

Convection coefficient $h_f = 600$ W m^{-2} K^{-1}

For applying the uniform thermal load at a given face all the nodes lying on that face are subjected to that thermal load. For the thermal stress analysis, coupled field analysis is used. The sequential method for the coupled field analysis has been used for thermal analysis. The sequential method involves two or more sequential analyses. The thermal analysis and the stress analysis are coupled by applying results from the thermal analysis as loads for the stress analysis. The nodal temperatures from the thermal analysis are applied as "body force" loads in the stress analysis.

Variation in thermal stresses along the x-axis direction is measured for three different material combinations as discussed. To determine the thermal stress at any particular x-axis location, the thermal stress of all the nodes at that particular x-axis location is measured. The average of all the nodal stresses at that particular location is considered as the average thermal stress at that location. It has been assumed that there is no change in the material properties along y-axis and hence the stresses are assumed to be constant along the y-axis direction.
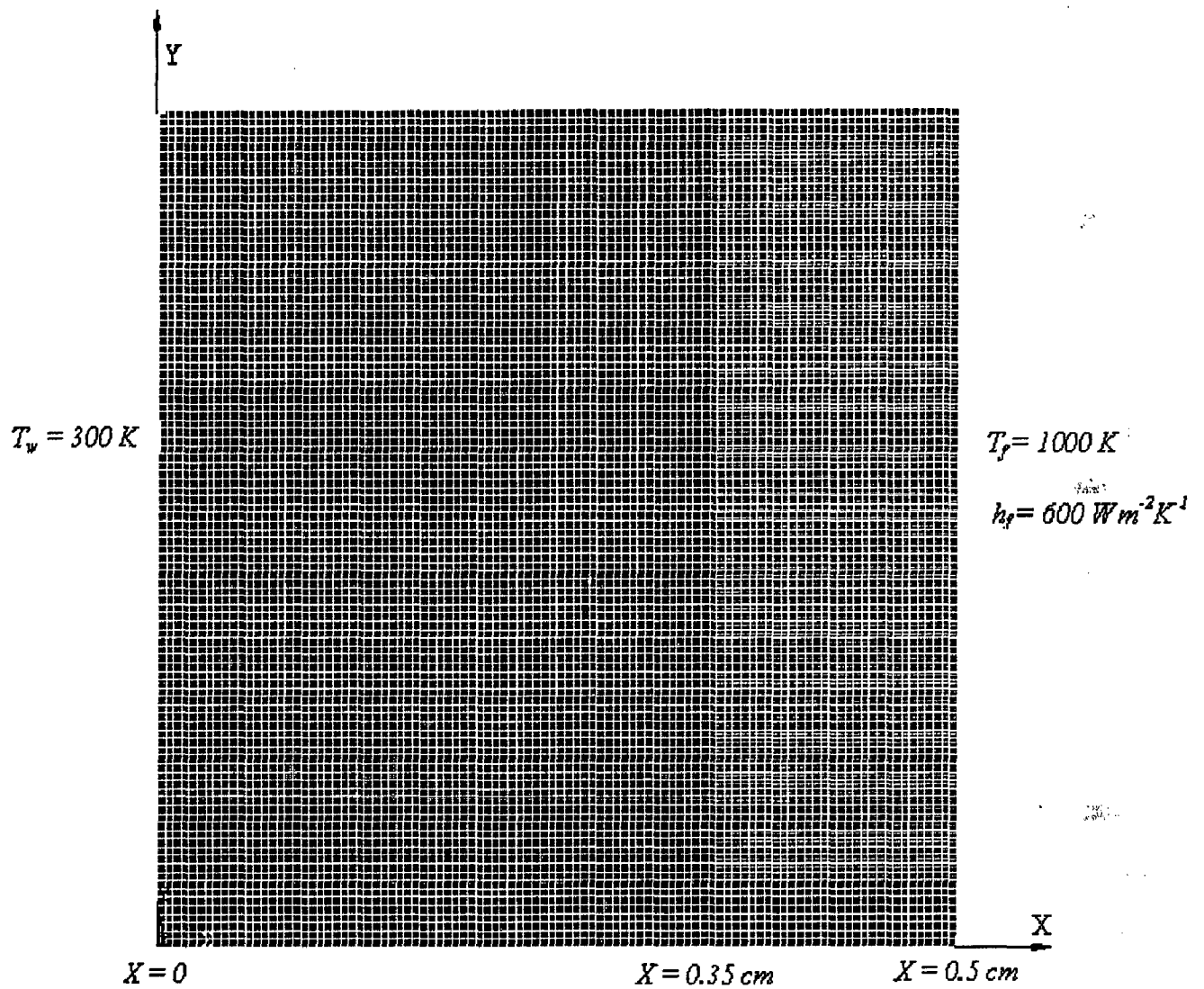
Fig. 4.13 A schematic showing model of a layered composite with thermal boundary conditions. Turquoise colour shows aluminium matrix and dark lavender colour shows alumina.

RESULTS AND DISCUSSION: EXPERIMENTAL WORK

The chapter outlines the results on the development of Functionally Graded Materials (FGM) synthesized by solidification processing and their characterization with respect to microstructure by optical and scanning electron microscopes and hardness by Vickers hardness test. In the last section, the results have been discussed.

5.1 MICROSTRUCTURE CHARACTERIZATION

The optical micrographs at different positions in the cast cylindrical FGM ingots and the graphical plots of variation of alumina content corresponding to optical micrographs across the section of the ingots at a given height have been shown in Figs. 5.1 to 5.36. Samples taken for the present investigation have radius of approximately 3.8 cm and height of 2.5 cm. The volume fraction of alumina particles has been estimated with the help of Dewinter software for determining the volume fraction of a phase.

Figures 5.1 (a) to (h) show the optical micrographs at magnification of 65X taken on the horizontal surface of the ingot along the radial distance from the centre to the outer radius just below the shrinkage cavity of $10Al/Al_2O_3$ FGM with overall alumina content 10 wt% of aluminium. The micrographs clearly reveal the presence of more alumina particles along with porosity at the centre and it decreases gradually from centre to the outer radius. Optical micrographs clearly show dark spherical particles of alumina of similar size as those added (see Fig.3.1), distributed in the aluminium matrix. The porosity also appears black and so, cannot be distinguished separately from the dark particles. The micrographs close to the outer radius, as shown in Fig. 5.1(h), reveals the absence of large alumina particles and there are fine dark spots which could either be fine alumina particles or pinhole porosities. Figure 5.2 shows the graphical plot of the variation of combined alumina and porosity content as revealed by the dark areas in the micrographs, with

increasing distance from the centre towards the outer radius of cast $10Al/Al_2O_3$ FGM ingot, just below the shrinkage cavity. Figure shows that the average volume fraction of combined alumina particles and porosity gradually decreases from the centre towards the outer radius.

Similarly, Figs. 5.3 to 5.11 show the optical micrographs at a magnification of 65X, depicting the radial variation of alumina content and porosity in the cast $10Al/Al_2O_3$ FGM ingot, followed by the graphical plots of the variation of alumina content with increasing distance from the centre towards the outer radius for each horizontal section, respectively at heights of 0.5 cm, 1.0 cm, 1.5 cm, 2.0 cm and 2.5 cm below the bottom of shrinkage cavity. The figures show that the combined alumina and porosity content decreases gradually as one moves from the centre towards the outer radius of the ingot at all the sections at different heights investigated. It may be noted that at a given radial distance, relatively higher volume fractions of alumina particles are observed at higher heights from the bottom of the ingot as shown in Fig. 5.12. The figure also reveals that a larger zone free of particle and porosity at the outer radius results when one moves from the top to the bottom of the cast ingot.

Figures 5.13 to 5.24 show the optical micrographs depicting the radial variation of alumina content in the cast $15Al/Al_2O_3$ FGM ingot, followed by the graphical plots of the variation of alumina content with increasing distance from the centre towards the outer radius for each section of micrographs, at different heights of 0 cm, 0.5 cm, 1.0 cm, 1.5 cm, 2.0 cm and 2.5 cm below the shrinkage cavity respectively, at a magnification of 50X. The micrographs clearly show decreasing amount of combined alumina particles and porosity as one moves from the centre to the outer radius at all the sections at different heights investigated here. The highest concentration of alumina and porosity is observed at the centre. It has been observed that the bottom layer of the ingot has a large zone free of particle or porosity. Figure 5.25 shows the combined result of variation of alumina and porosity content at different radial distances as one move from the centre towards the outer radius at different heights of 0 cm, 0.5 cm, 1.0 cm, 1.5 cm, 2.0 cm and 2.5 cm below the

shrinkage cavity. Higher alumina and porosity concentration has been observed at relatively higher heights and the concentration of alumina and porosity decreases from the top to the bottom.

Figures 5.26 to 5.35 reveal the optical micrographs showing the radial variation of alumina and porosity content in cast $20Al/Al_2O_3$ FGM ingot, followed by the graphical plot of the variation of alumina and porosity content with increasing distance from the centre towards the outer radius for sections at different heights of 0 cm, 0.5 cm, 1.0 cm, 1.5 cm and 2.0 cm below the bottom of shrinkage cavity, respectively, at a magnification of 50X. Figure 5.36 shows the graphical plot of the combined result of variation of alumina and porosity content at different radial distances as one moves from centre to the outer radius at different heights of 0 cm, 0.5 cm, 1.0 cm, 1.5 cm and 2.0 cm below the shrinkage cavity. Higher alumina and porosity concentration has been observed at relatively higher heights and the concentration of alumina and porosity decreases from the top to the bottom as obtained in previous ingots.

Comparisons of the variation of alumina and porosity content at different radial distances from the centre to the outer radius at a given distance below the shrinkage cavity of the three cast FGM ingots are shown in Figs. 5.37 to 5.41 respectively. Figure 5.42 shows the variation of the size of the zone free of particle and porosity in the cast ingot with increasing height. As the height decreases towards the bottom of the cast ingot, the size of the region free of particle and porosity increases as shown in Fig. 5.42. The ingot with higher alumina content has relatively smaller size of zone free of particle and porosity at a given height in the cast ingot.

Figures 5.43 to 5.48 show the scanning electron micrographs (SEM) depicting the radial variation of alumina content in the cast $10Al/Al_2O_3$, $15Al/Al_2O_3$, $20Al/Al_2O_3$ FGM ingots at heights of 0 cm and 2.5 cm below the shrinkage cavity, respectively. The SEM micrographs for all the three FGMs reveal good interfacial integrity, with no observable microvoids at the particle matrix interface. Figure 5.49 shows the nature of $Al-Al_2O_3$ interface at higher magnification indicating a reaction zone around the particles.

80
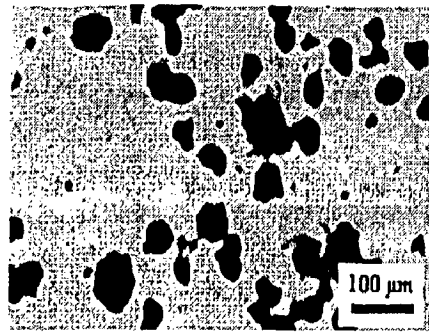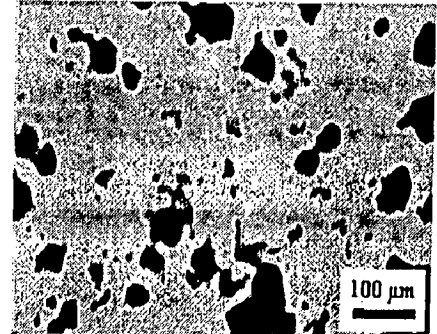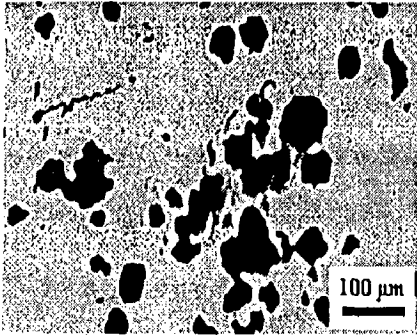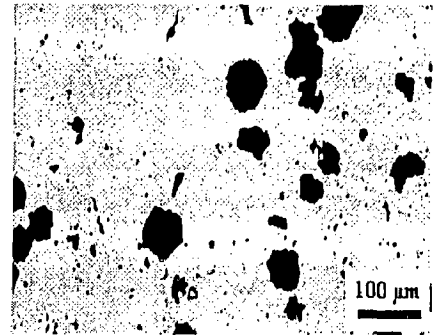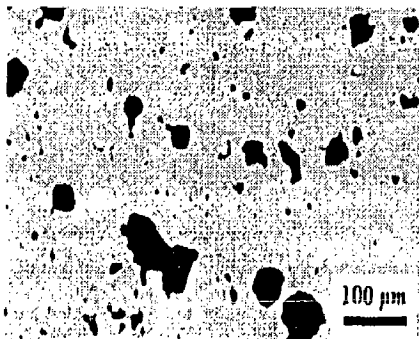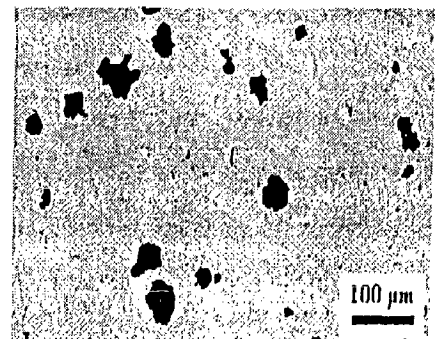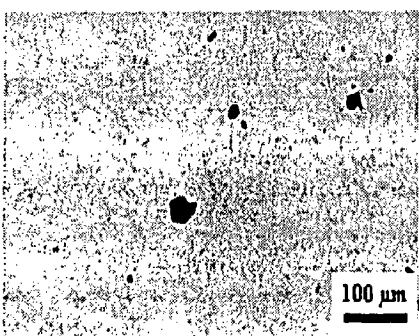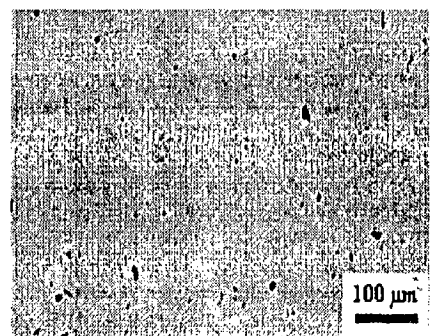
Fig. 5.1 Optical micrographs of $10Al/Al_2O_3$ FGM ingot showing the variation of particle content and porosity along the radial direction from the centre to the outer radius, just below the bottom of shrinkage cavity. The radial distance from the centre is indicated below each micrograph. Magnification: 65X.
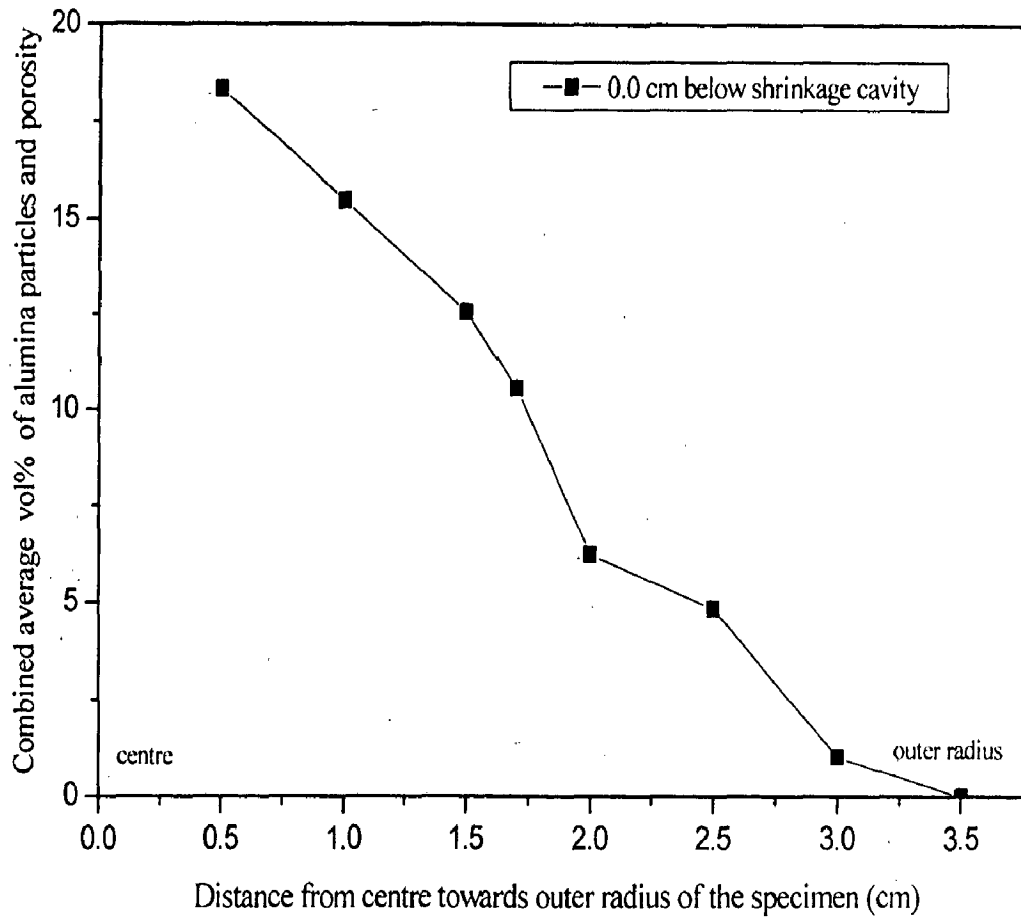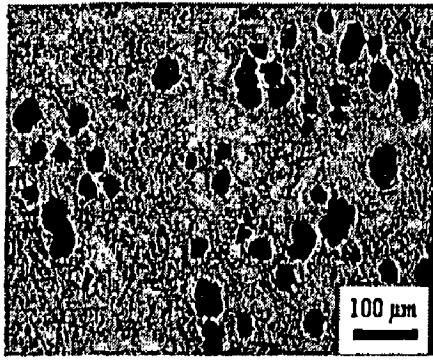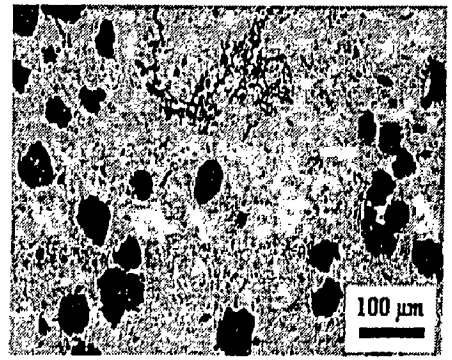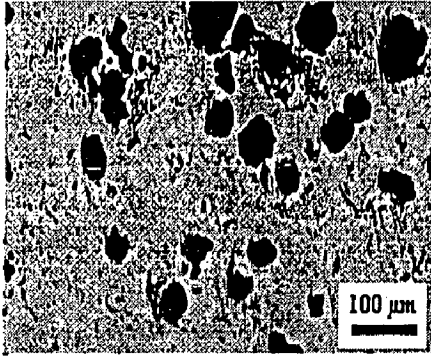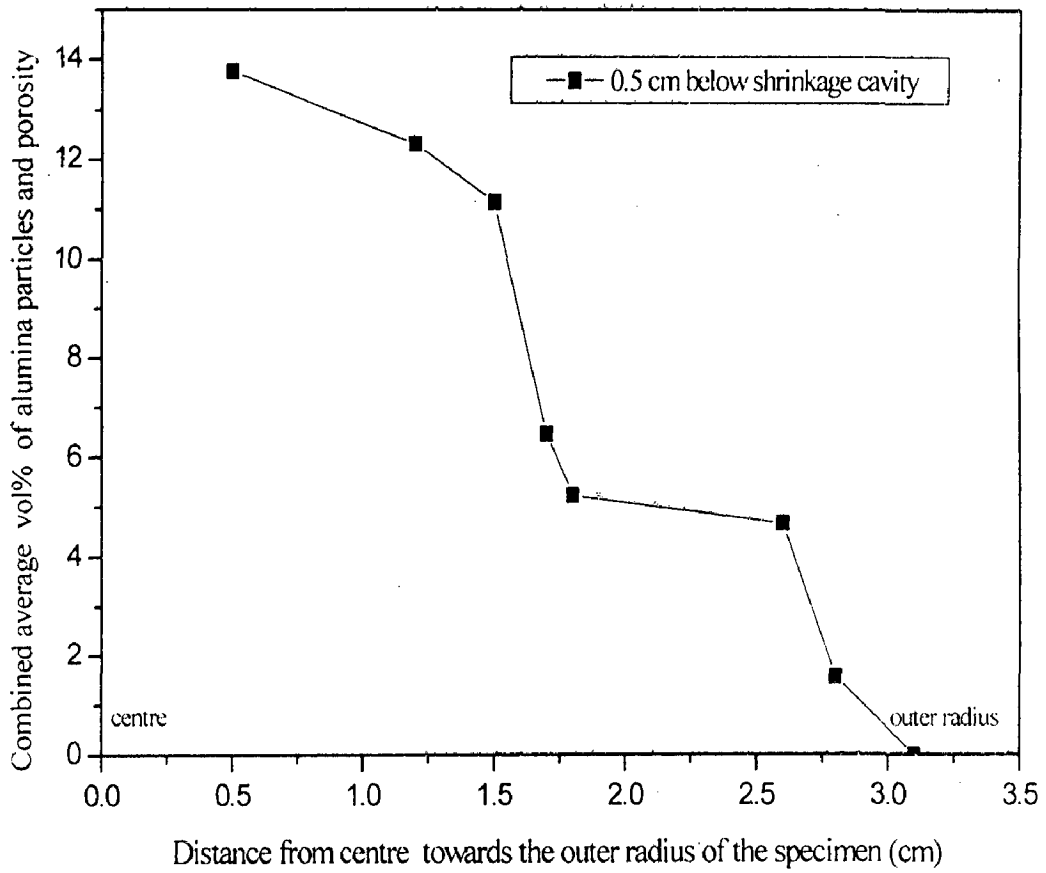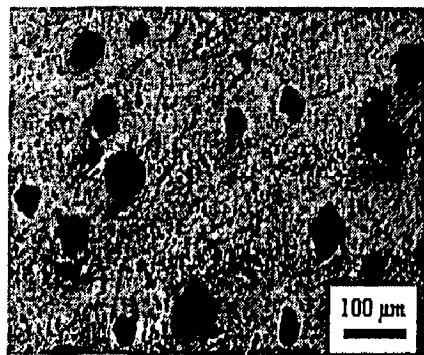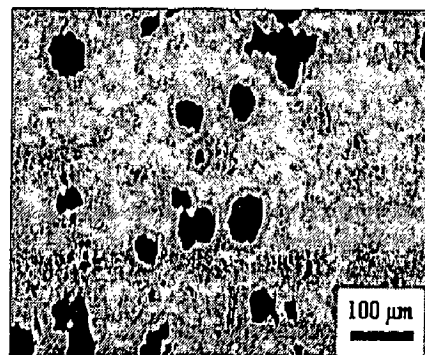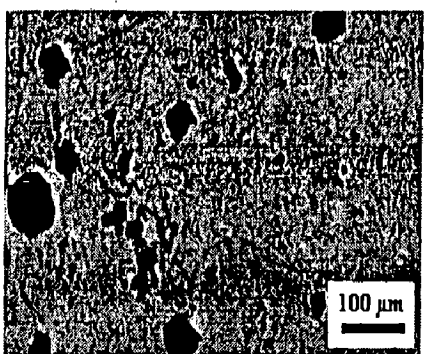
81

Fig. 5.2 The variation of alumina content and porosity with distance from the centre towards the outer radius of the cast $10Al/Al_2O_3$ FGM ingot just below the shrinkage cavity.
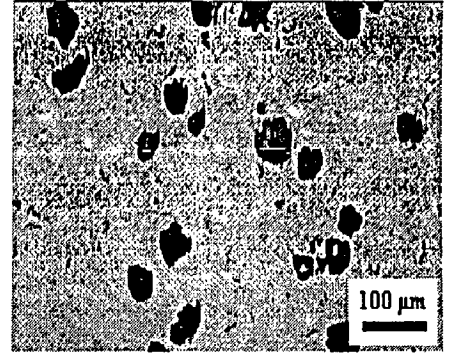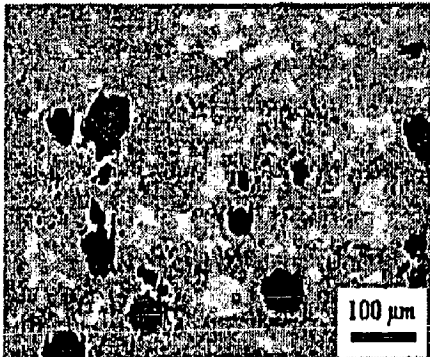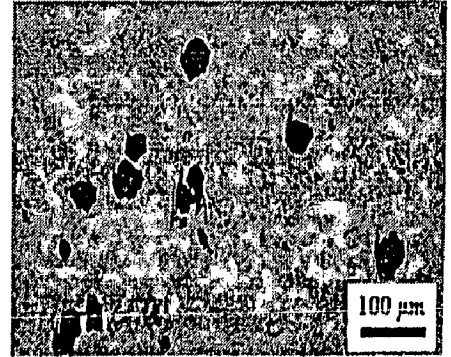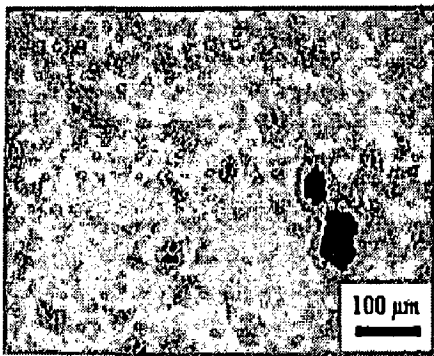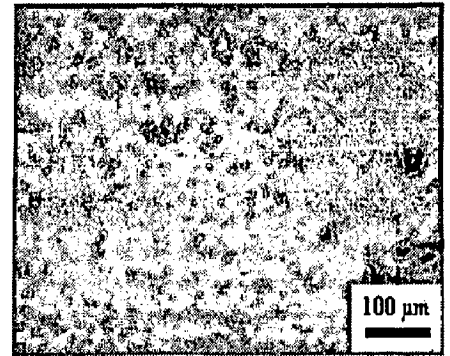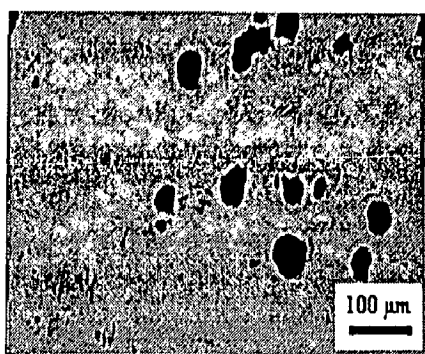
Fig. 5.3 Optical micrographs of 10Al/Al$_2$O$_3$ FGM ingot showing the variation of particle content and porosity along the radial direction from the centre towards the outer radius, 0.5 cm below the shrinkage cavity. The radial distance from the centre is indicated below each micrograph. Magnification: 65X.

Combined average vol% of alumina particles and porosity

14

— ■ — 0.5 cm below shrinkage cavity

12

10

8

6

4

2

centre

outer radius

0

0.0   0.5   1.0   1.5   2.0   2.5   3.0   3.5

Distance from centre towards the outer radius of the specimen (cm)

Fig. 5.4   The variation of alumina content and porosity with distance from centre towards the outer radius of the cast $10Al/Al_2O_3$ FGM ingot at 0.5 cm below the bottom of shrinkage cavity.
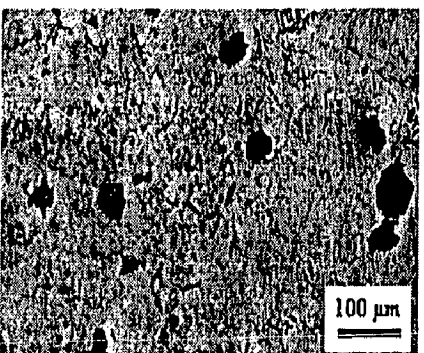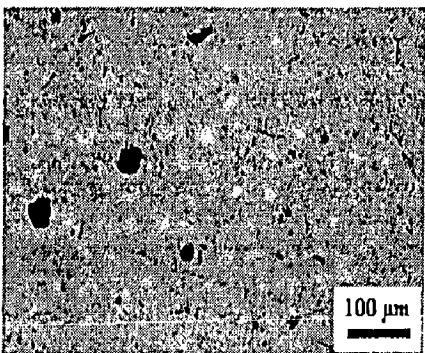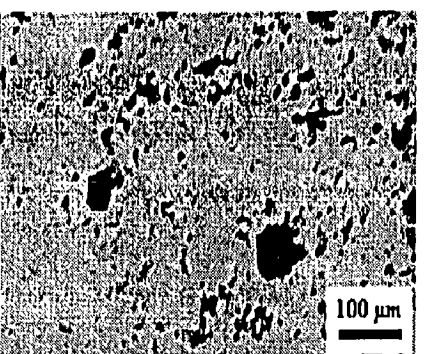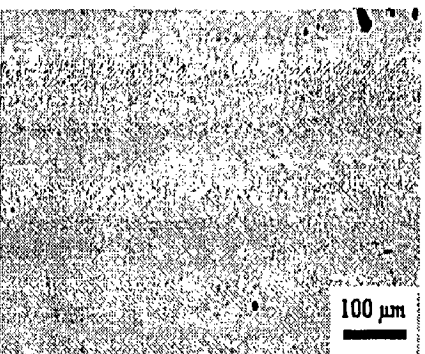
Fig. 5.5 Optical micrographs of 10Al/Al$_2$O$_3$ FGM ingot showing the variation of particle content and porosity along the radial direction from the centre towards the outer radius, 1.0 cm below the bottom of shrinkage cavity. The radial distance from the centre is indicated below each micrograph. Magnification: 65X.
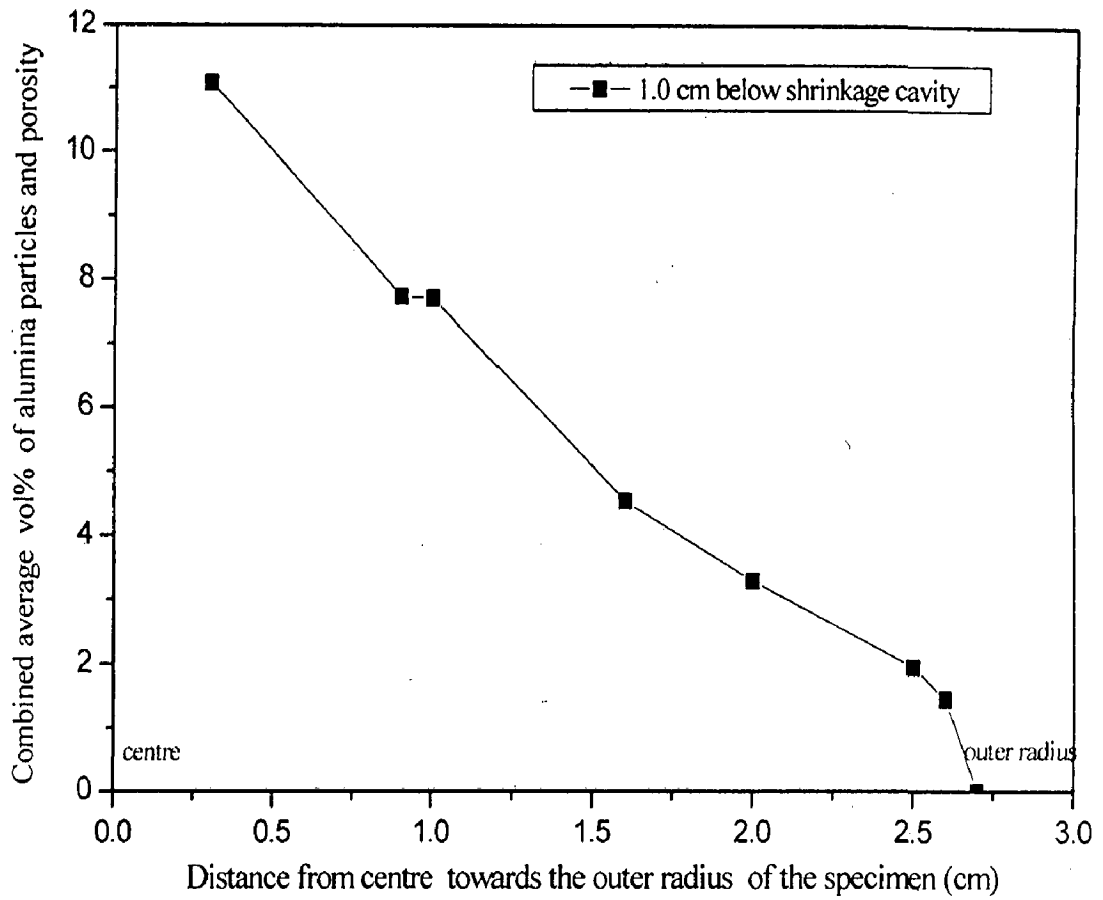
Fig. 5.6 The variation of alumina content and porosity with distance from the centre towards outer radius of the cast $10Al/Al_2O_3$ FGM ingot at 1.0 cm below the bottom of shrinkage cavity.
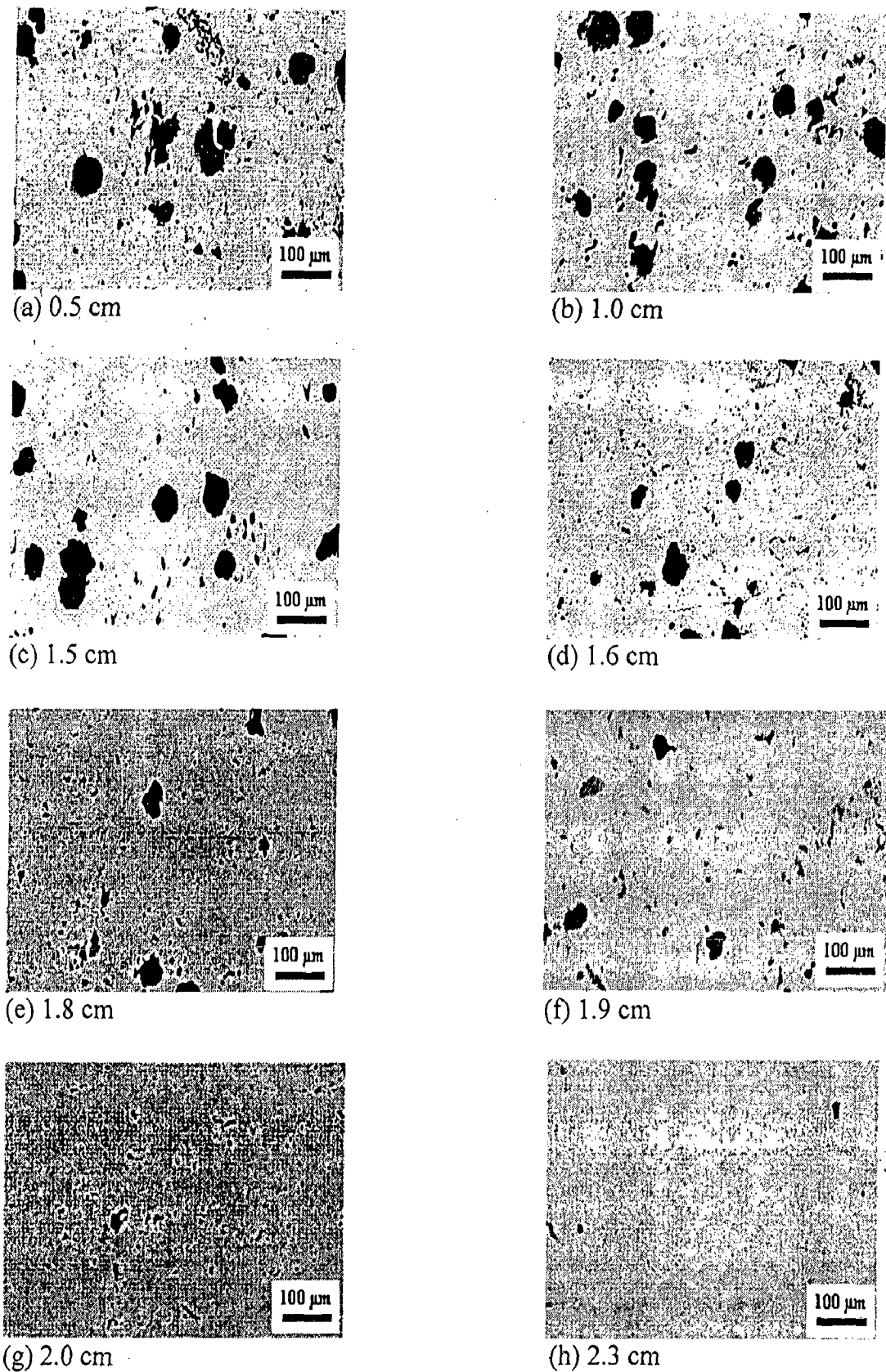
Fig. 5.7 Optical micrographs of 10Al/Al₂O₃ FGM ingot showing the variation of particle content and porosity along the radial direction from the centre towards the outer radius, 1.5 cm below the bottom of shrinkage cavity. The radial distance from the centre is indicated below each micrograph. Magnification: 65X.
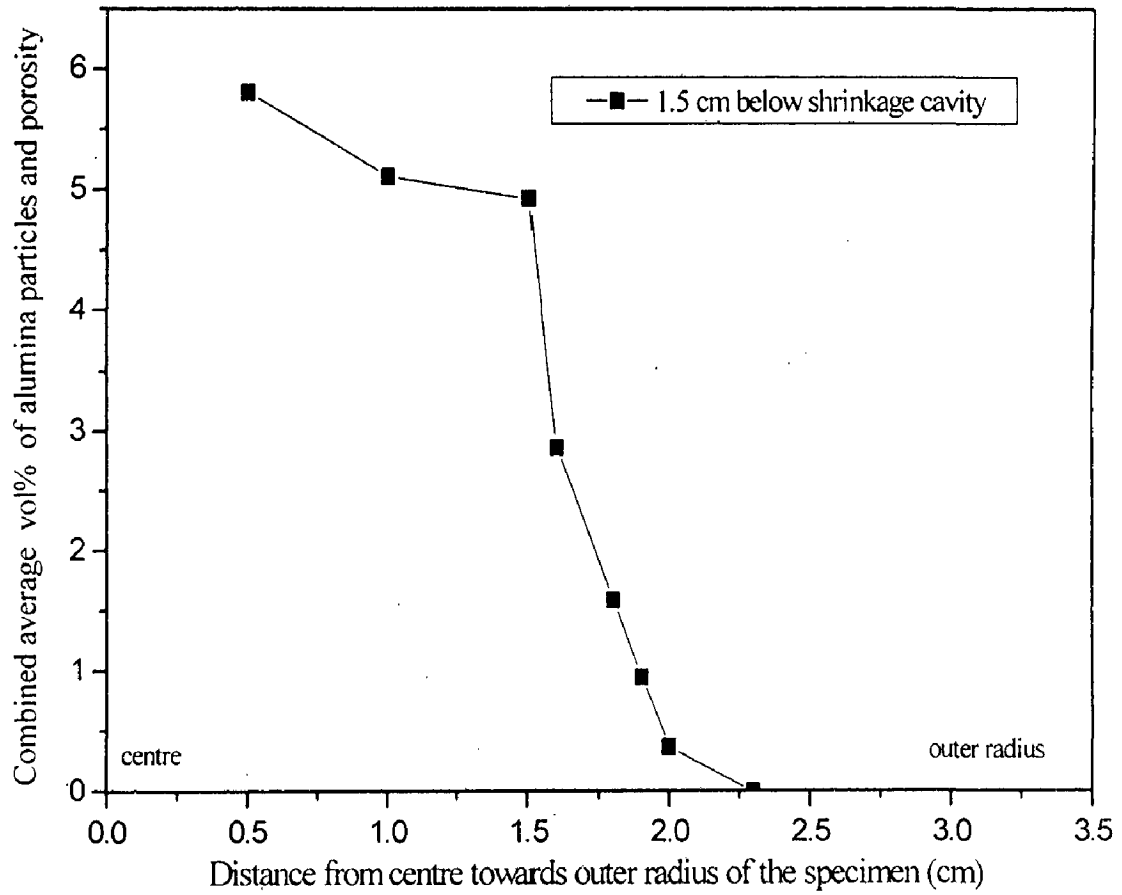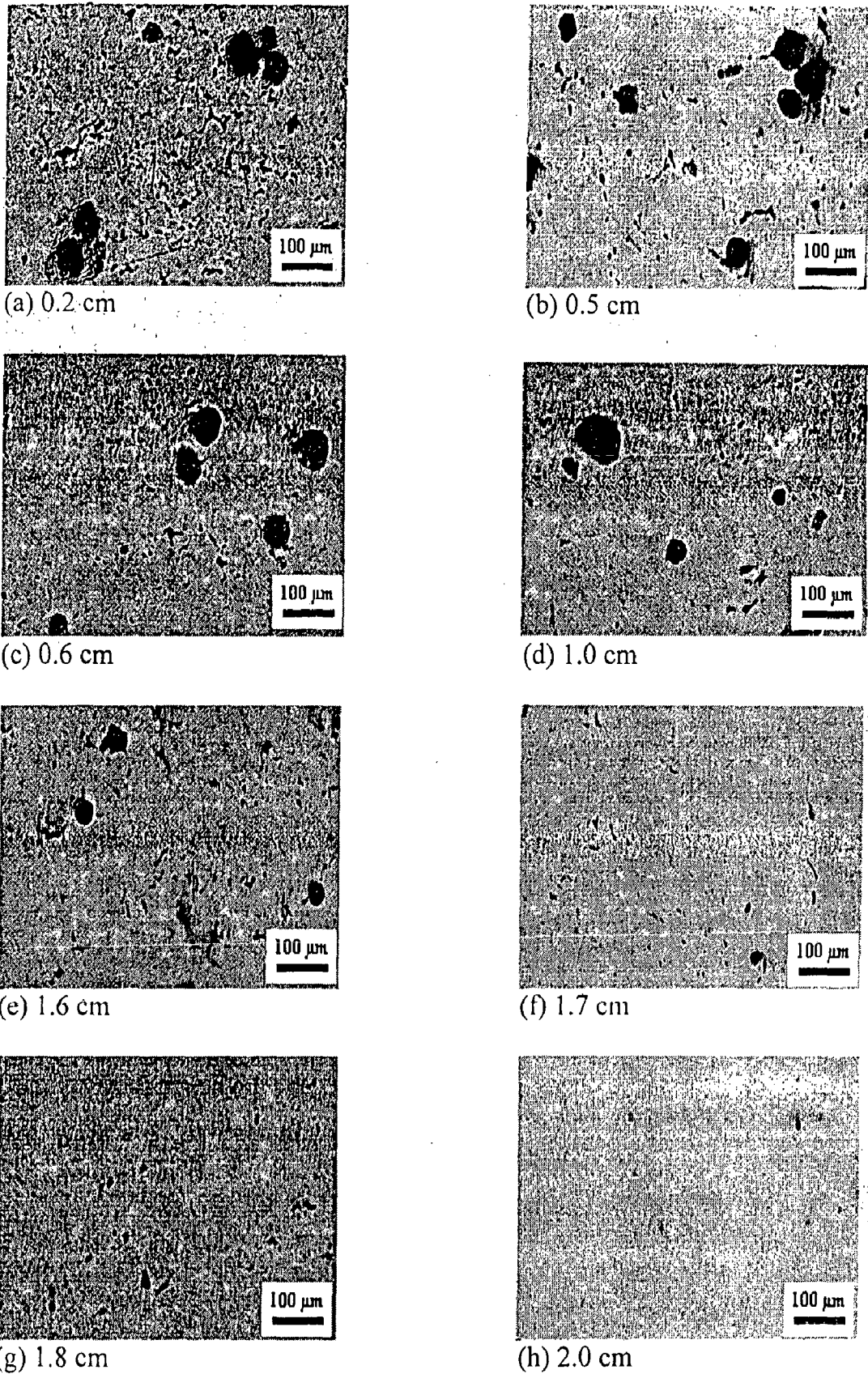
87

Fig. 5.8   The variation of alumina content and porosity with distance from the centre towards the outer radius of the cast $10Al/Al_2O_3$ FGM ingot at 1.5 cm below the bottom of shrinkage cavity.

(a) 0.2 cm

(b) 0.5 cm

(c) 0.6 cm

(d) 1.0 cm

(e) 1.6 cm

(f) 1.7 cm

(g) 1.8 cm

(h) 2.0 cm

Fig. 5.9 Optical micrographs of 10Al/Al$_2$O$_3$ FGM ingot showing the variation of particle content and porosity along the radial direction from the centre towards the outer radius, 2.0 cm below the bottom of shrinkage cavity. The radial distance from the centre is indicated below each micrograph. Magnification: 65X.
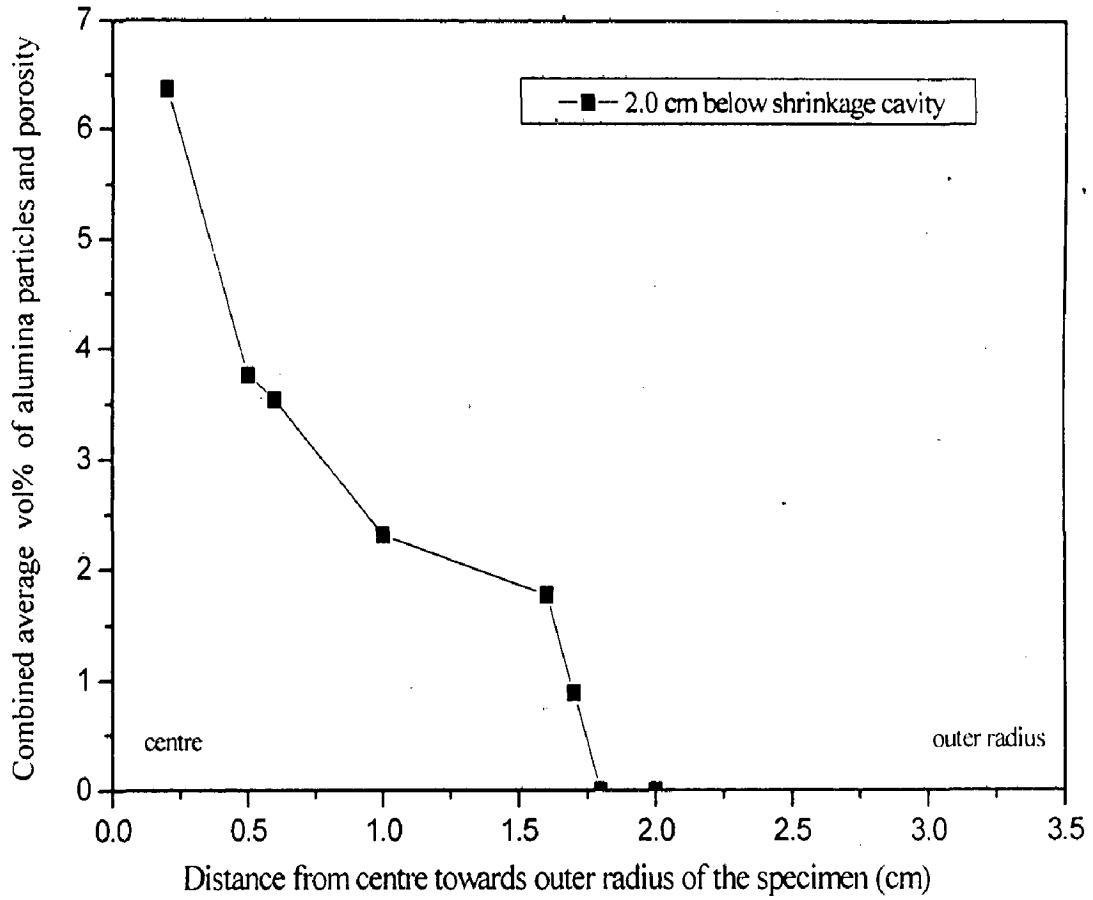
Fig. 5.10 The variation of alumina content and porosity with distance from the centre towards the outer radius of the cast $10Al/Al_2O_3$ FGM ingot at 2.0 cm below the bottom of shrinkage cavity.

(a) 0.2 cm   (b) 0.5 cm

Fig. 5.11 Optical micrographs of 10Al/Al₂O₃ FGM ingot showing the variation of particle content and porosity along the radial direction from the centre towards the outer radius, 2.5 cm below the bottom of shrinkage cavity. The radial distance from the center is indicated below each micrograph. Magnification: 65X.
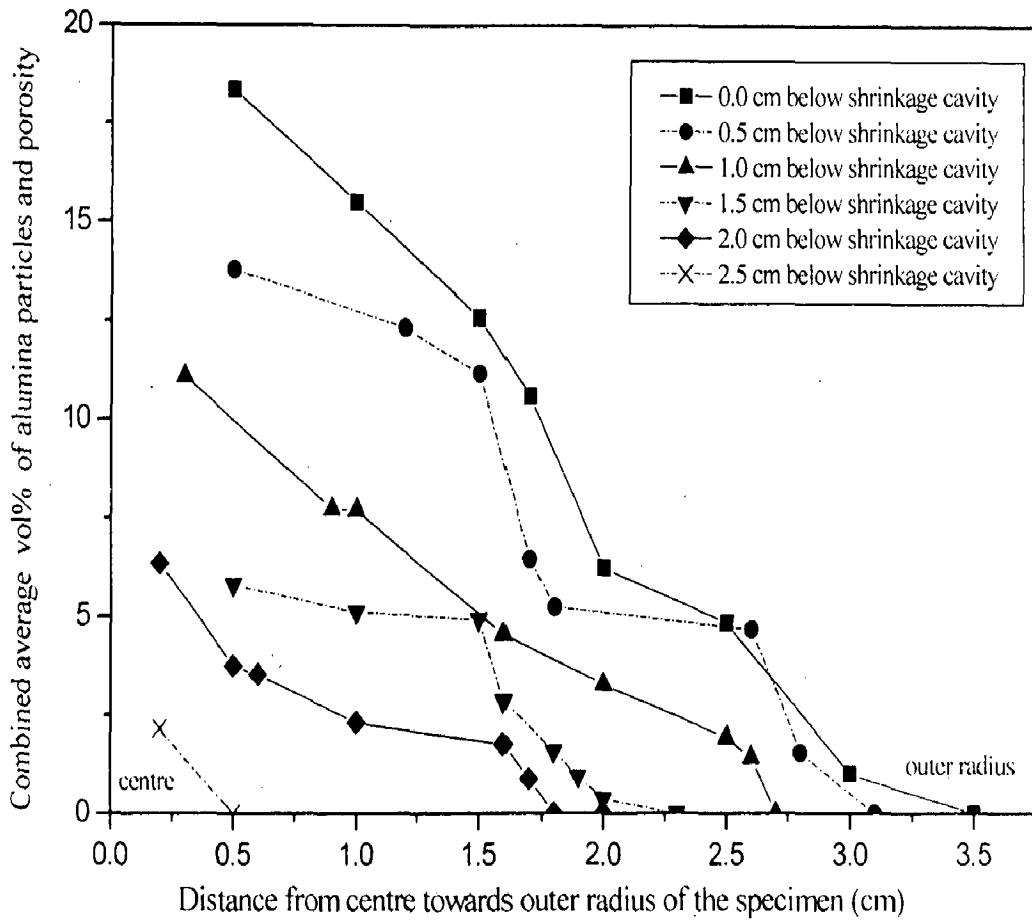

Fig. 5.12 The variation of alumina content and porosity at different radial distances from the centre towards the outer radius at different heights below the shrinkage cavity of cast 10Al/Al₂O₃ FGM ingot.
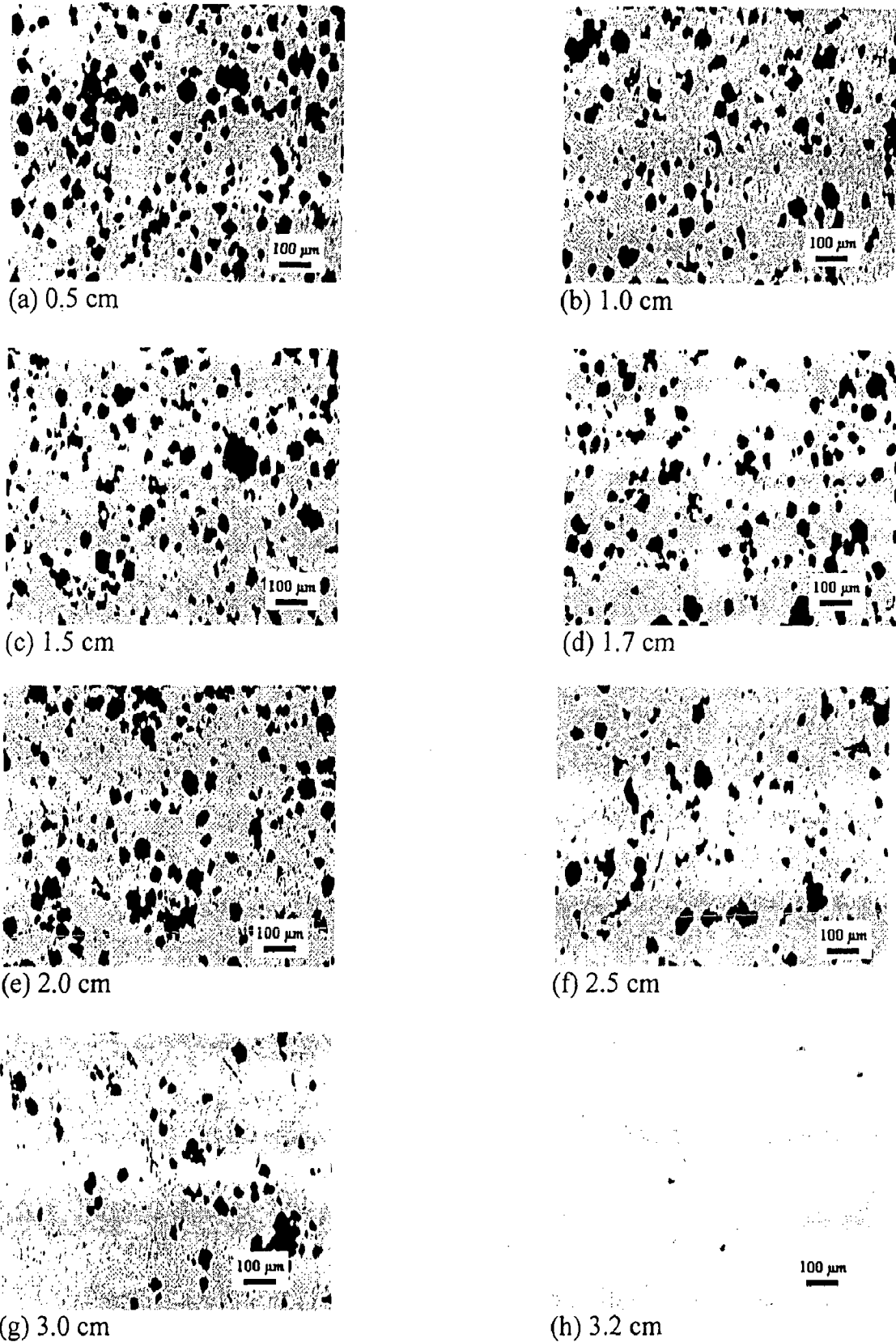
91

Fig. 5.13 Optical micrographs of 15Al/Al$_2$O$_3$ FGM ingot showing the variation of particle content and porosity along the radial direction from the centre towards the outer radius, 0 cm below the bottom of shrinkage cavity. The radial distance from the centre is indicated below each micrograph. Magnification: 50X.
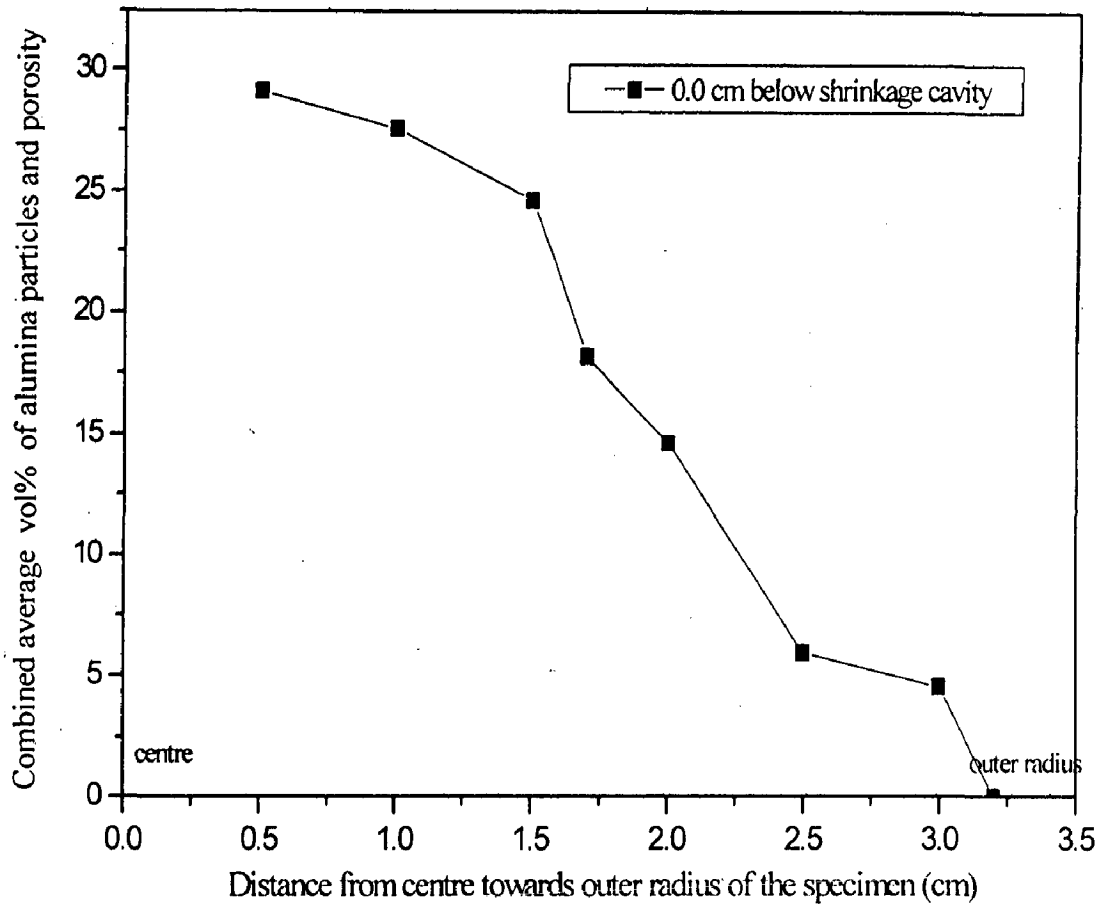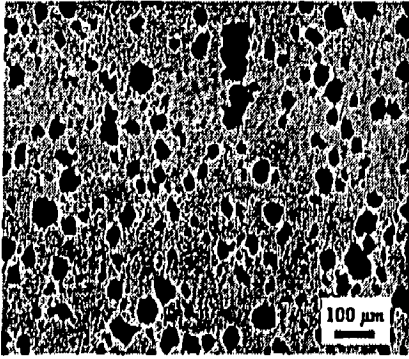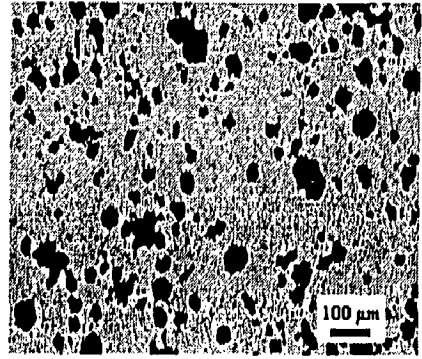
Fig. 5.14 The variation of alumina content and porosity with distance from the centre towards the outer radius of the cast 15Al/Al₂O₃ FGM ingot at 0 cm below the bottom of shrinkage cavity.

(a) 0.5 cm

(b) 0.9 cm

(c) 1.0 cm

(d) 1.2 cm

(e) 1.5 cm

(f) 1.7 cm

(g) 1.8 cm

(h) 2.0 cm

Fig. 5.15 Optical micrographs of 15Al/Al₂O₃ FGM ingot showing the variation of particle content and porosity along the radial direction from the centre towards the outer radius, 0.5 cm below the bottom of shrinkage cavity. The radial distance from the center is indicated below each micrograph. Magnification: 50X.
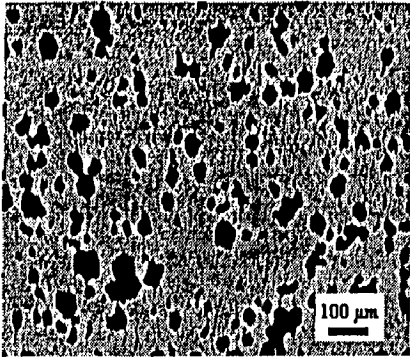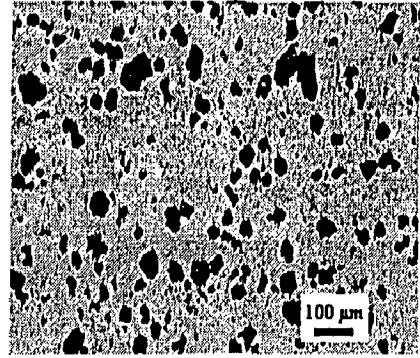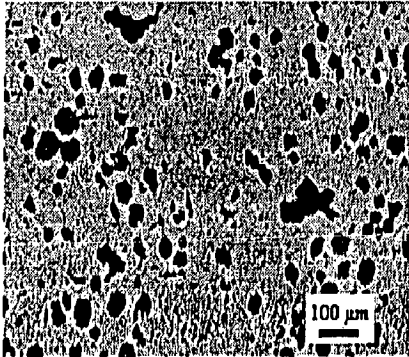
(i) 2.2 cm

(j) 2.6 cm

(k) 2.8 cm

(l) 3.1 cm

Fig. 5.16 The variation of alumina content and porosity with distance from the centre towards the outer radius of the cast 15Al/Al₂O₃ FGM ingot at 0.5 cm below the bottom of shrinkage cavity.
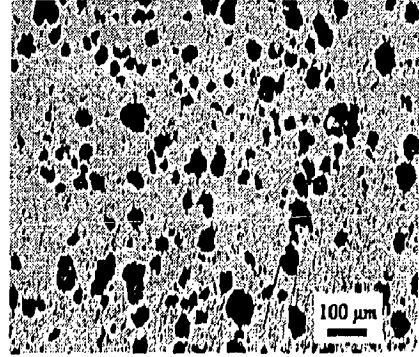
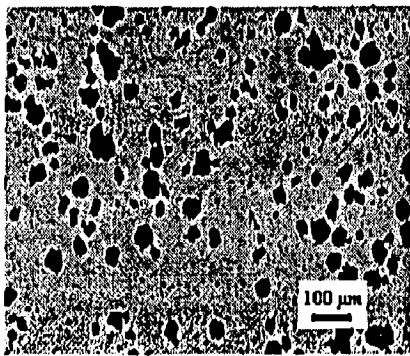(a) 0.3 cm

(b) 0.9 cm

(c) 1.0 cm

(d) 1.5 cm

(e) 1.7 cm

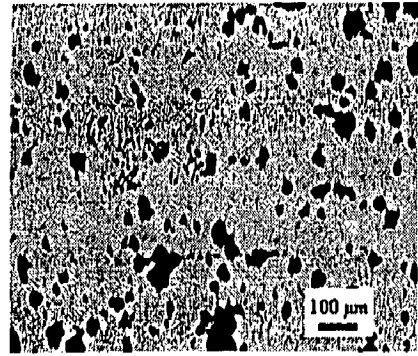(f) 2.2 cm

(g) 2.3 cm

(h) 2.6 cm

(i) 2.7 cm   (j) 3.0 cm

Fig. 5.17 Optical micrographs of $15Al/Al_2O_3$ FGM ingot showing the variation of particle content and porosity along the radial direction from the centre towards the outer radius, 1.0 cm below the bottom of shrinkage cavity. The radial distance from the center is indicated below each micrograph. Magnification: 50X.

Distance from centre towards outer radius of the specimen (cm)

Fig. 5.18 The variation of alumina content and porosity with distance from the centre towards the outer radius of the cast $15Al/Al_2O_3$ FGM ingot at 1.0 cm below the bottom of shrinkage cavity.
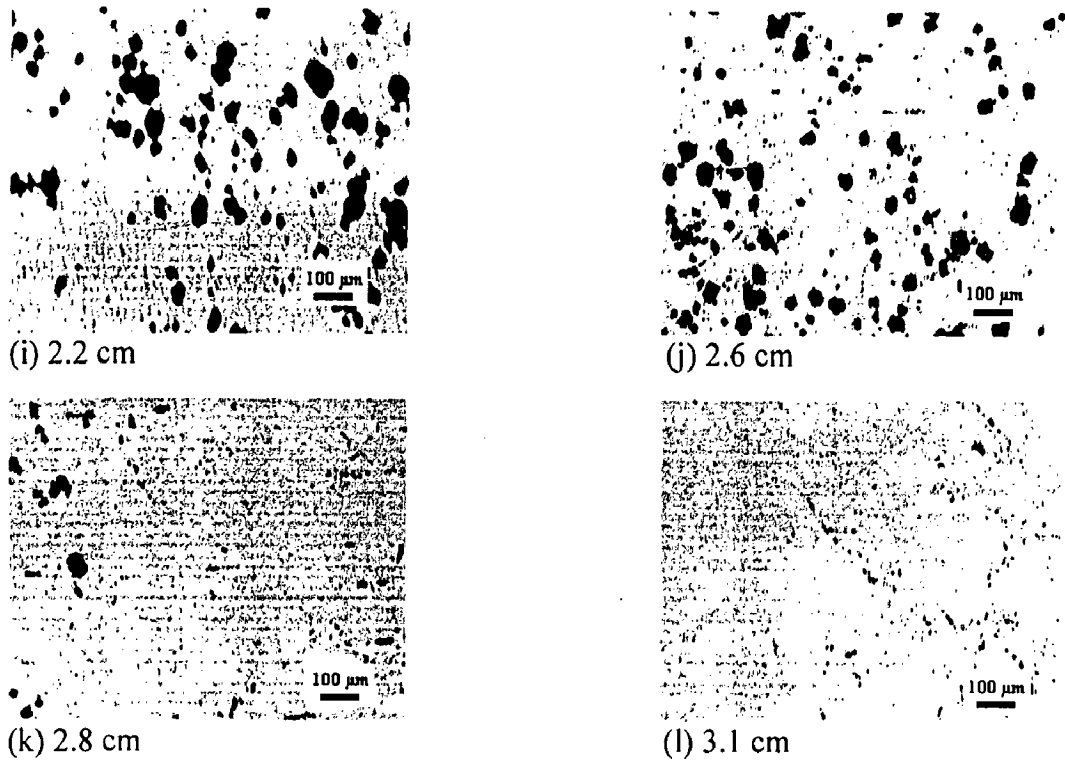
97

Fig. 5.19 Optical micrographs of 15Al/Al₂O₃ FGM ingot showing the variation of particle content and porosity along the radial direction from the centre towards the outer radius, 1.5 cm below the bottom of shrinkage cavity. The radial distance from the centre is indicated below each micrograph. Magnification: 50X.
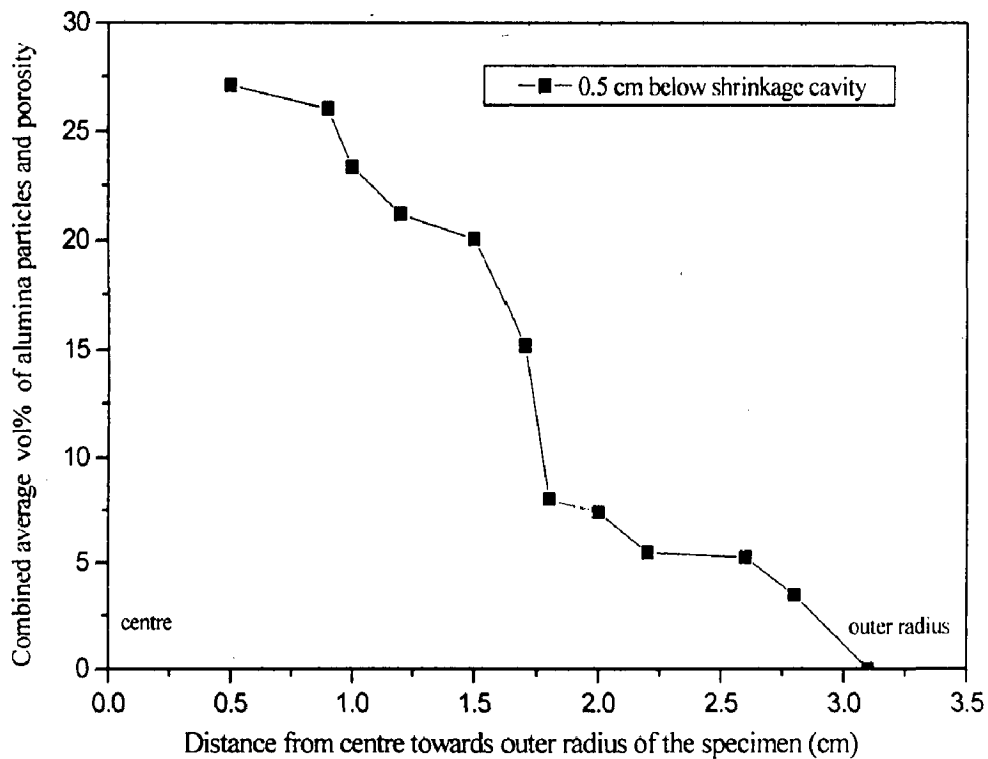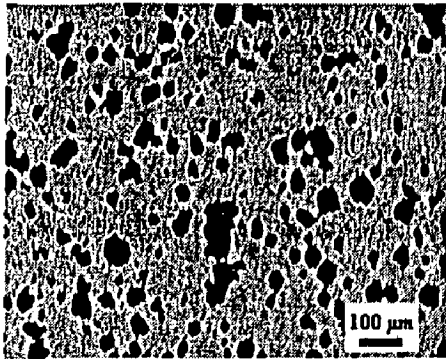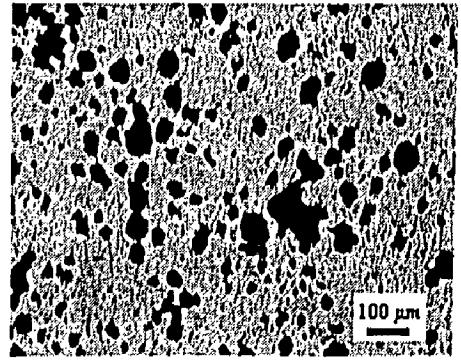
Fig. 5.20 The variation of alumina content and porosity with distance from the centre towards the outer radius of the cast 15Al/Al₂O₃ FGM ingot at 1.5 cm below the bottom of shrinkage cavity.

(a) 0.2 cm

(b) 0.5 cm

(c) 1.0 cm

(d) 1.6 cm

(e) 1.8 cm

(f) 2.0 cm

Fig. 5.21 Optical micrographs of 15Al/Al$_2$O$_3$ FGM ingot showing the variation of particle content and porosity along the radial direction from the centre towards the outer radius, 2.0 cm below the bottom of shrinkage cavity. The radial distance from the centre is indicated below each micrograph. Magnification: 50X.
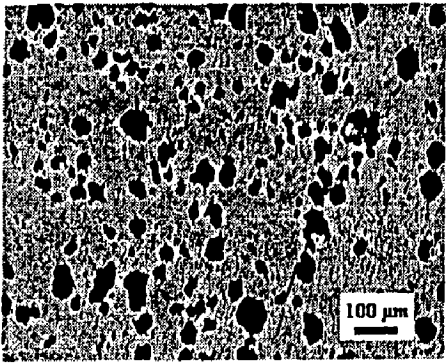
Fig. 5.22 The variation of alumina content and porosity with distance from the centre towards the outer radius of the cast 15 Al/Al₂O₃ FGM ingot at 2.0 cm below the bottom of shrinkage cavity.
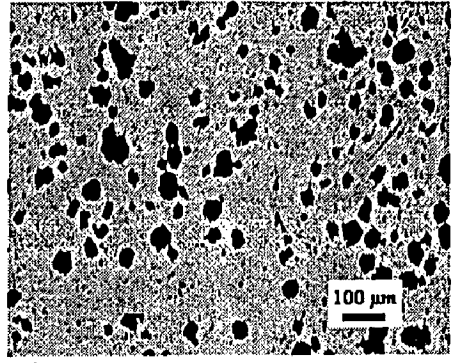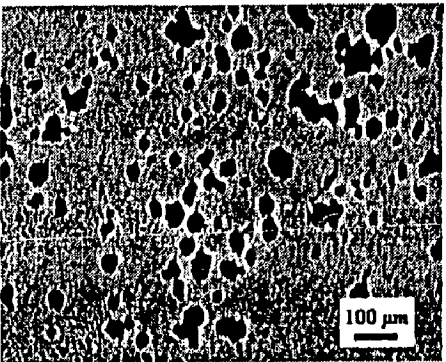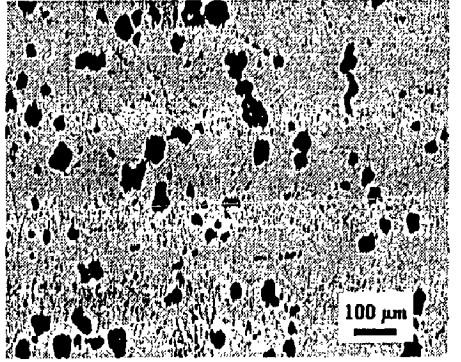
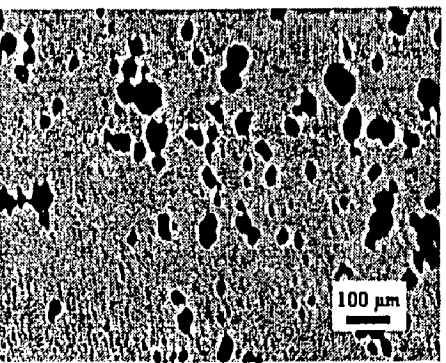(a) 0.2 cm   (b) 0.5 cm
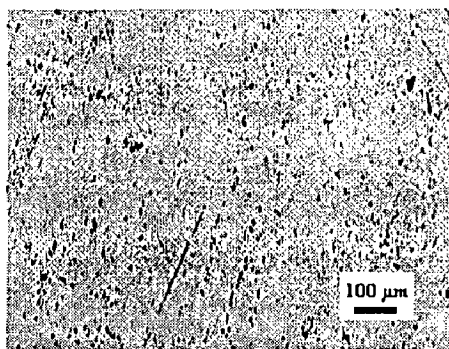
(c) 1.3 cm   (d) 1.5 cm
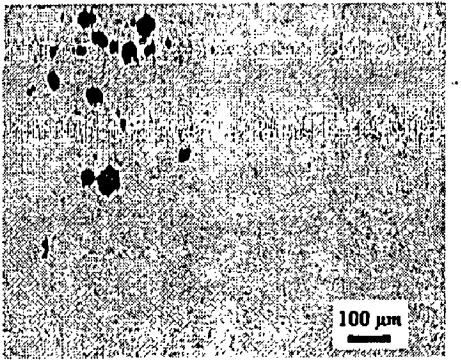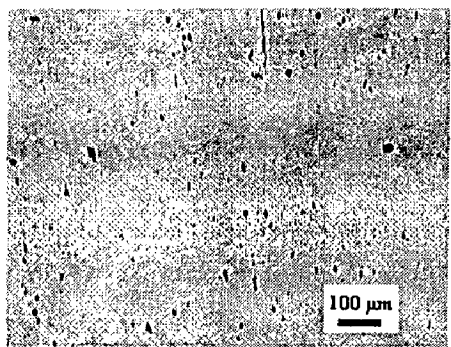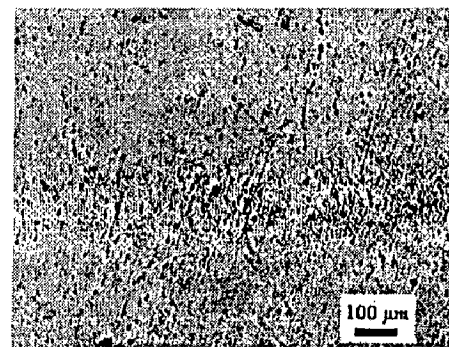
(e) 2.0 cm   (f) 2.5 cm

Fig. 5.23 Optical micrographs of 15Al/Al$_2$O$_3$ FGM ingot showing the variation of particle content and porosity along the radial direction from the centre towards the outer radius, 2.5 cm below the bottom of shrinkage cavity. The radial distance from the centre is indicated below each micrograph. Magnification: 50X.
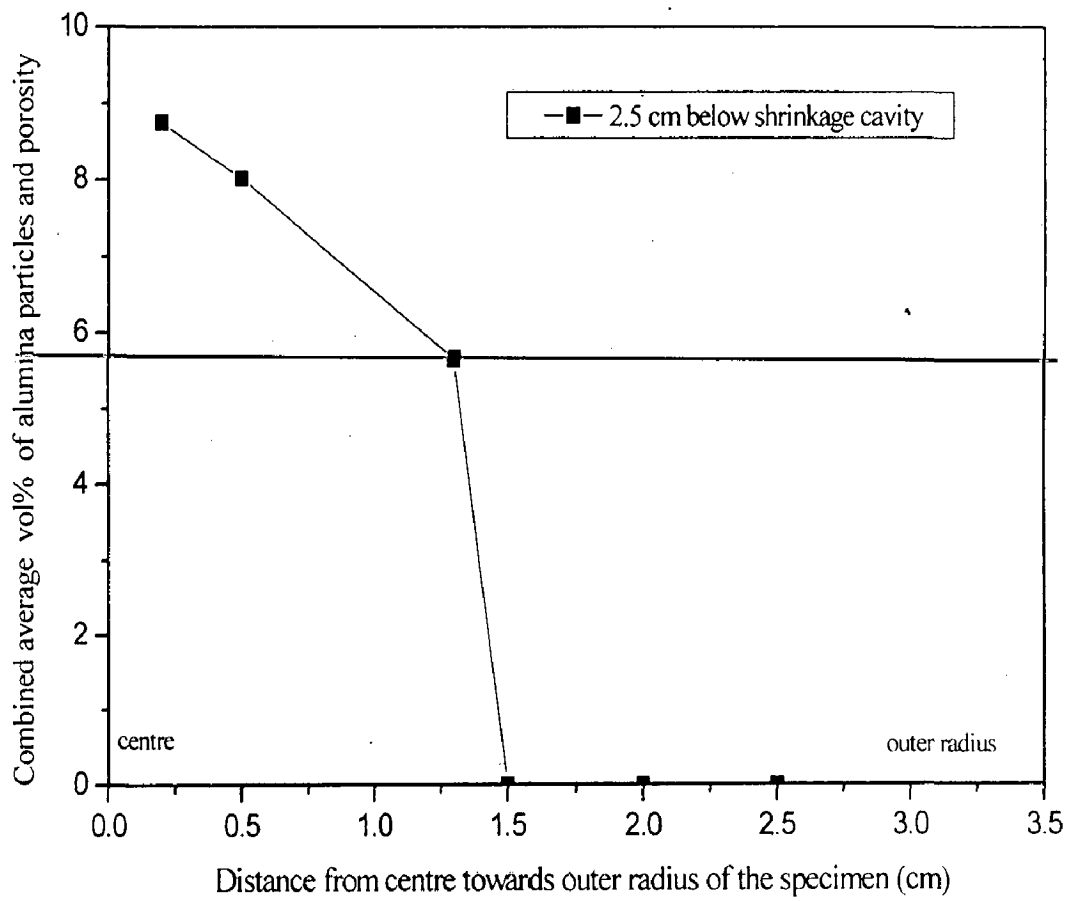
Fig. 5.24 The variation of alumina content and porosity with distance from the centre towards the outer radius of the cast 15Al/Al$_2$O$_3$ FGM ingot at 2.5 cm below the bottom of shrinkage cavity.

Fig. 5.25 The variation of alumina content and porosity at different radial distances from the centre towards the outer radius at different heights below the shrinkage cavity of cast 15Al/Al$_2$O$_3$ FGM ingot.
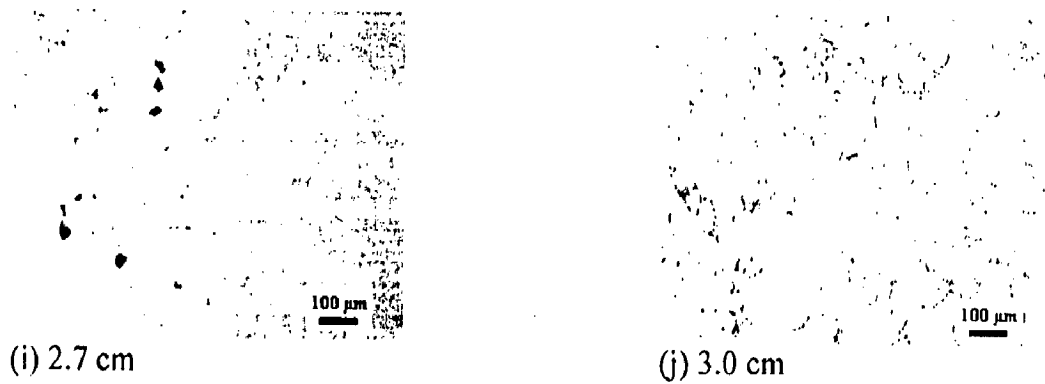
Fig. 5.26 Optical micrographs of 20Al/Al$_2$O$_3$ FGM ingot showing the variation of particle content and porosity along the radial direction from the centre towards the outer radius, 0 cm below the bottom of shrinkage cavity. The radial distance from the centre is indicated below each micrograph. Magnification: 50X.
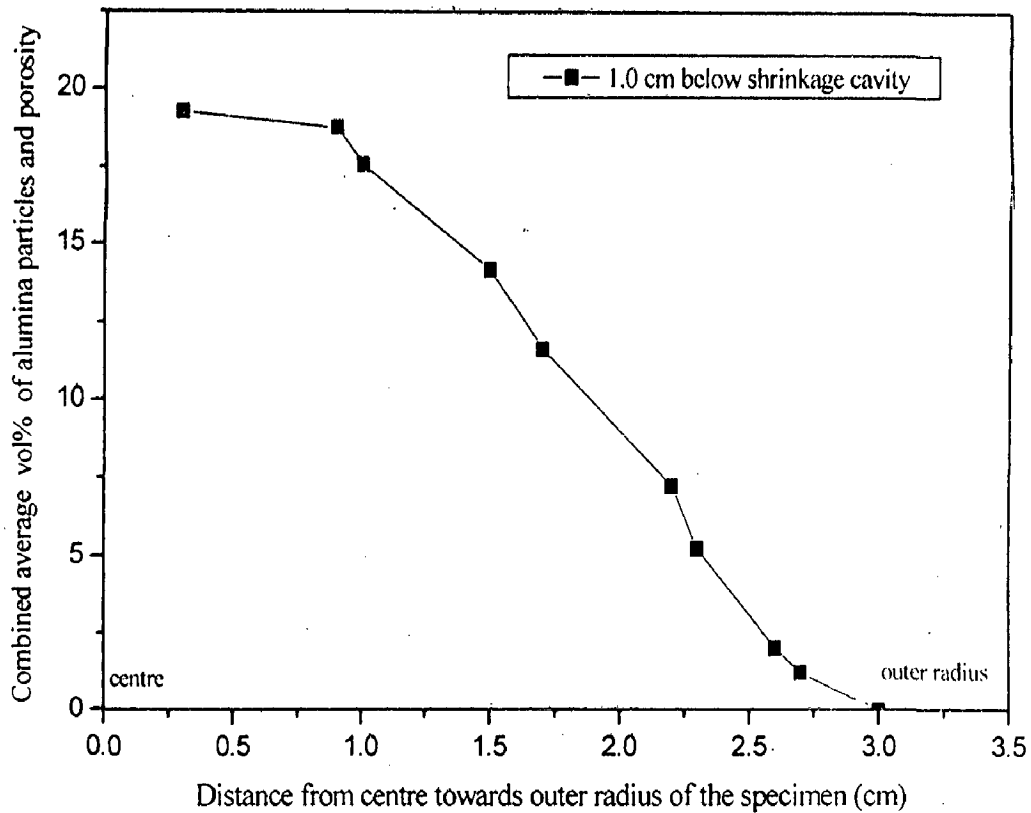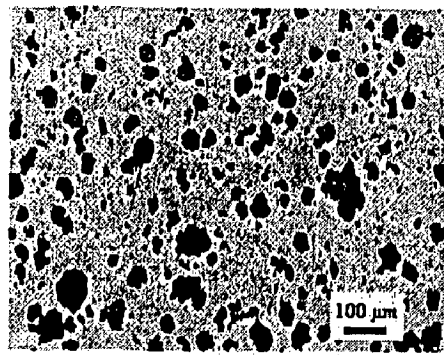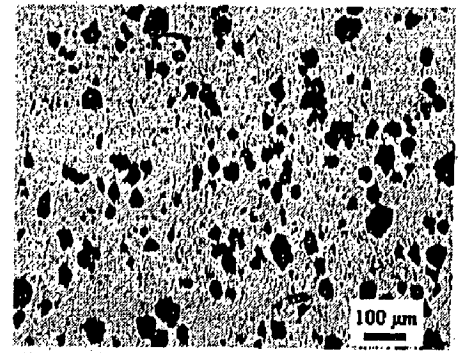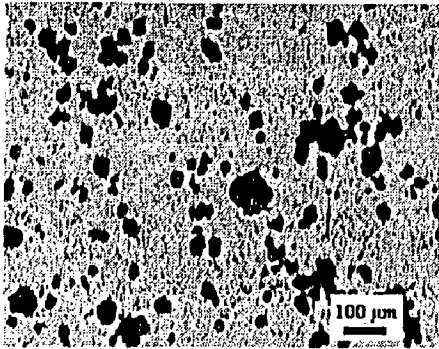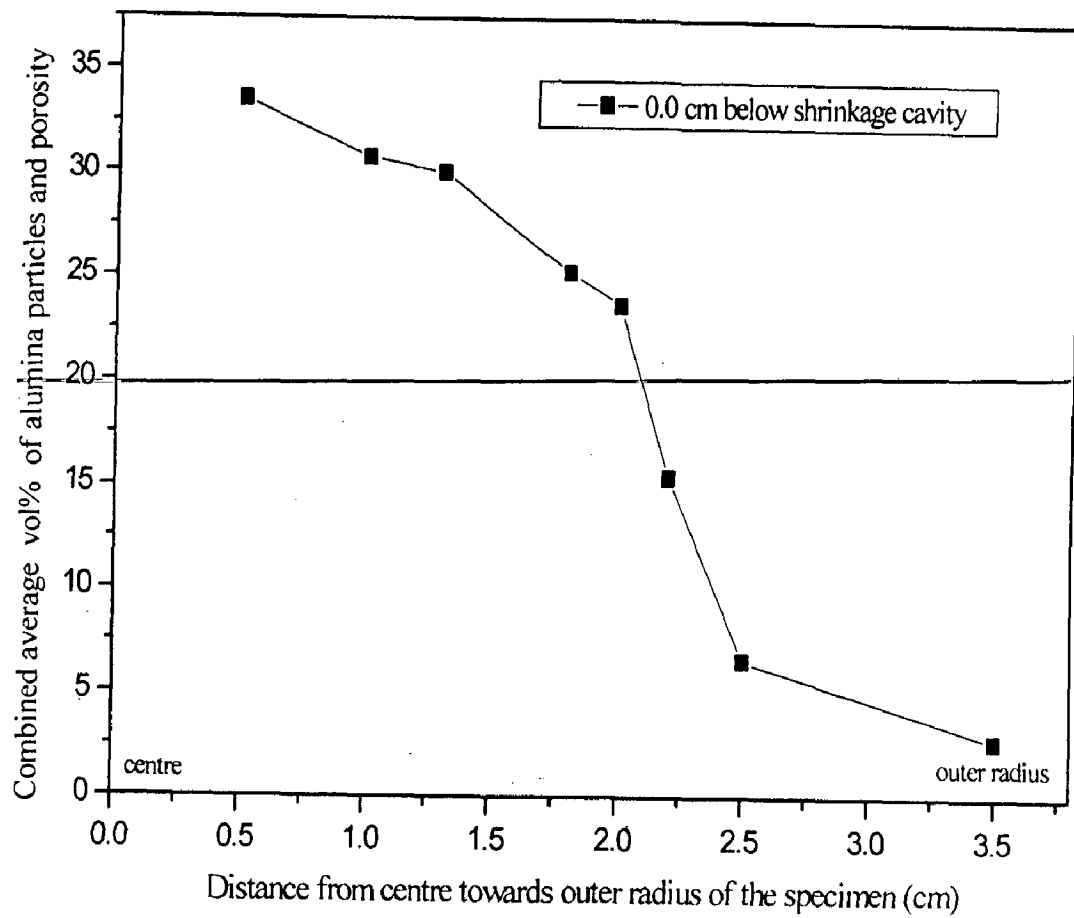
Fig. 5.27 The variation of alumina content and porosity with distance from the centre towards the outer radius of the cast 20Al/Al$_2$O$_3$ FGM ingot at 0 cm below the bottom of shrinkage cavity.
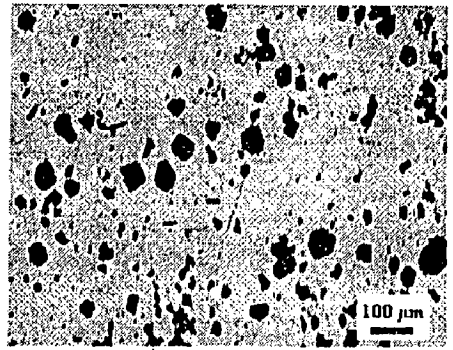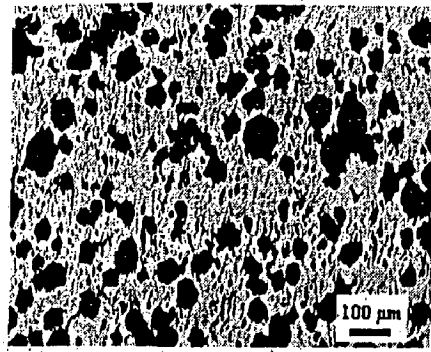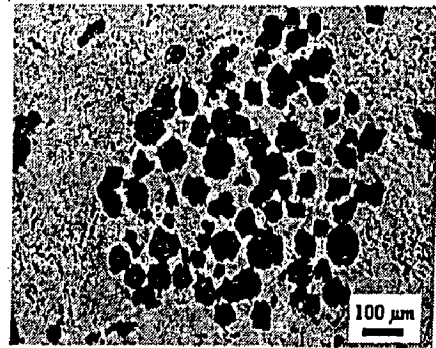
(a) 0.5 cm   (b) 1.0 cm
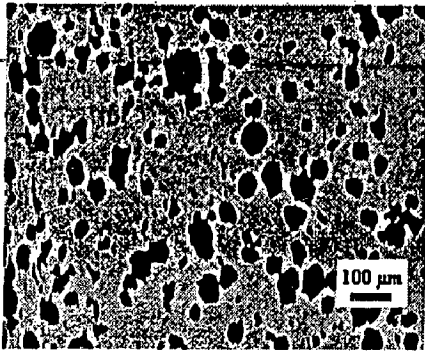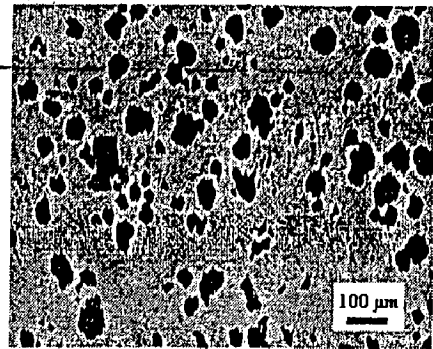
(c) 1.5 cm   (d) 1.7 cm
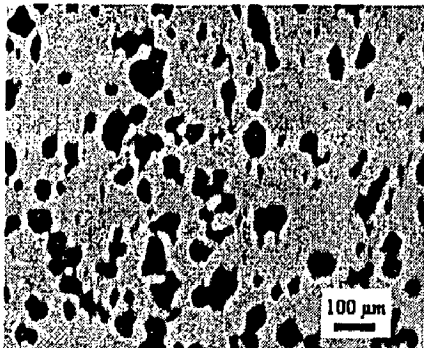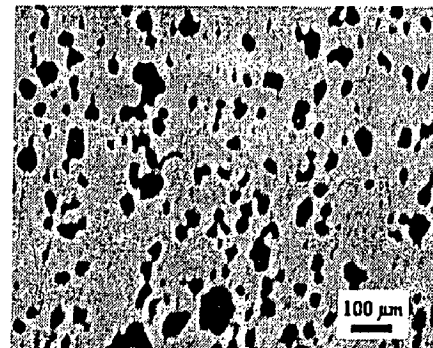
(e) 1.8 cm   (f) 2.0 cm
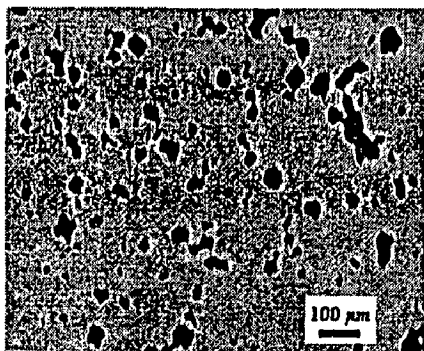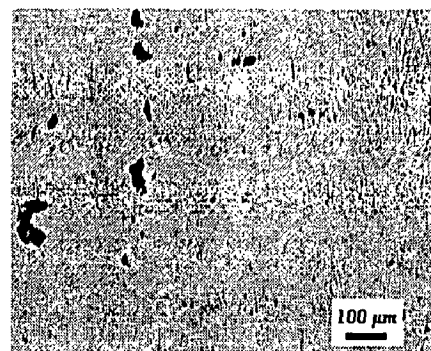
(g) 2.6 cm   (h) 3.5 cm

Fig. 5.28 Optical micrographs of 20Al/Al$_2$O$_3$ FGM ingot showing the variation of particle content and porosity along the radial direction from the centre towards the outer radius, 0.5 cm below the bottom of shrinkage cavity. The radial distance from the centre is indicated below each micrograph. Magnification: 50X.

107

Fig. 5.29 The variation of alumina content and porosity with distance from the centre towards the outer radius of the cast 20Al/Al$_2$O$_3$ FGM ingot at 0.5 cm below the bottom of shrinkage cavity.
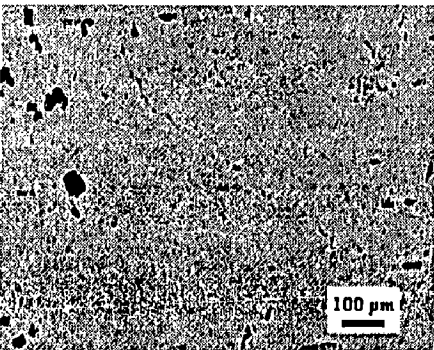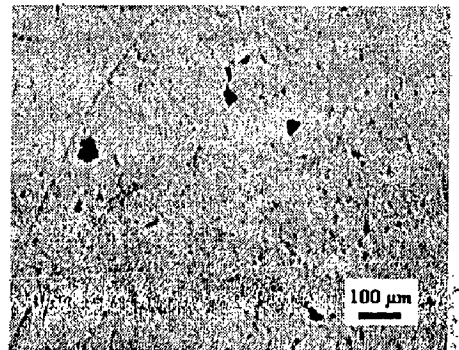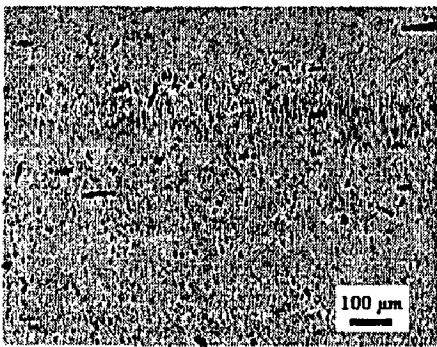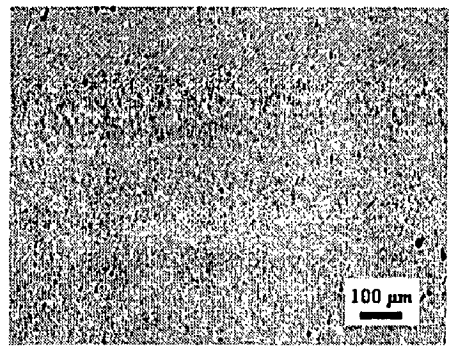
(a) 0.3 cm

(b) 0.9 cm

(c) 1.0 cm

(d) 1.7 cm

(e) 2.3 cm

(f) 2.5 cm

(g) 2.7 cm

(h) 3.0 cm
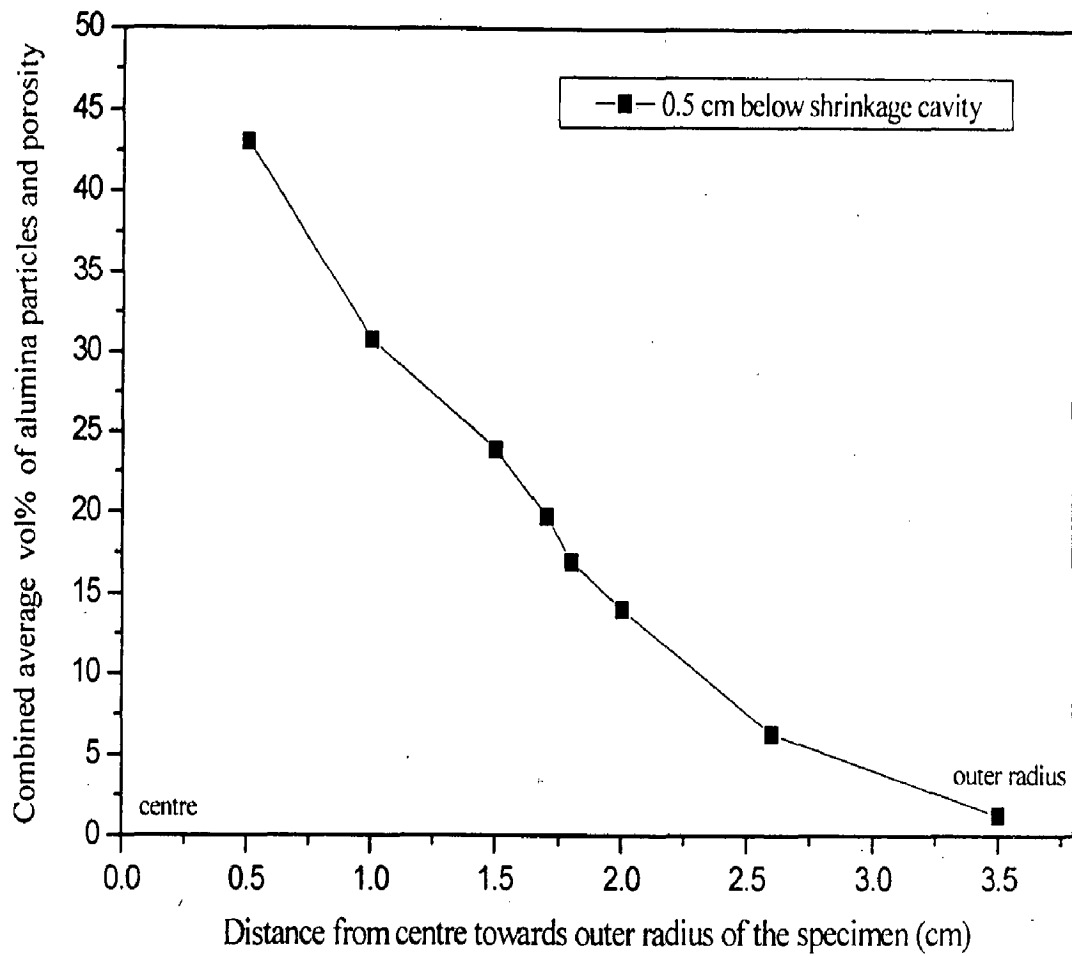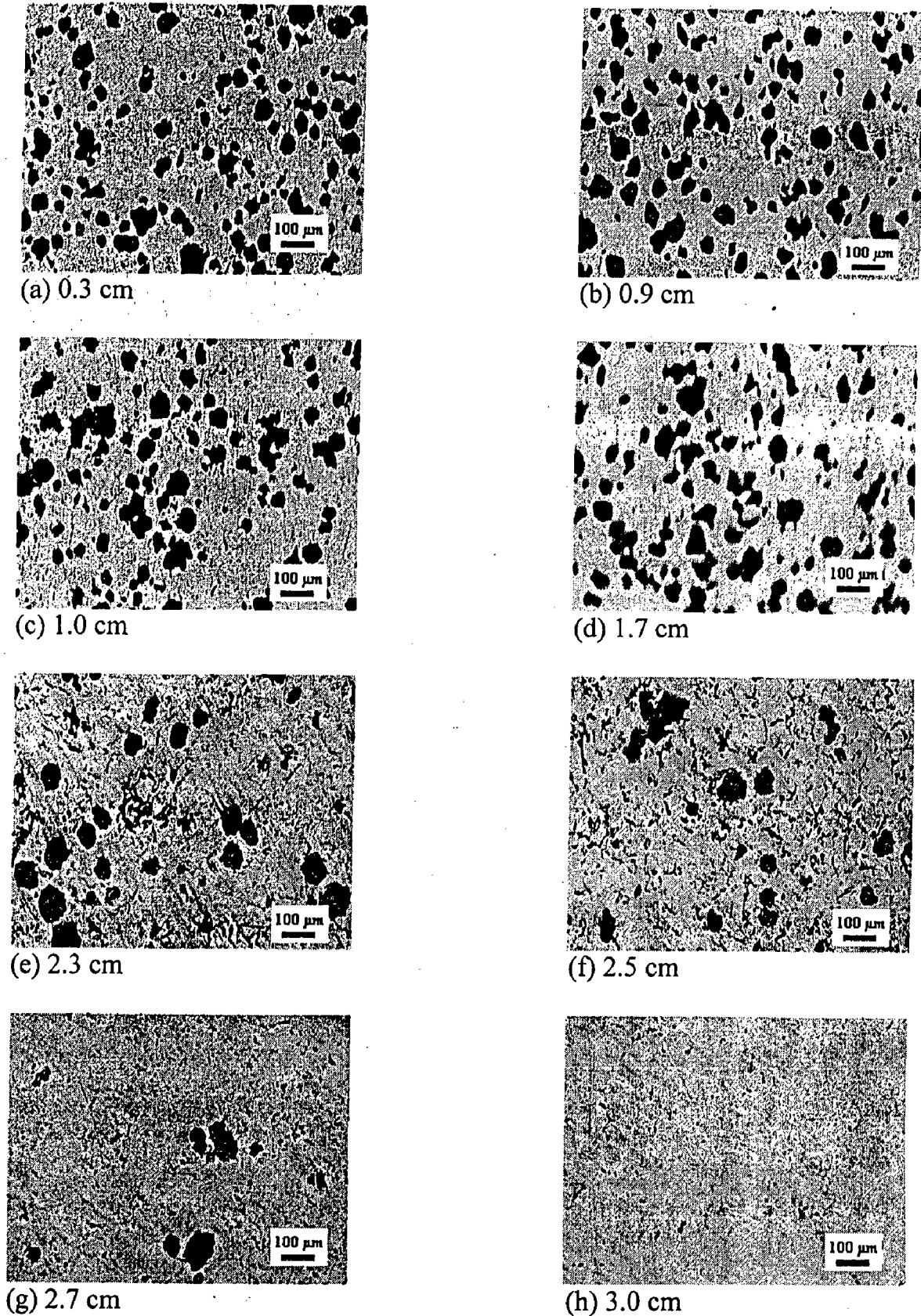
Fig. 5.30 Optical micrographs of 20Al/Al$_2$O$_3$ FGM ingot showing the variation of particle content and porosity along the radial direction from the centre towards the outer radius, 1.0 cm below the bottom of shrinkage cavity. The radial distance from the centre is indicated below each micrograph. Magnification: 50X.

Fig. 5.31 The variation of alumina content and porosity with distance from the centre towards the outer radius of the cast $20Al/Al_2O_3$ FGM ingot at 1.0 cm below the bottom of shrinkage cavity.
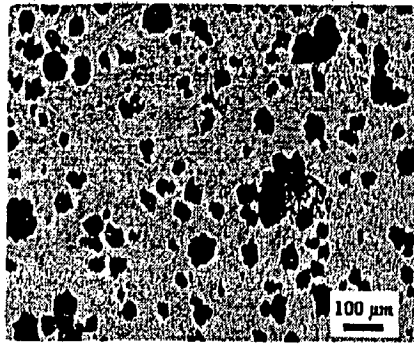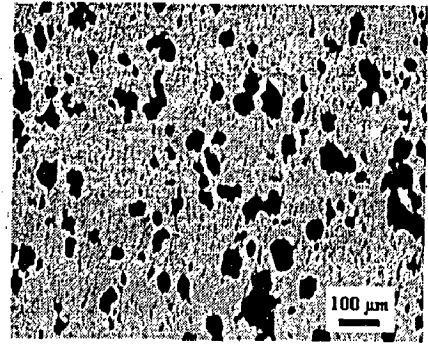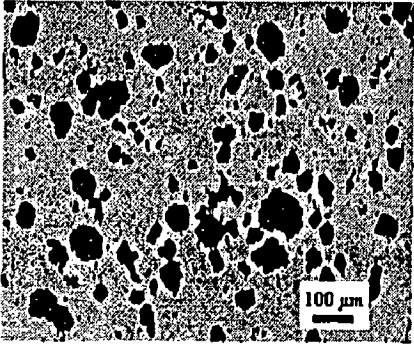
Fig. 5.32 Optical micrographs of $20Al/Al_2O_3$ FGM ingot showing the variation of particle content and porosity along the radial direction from the centre towards the outer radius, 1.5 cm below the bottom of shrinkage cavity. The radial distance from the centre is indicated below each micrograph. Magnification: 50X.
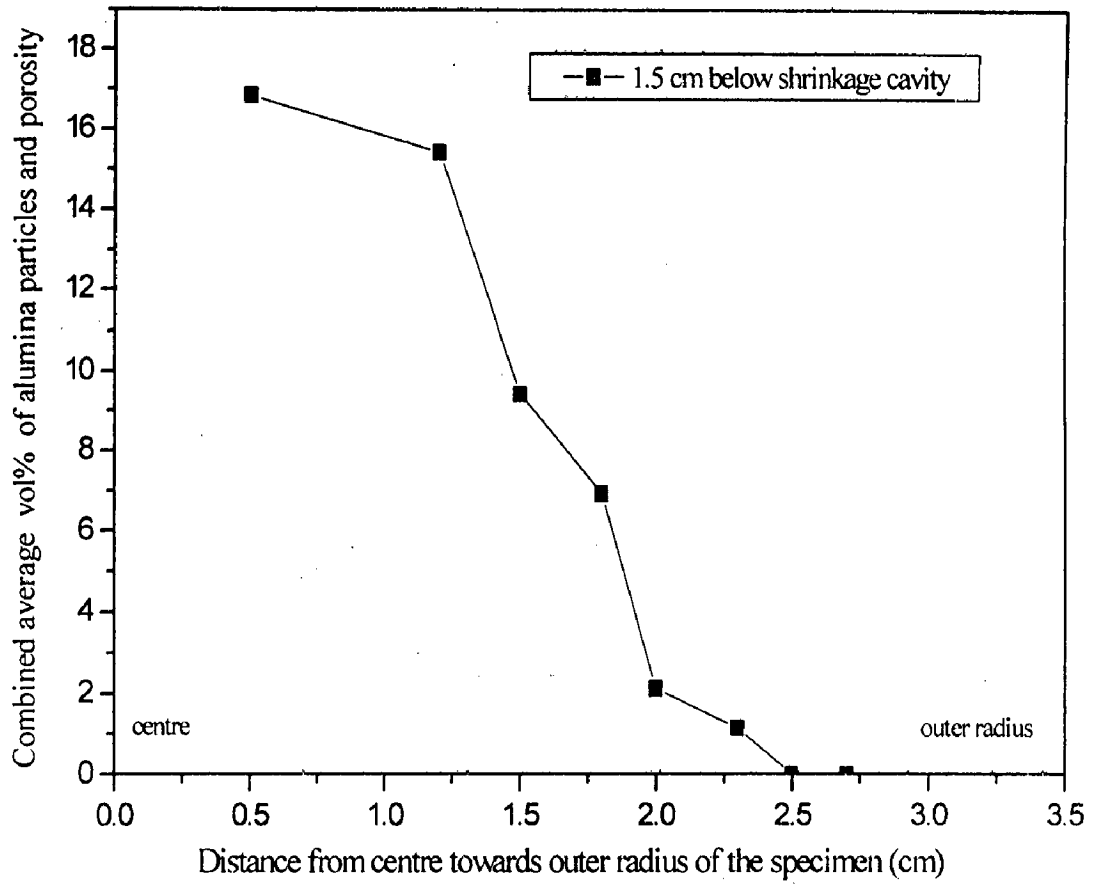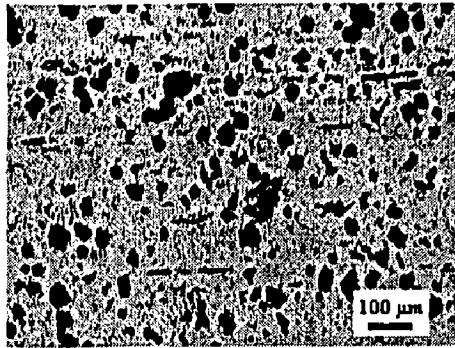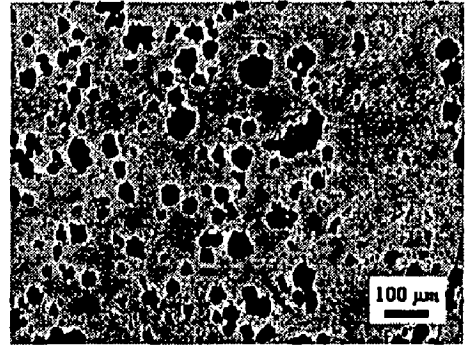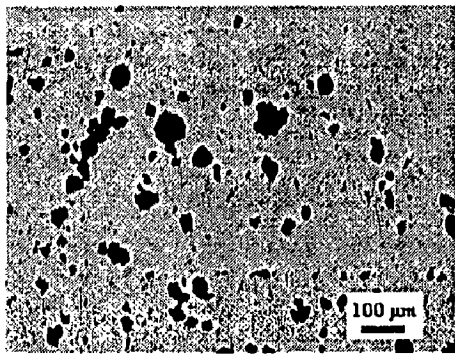
Fig. 5.33 The variation of alumina content and porosity with distance from the centre towards the outer radius of the cast 20Al/Al$_2$O$_3$ FGM ingot at 1.5 cm below the bottom of shrinkage cavity.
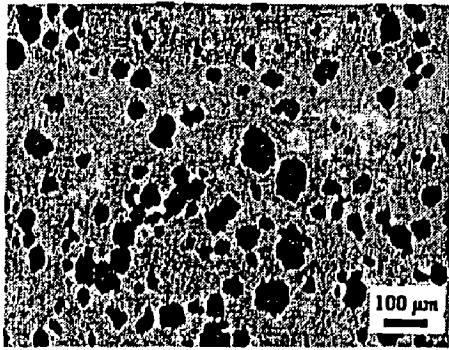
(a) 0.2 cm
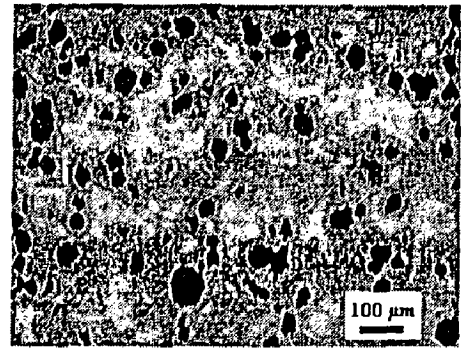
(b) 0.5 cm
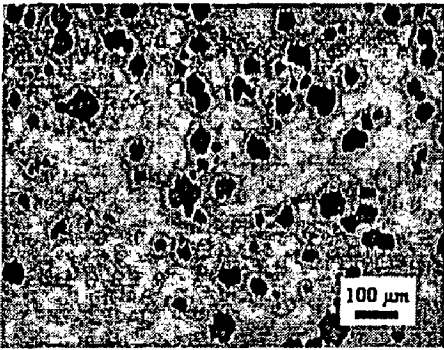
(c) 1.0 cm
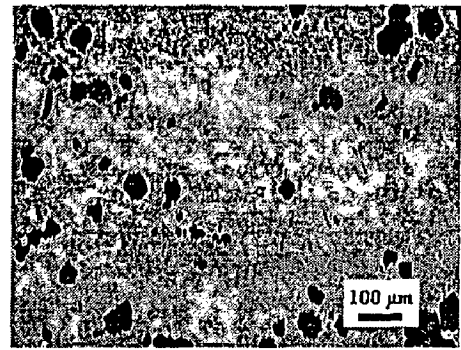
(d) 1.8 cm
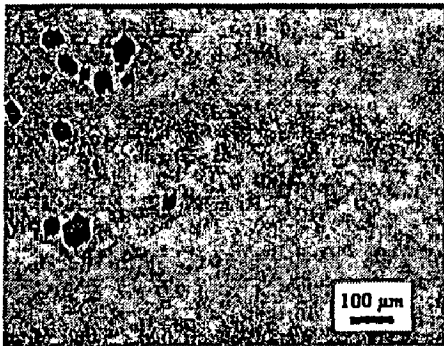
(e) 2.0 cm
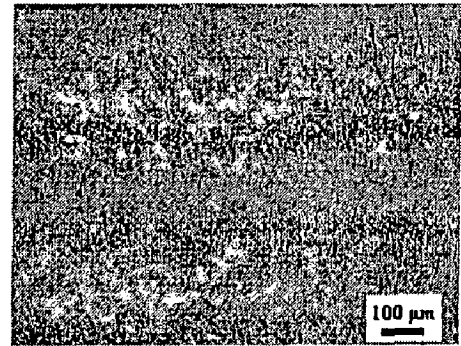
(f) 2.2 cm

Fig. 5.34 Optical micrographs of $20Al/Al_2O_3$ FGM ingot showing the variation of particle content and porosity along the radial direction from the centre towards the outer radius, 2.0 cm below the bottom of shrinkage cavity. The radial distance from the centre is indicated below each micrograph. Magnification: 50X.
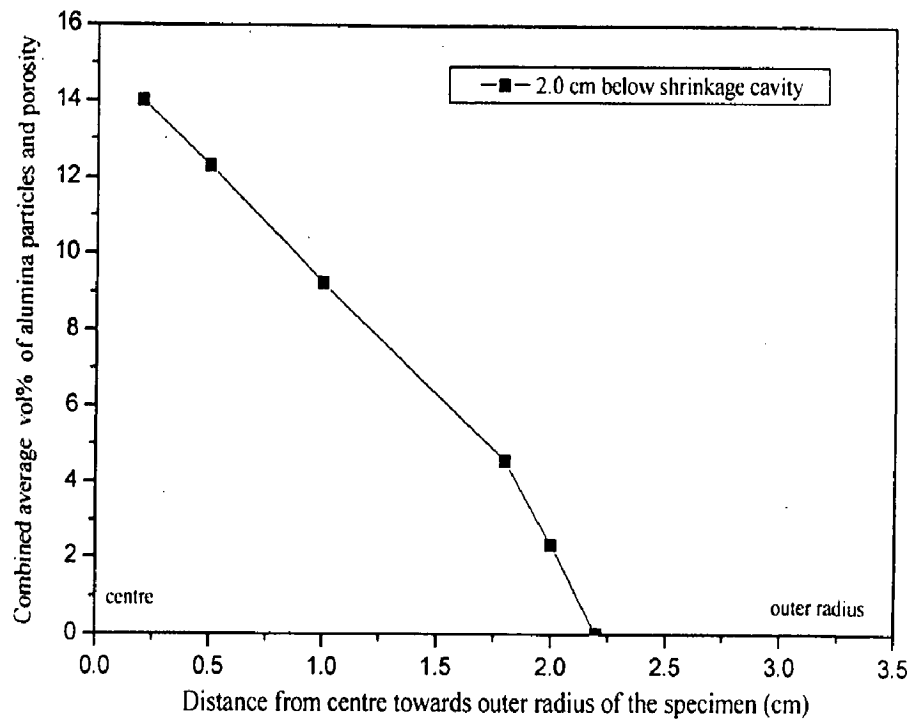
Fig. 5.35 The variation of alumina content and porosity with distance from the centre towards the outer radius of the cast 20Al/Al₂O₃ FGM ingot at 2.0 cm below the bottom of shrinkage cavity.
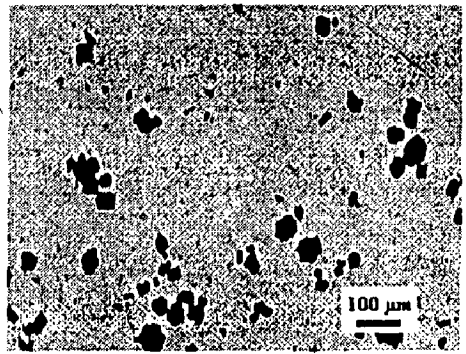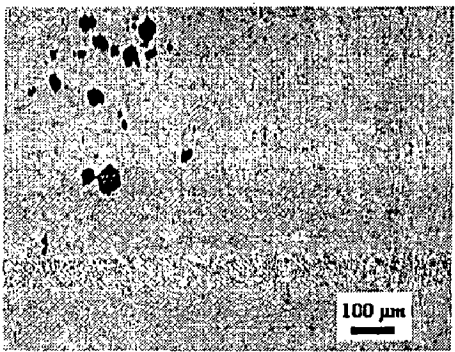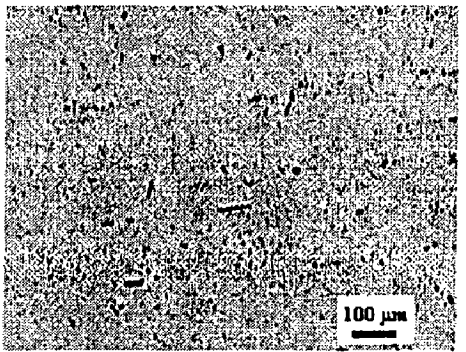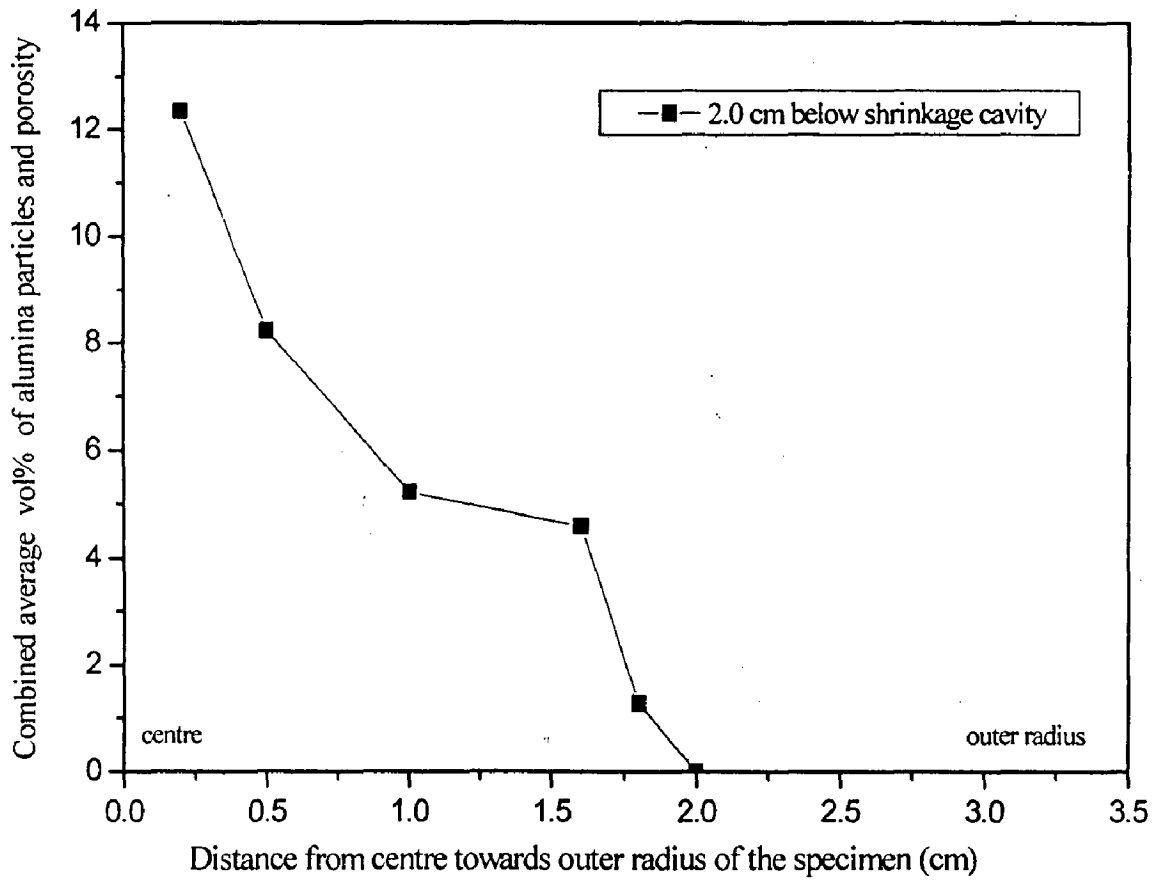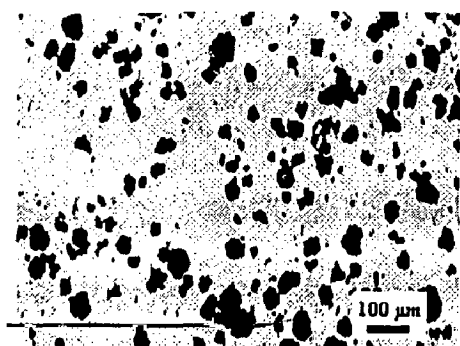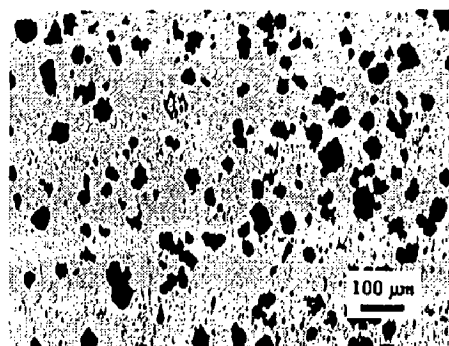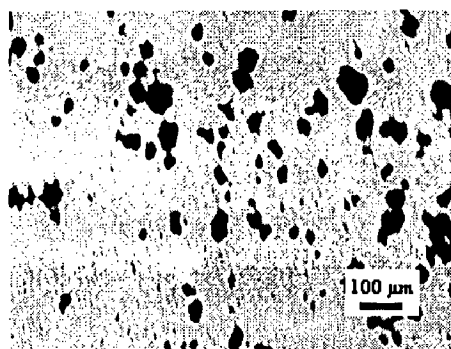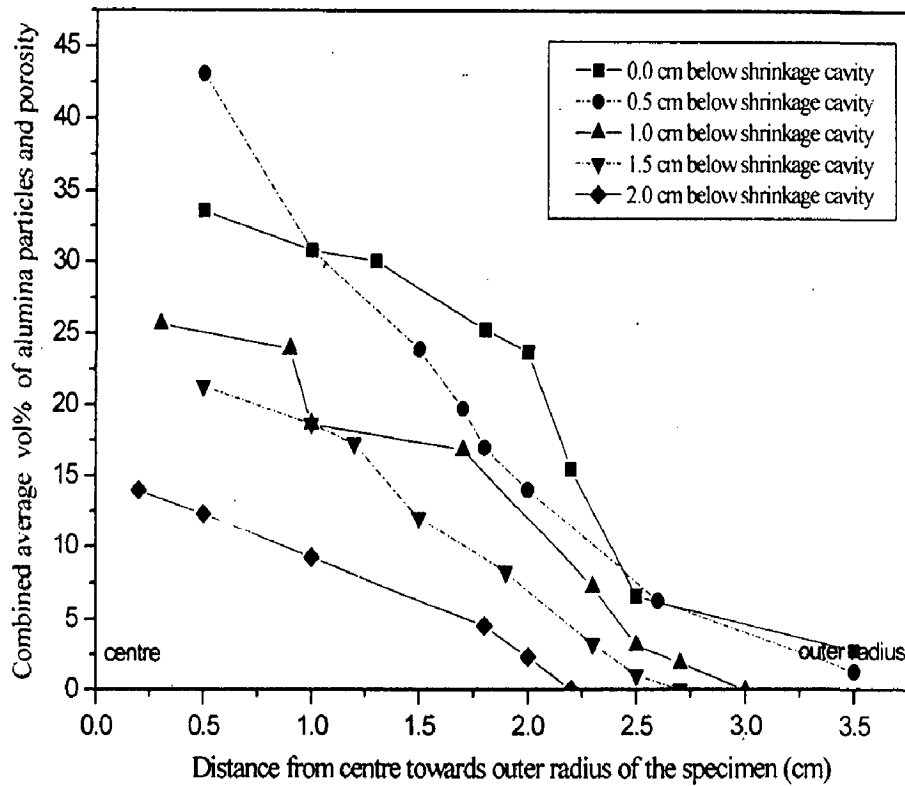

Fig. 5.36 The variation of alumina content and porosity at different radial distances from the centre towards the outer radius at different heights below the shrinkage cavity of cast 20Al/Al₂O₃ FGM ingot.
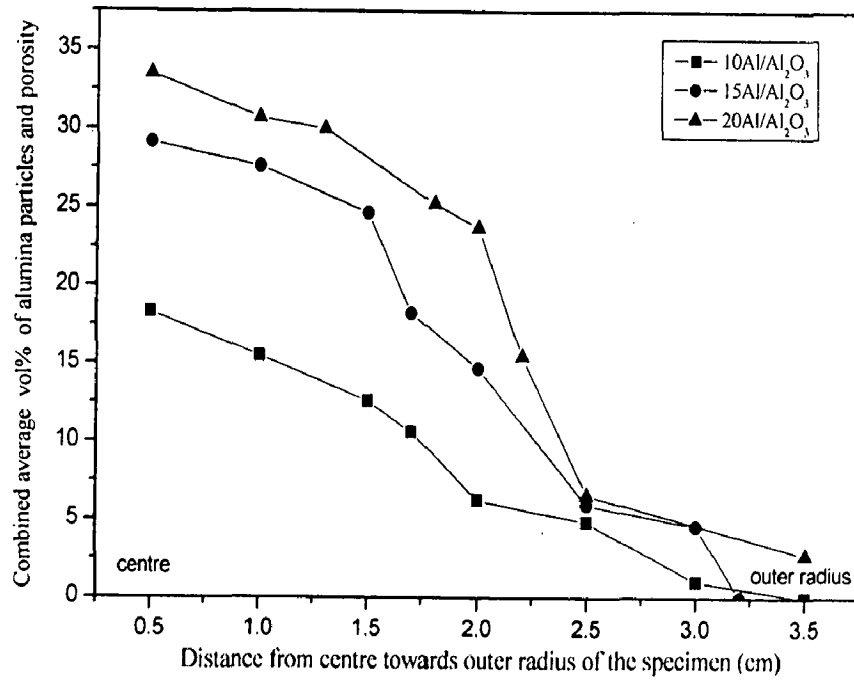
Fig. 5.37 The variation of alumina content and porosity at different radial distances from the centre towards the outer radius at the bottom of the shrinkage cavity of cast 10Al/Al₂O₃, 15Al/Al₂O₃, 20Al/Al₂O₃ FGM ingots.
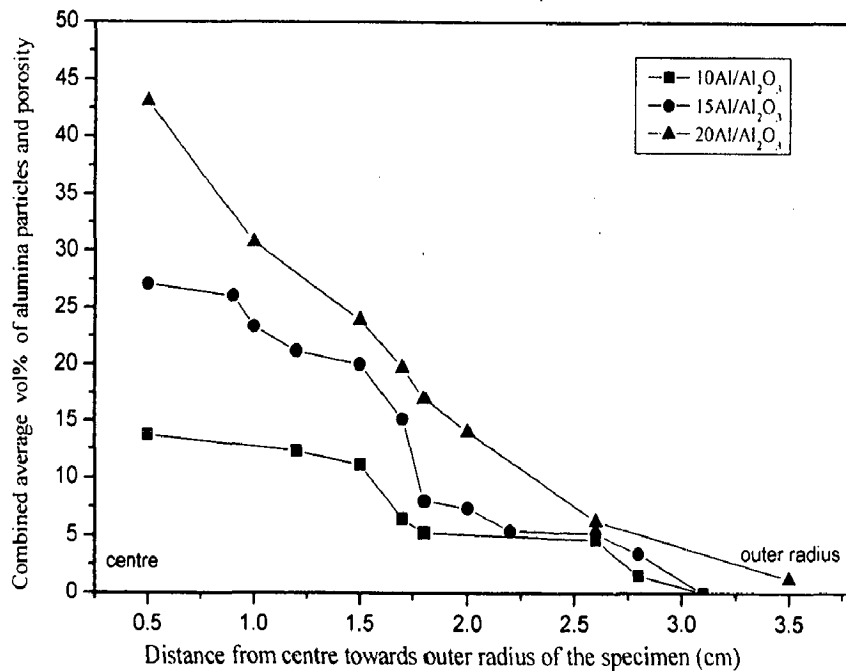
Fig. 5.38 The variation of alumina content and porosity at different radial distances from the centre towards the outer radius at a height of 0.5 cm below the shrinkage cavity of cast 10Al/Al₂O₃, 15Al/Al₂O₃, and 20Al/Al₂O₃ FGM ingots.
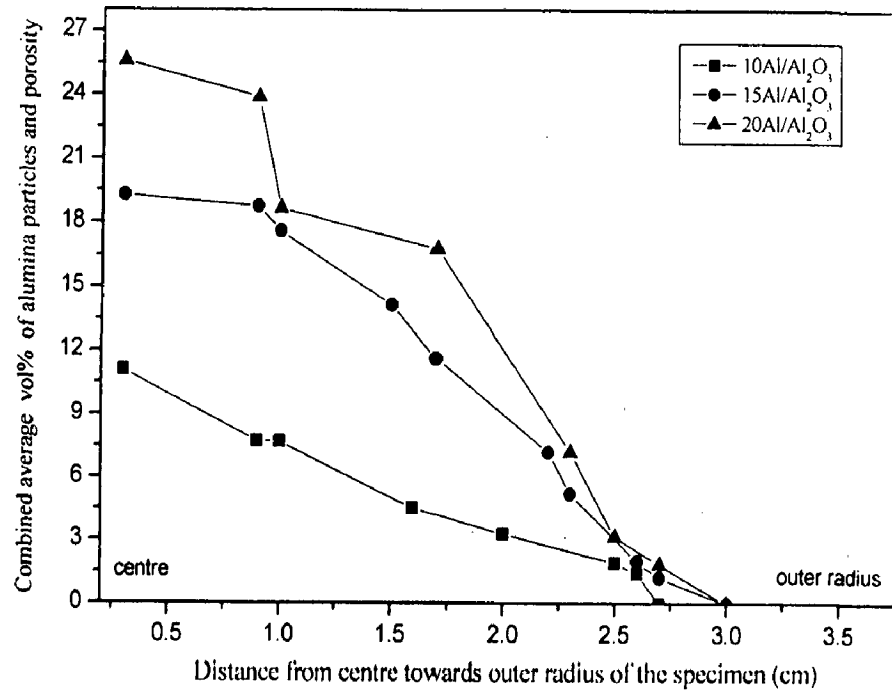
Fig. 5.39 The variation of alumina content and porosity at different radial distances from the centre towards the outer radius at a height of 1.0 cm below the shrinkage cavity of cast 10Al/Al₂O₃, 15 Al/Al₂O₃, 20Al/Al₂O₃ FGM ingots.
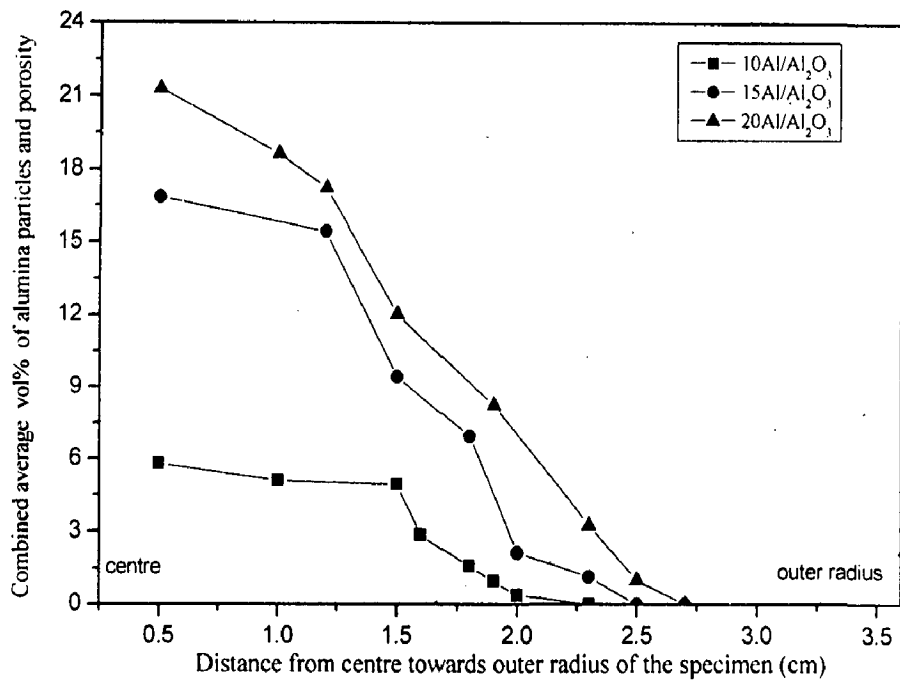
Fig. 5.40 The variation of alumina content and porosity at different radial distances from the centre towards the outer radius at a height of 1.5 cm below the shrinkage cavity of cast 10Al/Al₂O₃, 15Al/Al₂O₃, and 20Al/Al₂O₃ FGM ingots.
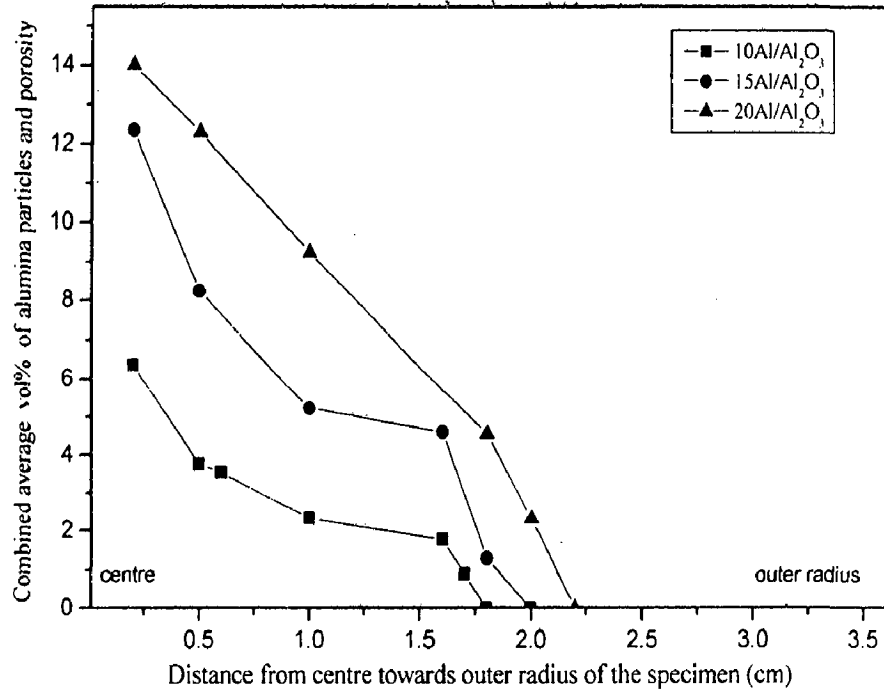
Fig. 5.41 The variation of alumina content and porosity at different radial distances from the centre towards the outer radius at a height of 2.0 cm below the shrinkage cavity of cast $10Al/Al_2O_3$, $15Al/Al_2O_3$, and $20Al/Al_2O_3$ FGM ingots.
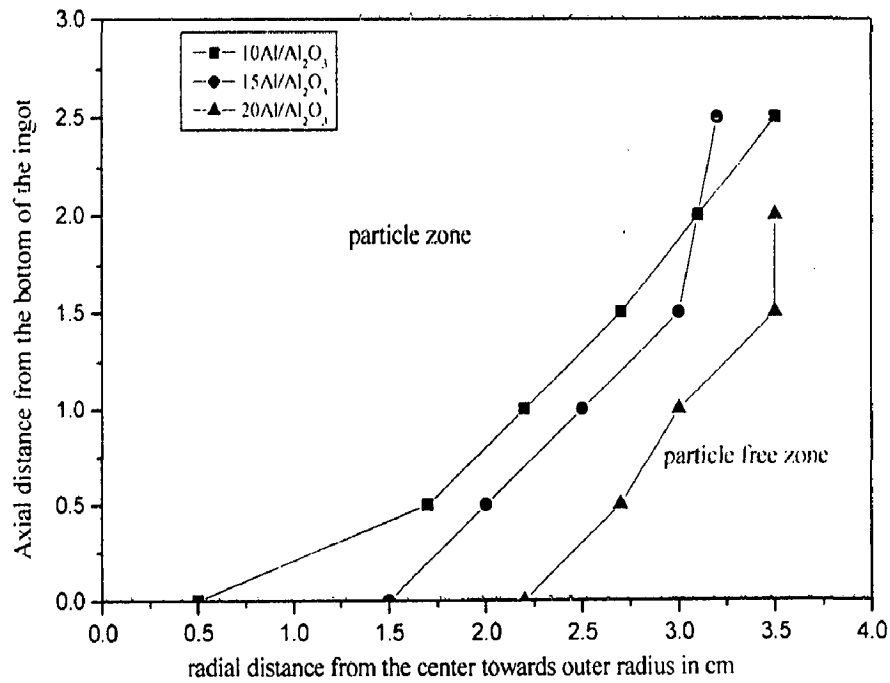
Fig. 5.42 The variation of the size of particle free zone obtained for the cast $10Al/Al_2O_3$, $15Al/Al_2O_3$, and $20Al/Al_2O_3$ FGM ingots.

117
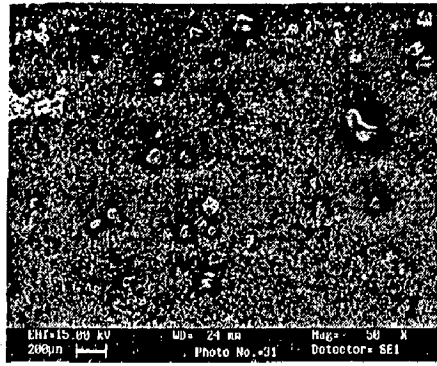
(a)
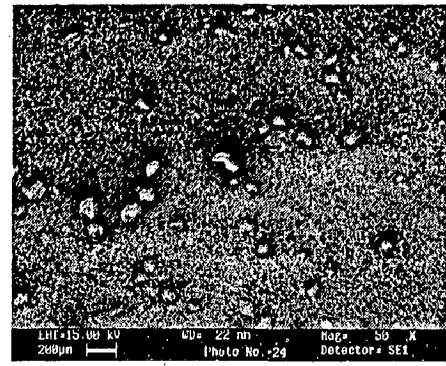
(b)
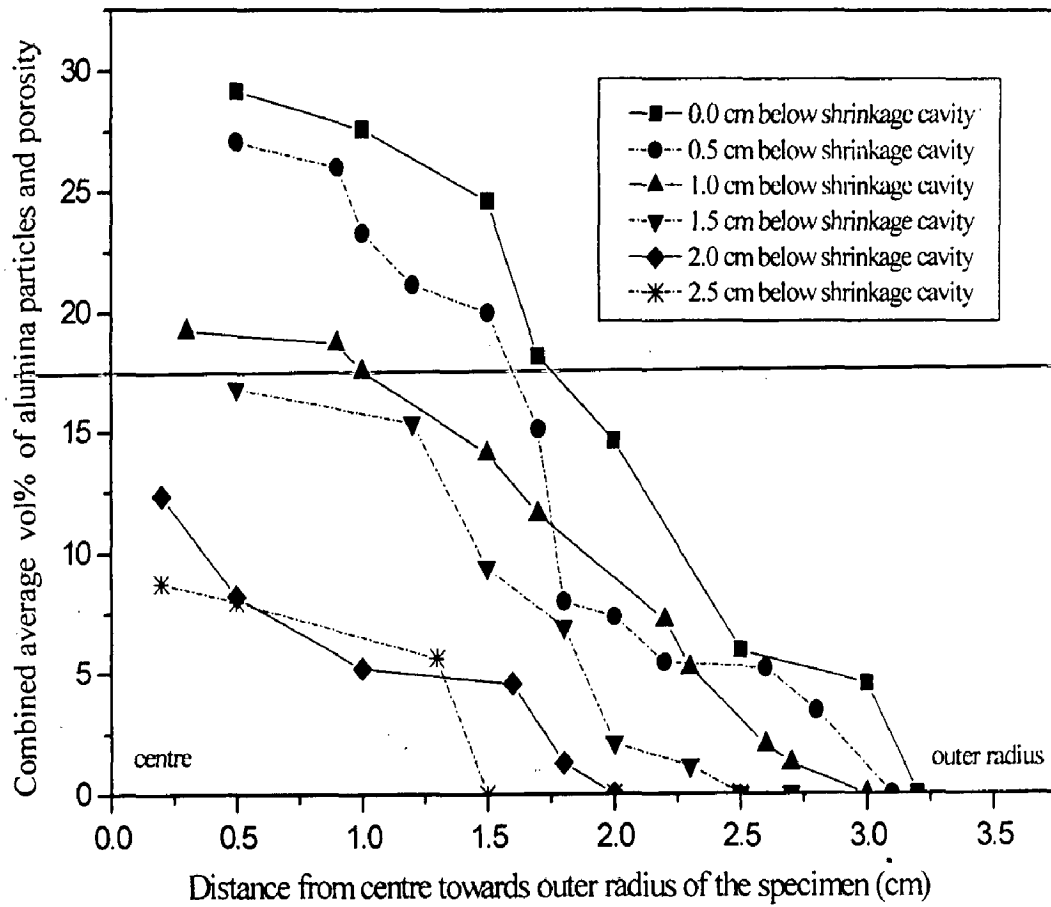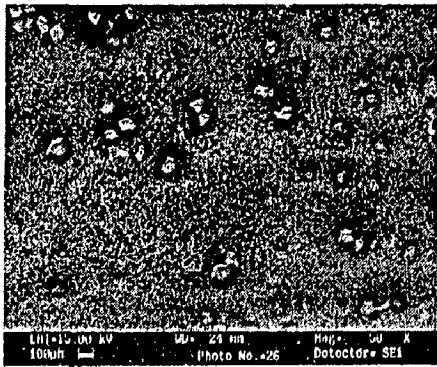
(c)
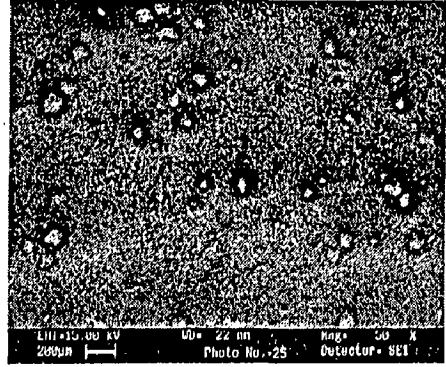
(d)
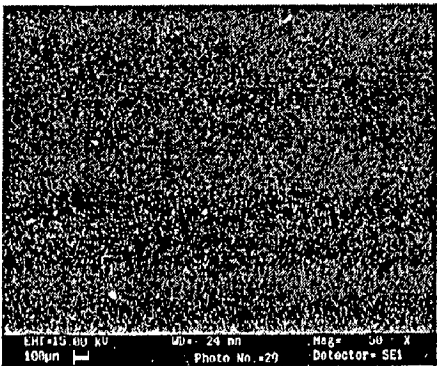
(e)
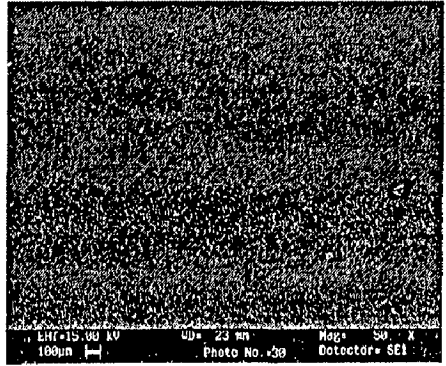
(f)

Fig. 5.43 SEM micrographs of 10Al/Al$_2$O$_3$ FGM ingot showing the variation of particle content along the radial direction from the centre towards the outer radius, just below the bottom of shrinkage cavity.
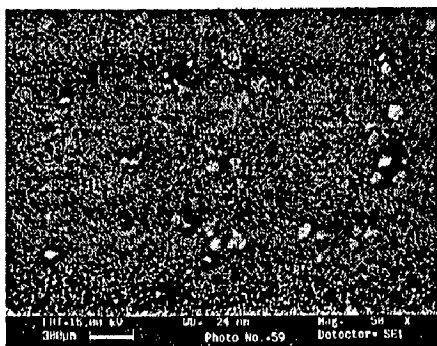
(a)
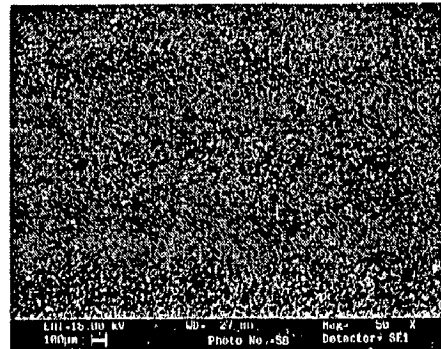
(b)

Fig. 5.44 SEM micrographs of 10Al/Al$_2$O$_3$ FGM ingot showing the variation of particle content along the radial direction from the centre towards the outer radius, at the base of the ingot.

118
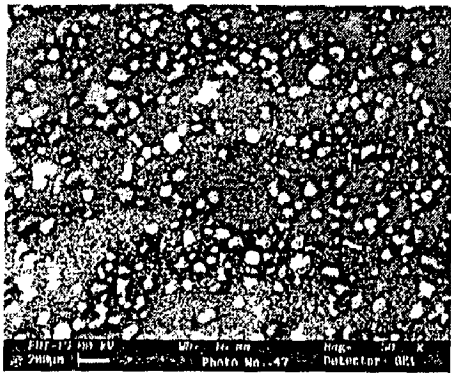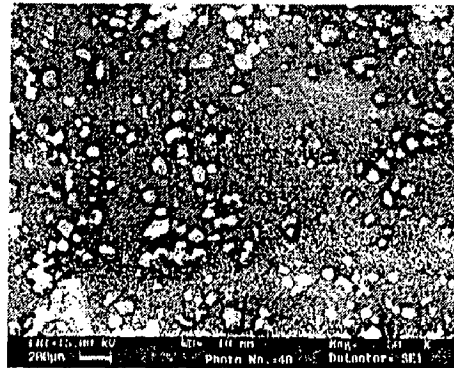
(a) (b)
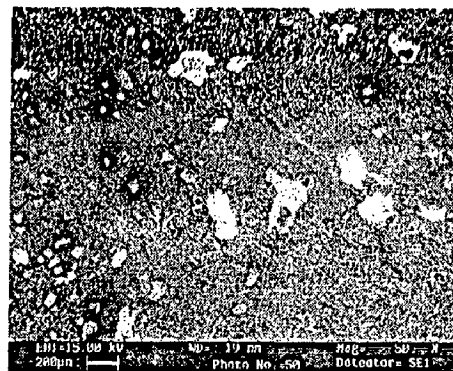
(c) (d)
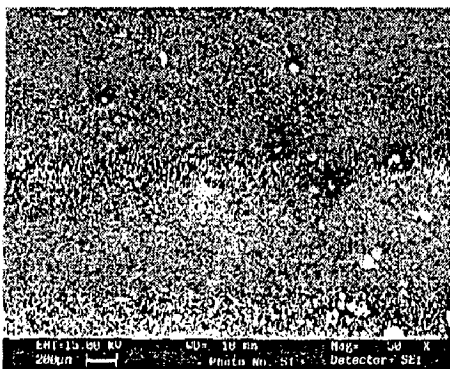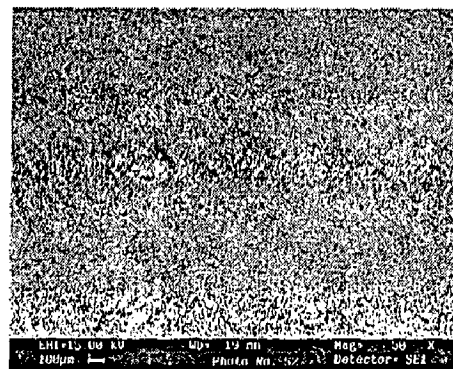
(e) (f)

Fig. 5.45 SEM micrographs of 15Al/Al₂O₃ FGM ingot showing the variation of particle content along the radial direction from the centre towards the outer radius, just below the bottom of shrinkage cavity.
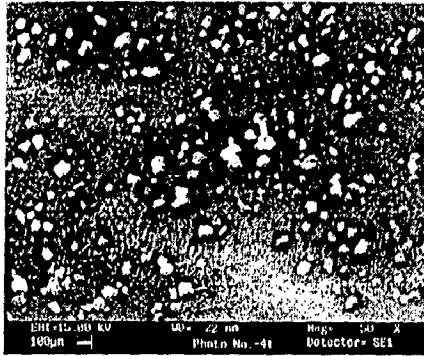
(a)
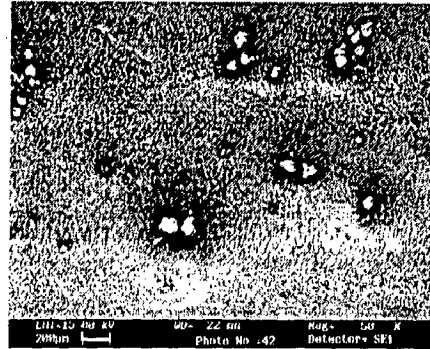
(b)
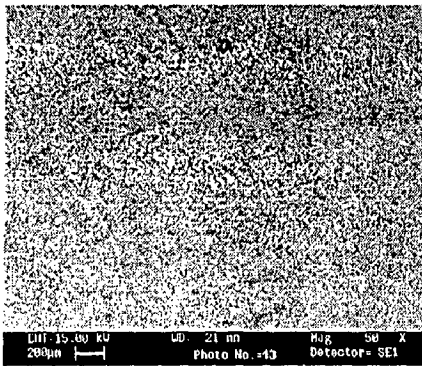
(c)
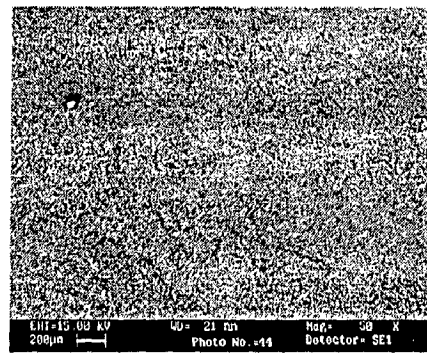
(d)
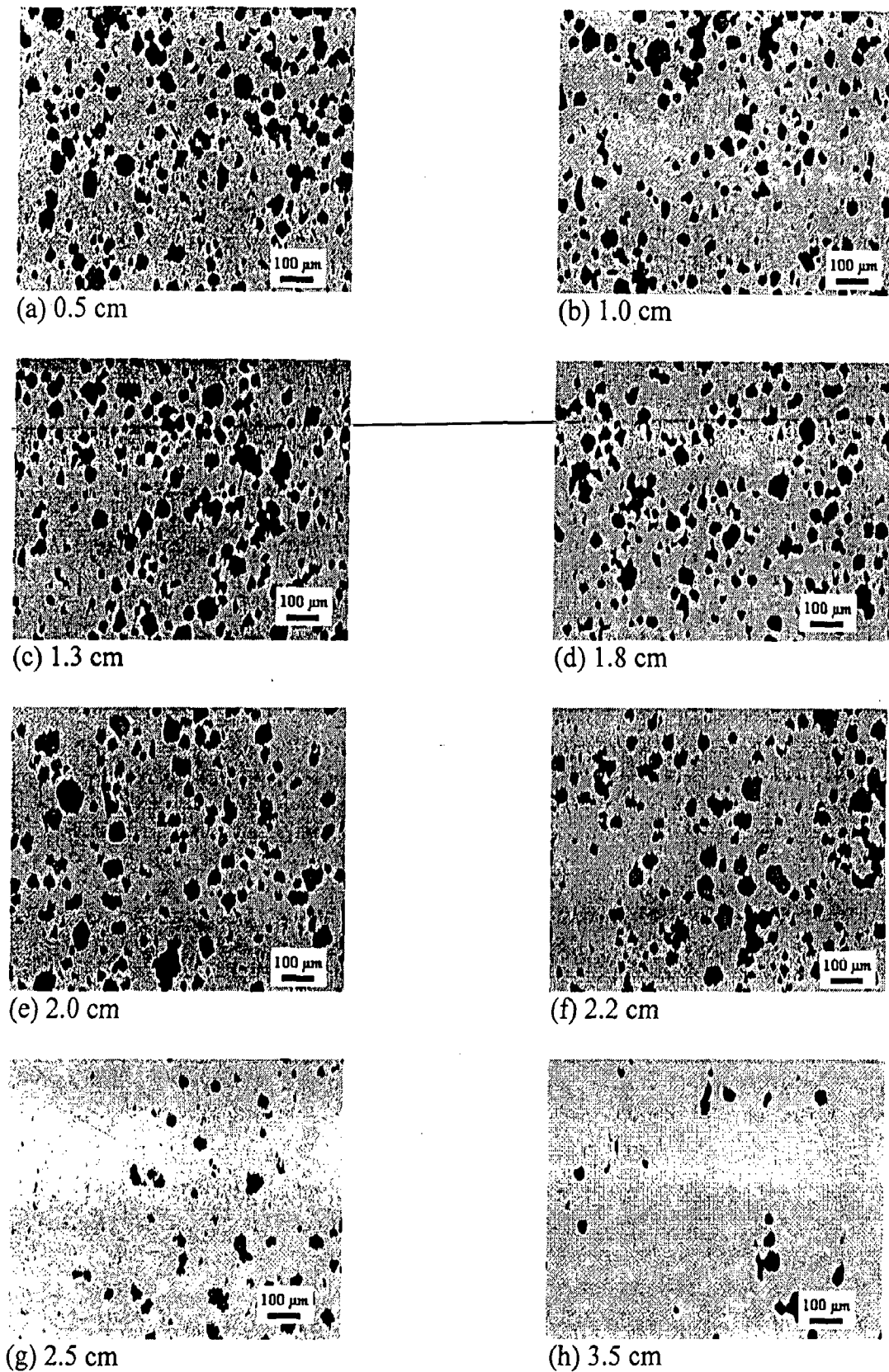
Fig. 5.46 SEM micrographs of 15Al/Al₂O₃ FGM ingot showing the variation of particle content along the radial direction from the centre towards the outer radius, at the base of the ingot.

120

(a)   (b)

(c)   (d)

(e)   (f)
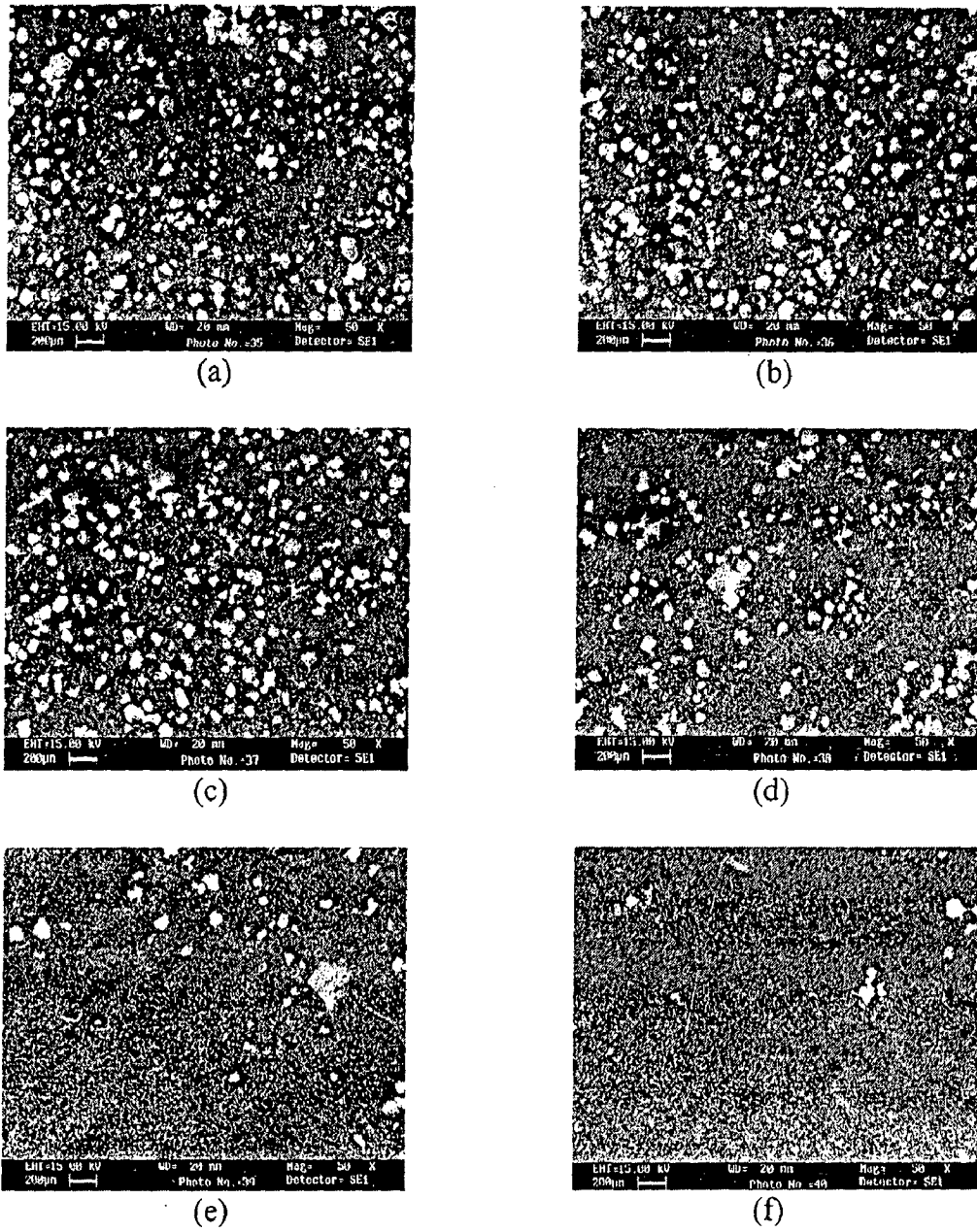
Fig. 5.47 SEM micrographs of $20Al/Al_2O_3$ FGM ingot showing the variation of particle content along the radial direction from the centre towards the outer radius, just below the bottom of shrinkage cavity.

(a)

(b)

(c)

(d)
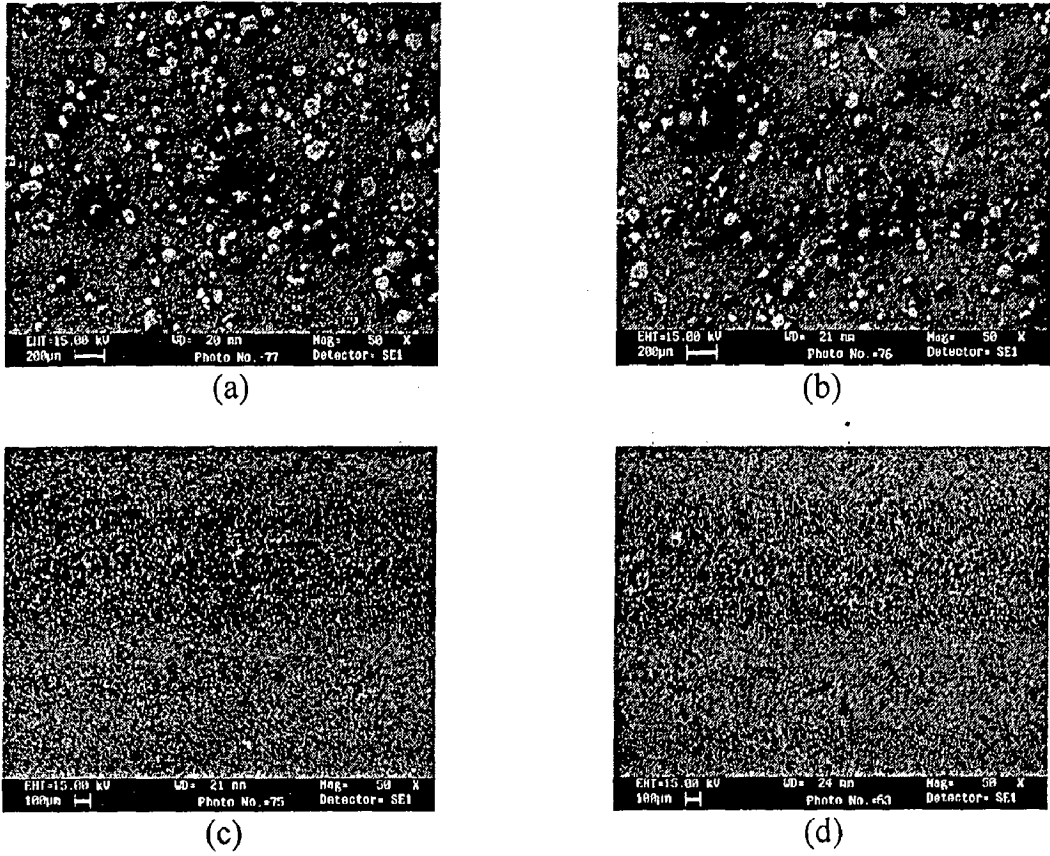
Fig. 5.48 SEM micrographs of 20Al/Al₂O₃ FGM ingot showing the variation of particle content along the radial direction from the centre towards the outer radius, at the base of the ingot.
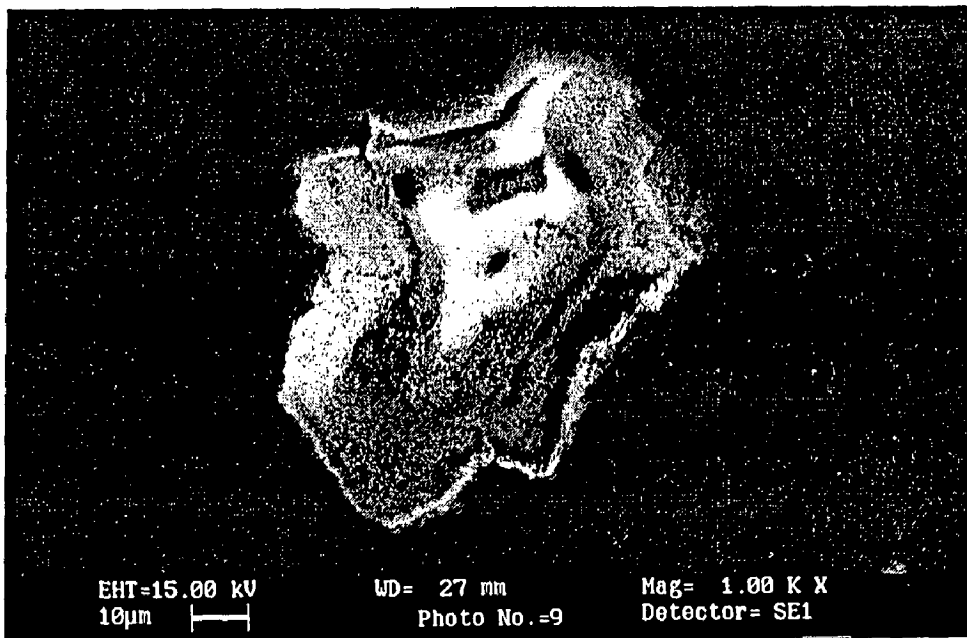
Fig. 5.49 SEM micrograph showing the nature of Al-Al₂O₃ interface of cast FGM ingot.

5.2 VARIATION OF VICKERS HARDNESS IN Al-Al₂O₃ FGM INGOTS

The variation of Vickers hardness with the distribution of alumina particles along the radial distance has been studied at different positions across the section of cast cylindrical FGM ingots. The Vickers Hardness distribution in the samples from as cast FGM ingots have been compared with those observed after annealing of samples. Figure 5.50 shows the results of variation of Vickers hardness along radial distances from the centre towards the outer radius at the top layer, middle layer and bottom layer of $10Al/Al_2O_3$ cast cylindrical FGM ingot, situated at 0 cm, 1.2 cm and 2.5 cm below the shrinkage cavity respectively. At a given height, higher hardness has been found near the centre and the hardness decreases gradually from the centre to the outer radius in both the as cast and annealed FGM. In general, higher hardness distribution has been observed at higher heights. It is also interesting to note that the particle free regions at higher heights have relatively higher hardness. The same trend of hardness variation as observed in cast FGM ingot are also observed along the radial distance in annealed ingot as shown in Figs. 5.51 to 5.53 for $10Al/Al_2O_3$ cast FGM ingot. However, at higher heights, there is larger difference between the hardness at the outer radius and that at the centre.

The variation of Vickers hardness along radial distances from the centre towards the outer radius of the top layer and the bottom layer of $15Al/Al_2O_3$ cast cylindrical FGM ingot, situated at 0 cm and 2.5 cm below the shrinkage cavity respectively, is shown in Fig. 5.54. Figures 5.55 and 5.56 show the separate results of Vickers hardness distribution along radial distances respectively at the top and the bottom of $15Al/Al_2O_3$ FGM ingot in both as cast and annealed condition. It is observed that relatively higher hardness value is observed at relatively higher heights of the cast ingot and after annealing the hardness is reduced. In annealed condition, FGM ingots show, in general, a relatively more smooth distribution of hardness along radial distances.

Figure 5.57 shows the results of variation of Vickers hardness along radial distances from the centre towards the outer radius for the top layer and bottom layer of $20Al/Al_2O_3$ cast cylindrical FGM ingot, situated at 0 cm and 2.5 cm below the shrinkage cavity respectively. Figures 5.58 and 5.59 show the separate results of Vickers hardness distribution along radial distances at different heights of $20Al/Al_2O_3$ FGM ingot in as cast as well as annealed conditions. Hardness decreases similarly as observed earlier when one moves from centre towards the outer radius of the ingot and there is a decrease in hardness under annealed condition although radial distribution of hardness remains similar to that in as cast condition.
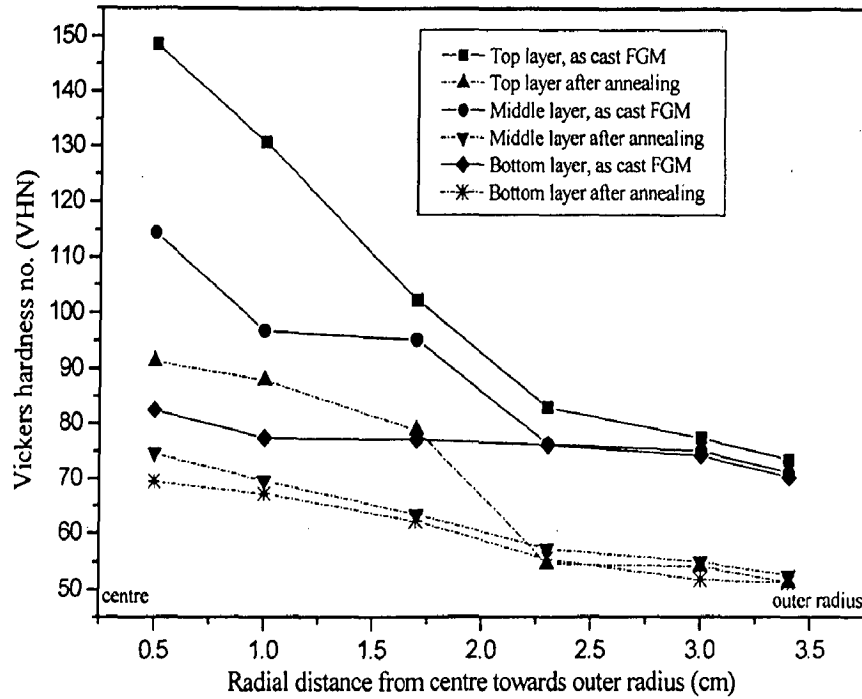
Fig. 5.50 The variation of hardness with increasing radial distance from the centre towards the outer radius at the top, middle and bottom layer, situated at 0 cm, 1.2 cm and 2.5 cm below the shrinkage cavity of $10Al/Al_2O_3$ FGM ingot.
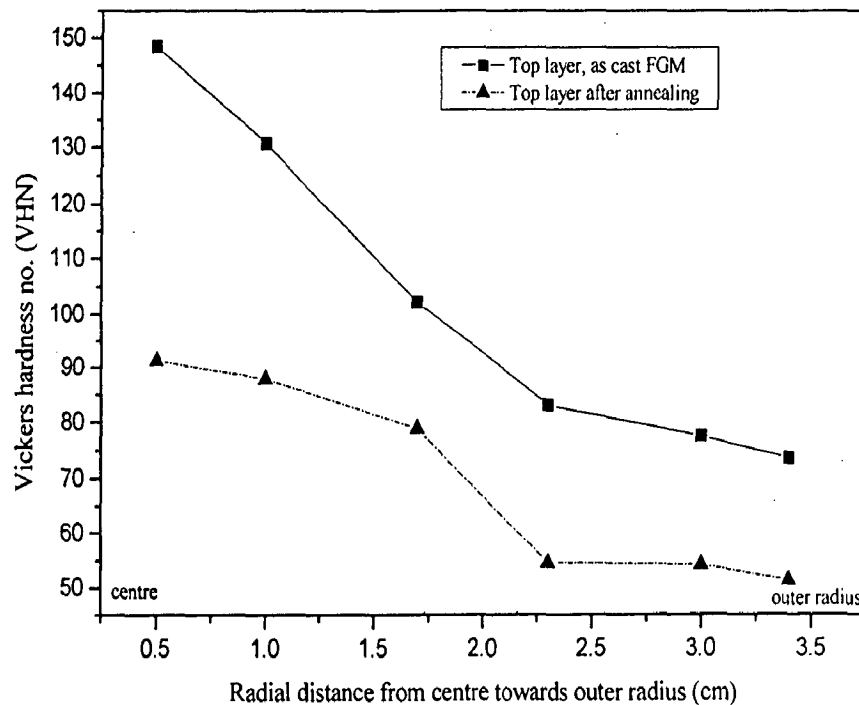
Fig. 5.51 The variation of hardness with increasing radial distance from the centre towards the outer radius at the top layer, situated below the shrinkage cavity of $10Al/Al_2O_3$ FGM ingot.
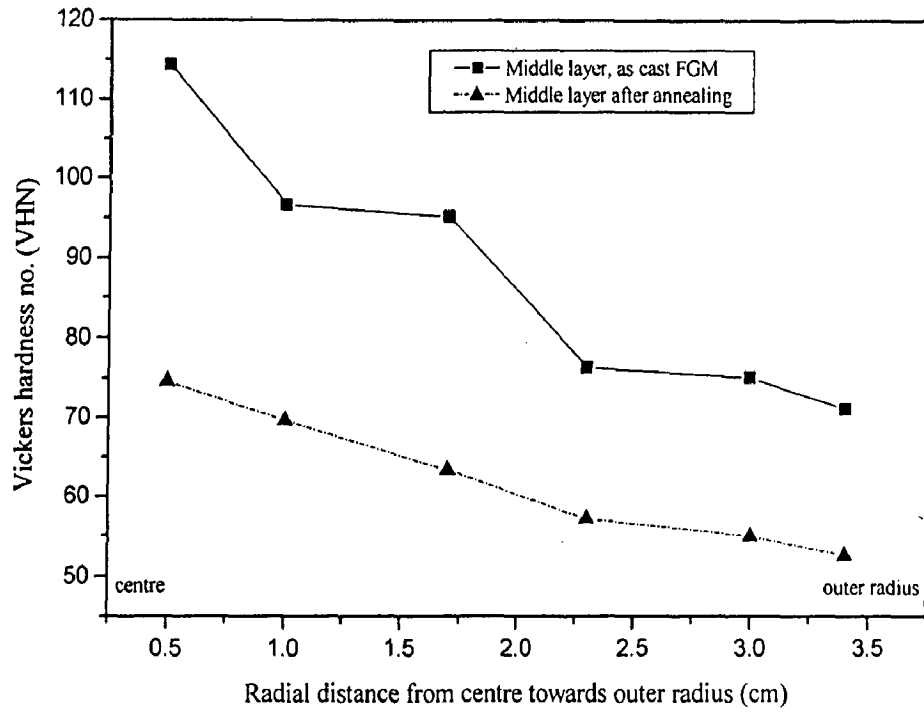
Fig. 5.52 The variation of hardness with increasing radial distance from the centre towards the outer radius at the middle layer, situated at 1.2 cm below the shrinkage cavity of $10Al/Al_2O_3$ FGM ingot.
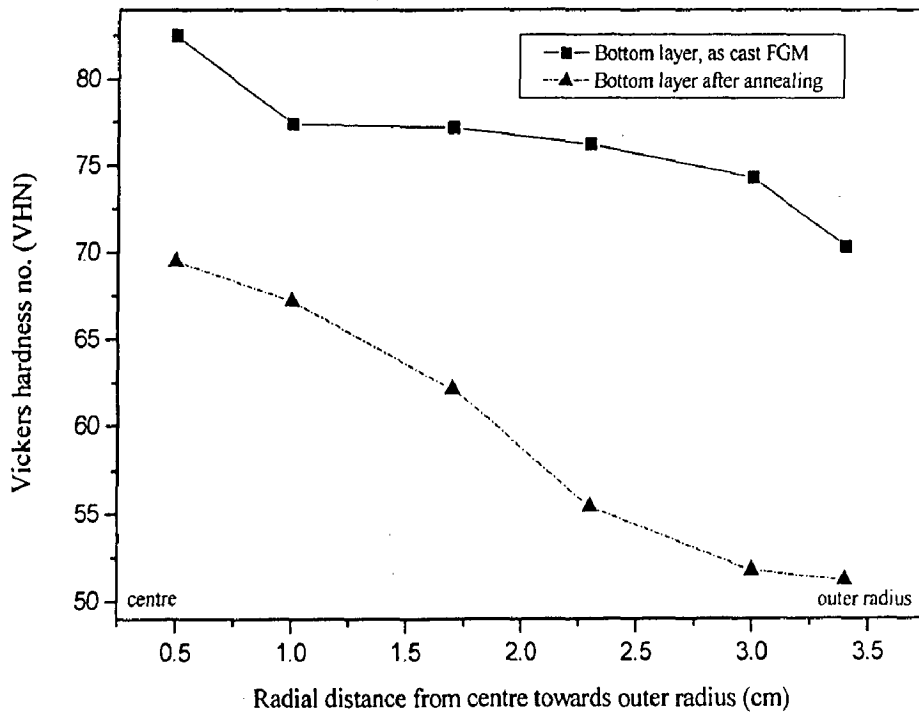
Fig. 5.53 The variation of hardness with increasing radial distance from the centre towards the outer radius at the bottom layer, situated at 2.5 cm below the shrinkage cavity of $10Al/Al_2O_3$ FGM ingot.

125
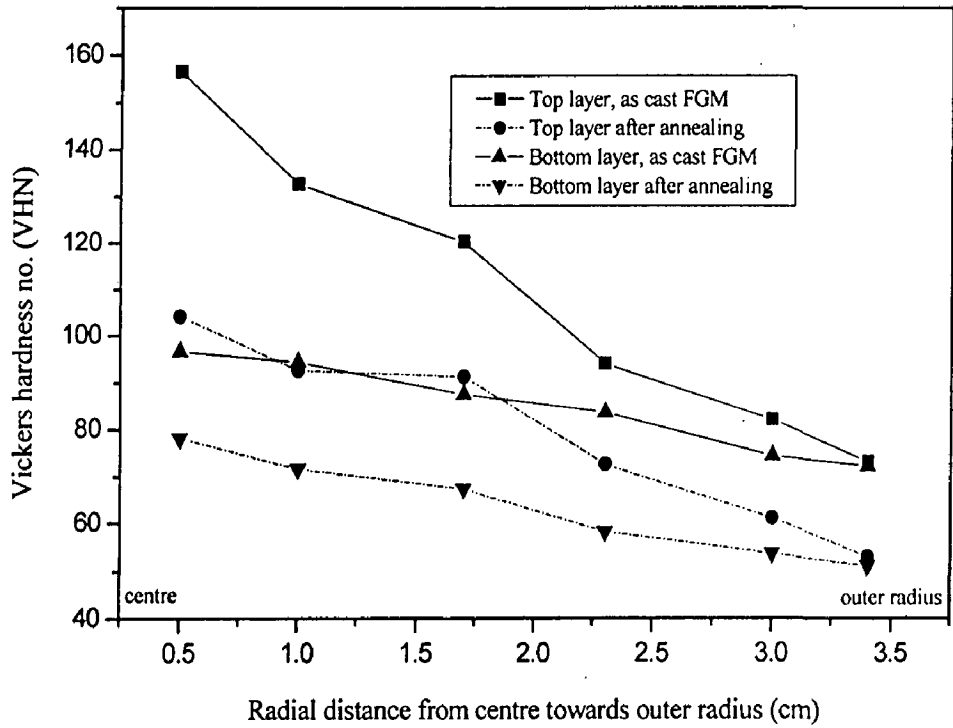
Fig. 5.54 The variation of hardness with increasing radial distance from the centre towards the outer radius at the top and bottom layer, situated at 0 cm and 2.5 cm below the shrinkage cavity of $15Al/Al_2O_3$ FGM ingot.
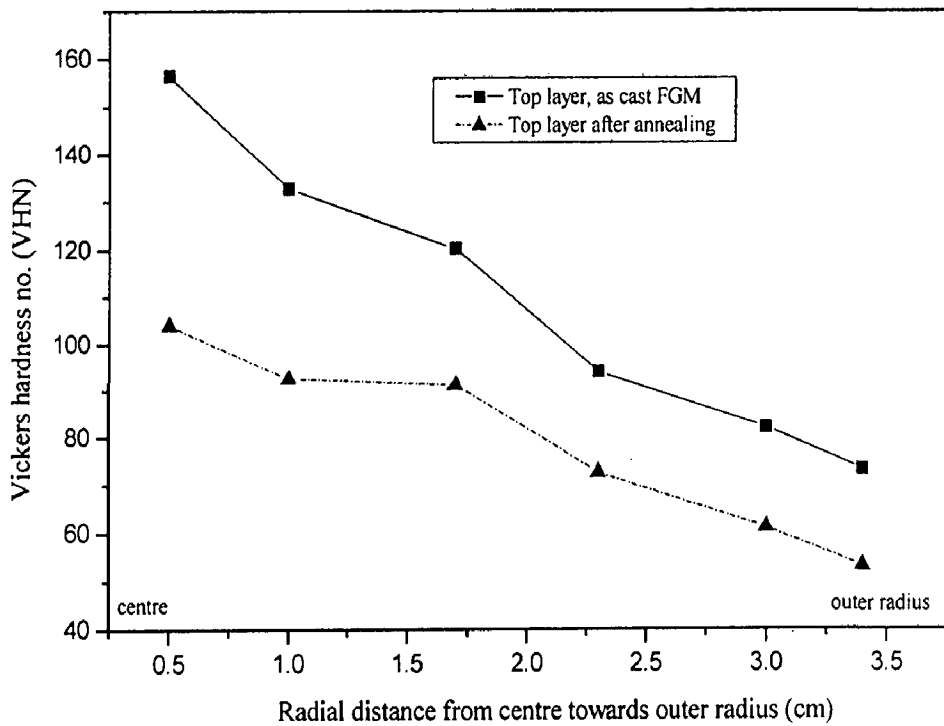
Fig. 5.55 The variation of hardness with increasing radial distance from the centre towards the outer radius at the top layer, situated below the shrinkage cavity of $15Al/Al_2O_3$ FGM ingot.
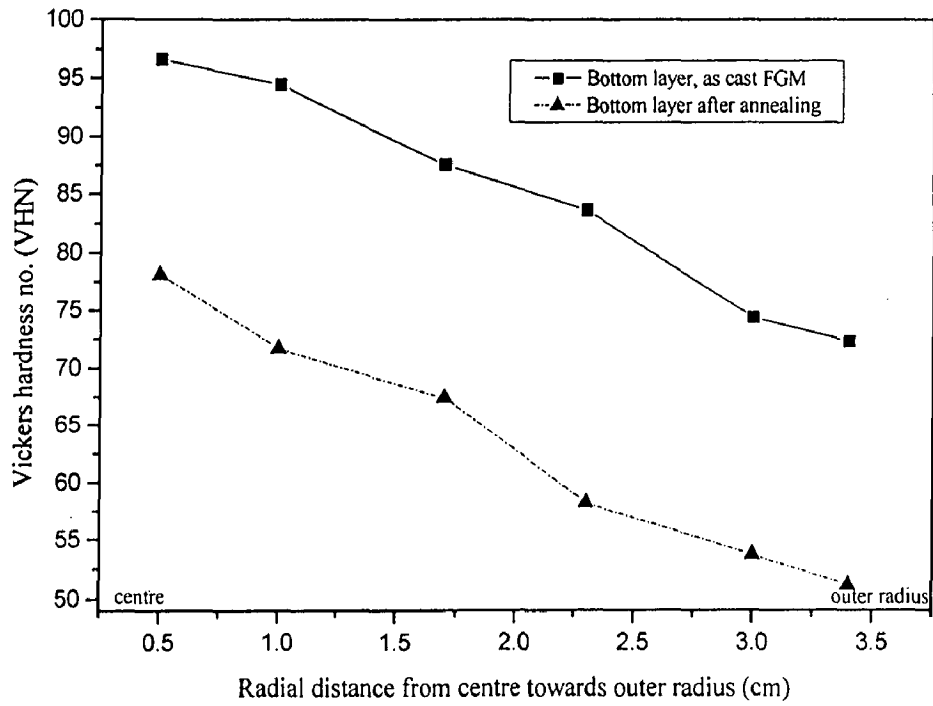
Fig. 5.56 The variation of hardness with increasing radial distance from the centre towards the outer radius at the bottom layer, situated at 2.5 cm below the shrinkage cavity of 15Al/Al₂O₃ FGM ingot.
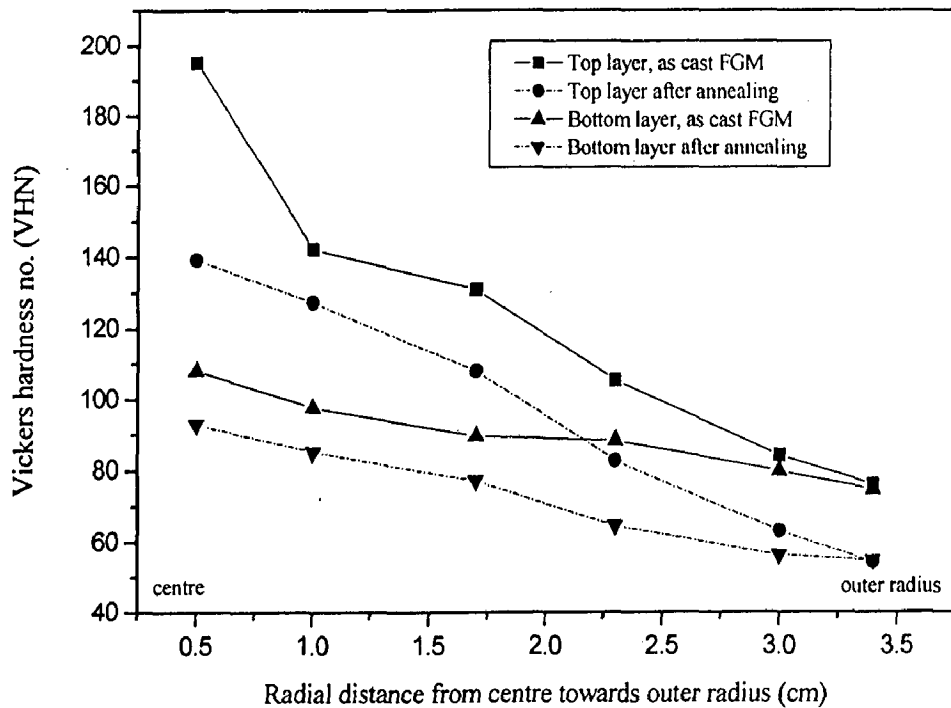
Fig. 5.57 The variation of hardness with increasing radial distance from the centre towards the outer radius at the top and bottom layer, situated at 0 cm and 2.5 cm below the shrinkage cavity of 20Al/Al₂O₃ FGM ingot.
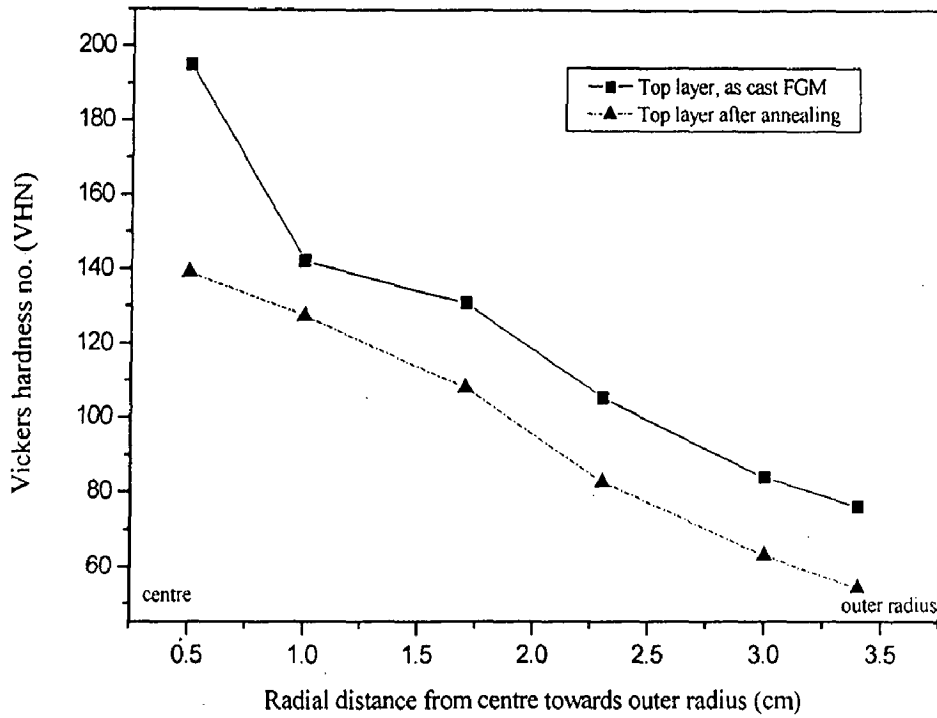
Fig. 5.58 The variation of hardness with increasing radial distance from the centre towards the outer radius at the top layer, situated below the shrinkage cavity of 20Al/Al$_2$O$_3$ FGM ingot.
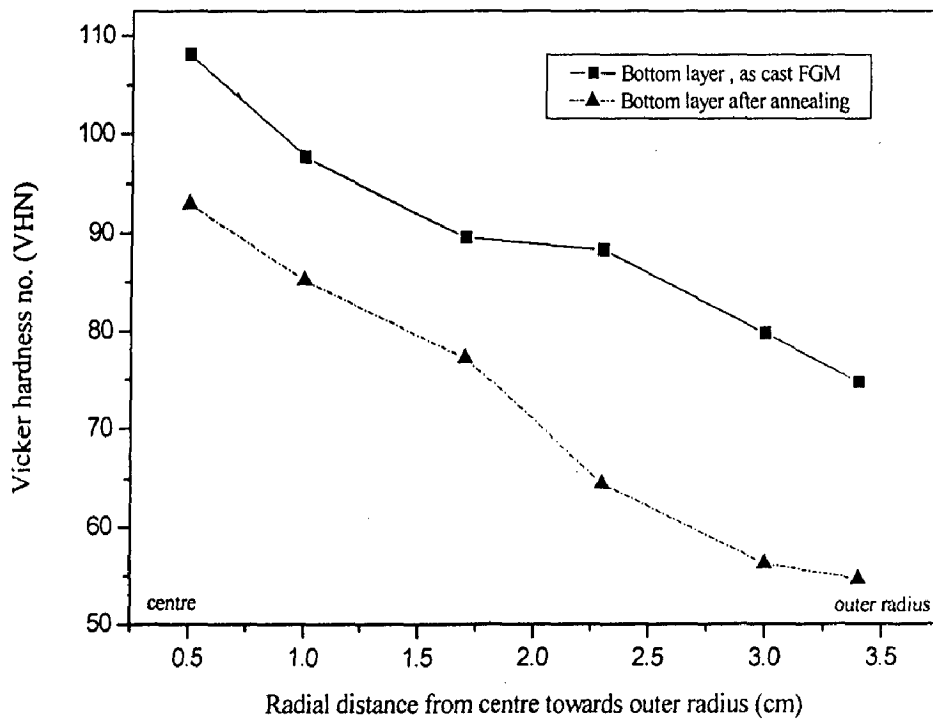
Fig. 5.59 The variation of hardness with increasing radial distance from the centre towards the outer radius at the bottom layer, situated at 2.5 cm below the shrinkage cavity of 20Al/Al$_2$O$_3$ FGM ingot.

5.3 DISCUSSION

The results of this study indicates that centrifugal casting techniques has been successfully used to synthesize Al and Al_2O_3 based Functionally Graded Materials (FGM) with the starting nominal weight percentage of alumina particles ranging from 10 to 20 %. From the micrographs and the graphical representation of alumina content, it has been observed that alumina content decreases gradually as one move from the centre towards the outer radius of the ingot at all the heights investigated. The progressive decrease in alumina content from the centre towards the outer wall is not in agreement with the theory that the higher centrifugal force acting on relatively denser alumina particles during rotation will force them relatively towards the outer wall leaving behind the lighter aluminium melt. It is also observed, as one moves down from the top to the bottom of cast ingot the alumina content decreases. This is also surprising in view of higher density of alumina particles relative to the melt.

It has been observed in the past that the particles are often associated with bubbles inside the melt. The bubbles generally originate from simultaneous suction of bubbles and particles at the bottom of vortex during particle transfer into the melt by stirring. It is also possible that the bubbles may have arisen due to expansion of gases in the crevices of irregular particles when relatively cold particles are incorporated in the melt. For this reason, one often observes cluster of particles inside pores in cast ingots of uniform composite (Ghosh and Ray, 1986).

It is apparent that the particles, in spite of addition of magnesium, have poor wettability and it makes bubble-particle detachment difficult. But clusters of particles inside pores have not been commonly observed in the cast FGM ingots synthesized in this study, as evident from optical micrographs. It is possible that centrifugal force acting on the bubble-particle combinations has helped detachment of the bubble-particle combinations from other bubble particle combinations, but the centrifugal force was not enough to detach particles from bubbles. The fact that at higher heights from the bottom, a larger amount of alumina is observed could be attributed to flotation of the bubble-particle combine due to its low density. It has been observed that at low rotational speeds during centrifugal casting the centrifugal force is not enough to detach bubble-particle combination and the effective particle density is lower than its actual density. The low effective density of bubble-particle combination results in particle distribution and

hardness decreasing radially from the centre to outer wall and axially from top to the bottom of the ingot.

From Figs. 5.50 to 5.59, it has been observed that at a given height, higher hardness has been found near the centre and the hardness decreases gradually from the centre towards the outer radius, following the general trend of variation of particle distribution as described above. The variation of hardness along radial distance at different heights follows the particle distribution, in general. However, there are local irregular changes in hardness which could be attributed to inhomogeneous matrix of cast ingots. The FGM ingots have been annealed to eliminate the effect of inhomogeneous cast structure of the matrix and it is observed that the hardness distribution has become much smooth in general although the hardness values have decreased.

RESULTS AND DISCUSSION: MODELLING

6.1 RESULTS AND DISCUSSION: UNIFORM COMPOSITES

The results for the modulus of elasticity have been obtained for uniform composites containing different amount of alumina particles. Results for modulus of elasticity for uniform composites with average particle contents varying from 10 vol% to 90 vol% in a step of 10 vol% have been obtained. The uniformly distributed particulate composite is isotropic at the macroscopic level. Hence, the modulus of elasticity obtained in any direction should be the same. In the present work y-axis direction has been chosen for uniaxial loading and for the determination of modulus of elasticity. At the outset, the effect of random distribution of particles on the modulus of elasticity for uniform composite models has been investigated. For this purpose, three different random distributions of particles have been realized for the same uniform composite by generating the random numbers independently for each distribution. Numerical results for models of uniform composite with randomly distributed particles containing particle contents from 10 vol% to 90 vol% in a step of 10 vol% have been obtained with each set of random numbers.

Figure 6.1 shows the variation of modulus of elasticity with particle content in uniform composites for three different distributions realized by generating three different sets of random numbers. From Fig. 6.1 it is evident that there is no significant difference in the observed values of modulus of elasticity for the three different sets of random numbers generated for each given particle content over the entire range of particle content in the model of uniform composites. The results for the modulus of elasticity indicate that though there may be variation in particle distribution locally for different sets of random numbers generated leading to difference in material properties locally at the micro level but the properties at the global level remain the same for a given average volume fraction of particles, so long as the particles of the same size are distributed randomly in the uniform composite. It also validates the use of a domain size of 5 mm x 5 mm for getting

getting the global properties of the composite. For composite samples of the size taken in the present study or bigger, random distribution of particles produces same macroscopic properties irrespective of the local variation in particle positions in different composite models due to the random distribution of particles. It is also quite natural for the real composite samples. The location of particles will be different in the different samples but at the global scale, they show almost the same mechanical properties.

The results for modulus of elasticity of the present modelling technique have been compared with the well established rule of mixture (ROM) and inverse rule of mixture (IROM). ROM and IROM may be assumed as the most conservative upper and lower bounds for the modulus of elasticity for uniform composites. Figure 6.2 shows the modulus of elasticity variation with particle vol% obtained from the present model and its comparison with ROM and IROM and it clearly indicates that the results of the present modelling technique are well within the bounds of rule of mixture (ROM) and inverse rule of mixture (IROM) results.

The results predicted by the present model for modulus of elasticity have also been compared with the well known Hashim-Shtrikman (1963) bounds. Hashim-Shtrikman (1963) has given bounds for shear and bulk modulus of a two phase composite material. With the results for shear modulus and bulk modulus the results for modulus of elasticity may be obtained for uniform composites. Figure 6.3 shows that the results for modulus of elasticity obtained from the Hashim-Shtrikman (1963) bounds over the entire range of particle content. The results from the present modelling technique are also presented in the same figure. The results from the present modelling technique are well within the Hashim-Shtrikman bounds as shown in Fig. 6.3.

The present model results for modulus of elasticity have also been compared with those given by Halpin–Tsai (1969) equation. It has been established in the past that Halpin-Tsai equation with ζ equal to 2 may be used to predict modulus of elasticity for most of the practical composite materials with good accuracy. Figure 6.4 shows the results for the modulus of elasticity obtained from Halpin-Tsai equation along with the results of the present work and it may be concluded that the present model results are in good agreement with the Halpin–Tsai equation results with $\zeta = 2$.
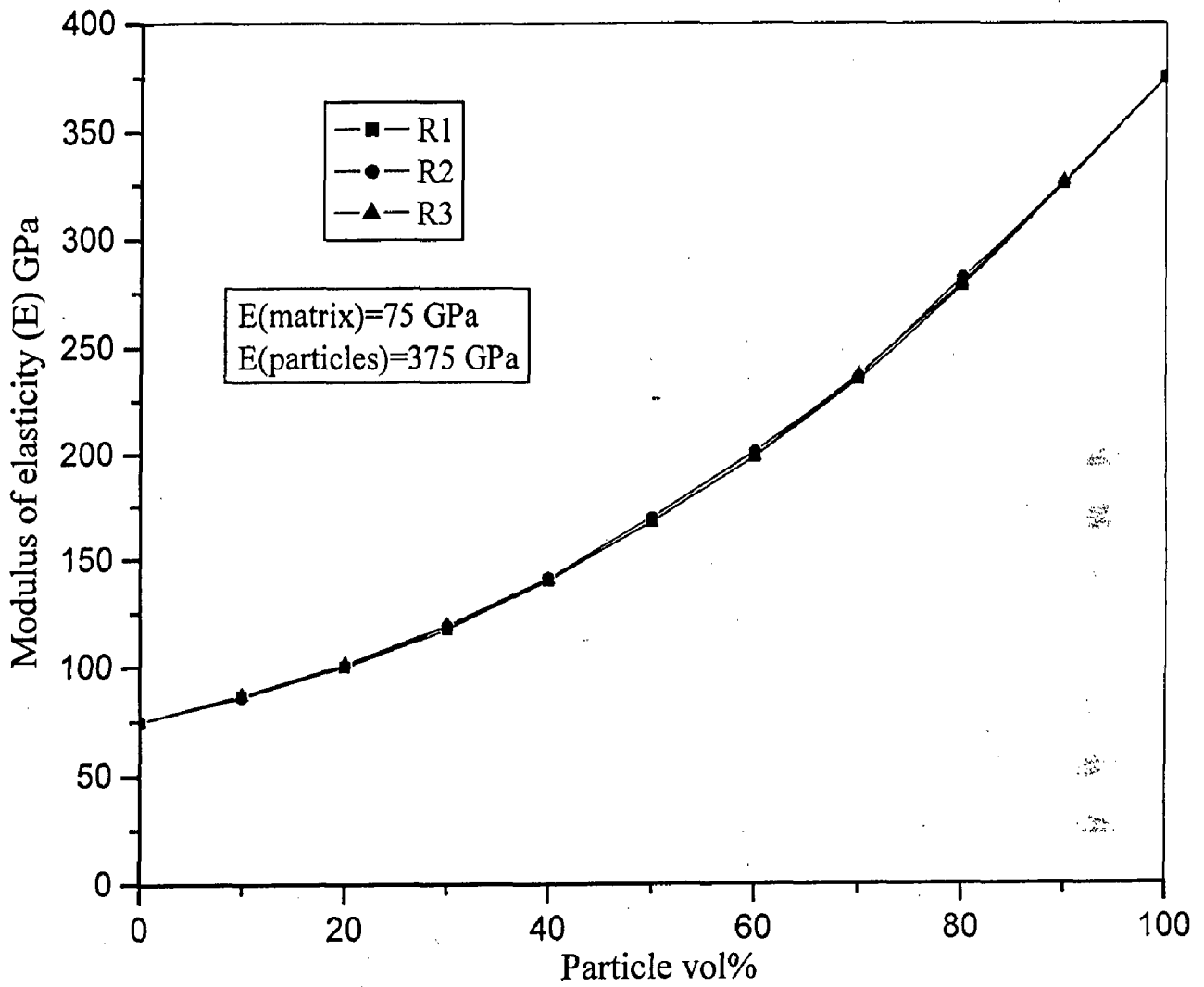
Fig. 6.1 Variation of modulus of elasticity with increasing particle contents in models of uniform composites as obtained with three different particle distributions generated by three different sets of random numbers (R1, R2 and R3).
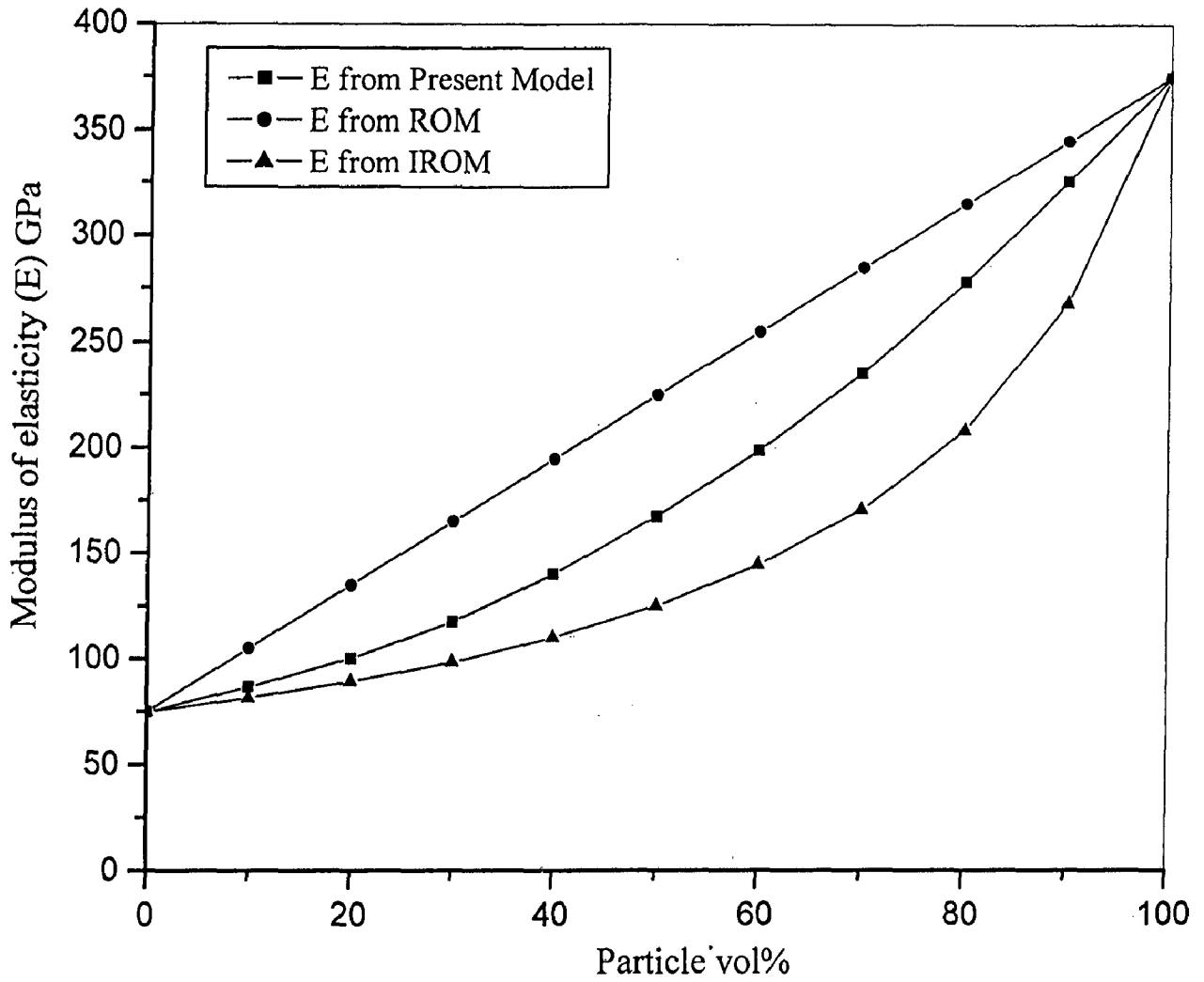
Fig. 6.2 Results for modulus of elasticity for the present model of composite with different average particle contents and their comparison with those estimated by rule of mixture and inverse rule of mixture.

134
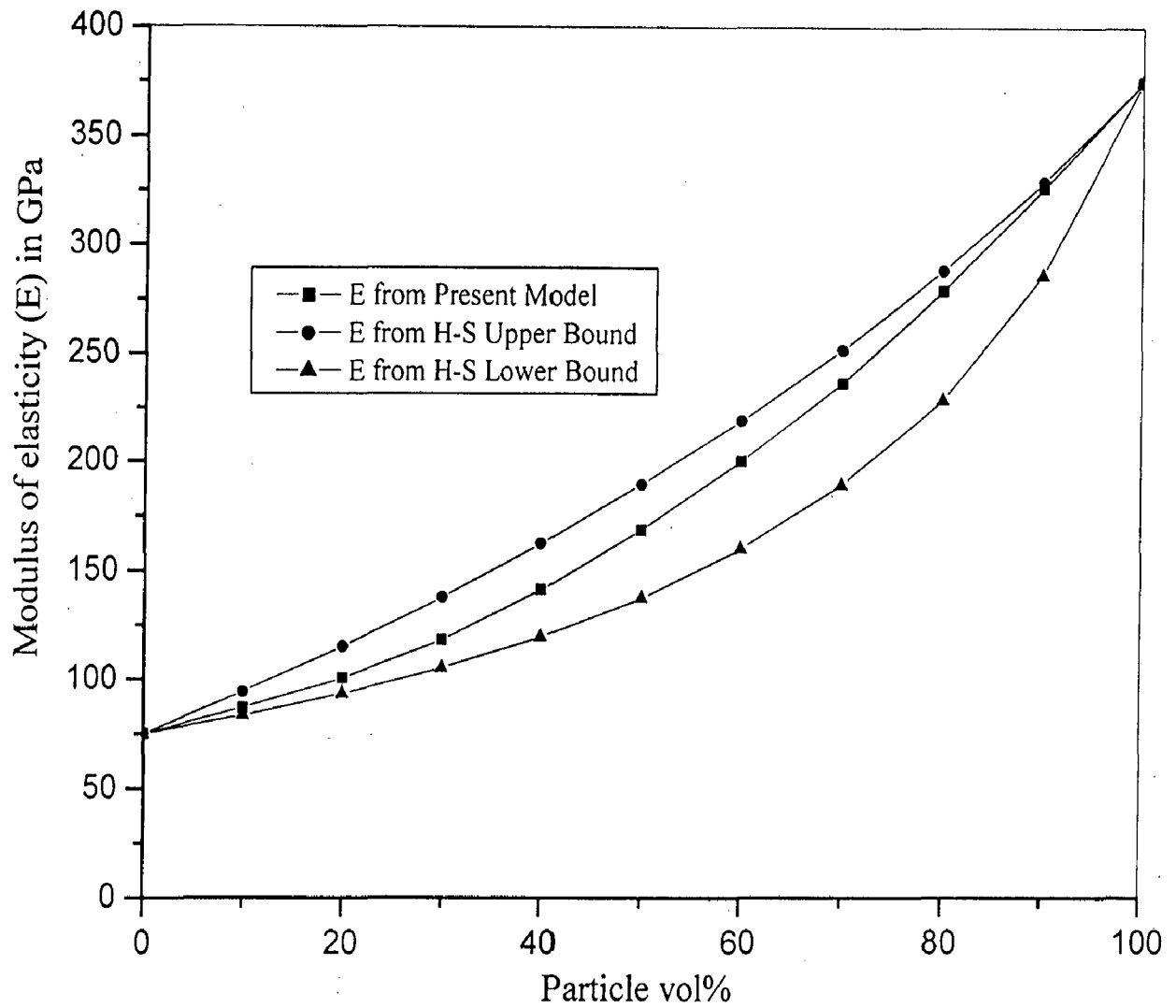
Fig. 6.3 Results for modulus of elasticity from the present model and their comparison with Hashim-Shtrikman (H-S) upper and lower bounds (Hashim-Shtrikman, 1963) for different average particle contents.
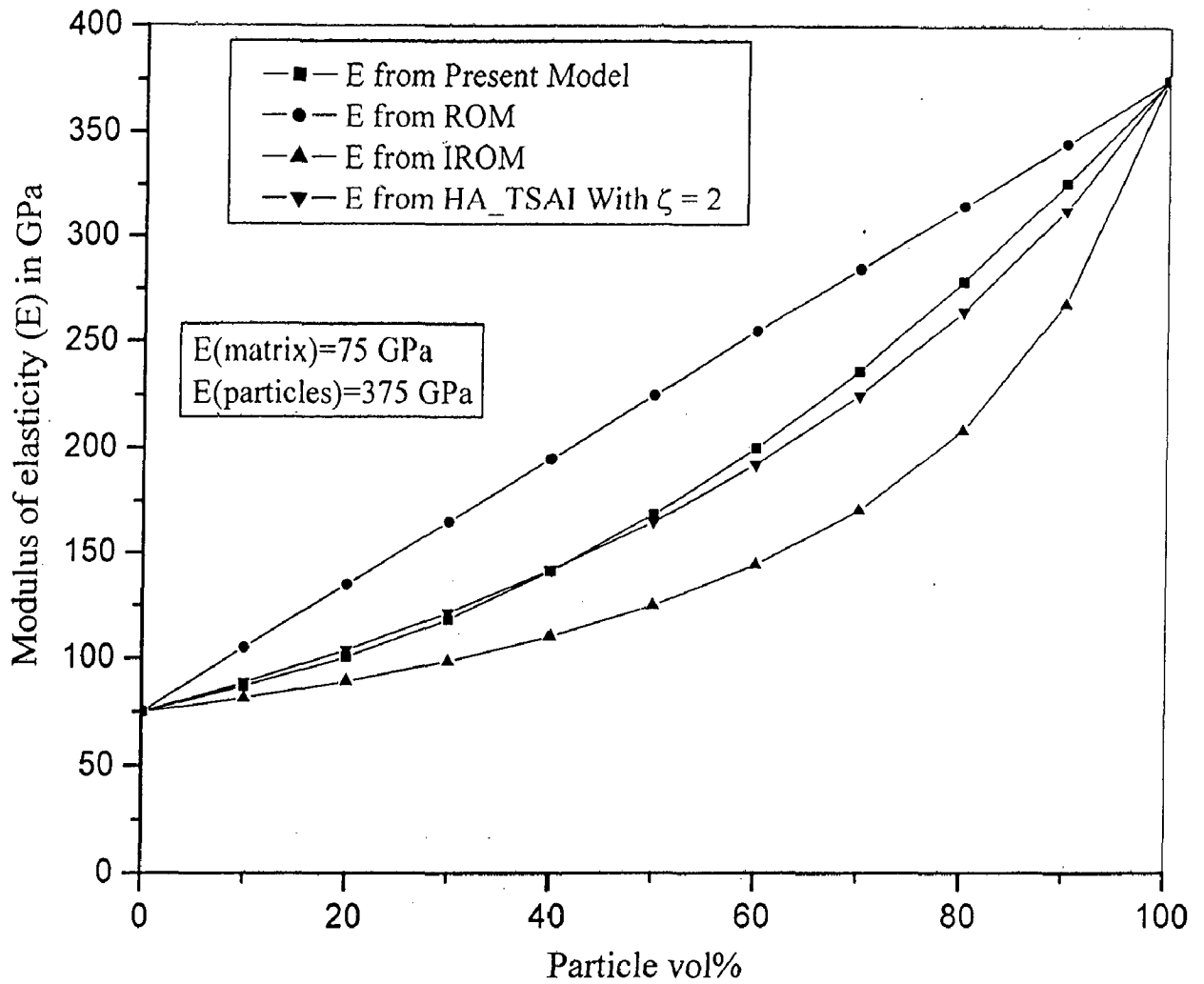
Fig. 6.4 Results for modulus of elasticity from the Halpin-Tsai (HA-TSAI) equation (Halpin-Tsai, 1968) with $\zeta = 2$ and its comparison with the results of the present model, rule of mixture (ROM) and inverse rule of mixture (IROM) for composites with different particle contents.

The present model results for modulus of elasticity are also compared with those given by Aradhya and Surappa (1991) with their model and experimental work for aluminium matrix composite reinforced with SiC particles. Figure 6.5 shows the results given by Aradhya and Surappa (1991) for modulus of elasticity of aluminium matrix composite reinforced with SiC particles obtained from their experimental work and model. The results obtained from Halpin-Tsai (1968) equation are also presented in the same figure. The present model results with similar material properties are also presented in the same figure. It has been observed that the present model results are in better agreement with the experimental results given by Aradhya and Surappa (1991) as well as Halpin-Tsai (1968) equation but slightly higher than the results of FEM model of Aradhya and Surappa (1991).

The results of the present modelling technique have been represented by the following simple equation for particle volume fraction upto 40% with reasonable accuracy.

$$E_c = V_f \times E_{rom} + (1 - V_f) \times E_{irom}$$ (6.1)

where, E_c = modulus of elasticity for composite

V_f = Particle volume fraction

E_{rom} = modulus of elasticity from rule of mixture

E_{irom} = modulus of elasticity from inverse rule of mixture

Equation 6.1 may be used for quick estimation of modulus of elasticity for particle reinforced composites up to 40 vol% of particles with good accuracy. Figure 6.6 shows the modulus of elasticity results from the Eq. 6.1 for different average particle contents and their comparison with the present model results.

Results for modulus of rigidity for the uniform composite models with different average particle contents have also been obtained. For this purpose, a shear load is applied on the model and on the basis of shear stress and shear strain averaged over all the elements, the modulus of rigidity results have been obtained. Figure 6.7 shows the results for variation of modulus of rigidity with increasing average particle content as estimated from the present model. Figure 6.7 also shows the modulus of rigidity variation estimated by rule of mixture (ROM) and inverse rule of mixture (IROM).The modulus of rigidity results obtained with Hashim's upper and lower bounds have also been presented in the same graph. Figure 6.7 indicates that the results for the modulus of rigidity with the present modelling technique are well within the bounds of rule of mixture and inverse rule of mixture and also within the bounds given by Hashim-Shtrikman (1963).

137

Non linear analysis has been performed on the present model to predict nonlinear deformation behaviour of the uniform composites. All the nodes at y = 0 are kept fixed and all the nodes at y = 5 mm were subjected to uniform displacement u_y = 0.01 mm so as to give the specimen a maximum strain of 0.002. This displacement is applied in 20 steps and the results for each step are noted. After each step loading, stress in each element is found out. If an element having matrix material properties is found to have yielded, the stress in that particular element is not increased any further and the element does not take any further load. To decide yielding of an element von Mises criterion of failure is used.

The stress distribution within the composite has considerable variation depending upon local particle distribution. The maximum stress in y-axis direction inside the uniform composite with a given particle content increases with increasing applied strain and also, for a given strain the maximum stress increases with increasing particle content as shown in Fig. 6.8(a). It is interesting that the maximum stress behaves nonlinearly which indicates plastic deformation in the local region. The range between maximum and minimum stresses at a given strain in a uniform composite with a given particle content also increases with increasing strain and attains fairly high values as given in Fig. 6.8(b). The stress distribution in even uniform composites is highly non-uniform and the range increases with particle content in the composite. The mean stress has also been included in Fig. 6.8(b) for comparison and to show that the range is often considerably larger than the mean, particularly at higher strain and higher particle content.

The average of elemental stresses and strains of all the elements in y-axis direction for each step are plotted to show the global nonlinear behaviour of uniform composites. Figure 6.9 shows the non linear global deformation behaviour of the model of uniform composites over the entire range of particle content and it clearly shows the transition from elastic to plastic region at a critical strain, which decreases with increasing particle content in the composite. The strain required for transition from elastic to plastic region for uniform composites with different particle contents is shown in Fig. 6.10. Similar results have been obtained by Bao and coworkers (1991) with their unit cell model.

The yield stress is one of the most important design parameter for any engineering component. In the present work yield stresses for the nonlinear model of composites with different average particle contents are obtained by the crossover method. In this method the stress at the point where the tangent of the plastic region intersects the tangent of elastic region is taken as the yield stress.
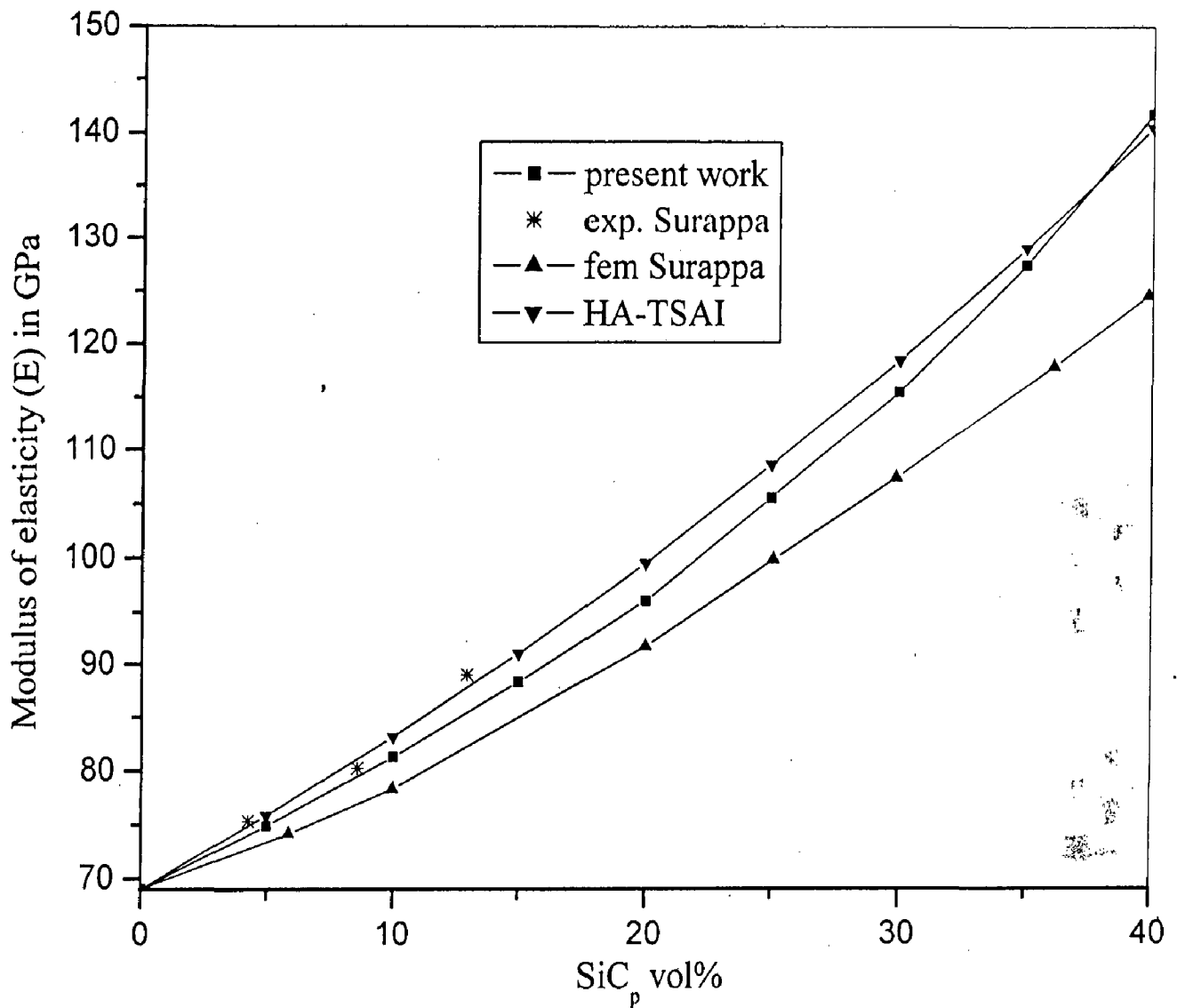
Fig. 6.5 Modulus of elasticity results for aluminium matrix composites reinforced with SiC particles given by Aradhya and Surappa (1991) from their experiments and modelling, and their comparison with those from the present model for Al-SiC composites and from Halpin-Tsai (HA-TSAI) equation (Halpin-Tsai, 1968) with $\zeta = 2$.
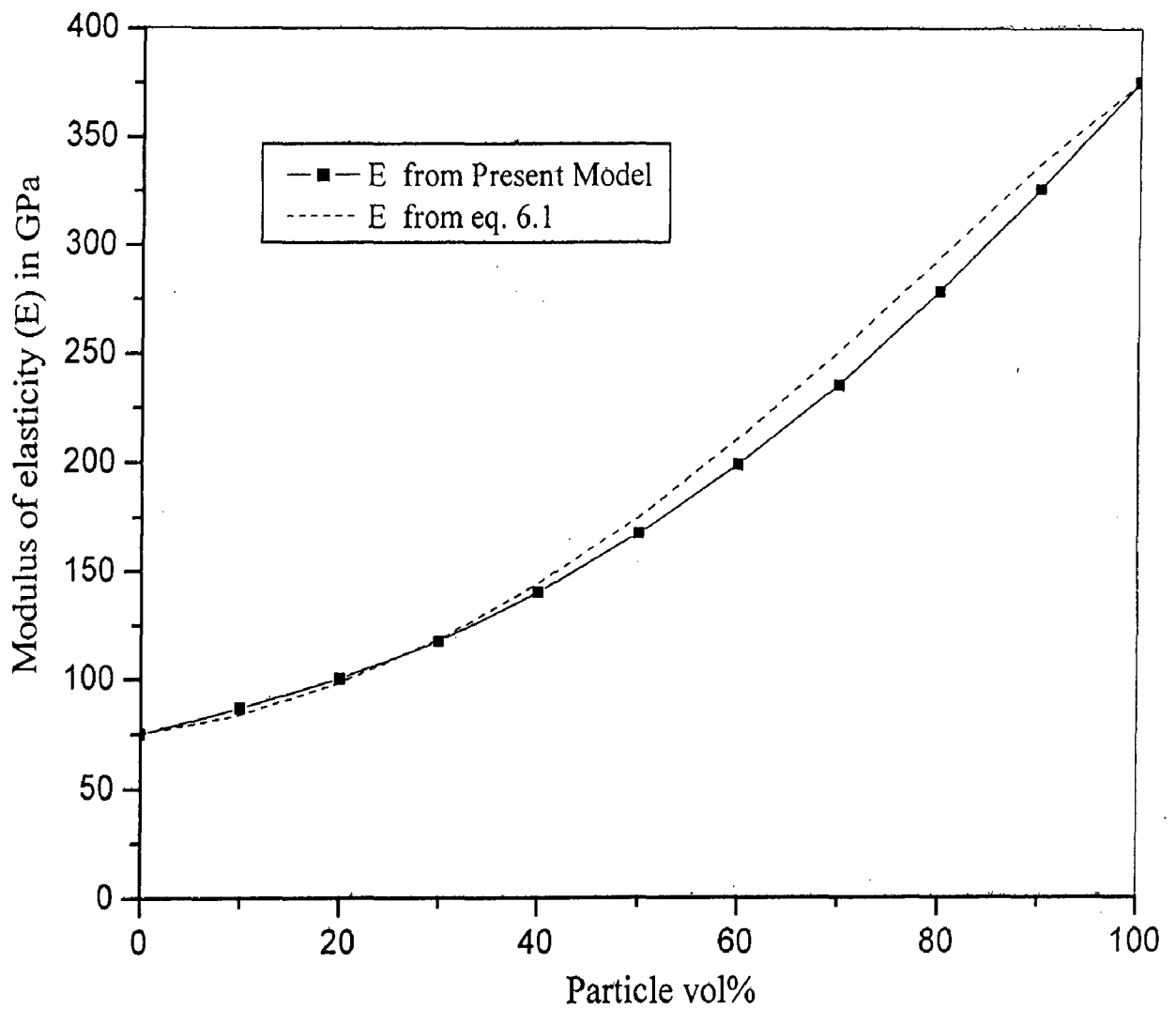
Fig. 6.6   Results for modulus of elasticity from the equation proposed from the results of present modelling technique.

140
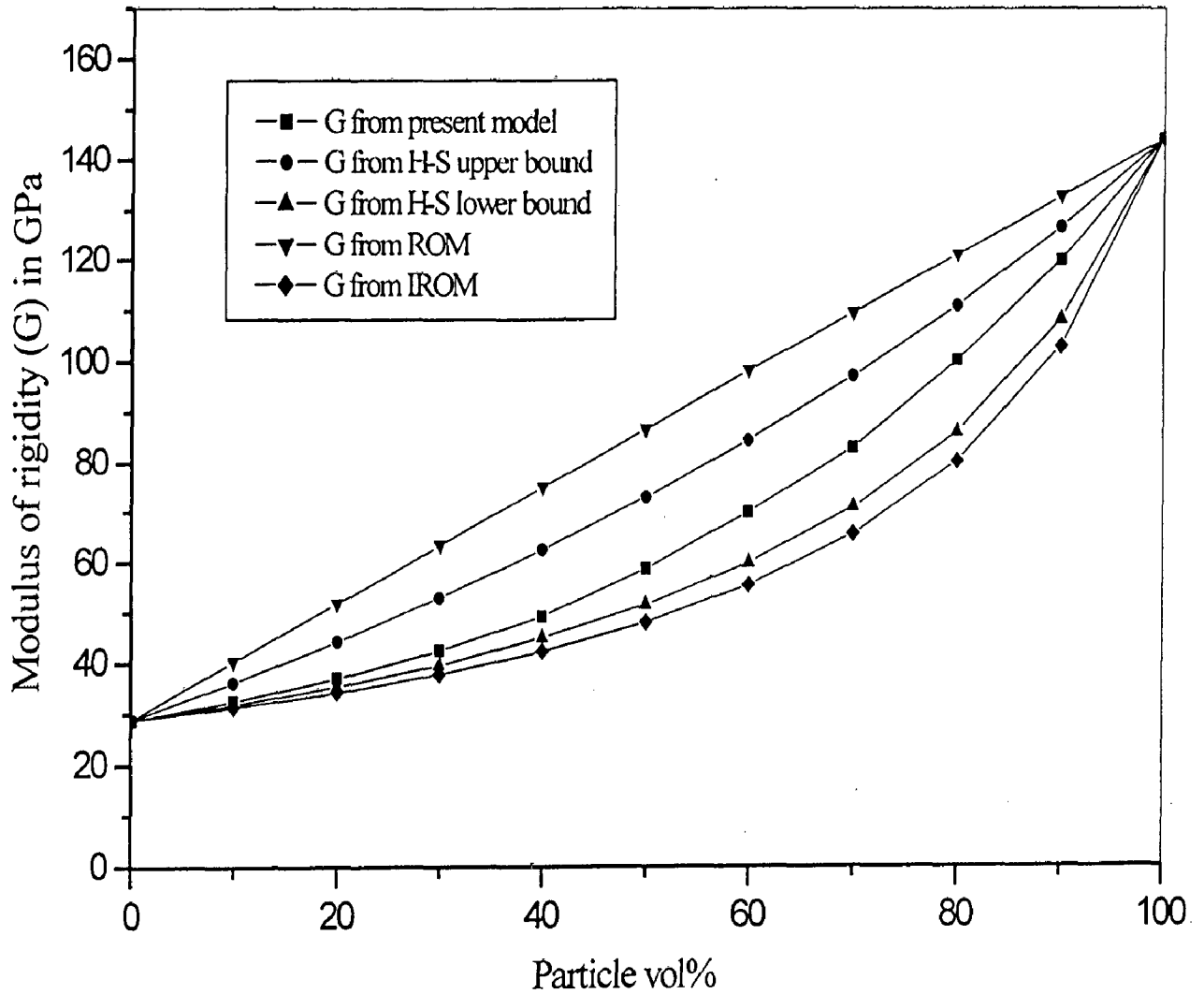
Fig. 6.7   Results for modulus of rigidity obtained from the present model for composites having different particle contents and their comparison with the estimates of Hashim-Shtrikman (H-S) bounds, rule of mixture (ROM) and inverse rule of mixture (IROM).

141
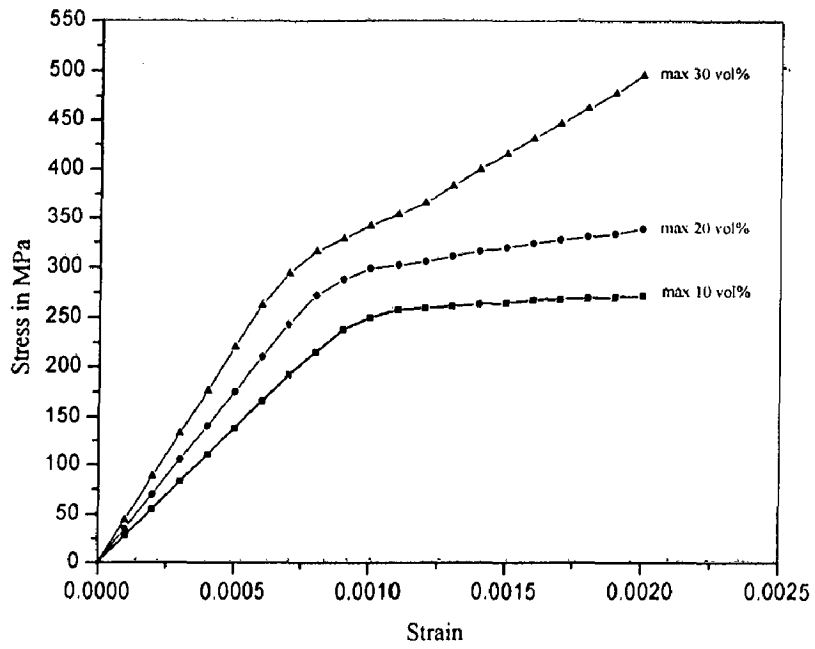
(a)
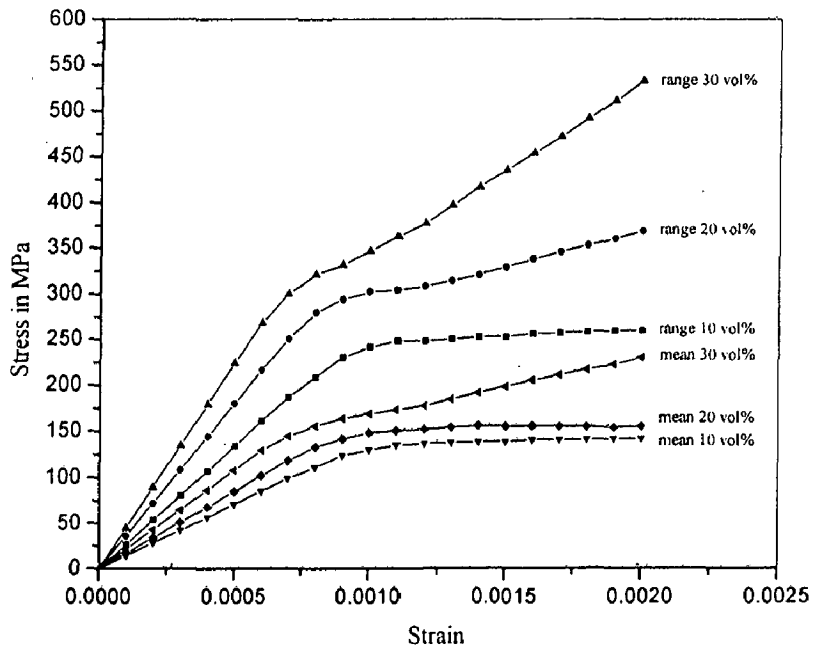
(b)

Fig. 6.8a,b The variation of stress within the uniform composite at different applied strains in terms of (a) maximum strain for different average particle content and (b) mean and range of the stress variations for the same particle contents.
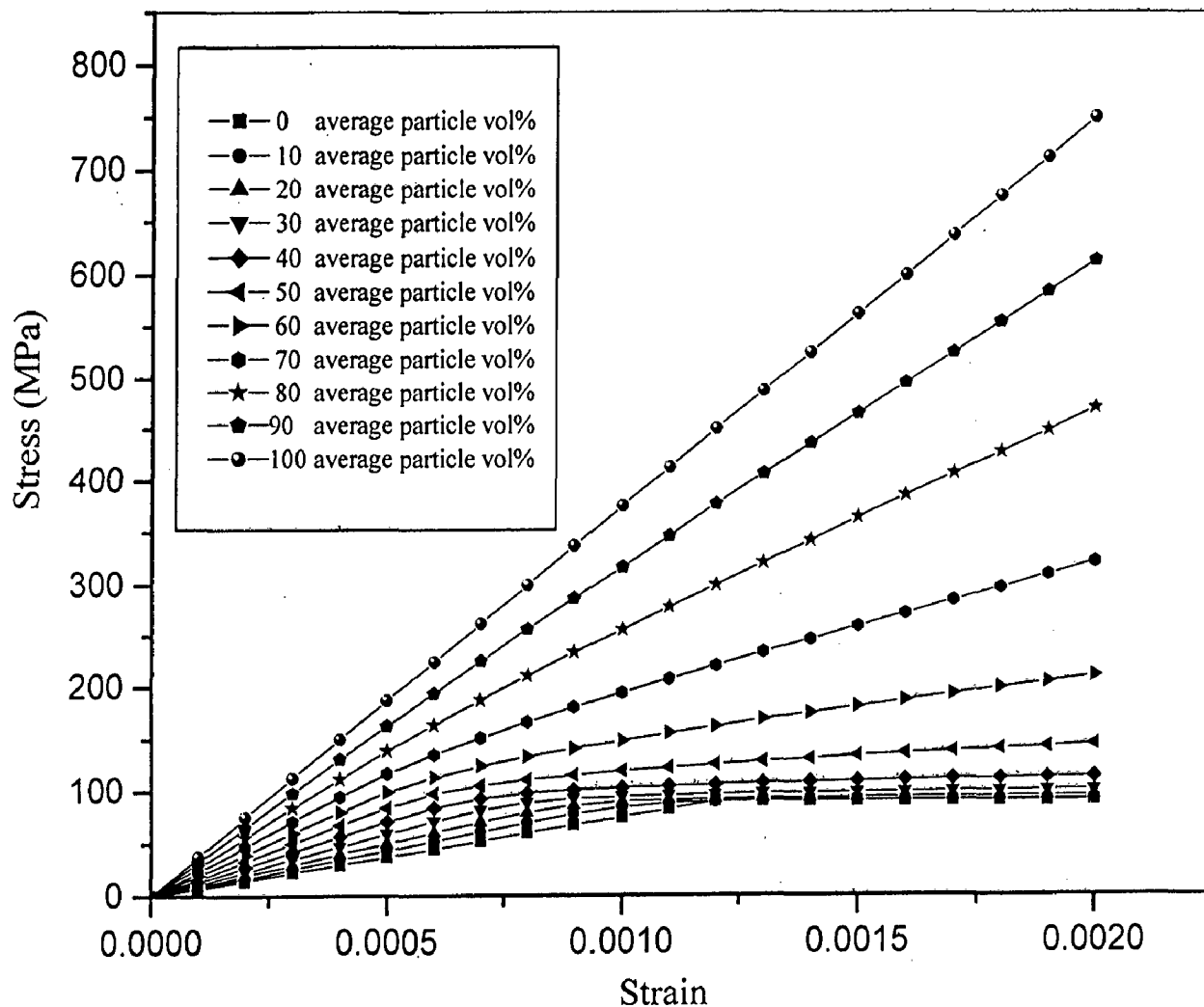
Fig. 6.9 Results for nonlinear behaviour of uniform composites with different average particle contents obtained from the nonlinear model used in the present study.
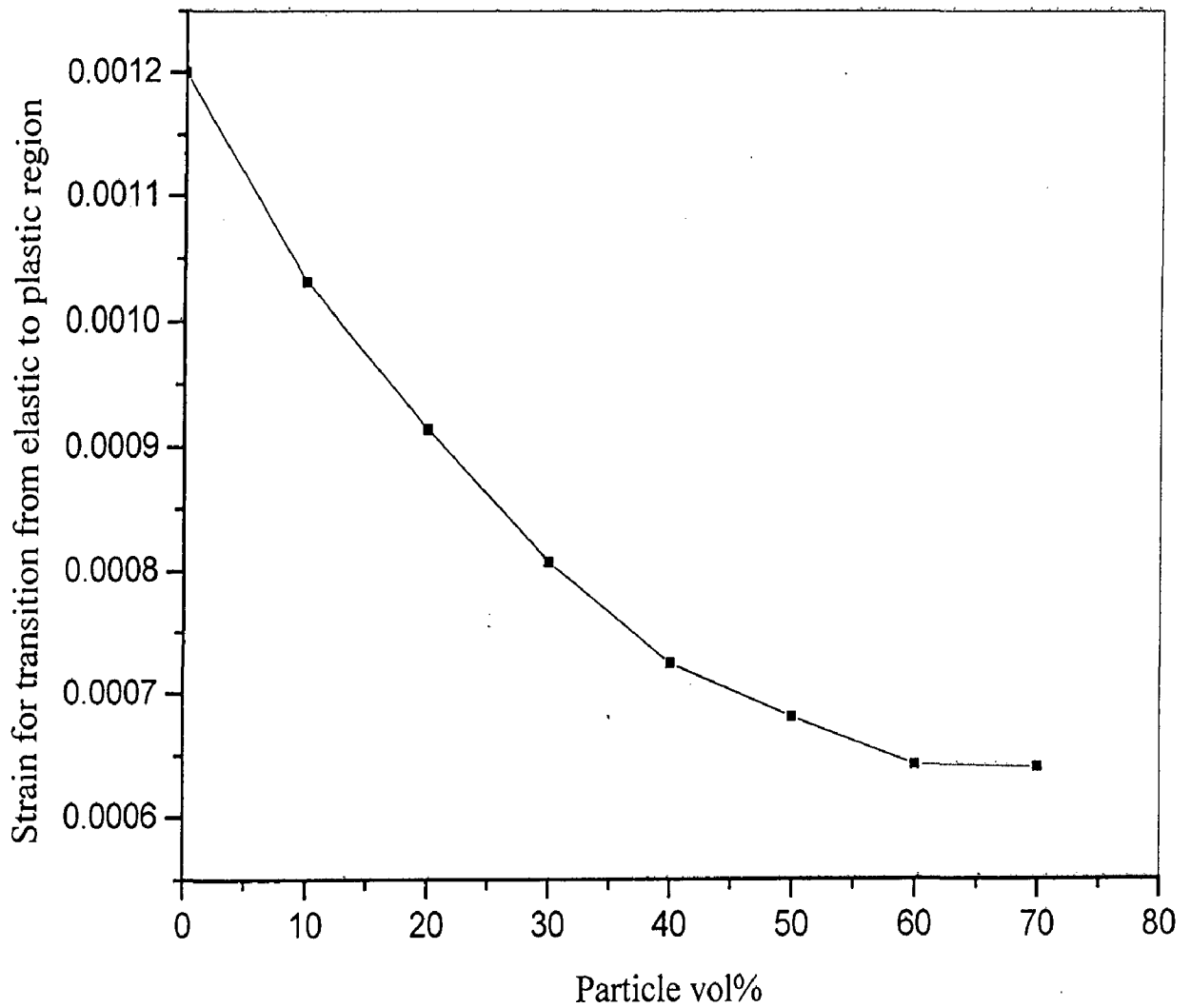
Fig. 6.10 Strain required for transition from elastic to plastic region for uniform composites with different particle contents.

144

With the help of curve fitting an empirical relation, Eq. 6.2, between the particle volume fractions and the yield stress have been found to obey the results of the present modelling technique fairly well and so, could be used to find out the yield stress for a uniform composite with a given particle volume fraction following the present modelling technique.

$$\frac{Y_c}{Y_m} = 1 + \alpha \, (V_f)^3 \qquad (6.2)$$

where, Y_c = yield stress of the composite at particle volume fraction V_f.

Y_m = yield stress at no particles i.e. the yield stress of the matrix.

α = a constant, its value is 2.1 for the present model results.

V_f = average particle volume fraction.

Figure 6.11 shows the variation of the yield stress with particle vol% for uniform composites as obtained from the present model and compares them with the results from the Eq. 6.2. It is obvious that the Eq. 6.2 may be used for a quick estimation of the yield stress of the particle reinforced composite with randomly distributed particles for the whole range of the average particle content following the present modelling method. This equation predicts the results of the present model with reasonable accuracy.

Bao and coworkers (1991) in their work have made a theoretical investigation of the role of non-deforming particles in reinforcing ductile matrix materials against plastic flow. They have used a unit cell model to find the elastic-plastic response of metal matrix composites. They have studied the variation of the ratio of flow stress of composite (σ_{oc}) to that of the same matrix (σ_o) with particle content under plane strain conditions. To compare the predictions of the present work with Bao and coworkers (1991), results are obtained for the present model under plain strain conditions. Figure 6.12 shows the comparison of the results of Bao and coworkers (1991) with the results of the present model. It is observed that for lower volume fraction both the models give quite similar results. But for the higher volume fractions of particle in composite, the results of the present model give relatively higher estimates for the flow stress ratio. The results of the present model may be closer to reality in view of the clustering of the particles, which takes place at higher volume fractions. The clustering of the particles causes a rapid increase in the limit flow stress of the composites at higher particle volume fractions and the unit cell model of Bao and coworkers (1991) does not accommodate such clustering.

145
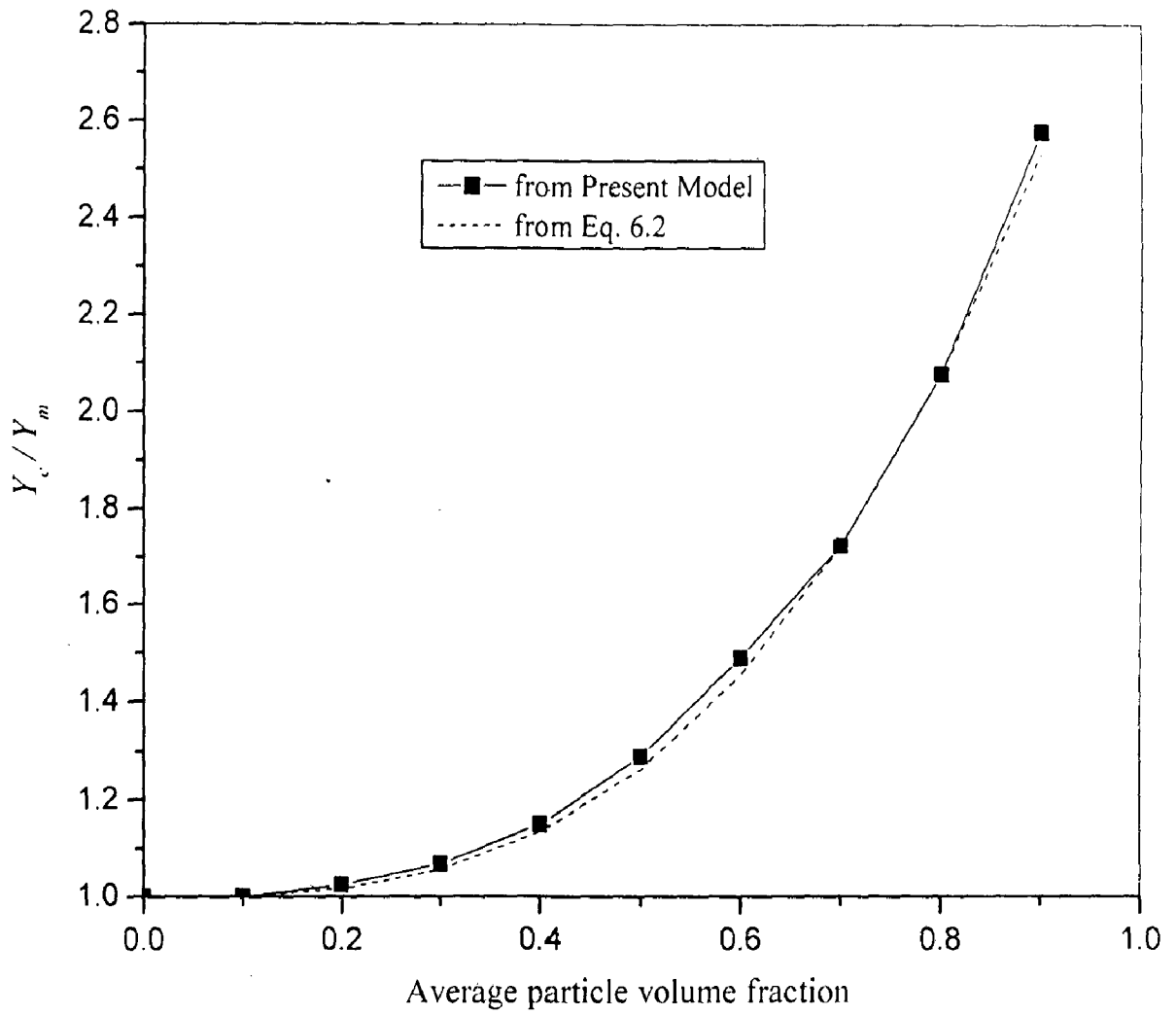
Fig.6.11 Results for the variation of the yield stress ratio of composite and matrix with average particle volume fraction and its comparison with the proposed equation. (Y_c is yield stress for composite, Y_m is yield stress for matrix)

146
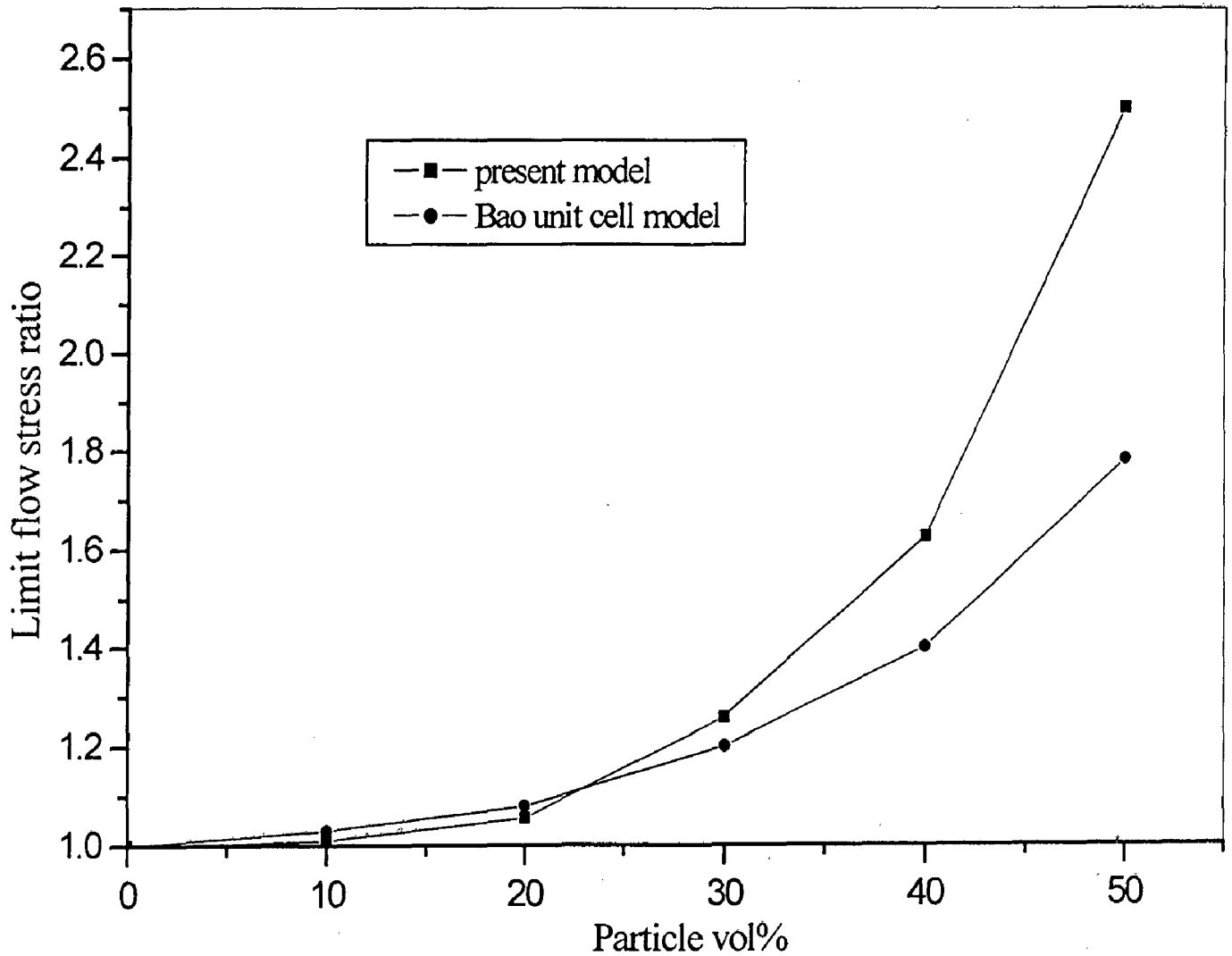
Fig.6.12 Dependence of limit flow stress ratio on particle vol% with the present model and its comparison with Bao unit cell model (Bao and coworkers, 1991) under plane strain conditions.

6.2 RESULTS AND DISCUSSION : UNIFORM COMPOSITES WITH DIFFERENT PARTICLE SHAPES

The effect of particle shape on the elastic modulus and yield stress of the uniform composites have been investigated with the help of present modelling technique. For this uniform composite model with 20 vol% average particle content has been considered. Four different shapes of particles are investigated. These particles are designated as *1*1, 1*4, 2*2* and *4*1*. Particle of shape *1*1* represents the particle made of one element, *1*4* represents the particle made of four neighbouring elements in y-axis direction, *4*1* represents the particle made of four neighbouring elements in x-axis direction and *2*2* represents the four neighbouring elements in the area of two grid elements in x-axis direction and two grid elements in y-axis direction.

The models are subjected to load in the y-axis direction for step by step uniform displacement of the perpendicular boundary. The stress-strain behaviour is obtained in the y-axis direction for uniform composite models. Figure 6.13 presents the stress-strain behaviour of the uniform composites in the y-axis direction for different particle shapes. The modulus of elasticity and yield stress of the uniform composites have been obtained. Figure 6.14 presents the results for the modulus of elasticity for uniform composites with the four different types of particle shapes. It is observed that the value for the modulus of elasticity for the composite with particles *4*1*, elongated in x-axis direction is the lowest. The modulus of elasticity for the composite with *2*2* types of particles is 3-4% higher than the composite with *4*1* types of particles. The modulus of elasticity values for the composite with *1*4* types of particles is the highest. It is 13% higher than the composite with *4*1* types of particles. The modulus of elasticity values for the composite with *1*1* types of particles is in between the modulus of elasticity values for composites with *1*4* and *2*2* types of particles. It is 9% lower than the composite with *1*4* types of particles and 3% higher than the composite with *2*2* types of particles. Thus, the orientation of particles is important in deciding the effectiveness of the reinforcement. Figure 6.15 shows the yield stress for the uniform composites investigated. It has been observed that the yield stress for the uniform composites with particles of type *1*4*, elongated in y-axis direction is higher by about 3-4% in comparison to those in the composites with two other types of particles, *4*1* and *2*2*. The particles, *2*2*, in the uniform composite results in slightly higher yield stress compared to that in composite having the same average particle content

of *4*1* particles. The yield stress for the composite with *1*1* types of particles is in between the yield stress for composites with *1*4* and *2*2* types of particles.

The investigations for modulus of elasticity are according to the rule of mixture (ROM) and inverse rule of mixture (IROM), which gives higher and lower bounds for the modulus of elasticity respectively. These rules are basically applicable for fiber reinforced composites. According to these rules when the fibers are along the loading directions the effective modulus is determined by the rule of mixture (ROM). When the fibers are transverse to the loading direction, the effective modulus is determined by the inverse rule of mixture (IROM). The *4*1* type of particles which may be considered small fibers transverse to the loading direction, results in lower values of modulus of elasticity. The *1*4* type of particles may be considered small fibers along to the loading direction and results in highest value of the modulus of elasticity among the particles investigated.
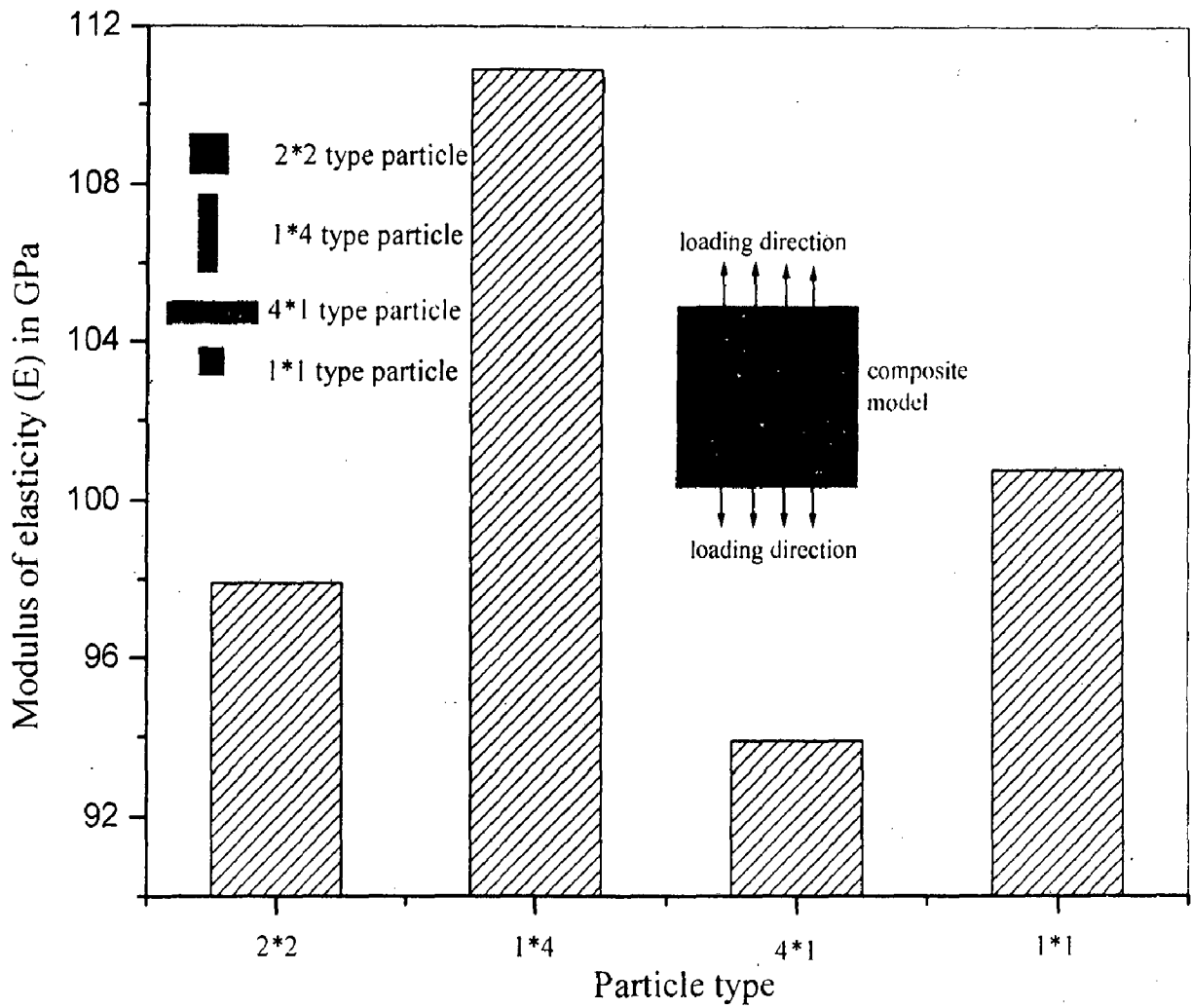
Fig. 6.14 Modulus of elasticity in the direction of loading of uniform composites having particles of different shapes but average particle content of 20 vol%.
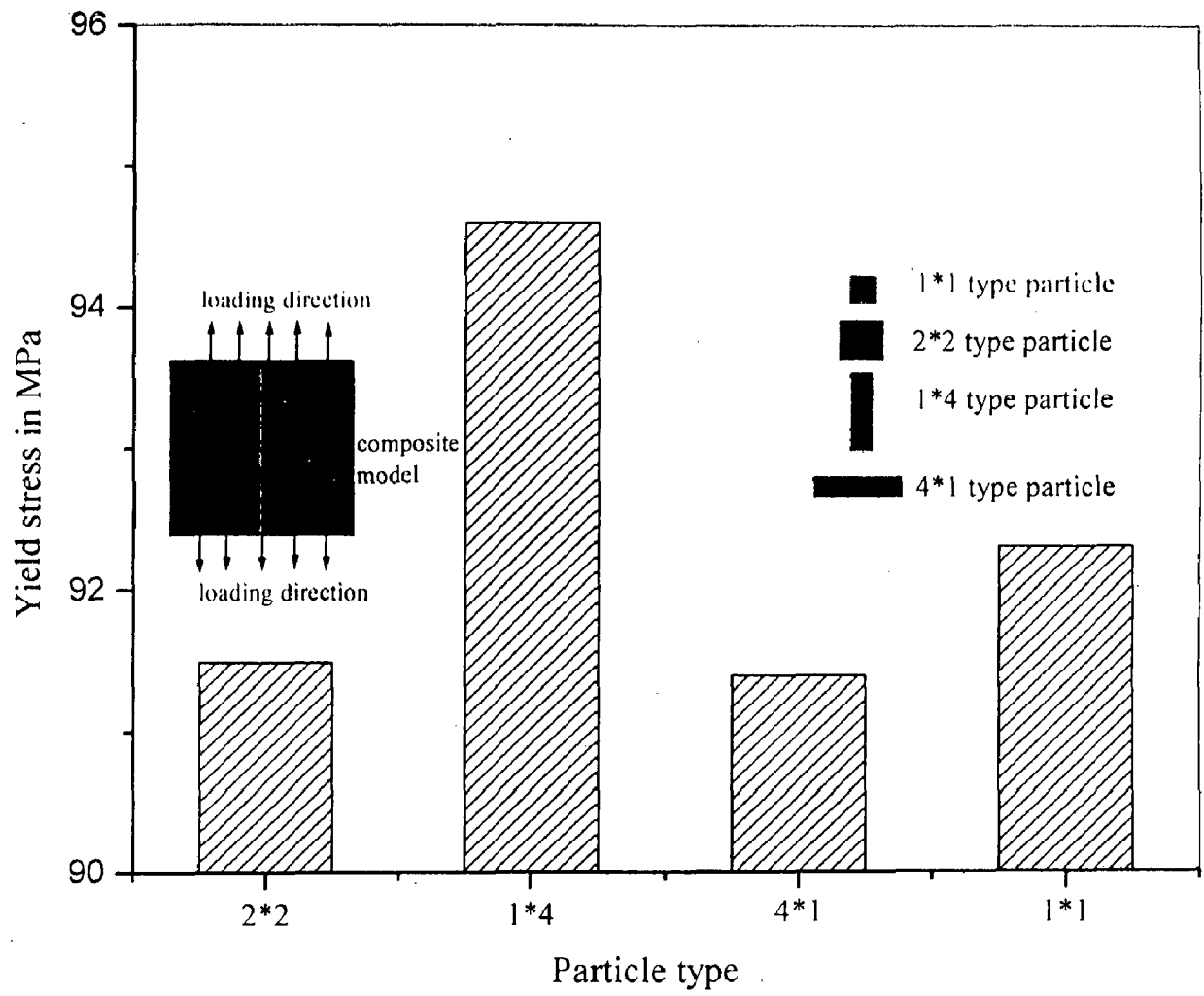
Fig. 6.15 Yield stress in the direction of loading of uniform composites having particles of different shapes but average particle content of 20 vol%.

6.3 RESULTS AND DISCUSSION : UNIFORM COMPOSITES WITH POROSITY

Numerical results have been obtained for the variation of modulus of elasticity of the particle reinforced uniform composites with increasing particle contents from 0 vol% to 100 vol%, with porosities. Three different porosity contents of 2.5 vol%, 5.0 vol% and 7.5 vol% in uniform composites have been investigated. The porosities are of the same size as that of particle and randomly distributed over the entire composite model. Load is applied to cause uniform displacement at the edge y = 5 mm of the 2D square specimen of the composite and the other edge at y = 0 is kept fixed. The effective modulus of elasticity in y-axis direction is obtained from the average elemental stress-strain relationship of the composite, obtained in the y-axis direction of the specimen. Plane stress condition is assumed in the present work. Figure 6.16 shows the variation of the modulus of elasticity with increasing particle contents in different composites containing 2.5, 5.0 and 7.5 vol% of porosity. The results for the variation of the modulus of elasticity with particle content in composite models without porosity have also been plotted in Fig. 6.16 for comparison. It is observed that the Young's modulus of the composites decreases with increasing porosity content and the extent of decrease is more at higher particle contents.

The results of the present model for modulus of elasticity have been compared with Sprigg's equation.

$$X = X_0 \exp(-b \times V_{fp}) \qquad (2.1)$$

In the Eq. 2.1, X is a particular mechanical property (which is modulus of elasticity here), V_{fp} is the volume fraction of porosity, b is an empirical constant and the subscript 0 indicates zero porosity. Figure 6.17 shows the relation between $\ln(X/X_0)$ and porosity content for different particle vol%. On the basis of Fig 6.17, the values of constant b are obtained for different particle contents in the composites and Fig 6.18 shows the variation of constant b with particle content. In the present work b varies from 2.15 to 2.58 for different particle contents. It indicates that the results of the present model for modulus of elasticity with porosity (particle size pores with uniform random distribution) for composites with particle content varying from 0 vol% to 100 vol% may be given by Sprigg's equation with constant b varying within a range of 2.15 to 2.58. An empirical relation for the variation of constant b with particle volume fraction may be given by the following equation.

$$b = 2.58 - 1.75(V_f - 0.5)^2 \qquad (6.3)$$

Nonlinear analysis has also been performed to predict the effect of porosity on the yield strength. Nonlinear analysis is performed with four different types of pores represented by *1*1*, *1*4, 2*2* and *4*1* in the present study. The notation *m*n* represents the pore introduced by the removal of *m* × *n* elements where *m* represents the length of *m* grid elements in *x-axis* direction and *n* similarly represents the length of *n* grid elements in y-axis direction. Thus, *1*4* and *4*1* represent pores elongated respectively in y-axis and x-axis directions with aspect ratios of 1:4 and 4:1 but having the same area as the square pore represented by *2*2* which has aspect ratio of unity. For each size and shape of the pore, the pores are randomly distributed in a composite containing 30 vol% of particles. The porosity contents in the composites are 2.5 vol%, 5.0 vol% and 7.5 vol%.

For the nonlinear analysis, the edge of the composite at y = 0 is kept fixed but the edge at y = 5 mm is subjected to a uniform total displacement u_y = 0.01 mm to give a maximum strain of 0.002 in 20 equal steps and the results for each step are noted. The average elemental stresses and strains in y-axis direction for each step are plotted to show the stress-strain behaviour of the composites containing 2.5, 5.0 and 7.5 vol% porosity as shown respectively in Fig. 6.19, Fig. 6.20 and Fig. 6.21 for different pore types. It is observed that smaller size of porosity as in *1*1* causes relatively less damage to load bearing capacity of the uniform composite compared to *2*2*, larger pores of similar shape as evident from the relatively lower stress–strain curve for the latter type of pore in a uniform composite having the same average particle content of 30 vol%. The most damaging feature appears to be the elongation of pores transverse to the loading direction as evident from the lowest stress-strain curve for *4*1* pores which is even lower than *2*2* types of pores having the same individual area. It is interesting to note that the stress-strain curve for a material with *1*4* pores is higher than that containing *2*2* pores which have a higher length in the transverse direction to loading. So the size of the pores, its aspect ratio and orientation with respect to loading direction, together determine the yield strength of the composite material containing porosity.

On the basis of the stress-strain curves, the modulus of elasticity and the yield stress in y-axis direction (loading direction) are obtained for materials containing different pore types as shown in Figs. 6.22 and 6.23 respectively. It is clear from these figures that the modulus of elasticity as well as yield strength is affected by the pore type to a great extent.

154
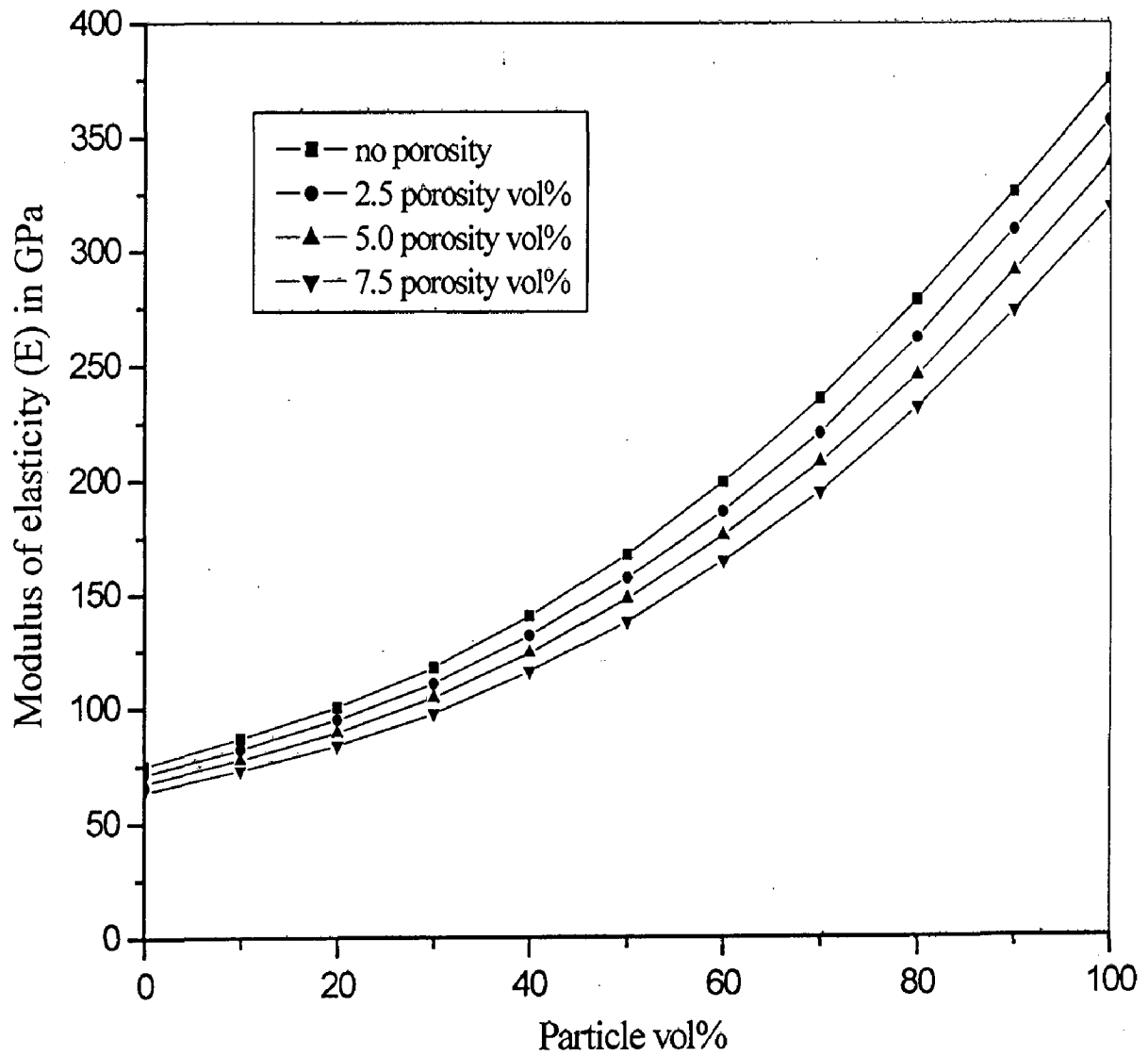
Fig. 6.16 Effect of porosity (particle size pores randomly distributed) on modulus of elasticity of uniform composites.
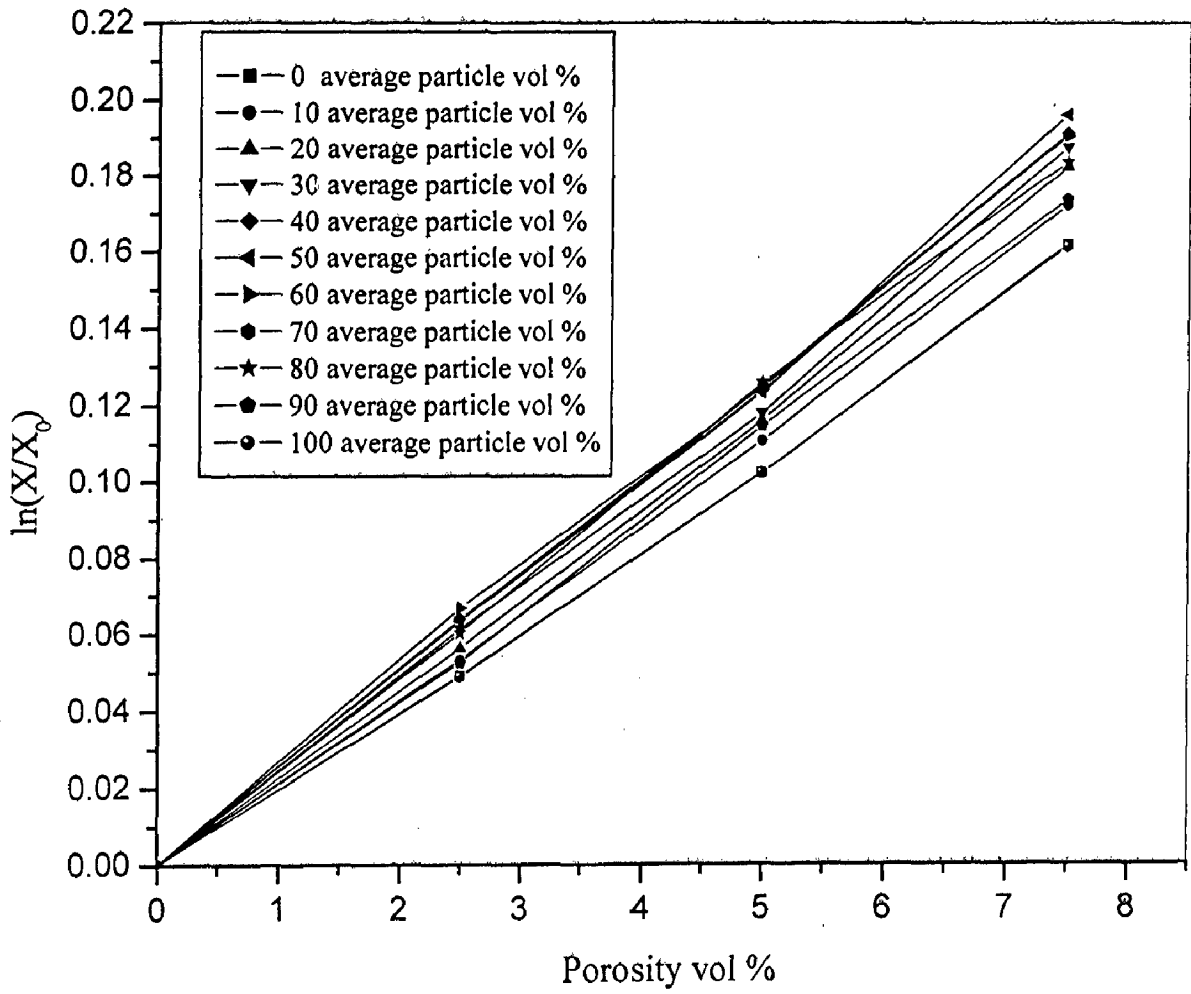
Fig. 6.17 The variation of *ln(X/X₀)* with porosity vol% for different particle vol%.
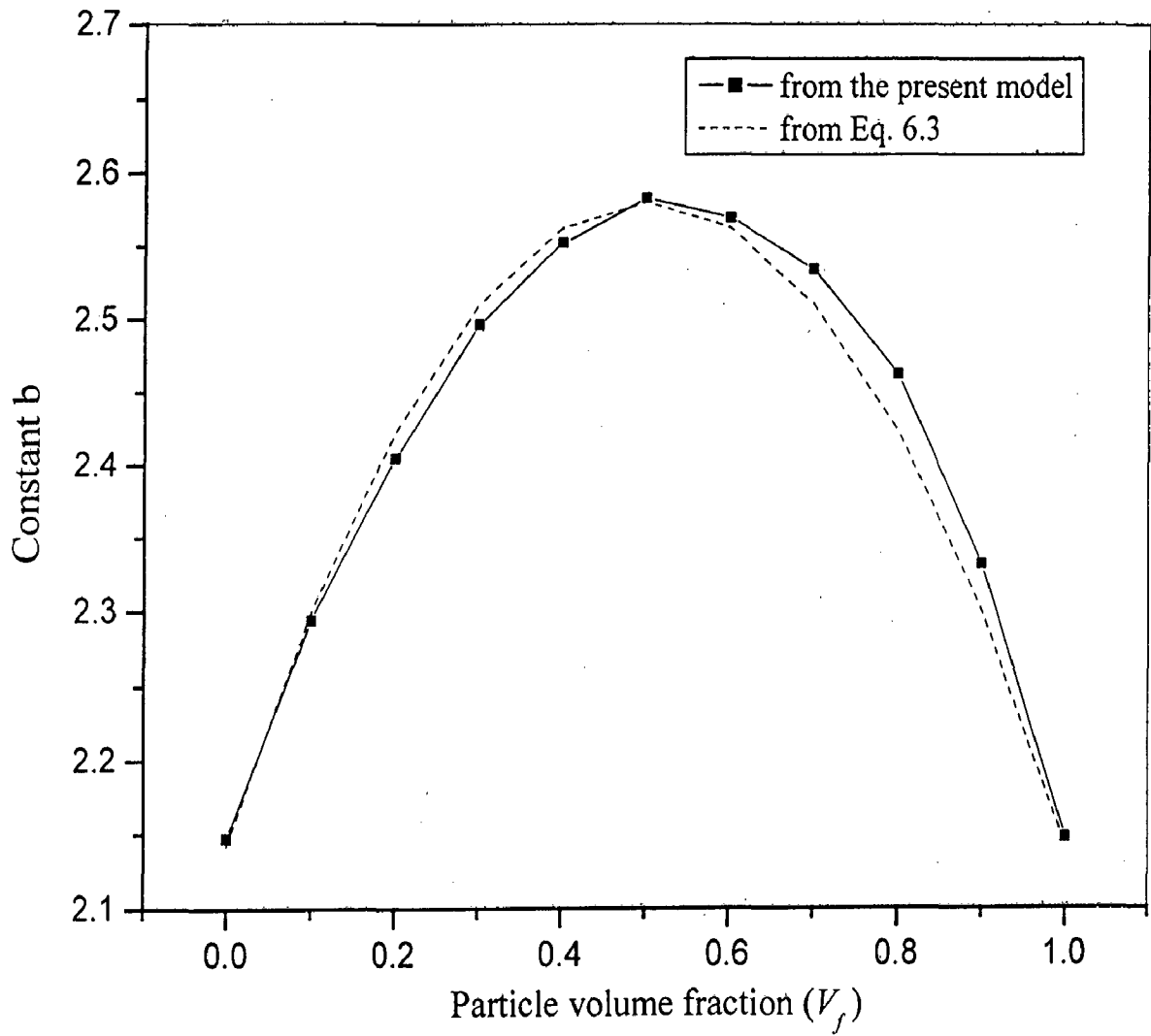
Fig. 6.18 The variation of constant *b* of Sprigg's equation for composites with different particle volume fractions.
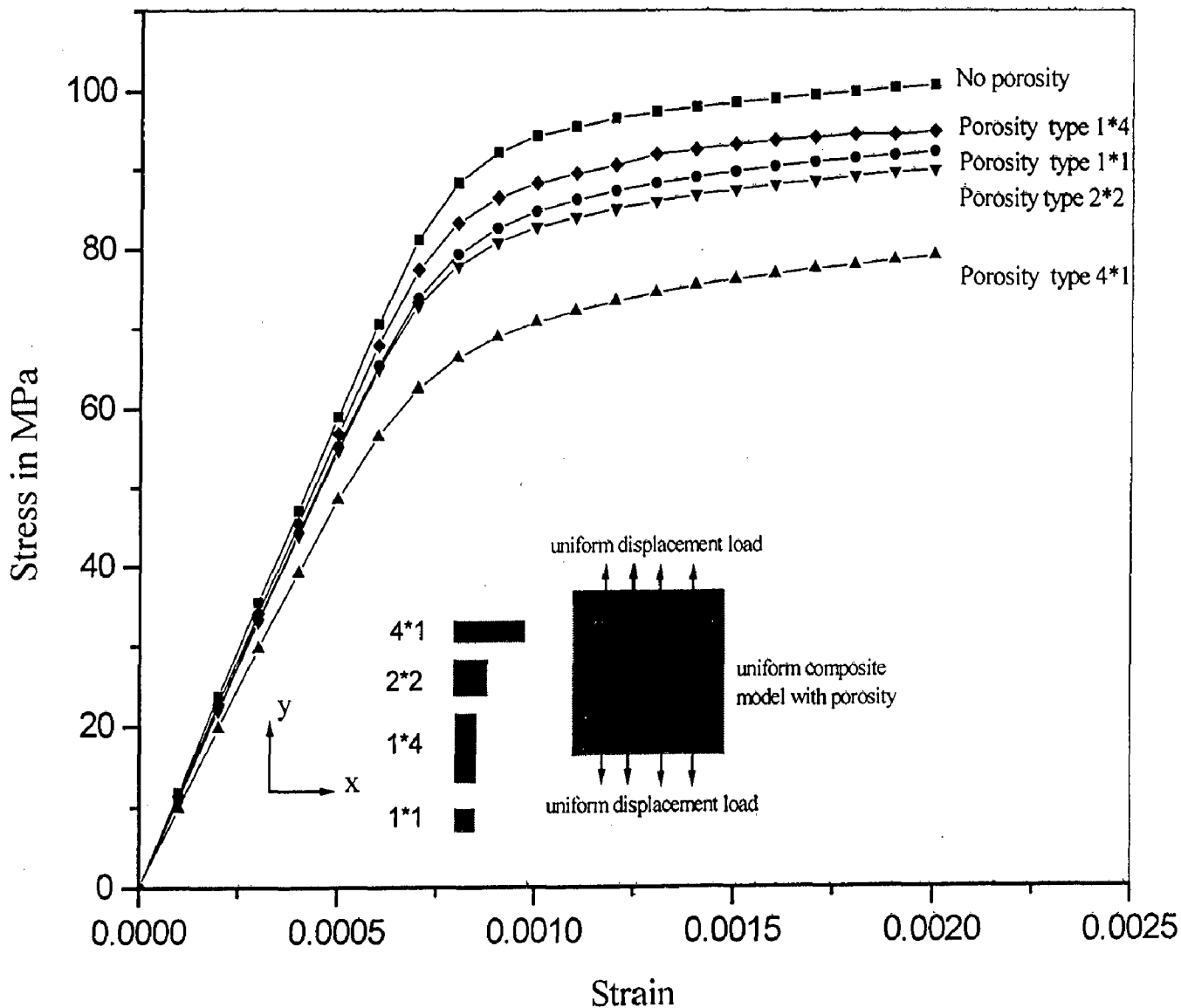
Fig. 6.19 Stress-strain behaviours of composites with 30 vol% randomly distributed particles and 2.5 vol% porosity of different sizes and aspect ratios.
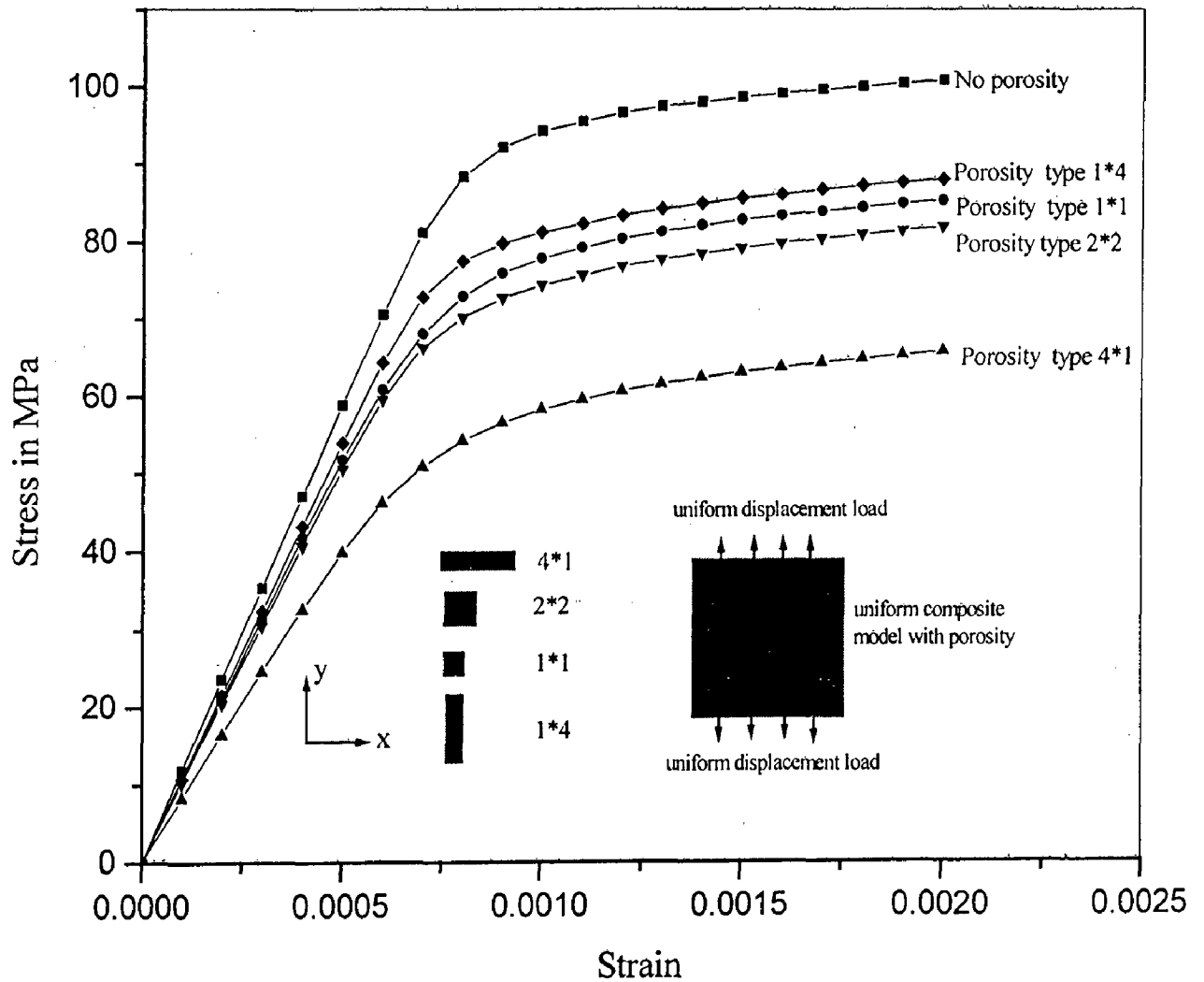
Fig. 6.20 Stress-strain behaviours of composites with 30 vol% randomly distributed particles and 5.0 vol% porosity of different sizes and aspect ratios.
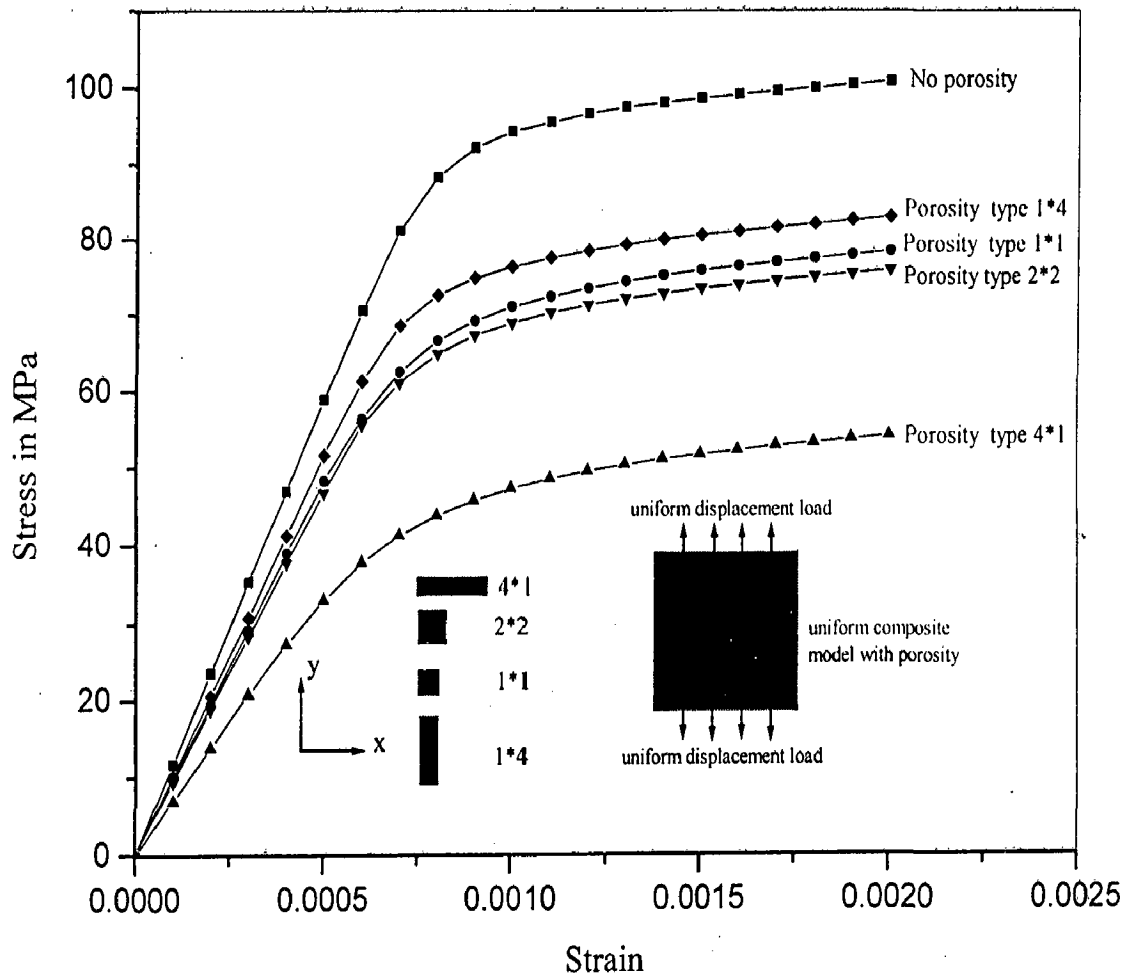
Fig. 6.21 Stress-strain behaviours of composites with 30 vol% randomly distributed particles and 7.5 vol% porosity of different sizes and aspect ratios.
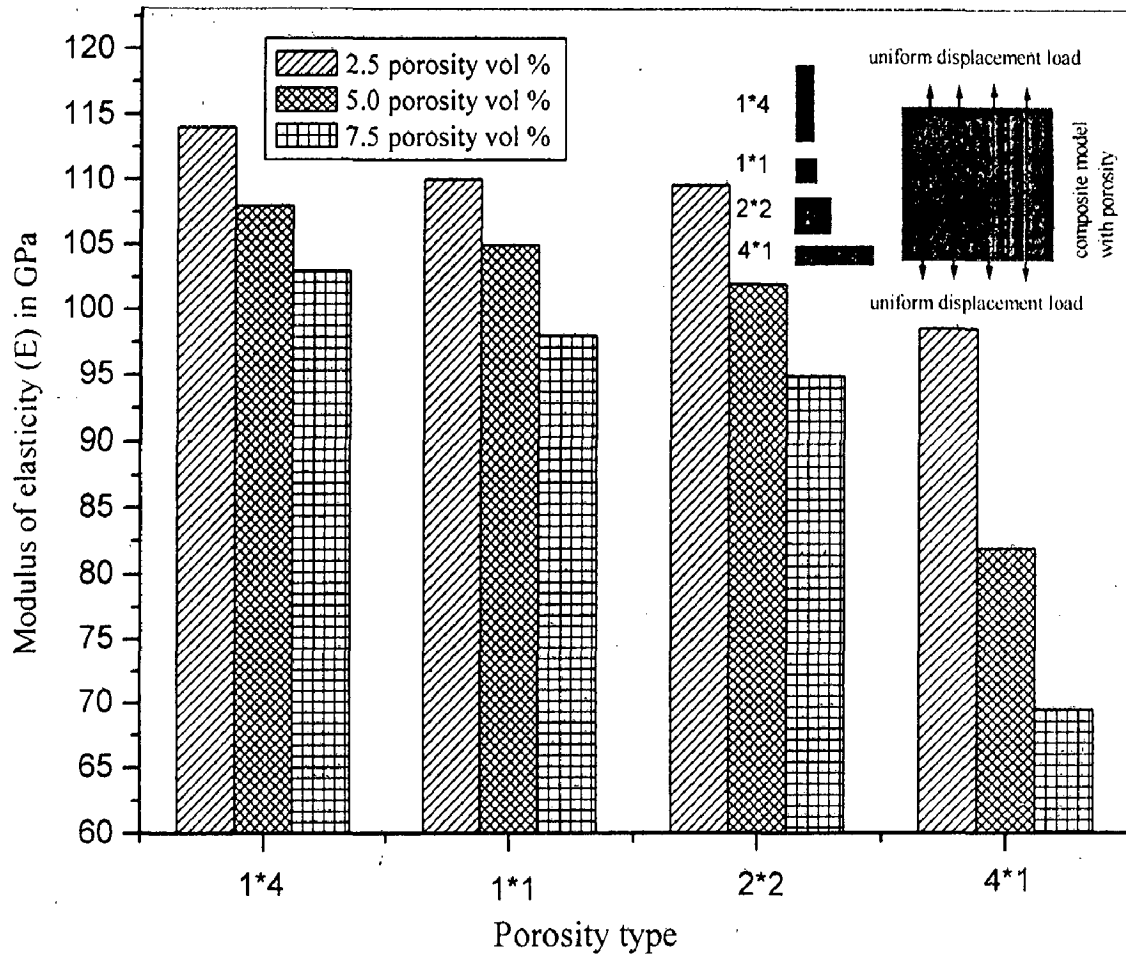
Fig. 6.22 Effect of porosity type on modulus of elasticity of the uniform composites with randomly distributed particles (30 vol% particle content). Modulus of elasticity without porosity is 118 GPa.

161
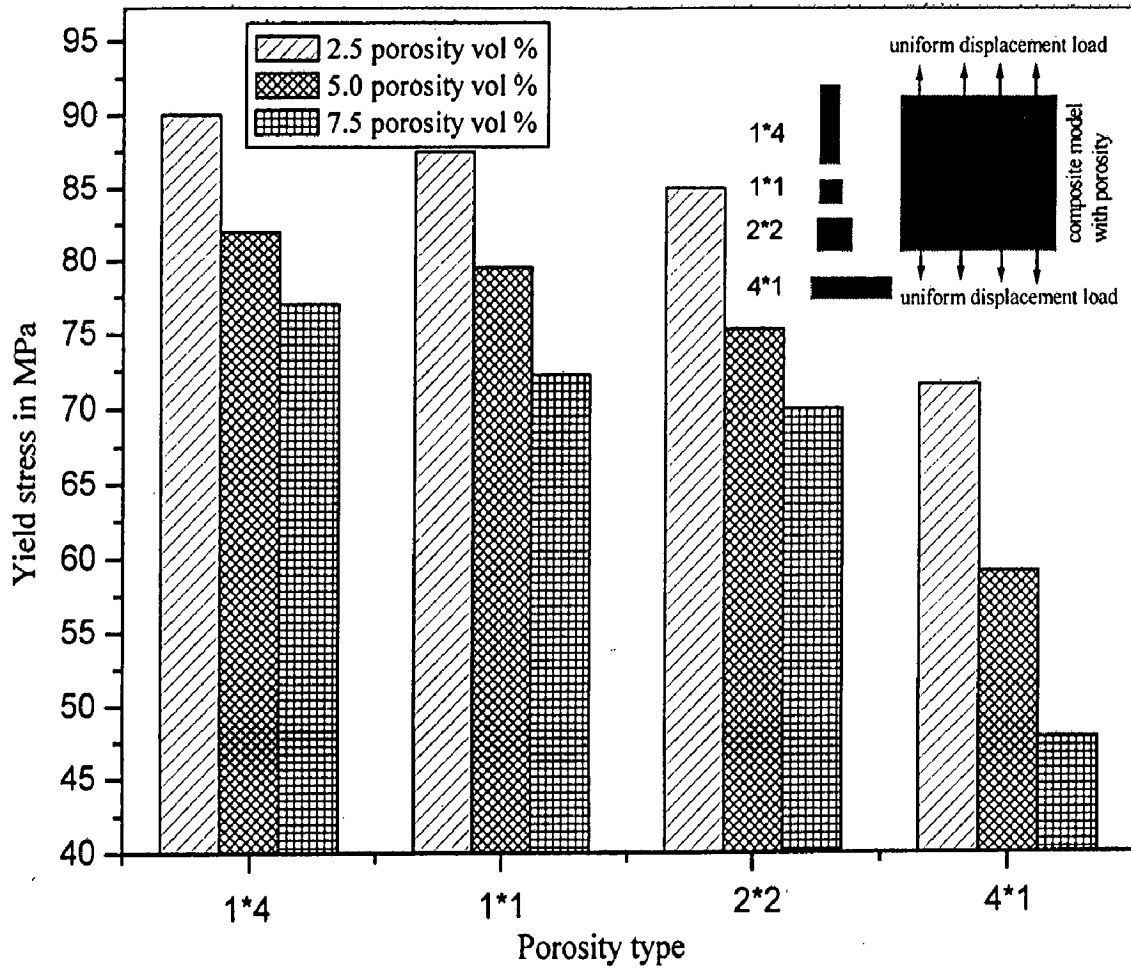
Fig. 6.23 Effect of porosity type on the yield strength of the composite with randomly distributed particles (30 vol% particle content). Yield strength without porosity is 96 MPa.

162

These results show that for 7.5 vol% of porosity, the yield strength of a composite with 30 vol% of particles is reduced from 77 MPa to 47.8 MPa when the pore type changes from $1*4$ to $4*1$, which are the least and the most damaging pore types considered in the present work. Thus, there could be 38% reduction in the yield strength depending on the shape, size and orientation of pores for the same porosity content.

Similarly, for the elastic modulus, there could be 33% reduction when the porosity type changes from $1*4$ to $4*1$ for 7.5 vol% of porosity. These results also show that for the same porosity type (type $1*4$) the reduction in the modulus of elasticity is only 5.3% when the porosity content increases from 2.5 to 5 vol%. Also, the results for yield strength show that there is only 9% reduction in the yield stress for the same porosity type (type $1*4$) when the porosity content increases from 2.5 to 5 vol%. These results clearly indicate the dominance of the porosity type on the mechanical properties of the composites.

Tekmen and coworkers (2003) have discussed the effect of porosity on the mechanical behaviour of Al-Si-Mg/SiC$_p$ composite. In their experimental work, they have concluded that increased porosity content decreases both the elastic modulus as well as the yield strength of the composites. They have also concluded that the average porosity content is not a reliable parameter to predict the mechanical properties of the composites. The existence of large pores extending in the direction perpendicular to that of loading is more effective in damaging mechanical properties than the overall porosity content. The results of the present model are also in agreement with the experimental results of Tekmen and coworkers (2003), as evident from Fig. 6.22 and Fig. 6.23. These results show that there is a big variation in modulus of elasticity as well as yield strength due to different porosity types with the same porosity content.

The relative effect of porosity on composites with different particle contents has also been investigated in the present work. Three different particle contents of 10, 20 and 30 vol% are investigated for three different levels of porosity - 2.5, 5.0 and 7.5 vol%. The ratio of yield stress with porosity and without porosity (Y_p/Y_0) has been plotted with vol% of porosity in Fig. 6.24. It shows that the rate of reduction in yield stress with increasing porosity is higher for lower particle contents in the MMCs. Ghosh (1986) has studied the effect of porosity on the mechanical behaviour of Al-Al$_2$O$_3$ metal matrix composites. His experimental results also show the same trend. The comparison of his linearized experimental results with the results of the present model for porosity types $1*4$ and $4*1$ is presented in Fig. 6.25. His results are in between these two extreme types of porosities. Although his results are closer to the $4*1$ type of porosity.
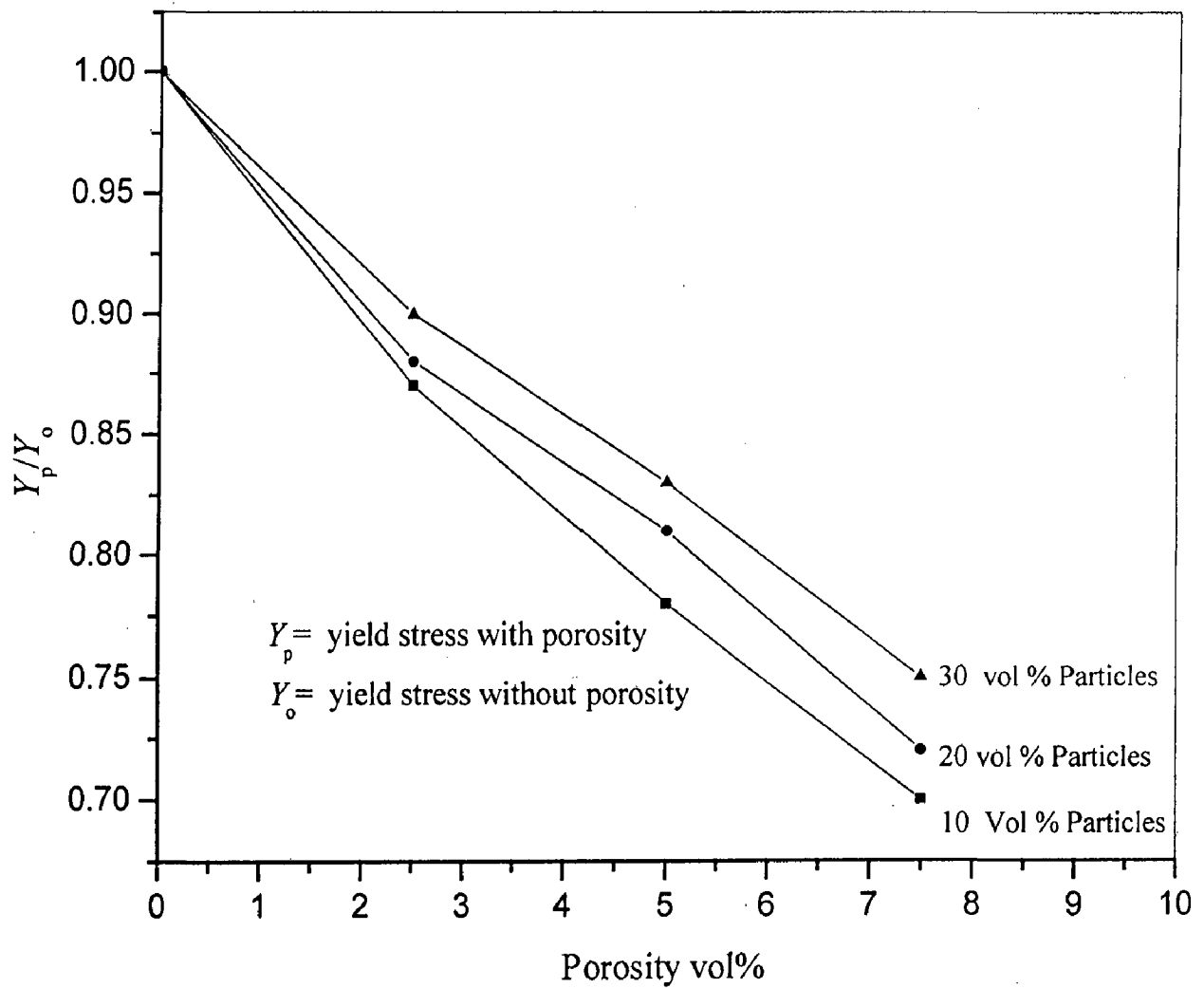
Fig. 6.24 Effect of porosity on the yield strength ratio for the composites with randomly distributed particles and pores (type *I*I*), containing different amount of particles.
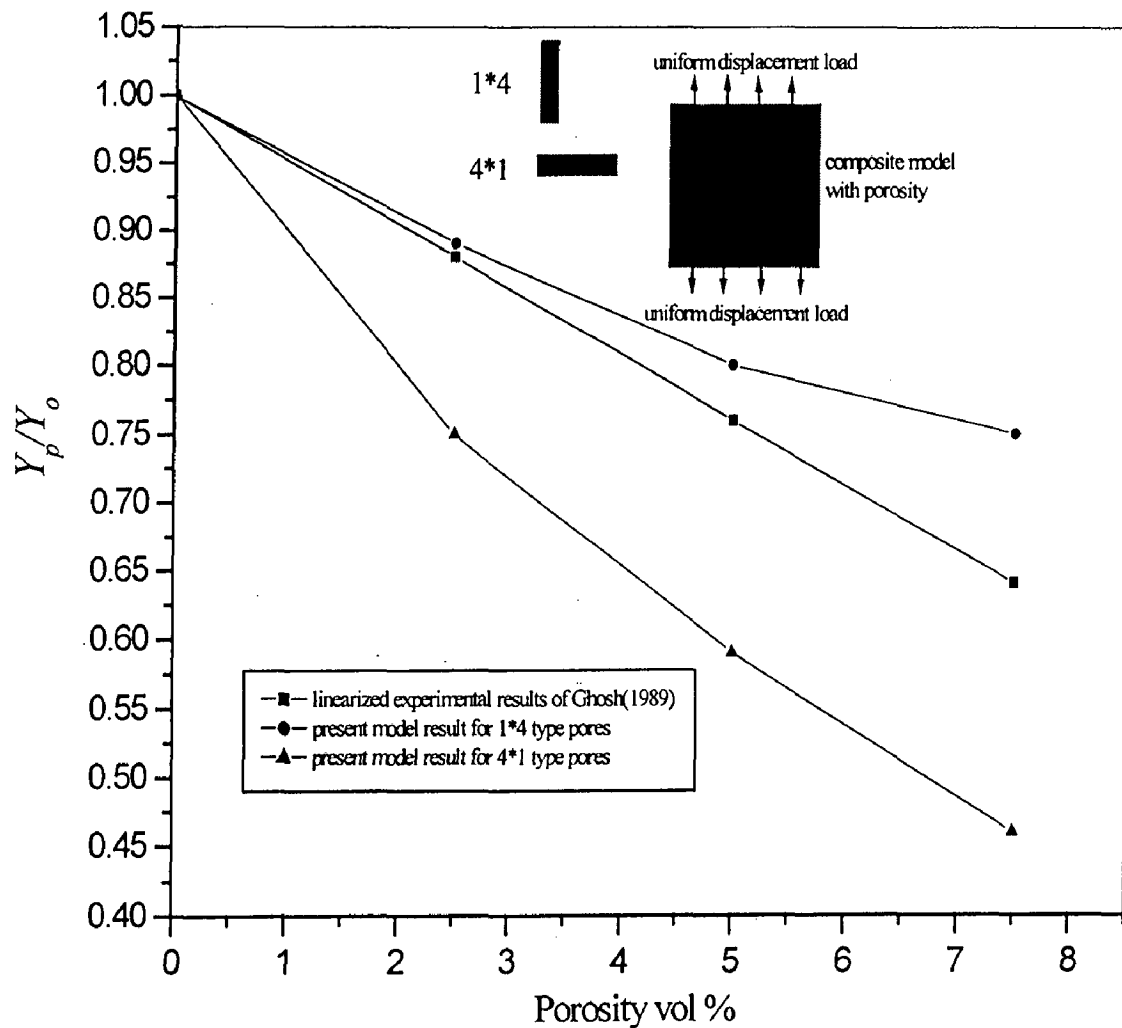
Fig. 6.25 Comparison of present model results with the experimental results of Ghosh (1986) for 10 vol% particle content. (Y_p is yield stress with porosity, Y_o is yield stress without porosity)

6.4 RESULTS AND DISCUSSION: FUNCTIONALLY GRADED MATERIALS (FGMs)

The results obtained for the uniform composites with and without porosity and their comparison with those in the literature give the necessary confidence in the present modelling technique in the domain of uniform composites. The same modelling technique has, therefore, been employed to model functionally graded materials and it is expected that this model will predict the properties of Functionally Graded Materials (FGMs) quite reasonably.

First, the results for FGM models for modulus of elasticity are obtained. FGM models with gradation of particles in x-axis direction are considered. Global values for modulus of elasticity for both gradation and non gradation directions are obtained. FGM models with polynomial variation in particle concentration in x-axis direction with 0% particle concentration at one end and 100% particle concentration at the other end are considered. The plane stress condition is assumed in the present numerical analysis. Figure 6.26 shows the results for the modulus of elasticity in gradation direction (x-axis) as well as non gradation direction (y-axis). The results for the uniform composites are also presented for comparison. The ROM and IROM results for the uniform composites are also shown in the same figure. The results show that the global average values of modulus of elasticity in the gradation direction (x-axis direction) are lower than those of the uniform composite models for the same average particle content. But in the non gradation direction (y-axis direction) these values are higher than those in the uniform composite models, which is interestingly almost the average of the moduli observed in x-axis and y-axis direction. Both the results in gradation and non gradation direction fall well within the rule of mixture and the inverse rule of mixture. The above results may be justified with the help of an example of two springs. One is harder while another is softer. When these springs are kept in parallel, similar in configuration for the particle rich and the particle poor regions for loading in y-direction, the harder spring dominates in the modulus of elasticity. When these springs are kept in series, similar in configuration for loading in x-direction, the softer spring dominates the modulus of elasticity, as reflected in the results of the present model.

The linear analysis on the FGM models has been extended to gradation in particle concentration in both the directions of x-axis and y-axis. The nature of gradation is the

same in both the directions. The gradation of the particles is taken from 0% at the corner (0,0) to 100% at the other corner (0.5 cm, 0.5 cm) and follows the same polynomial distribution in both the directions. Figure 6.27 presents the global values of modulus of elasticity for the FGM models with different average particle contents with particle concentration gradation in both the directions. The results of modulus of elasticity for the uniform composite models are also presented in the same graph for comparison. It is observed that the modulus of elasticity results for the FGM models with gradation in both directions are almost equal to those obtained for uniform composites with the same average particle content.

Nonlinear analysis has been performed for the FGM models with gradation in particle concentration in one direction (x-axis direction). Global non linear behaviour of FGM models in non gradation direction (y-axis direction) is estimated. For this purpose, all the nodes at y = 0 are kept fixed and all the nodes at y = 5 mm are subjected to total uniform displacement u_y = 0.01 mm to give a maximum strain of 0.002. This total displacement is applied in 20 steps and the results for each step are noted. The average elemental stresses and strains in y-axis direction for each step are plotted to obtain the nonlinear behaviour of FGM models. The particles are considered linear elastic with the modulus of elasticity of 375 GPA. The matrix is elastic-perfectly plastic with modulus of elasticity of 75 GPa and yield stress of 90 MPa.

Figure 6.28 presents the non linear behaviour of the FGM models in the non gradation direction. On the basis of the nonlinear behaviour of the FGM models the yield strength has been found by the crossover method. Figure 6.29 shows the yield stress variation of FGM models for different average particle contents. The results for yield strength shown in Fig. 6.29 may be fitted by the following linear empirical relation till particle content of about 60 vol%:

$$\frac{Y_f}{Y_m} = 1 + \alpha\,(V_f) \tag{6.4}$$

where, Y_f = yield stress of the FGM for average particle volume fraction V_f.

Y_m = yield stress at no particles i.e. yield stress of the matrix.

α = an empirical constant, its numerical value is 1.2 in this equation for the FGM investigated in the present work.

V_f = average particle volume fraction.
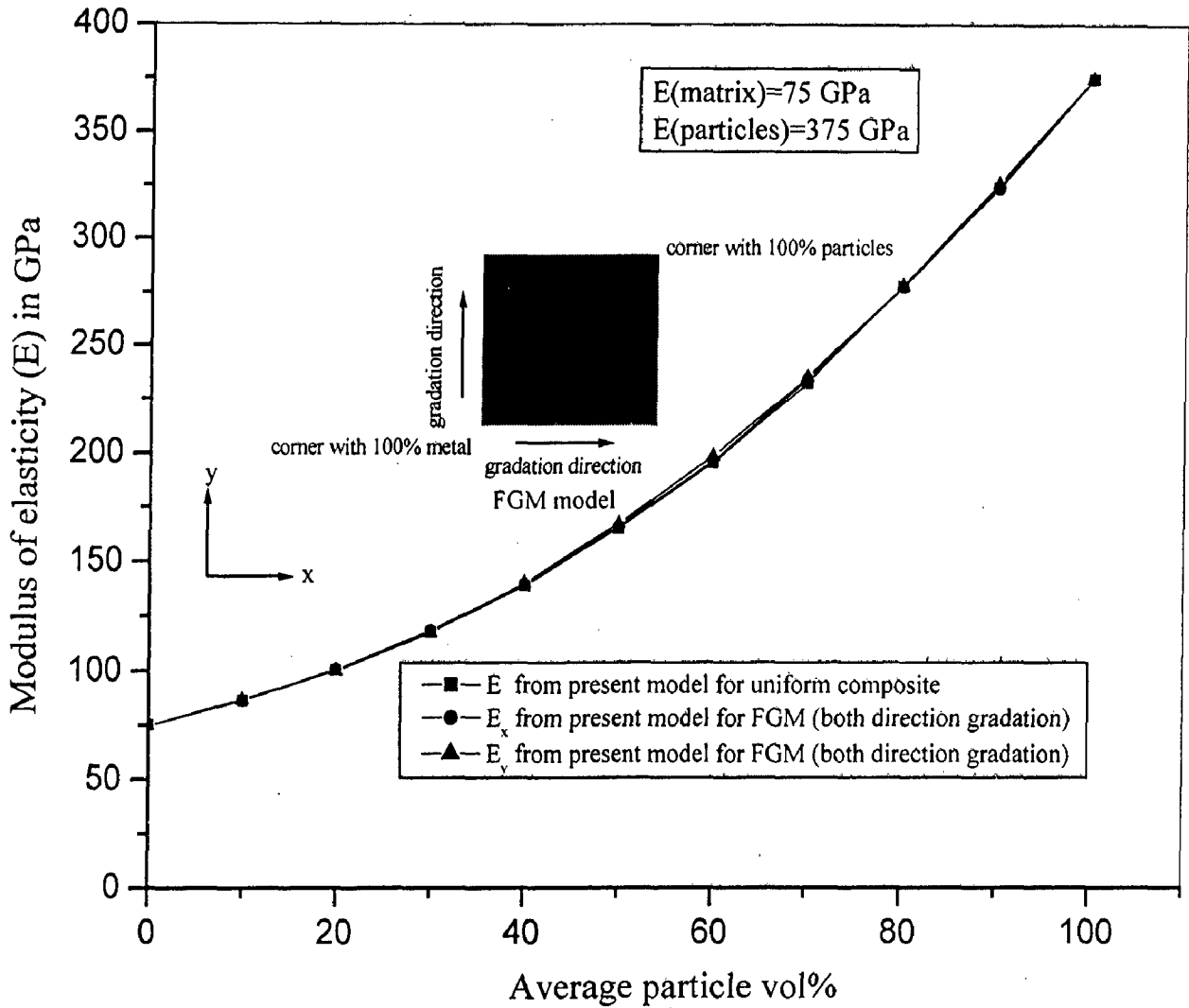
Fig. 6.27 Variation of global modulus of elasticity with different average particle contents in the FGMs having particle concentration gradation in both x-axis and y-axis directions following polynomial equation $c(xy) = 100(xy)^n /l^{2n}$, with no particles at corner (0, 0) and 100% particle concentration at corner (l, l).Here l is the edge length of the square model.

169
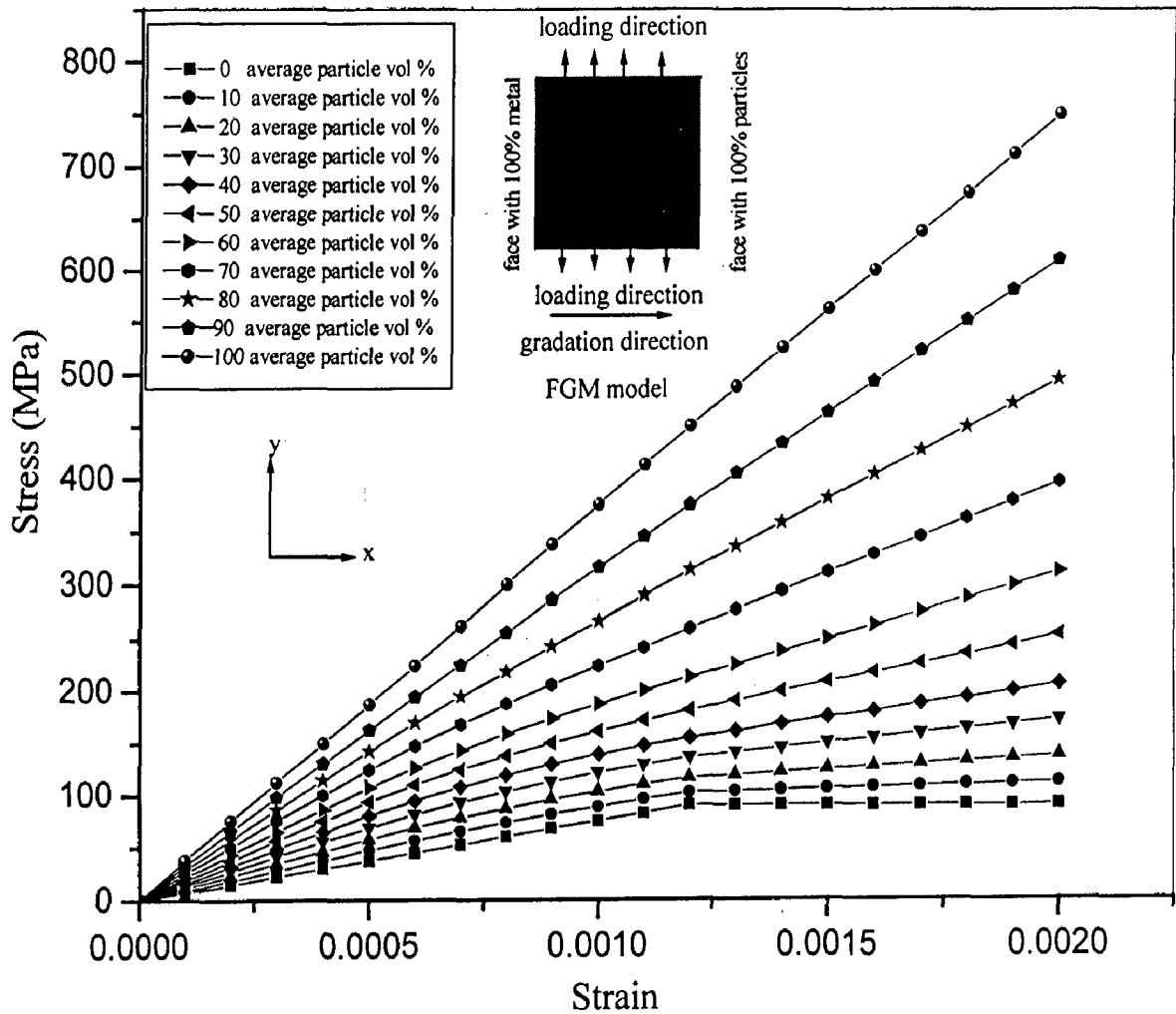
Fig. 6.28 The global non linear stress-strain behaviour in the non gradation (y-axis) direction for FGMs containing different average particle contents. Particle distributed in x-direction following polynomial equation $c(x) = 100(x/l)^n$ for different average particle contents, where $c(x)$ is the concentration of particles in vol% at any location, x, in FGM of length l in x-direction.
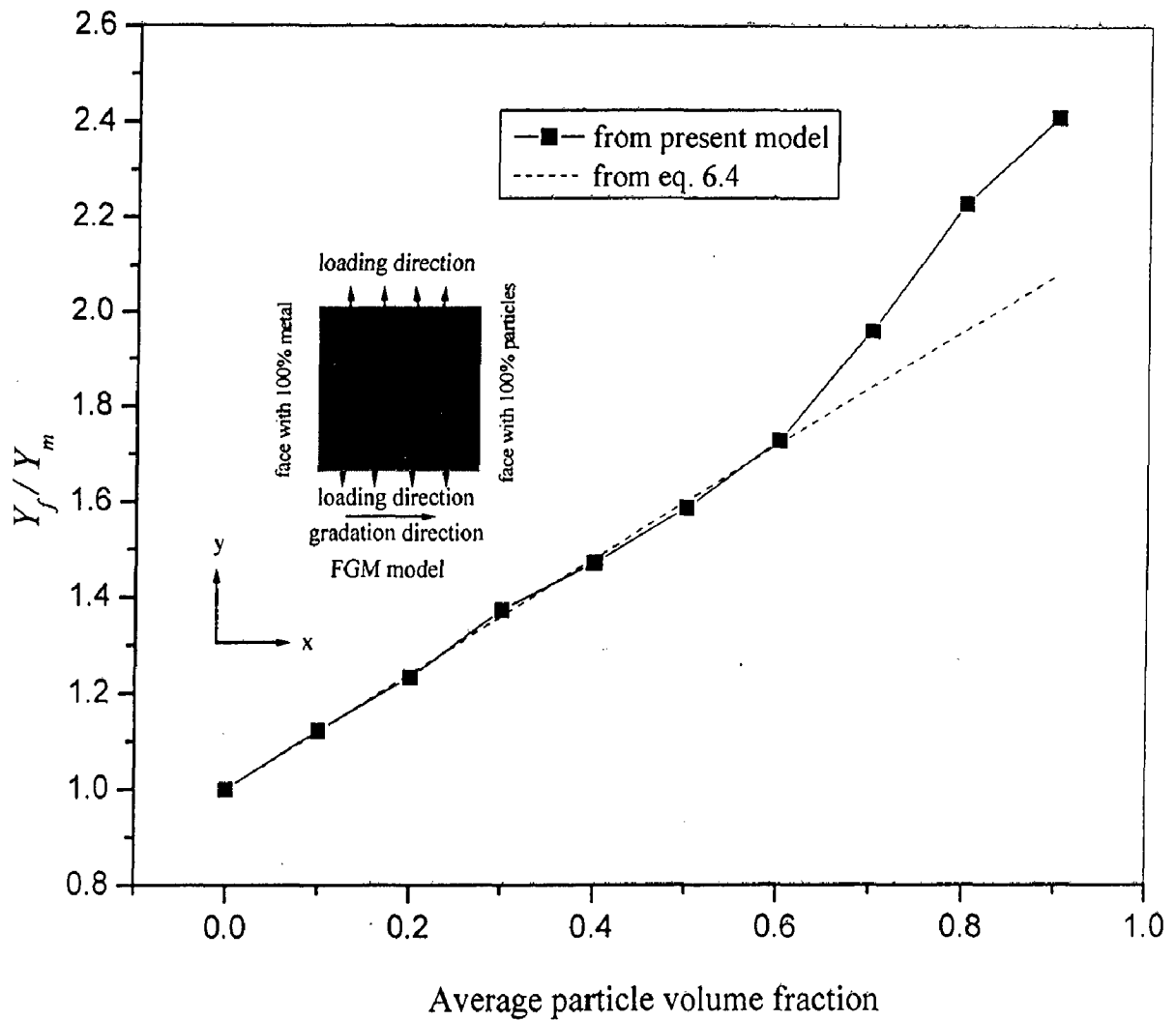
Fig. 6.29 The variation of global values of the yield stress for FGMs with different average particle volume fractions in the non gradation direction (y-axis direction). Particle distributed in x-direction following polynomial equation $c(x) = 100(x/l)^n$ for different average particle contents, where $c(x)$ is the concentration of particles in vol% at any location, x, in FGM of length l in x-direction. The results from Eq. 6.4 are also presented. (Y_f is yield stress for FGM, Y_m is yield stress for matrix)

The yield stress results obtained from the empirical equation are also presented in Fig. 6.29, which indicates that the above empirical relation in Eq. 6.4 may be used as a quick tool to present the results of the present modelling technique in non gradation direction up to average particle content of 60 vol%, distributed following the polynomial equation with 0 vol% particle content at one end to 100 vol% particle content at the other end and variation in particle concentration in one direction only.

The results of the nonlinear analysis for the global behaviour in gradation direction (x-axis direction) are also obtained for FGM models with particle distribution graded in x-axis direction from 0% particle concentration at x = 0 and 100% particle concentration at the other end, x = 5 mm, with polynomial distribution in between. For applying load all the nodes having coordinate x = 0 are kept fixed and all the nodes at x = 5 mm are subjected to uniform total displacement u_x = 0.01 mm to give a maximum strain of 0.002. This total displacement is applied in 20 steps and the results for each step are noted. The average elemental stresses and strains in x-axis direction for each step are plotted to show the nonlinear stress-strain behaviour of FGM models. Figure 6.30 shows the nonlinear deformation behaviour of the FGM models in the gradation direction. On the basis of nonlinear behaviour of the FGM models in gradation direction the yield stress variation of the FGM models is obtained with the help of crossover method. Figure 6.31 shows the global values for yield stress for the FGM models in the gradation and non gradation directions. The yield stress behaviour of uniform composite models is also presented in the same figure for comparison. The results indicate that in the gradation direction FGM models show the same yield stress behaviour as those of the matrix up to almost the average particle content of 70 vol% and it is lower than those estimated for uniform composite models. It shows that in the gradation direction FGM models show poor yield stress properties at the global scale compared to uniform composite model for the same average particle content.

The effect of porosity on the yield stress in the non gradation direction of FGM models has also been investigated. The yield stress behaviour has been investigated for four different levels of porosity - 0, 2.5, 5.0 and 7.5 vol%, in FGM model with average particle content of 30 vol% distributed in x-axis direction following polynomial equation from 0 vol% particle concentration at one end to 100 vol% particle concentration at the other end. Porosities considered are of the same size as that of particle and are randomly

distributed over the whole matrix. Figure 6.32 shows the effect of porosity on the yield strength of FGM model with average particle content of 30 vol%. The results for yield strength for the uniform composite models containing similar levels of porosity are also presented in the same figure for comparison. From Fig. 6.32 it may be concluded that the FGM models as well as uniform composite models show similar response to uniformly distributed porosity.

FGMs have a graded variation of particles in the microstructure along a particular direction. Hence FGMs exhibit variations in the properties along the gradation direction. In the next step, the variation of FGM properties along the dimensions is investigated. FGM models with particle concentration gradation in x-axis direction are considered. As there is no gradation of the particles distribution along the y-axis direction, the properties may be assumed uniform along the y-axis around a given x. That is, there is no variation in the properties along the y-axis direction. To estimate the variation in the modulus of elasticity inside the FGM model along the gradation, the modulus of elasticity values are calculated at eleven different locations along the gradation in the direction of x-axis. For this purpose the FGM model is divided in 10 equal parts along the x-axis. To find the modulus of elasticity in y-axis direction the nodes at y = 0 is kept fixed and at y = 5 mm all the nodes are subjected to uniform displacement. To estimate the modulus of elasticity at a particular location along x-axis the stresses and strains of all the nodes having that x coordinate have been obtained. The average of all the nodal stresses in y direction at a particular x location has been assumed to be as the average stress in y-axis direction at that location. The average of all the nodal strains in y-axis direction at that particular x location is assumed to be the average strain at that location. On the basis of the average stress and average strain at that particular location, the Young's modulus in y-axis direction at that particular location has been estimated. The same procedure is repeated for all the eleven locations along the x-axis. This procedure is repeated for different FGM models having different average particles vol% with gradation of particles from 0% particles concentration at one end to 100% particles concentration at the other end with particles distributed with polynomial distribution.

Figure 6.33 shows the modulus of elasticity variation inside the FGM models along the gradation direction (x-axis direction) for FGM models with different average particle contents. It shows that the modulus of elasticity results obtained at different locations follow almost the similar trend as of the gradation in particle concentration.
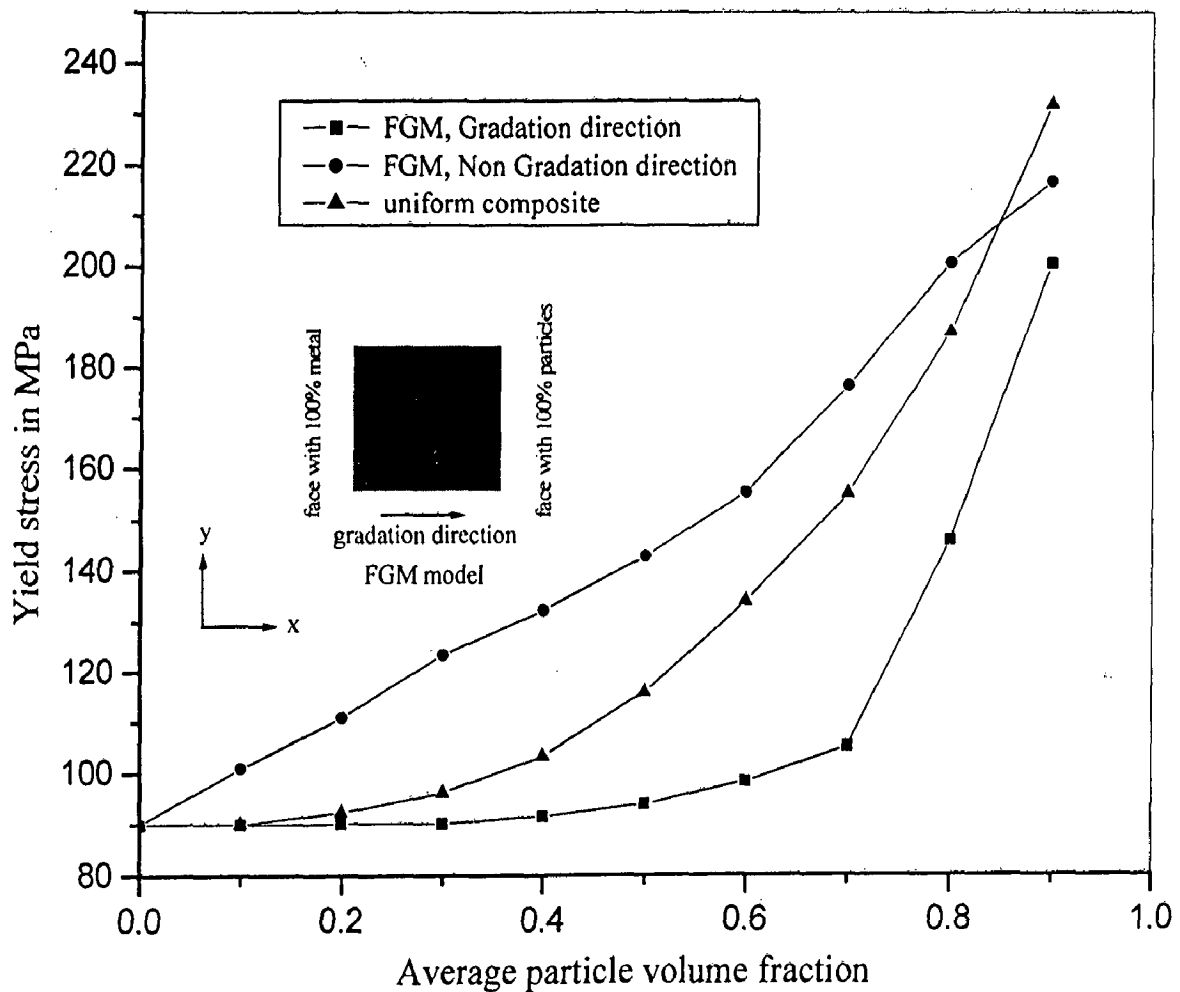
Fig. 6.31 Variation of the yield stress for FGMs with different average particle contents in the non gradation direction and the gradation direction, when the particles are distributed following polynomial equation from 0 vol% particle concentration at one end to 100 vol% at the other end. The results for uniform composite models are also presented.
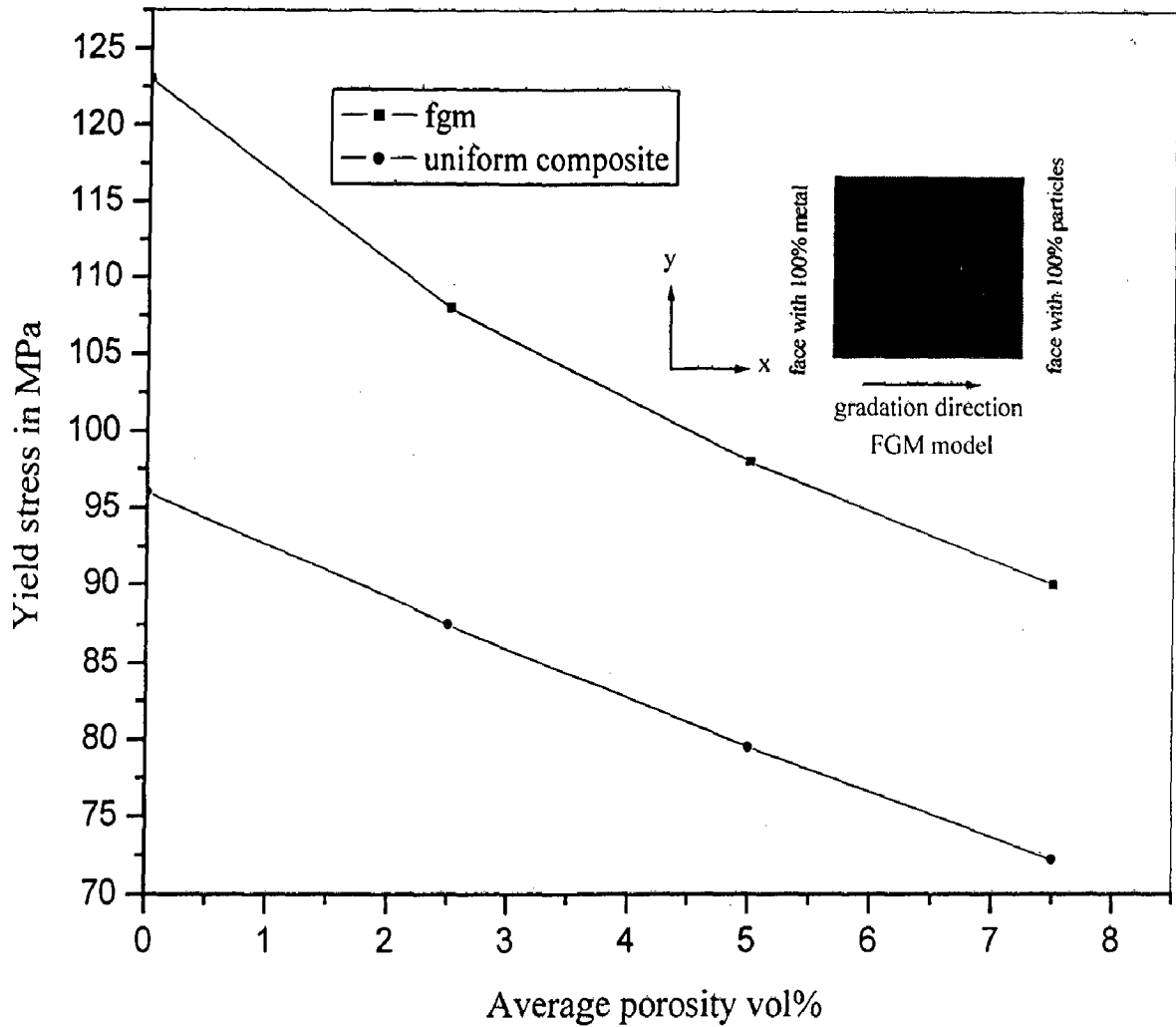
Fig. 6.32 Effect of porosity on the yield strength as estimated for loading in the non gradation (y-axis) direction for the FGMs with average particle content of 30 vol% and its comparison with the uniform composite model having 30 vol% particles and similar levels of porosity. Particle concentration gradation in FGM is in x-axis direction only.
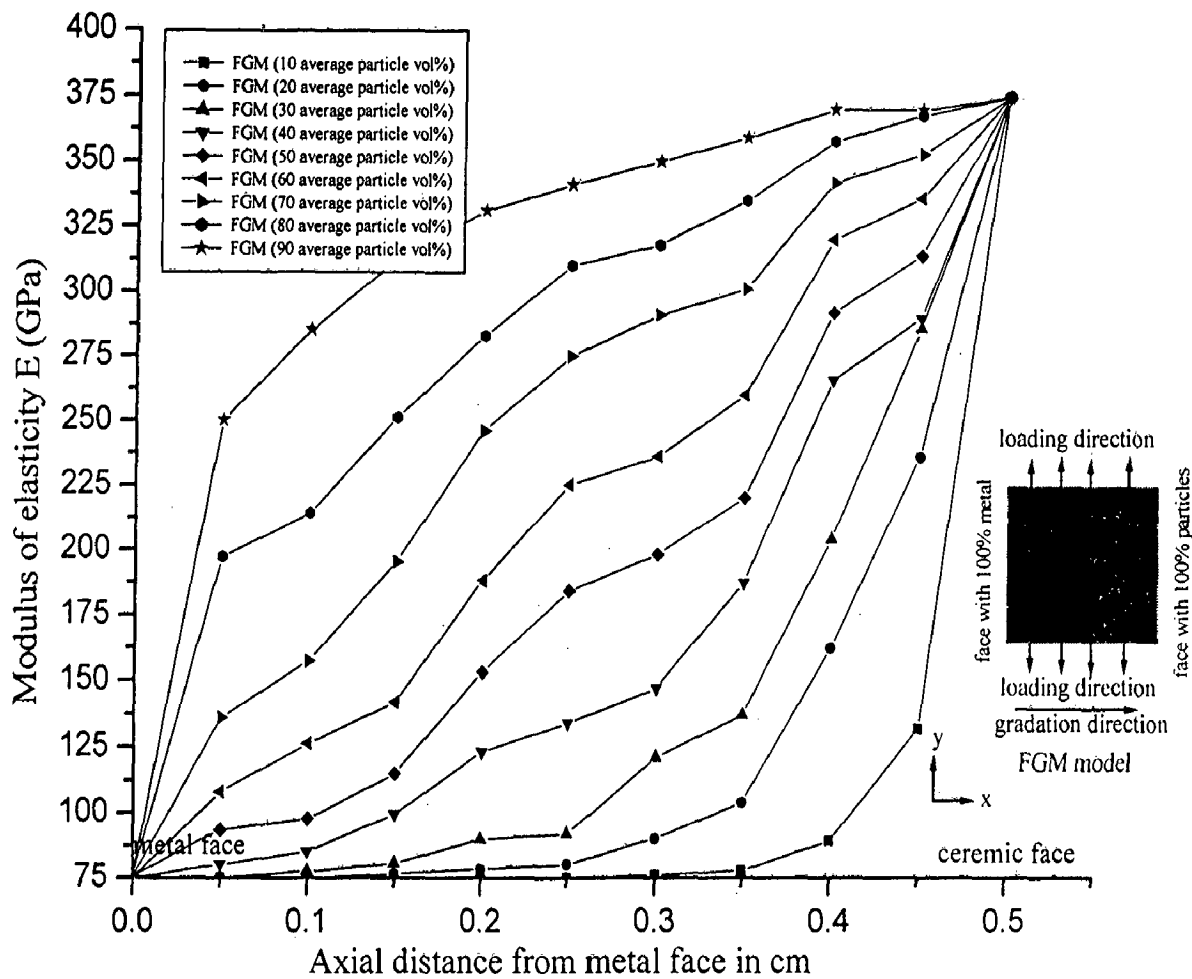
Fig. 6.33 Local variation of modulus of elasticity along the gradation in x-axis direction in FGMs with different average particle content, loaded in y-axis direction. Particle distributed in x-direction following polynomial equation $c(x) = 100(x/l)^n$ for different average particle contents, where $c(x)$ is the concentration of particles in vol% at any location, x, in FGM of length l in x-direction.

6.5 RESULTS AND DISCUSSION: FGMs WITH DIFFERENT GRADATIONS IN PARTICLE DISTRIBUTION

FGM models with average particle content of 30 vol% are investigated for different gradation in particle distribution and their impact on global values of modulus of elasticity and yield stress. For polynomial distribution of particles in the gradation direction of x-axis, with 10 vol% particle concentration at one end to different particle concentrations at the other end to arrive at the average particle content of 30 vol%, Fig. 4.11 in chapter-4 shows the seven different particle concentration profiles represented by a to g. The polynomial distribution of particles is given by the following equation.

$$c(x) = a_1 + (a_2 - a_1)\left(\frac{x}{l}\right)^n \qquad (4.39)$$

The distributions shown in Fig. 4.11 correspond to a_2 values of 100, 90, 80, 70, 60, 50 and 40 vol% respectively and the corresponding values of exponent 'n' are 3.5, 3.0, 2.5, 2.0, 1.5, 1.0 and 0.5 respectively. In fact a_2 and n for the case of average 30 vol% particles and a_1 equal to 10 vol% may be related as $a_2 = 30 + 20n$ using Eq. 4.40.

Figure 6.34 shows the stress-strain behaviour for these different FGM models for loading in the non gradation direction of y-axis. On the basis of the behaviour shown in Fig.6.34, the modulus of elasticity and the yield stress results for FGM models having different gradation distributions have been obtained. The variations of modulus of elasticity and yield stress in FGM containing an average of 30 vol% of particles distributed with the varying exponent, n, of polynomial gradation profile, are shown respectively in Fig. 6.35 and Fig. 6.36. It is observed that the global values of modulus of elasticity and yield stress of FGMs are significantly affected by the type of the gradation of the particles as characterized by exponent n. For an FGM with an average particle concentration of 30 vol% there is 12% increase in the modulus of elasticity and 22% increase in the yield stress with increasing gradient of distribution of particles.

FGM models with linear variation in particle concentration have also been investigated. Figure 4.12 in chapter-4 shows the different linear particle concentration profiles represented by h to m for fixed average particle content of 30 vol%. The different

profiles h to m may be characterized by a non-dimensional slope of the profile defined as $\tan\theta = (a_2 - a_1)/100$. It is apparent that the slope $\tan\theta$ will vary from 0.6 to 0.1 for profiles ranging from h to m. Figures 6.37(a) and (b) show the particle distribution in the grid for slopes $\tan\theta = 0.3$ and 0.4 respectively for an average particle content of 30 vol%.

The nonlinear stress-strain behaviours for these different FGM models with linear gradation of particles are shown in Fig. 6.38. On the basis of these behaviours the results for the modulus of elasticity and yield stress have been obtained. The variations of modulus of elasticity and yield stress with the slope of the linear gradation are presented in Figs. 6.39 and 6.40. Both the modulus of elasticity and yield stress increase approximately by 6% when the slope of linear distribution increases from $\tan\theta = 0$ to 0.6. Linear gradations are not as steep as the gradations obtained with polynomial distribution of particles. Therefore the extent of increase in the modulus of elasticity and yield stress for the linear gradations is relatively less compared to those observed for polynomial distribution of particles. For yield stress it is observed that at lower slopes below $\tan\theta = 0.3$, the yield stress increases slowly from that of uniform composites but beyond $\tan\theta = 0.3$, there is a steep rise in yield stress as shown in Fig. 6.40. This is possibly due to considerable crowding of particles at the particle rich end for a slope beyond $\tan\theta = 0.3$ as shown in Fig.6.37 (a) and (b), which makes particle rich region stiff delaying the onset of plastic deformation.
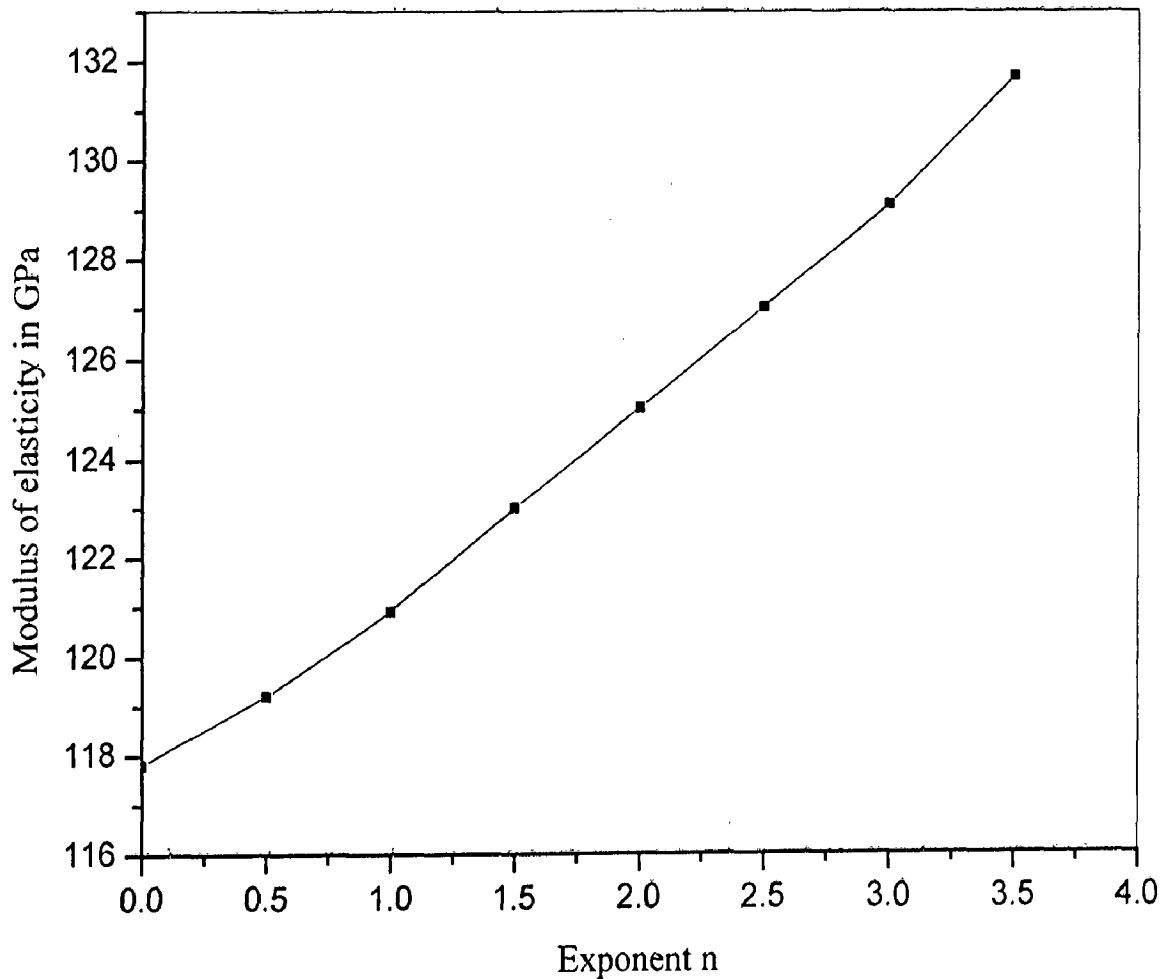
Fig. 6.35 The variation in modulus of elasticity of FGMs in non gradation direction with exponent, n, of polynomial equation, $c(x) = a_1 + (a_2-a_1)(x/l)^n$, used to distribute an average particle content of 30 vol% where, $c(x)$ is the concentration of particles in vol% at any location x in FGM of length l in x-direction. a_1 and a_2 are particle concentrations in vol% at locations x=0 and x = l respectively. a_1, the particle concentration at location x = 0 is kept constant at 10 vol% but a_2 varies with n following linear equation, $a_2 = 30 + 20\, n$.

181
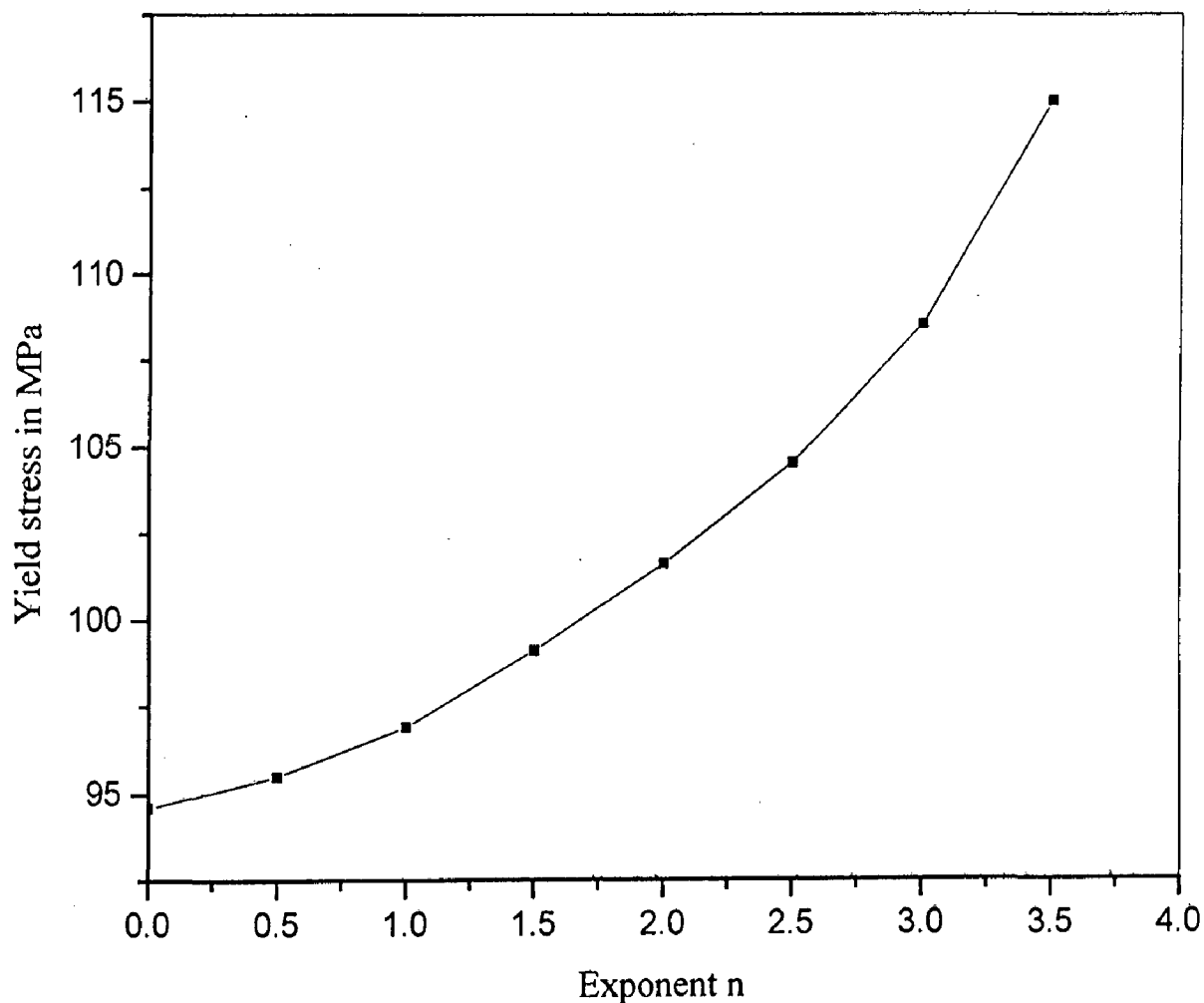
Fig. 6.36 The variation in yield stress of FGMs in non gradation direction with exponent, n, of polynomial equation, $c(x) = a_1 + (a_2-a_1) (x/l)^n$, used to distribute an average particle content of 30 vol% where, $c(x)$ is the concentration of particles in vol% at any location x in FGM of length l in x-direction. a_1 and a_2 are particle concentrations in vol% at locations x = 0 and x = 1 respectively. a_1, the particle concentration at location x = 0 is kept constant at 10 vol% but a_2 varies with n following linear equation, $a_2 = 30 + 20 n$.

tanθ = 0.3

(a)
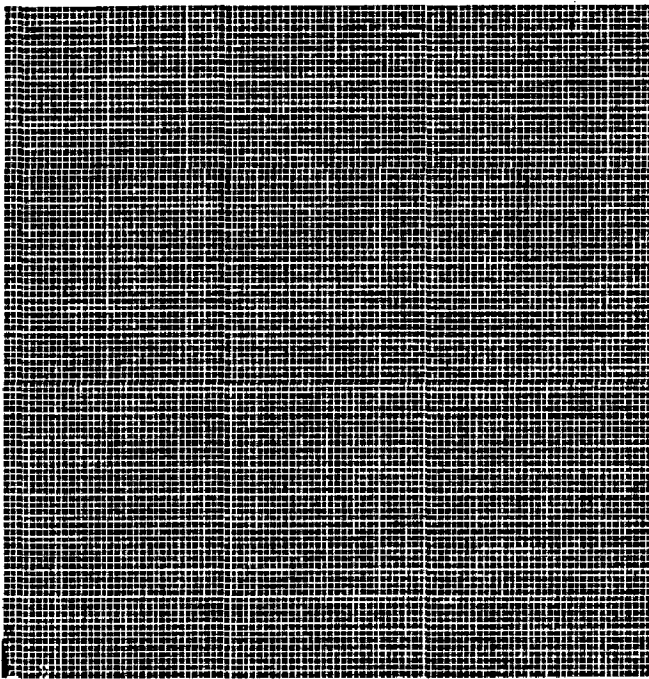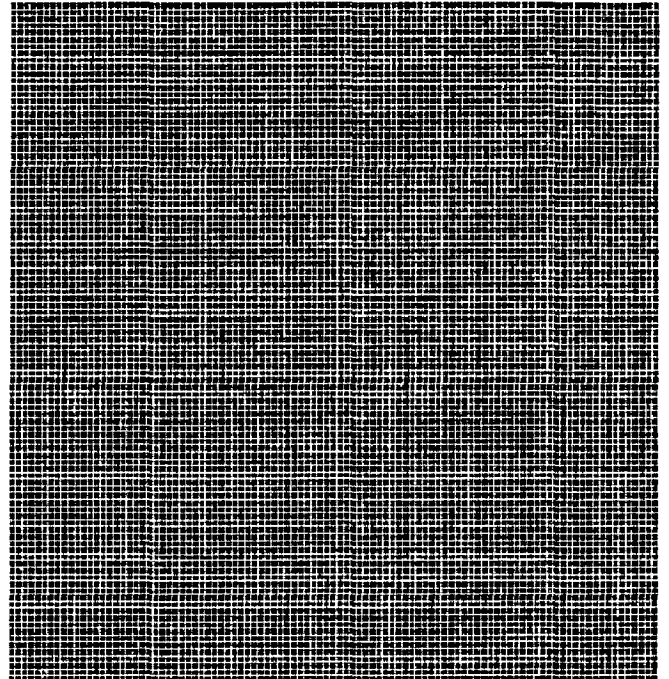
tanθ = 0.4

(b)

Fig. 6.37a, b A schematic showing the comparison of particle distribution in FGM models with linear distribution profiles having slopes tan θ = 0.3 and 0.4 respectively for 30 vol% average particle content.
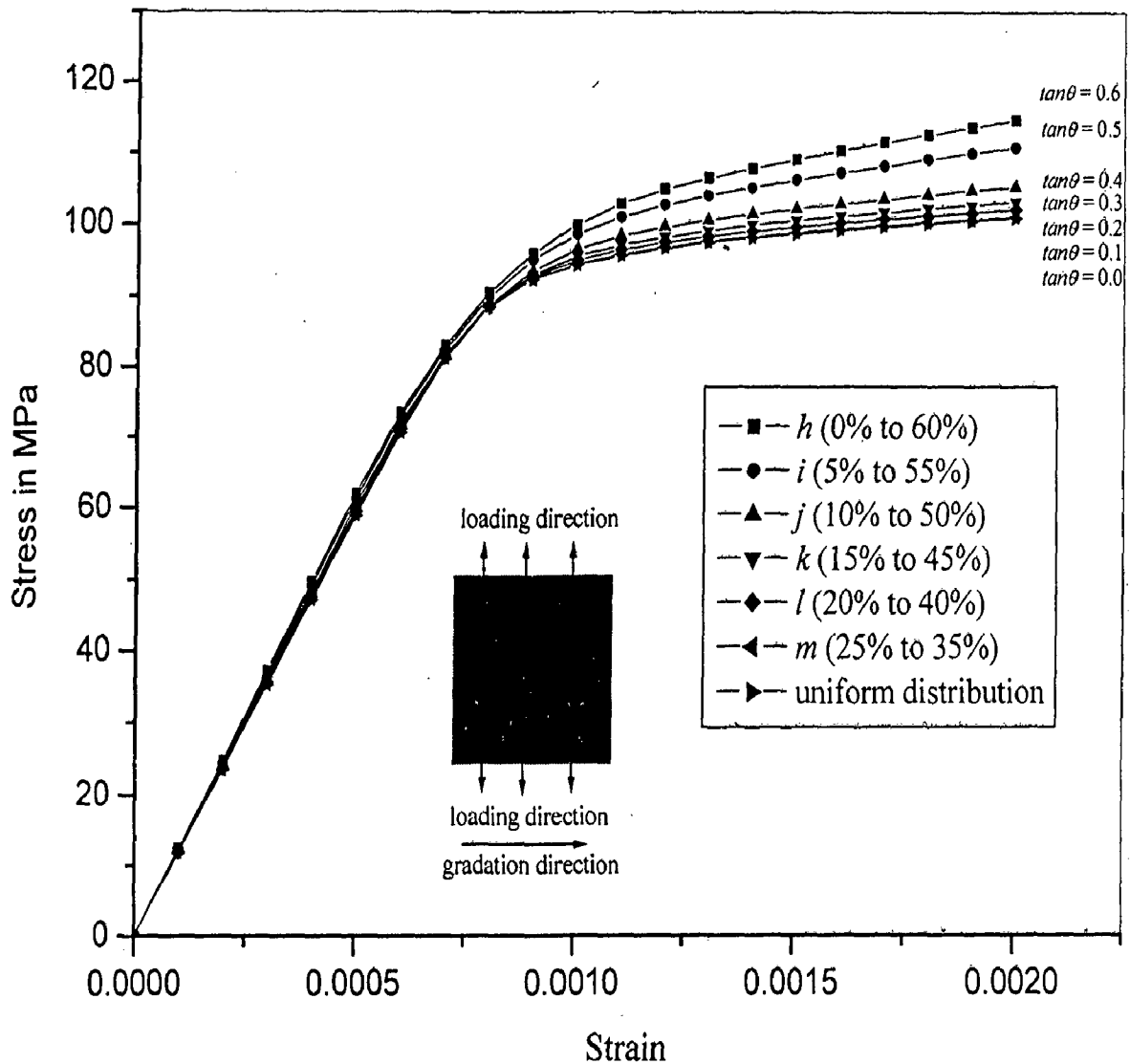
Fig. 6.38 Global non-linear stress-strain behaviour under loading along y-axis of FGMs with average particle content of 30 vol%, distributed with linear gradation of particles in x-axis following profiles shown in Fig. 4.12. The slopes of the linear gradation are shown with all non linear behaviours.
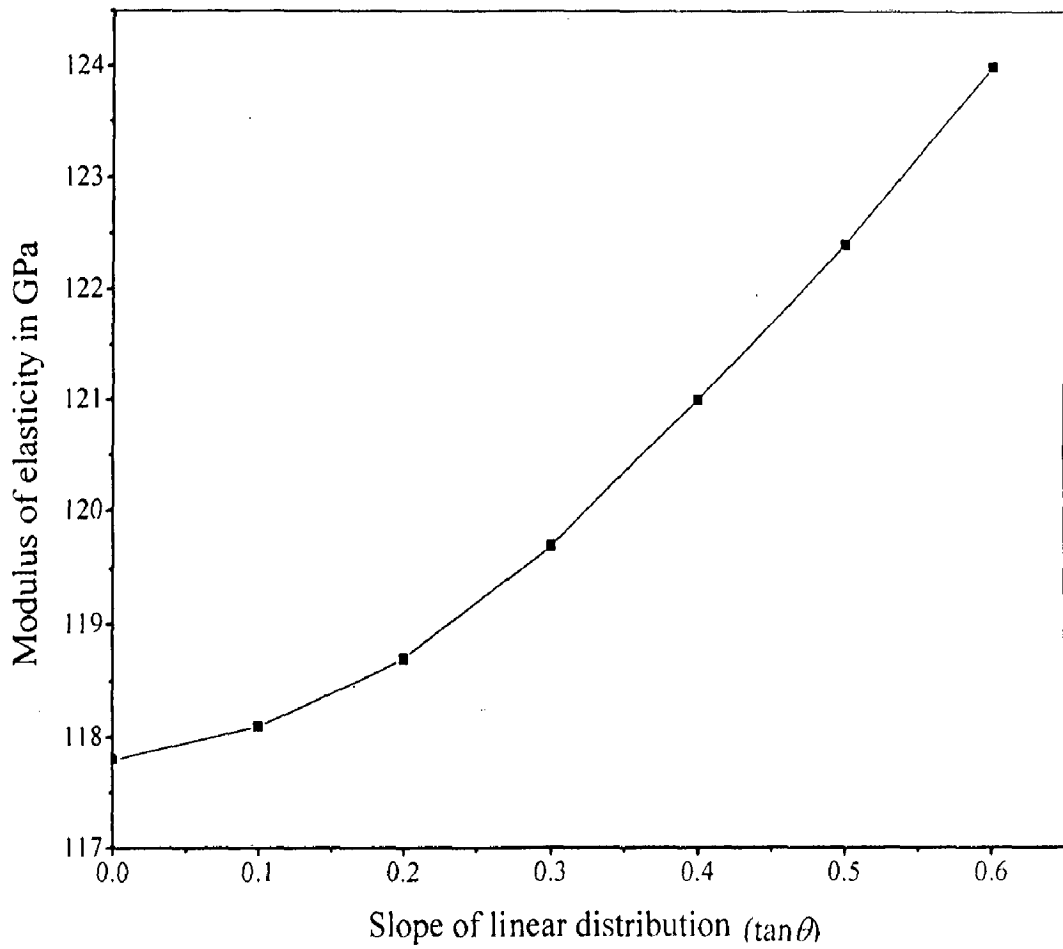
Fig. 6.39 The variation in modulus of elasticity in non gradation direction with slope (tanθ) of linear gradation of particles in FGMs with average particle content of 30 vol%.

185

Fig. 6.40 The variation in yield stress in non gradation direction with slope $(\tan\theta)$ of linear gradation of particles in FGMs with average particle content of 30 vol%.

6.6 RESULTS AND DISCUSSION : TEMPERATURE DISTRIBUTION AND THERMAL STRESSES

For the thermal analysis, the temperature distribution is obtained by imposing the thermal boundary conditions on different models. Three different types of materials combinations are considered in the present analysis - a layered composite plate as shown in Fig. 4.13 in chapter-4, a uniform composite model with 30 vol% of particles and a FGM model with an average particle content of 30 vol% distributed with gradation in x-axis direction from 0 vol% of particles at one end to 100 vol% of particles at the other end. The temperature variation in y-axis direction is assumed to be negligible. Figure 6.41 shows the variation in the temperature inside different models along the x-axis for the imposed boundary conditions as shown in the Fig. 4.13 in Chapter-4.

The thermal stresses are obtained after imposing the structural boundary conditions on different models using coupled field analysis. The results for the thermal stresses are obtained when the plates are constrained to move in x-axis direction. Figures 6.42 and 6.43 show the variation of average thermal stresses σ_{yy} and σ_{xx} at different locations along x-axis direction for different models investigated. The study of the thermal stresses in the FGM model and the layered metal-ceramic model are of major interest. When the plates are constrained to move in the x-axis direction, the average thermal stresses in y-axis direction (σ_{yy}) for the strip composite plate suddenly becomes very high at the interface, as indicated by Fig. 6.42. These stresses are responsible for peeling off the outer ceramic layer due to their exceeding interfacial strength of metal-ceramic interface. For the case of FGM model there is smooth variation in the average stresses and the heat flux at the lower temperature side is also low. Although uniform composite also have smooth variation in thermal stresses, but there is fairly high heat flux to the low temperature side. The variation in σ_{xx} is smooth for all the three cases.
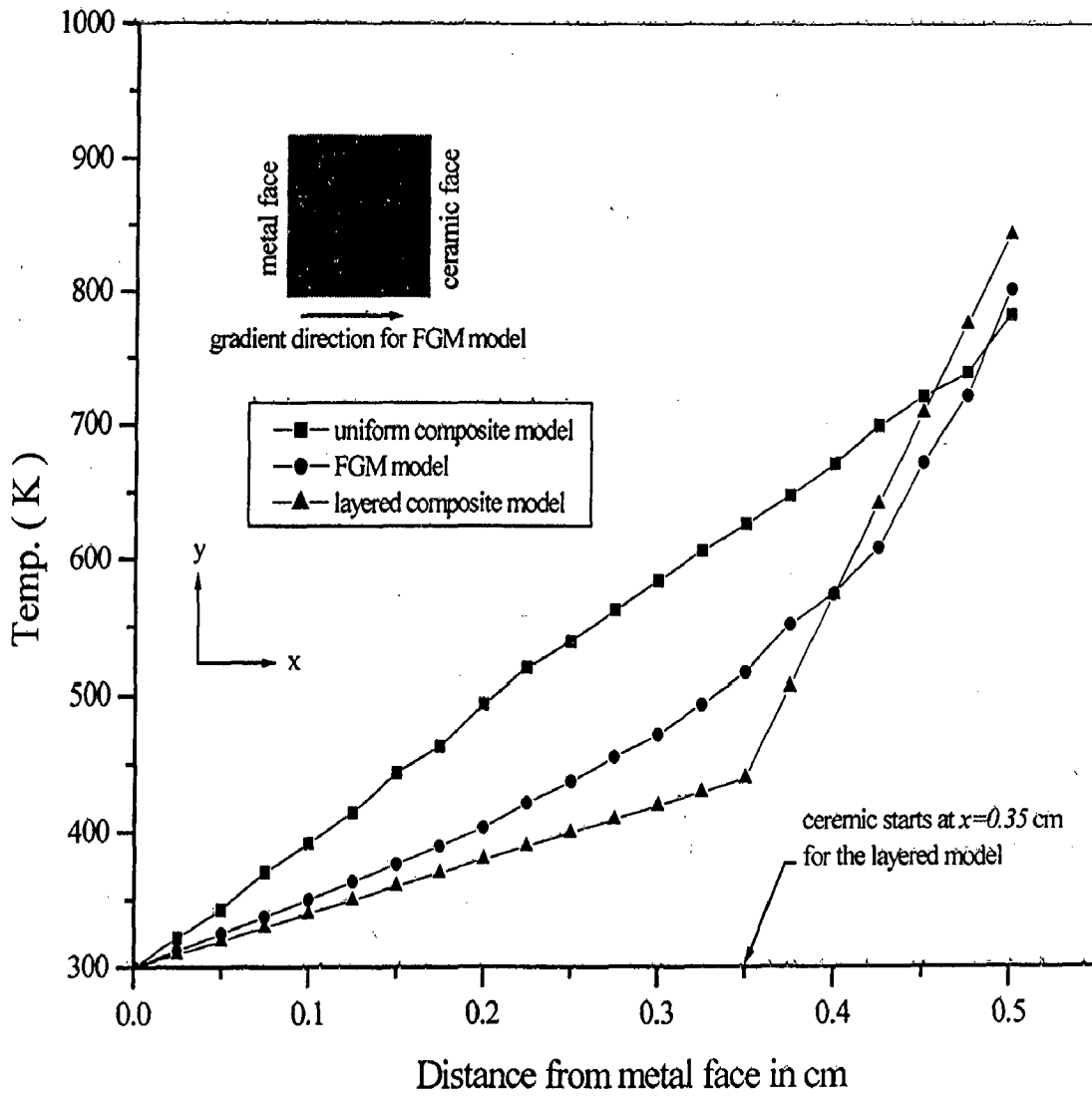
Fig. 6.41 Temperature distribution along the x-axis for the thermal boundary conditions (as shown in Fig. 4.13) in different plate models of layered metal-ceramic, uniform composite and FGM containing the same average ceramic particle content of 30 vol%.
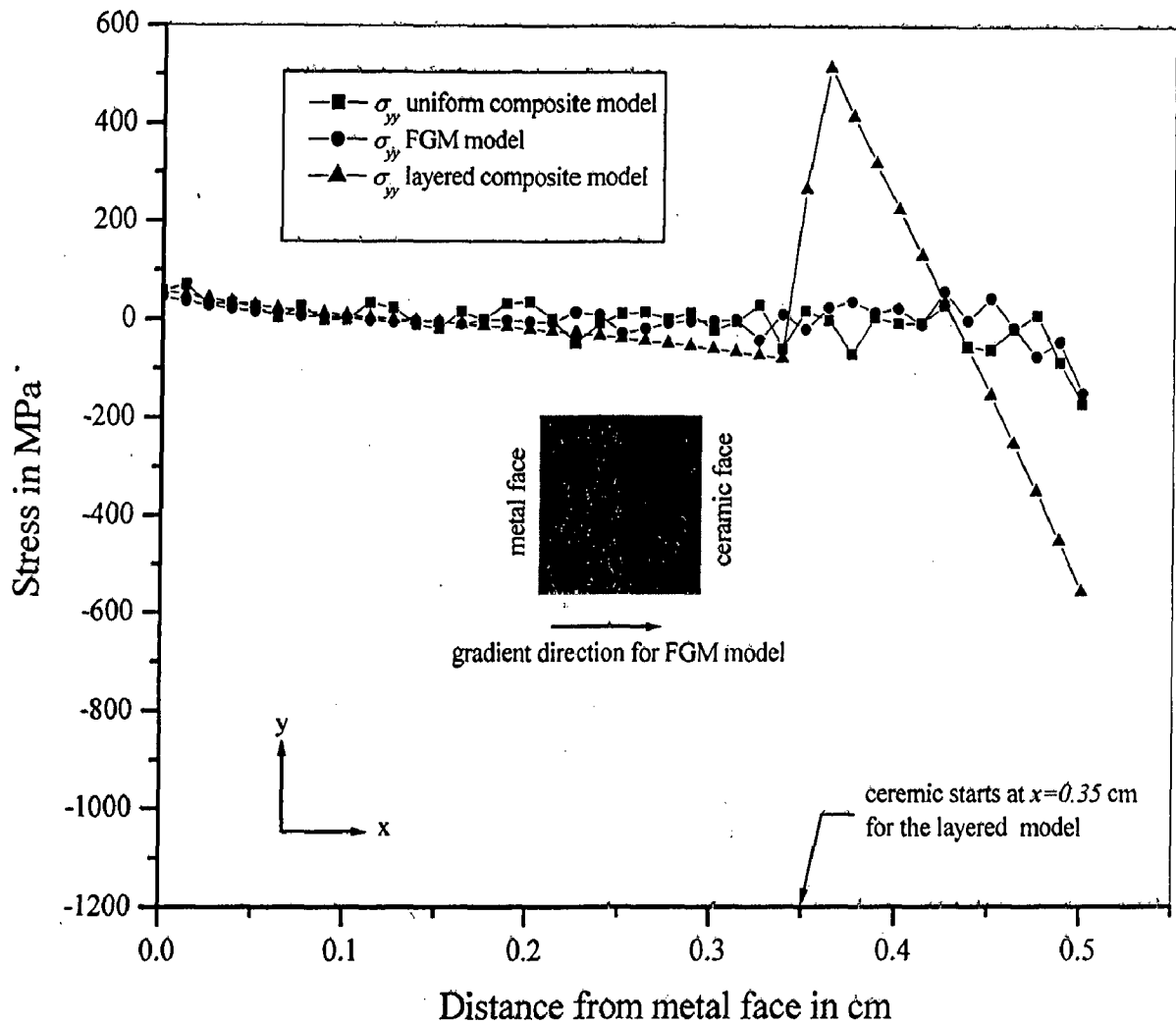
Fig. 6.42 Average normal stresses, σ_{yy}, in y-axis direction developed inside the layered metal-ceramic, uniform composite and FGM plates when constrained to move in x-axis direction for thermal boundary conditions (as shown in Fig. 4.13).
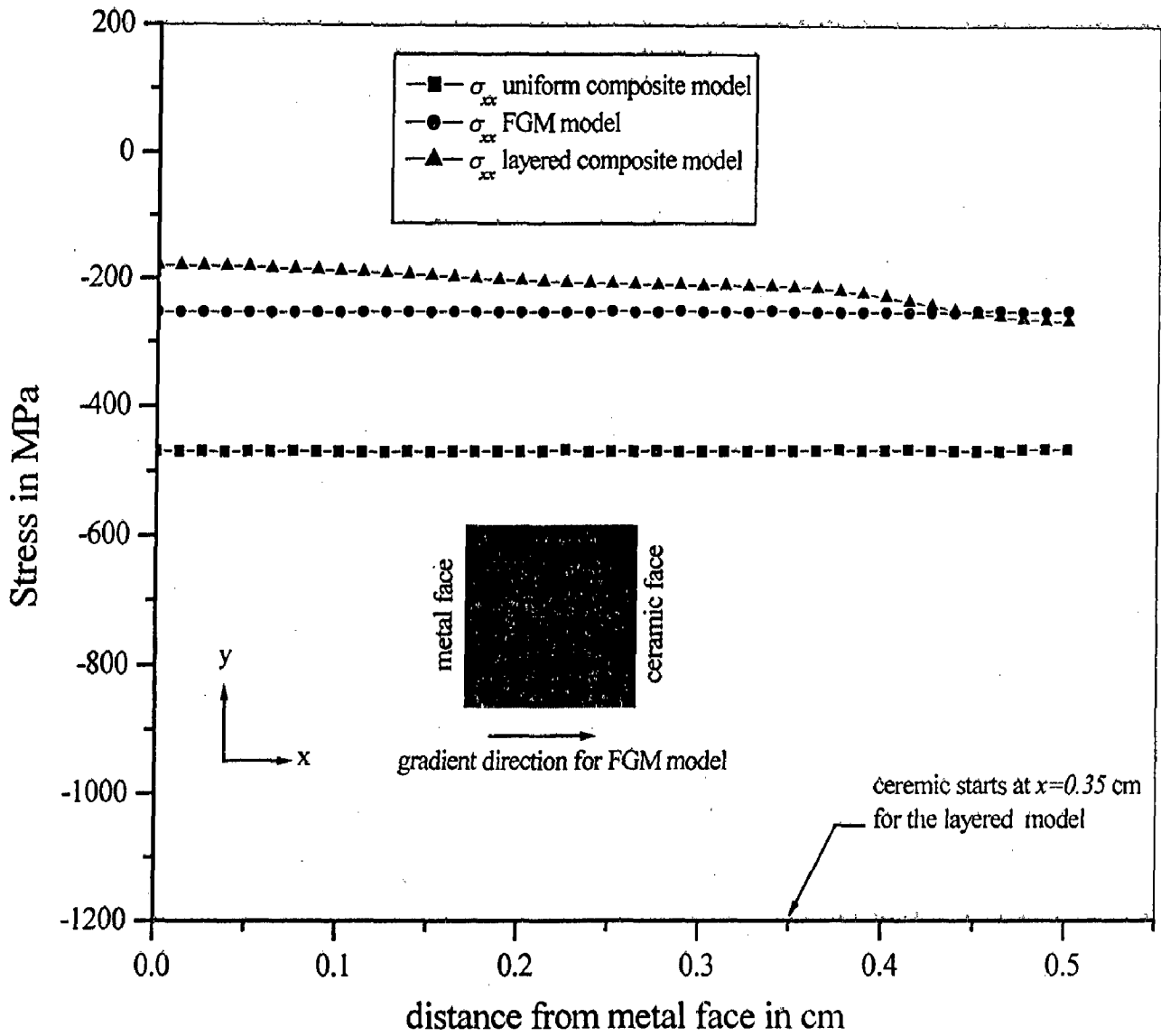
Fig. 6.43 Average normal stresses, σ_{xx}, in x-axis direction developed inside the layered metal-ceramic, uniform composite and FGM plates when constrained to move in x-axis direction (as shown in Fig. 4.13).

6.7 ANALYSIS OF FGM INGOT SYNTHESIZED IN THE PRESENT WORK WITH THE PRESENT MODELLING METHOD

The FGM sample obtained from FGM ingot designated as $20Al/Al_2O_3$ containing an average 20 wt% of alumina particles has been analyzed with the help of present modelling method. The FGM ingot is divided into five equal size layers as shown in Fig. 6.44. Particle volume fractions at the top of the each layer are shown in Fig. 6.45 as measured from optical micrographs with the help of point count technique. The top surface of the layer 1 is just below the shrinkage cavity of the FGM ingot. Similarly the top surfaces of the layer 2, layer 3, layer 4 and layer 5 are 0.5 cm, 1.0 cm, 1.5 cm, and 2.0 cm below the shrinkage cavity respectively. The particle distributions at the top surfaces of the layers are taken to represent the particle distribution in the layers and are modelled using the present modelling technique. It is assumed that there is no particle concentration gradation in the circumferential z-axis direction as the gradation is confined to the radial direction (x-axis) of the cylindrical cast ingot. The axial direction of the cylindrical cast ingot is the y-axis direction and it has no gradation of particle within a layer but the concentration at x = 0 in different layer varies following the particle content as given in Fig. 6.45. It is assumed that the particle volume fraction at the center of the FGM ingot is same as in the location nearest to the center.

For the modelling of the layers of FGM sample, a domain size of 3.5 cm x 0.5 cm representing the x-y section of a given layer is considered. This area is meshed with plane42 square elements with an edge length of 50 μm representing a particle size. The particle distribution is achieved with the help of a FORTRAN program as discussed in Chapter 4. The particle volume fractions are assigned at different locations in the FORTRAN program according to the variation shown in Fig. 6.45. Linear variation in particle concentration is taken between two consecutive locations as it is also shown in Fig. 6.45. All the elements are divided in two lists with the help of the FORTRAN program. One list of elements represents the particles and the other represents the matrix material. Elements representing particles are distributed randomly according to the volume fractions at different locations. Matrix properties and particle properties are assigned to the elements representing matrix and particles respectively. In this way five FGM models are obtained representing the layers 1 to 5. First the global properties of these FGM models are obtained in the y-direction.

Figure 6.46 shows the nonlinear stress-strain behaviour of different layers loaded in the axial y-direction. Modulus of elasticity and yield stress of different layers obtained from the stress-strain behaviour in the y-direction are shown in Figs. 6.47 and 6.48 respectively. The average particle content are found to be 21.2%, 20%, 13.2%, 10% and 5.6% in layers 1, 2, 3, 4 and 5 respectively. The results for the modulus of elasticity and yield stress for the uniform composite models with these average particle contents are also presented in the same figures. The yield strength and modulus of elasticity of the FGMs are better than that of the uniform composites with the same average particle contents in the non gradation direction (y-axis).

In the next step the global properties of these FGM models are obtained in the gradation direction of x-axis. For this, the nonlinear stress-strain behaviour of different layers is obtained in the gradation direction as shown in Fig. 6.49 and the modulus of elasticity and yield stress are obtained for each layer. Figure 6.50 shows the modulus of elasticity of different layers in the gradation direction. Figure 6.51 shows the yield stresses of different layers. The results for the modulus of elasticity and yield stress for the uniform composite models with the same average particle contents are also presented in the same figures. The yield strength and modulus of elasticity of the FGMs are poor than that of the uniform composites with the same average particle contents in the gradation direction (x-axis) as it has already been observed in the results for FGM.

The global nonlinear behaviour of layer 1 is also investigated with porosity. It has been observed that in the cast composites, particles are associated with porosities. As the level of reinforcement increases, the level of porosity also increases. It can be said that there will be gradation in the level of porosity also in the case of cast ingots of functionally graded materials. An average 5 vol% of porosity with pores of particle size is investigated with different linear gradient variations. Figure 6.52 shows the different linear variations in the porosity content in the gradation direction of particle distribution in FGM, marked p_1 to p_4. Figure 6.53 shows the nonlinear stress-strain behaviour for loading in axial y-direction of layer 1 with 5 vol% average porosity distributed following different linear variations. The stress strain curves are very close for different porosity distributions. It is observed that although there is a reduction in the yield strength and the modulus of elasticity as the slope of the linear variation increases, this reduction is not substantial.
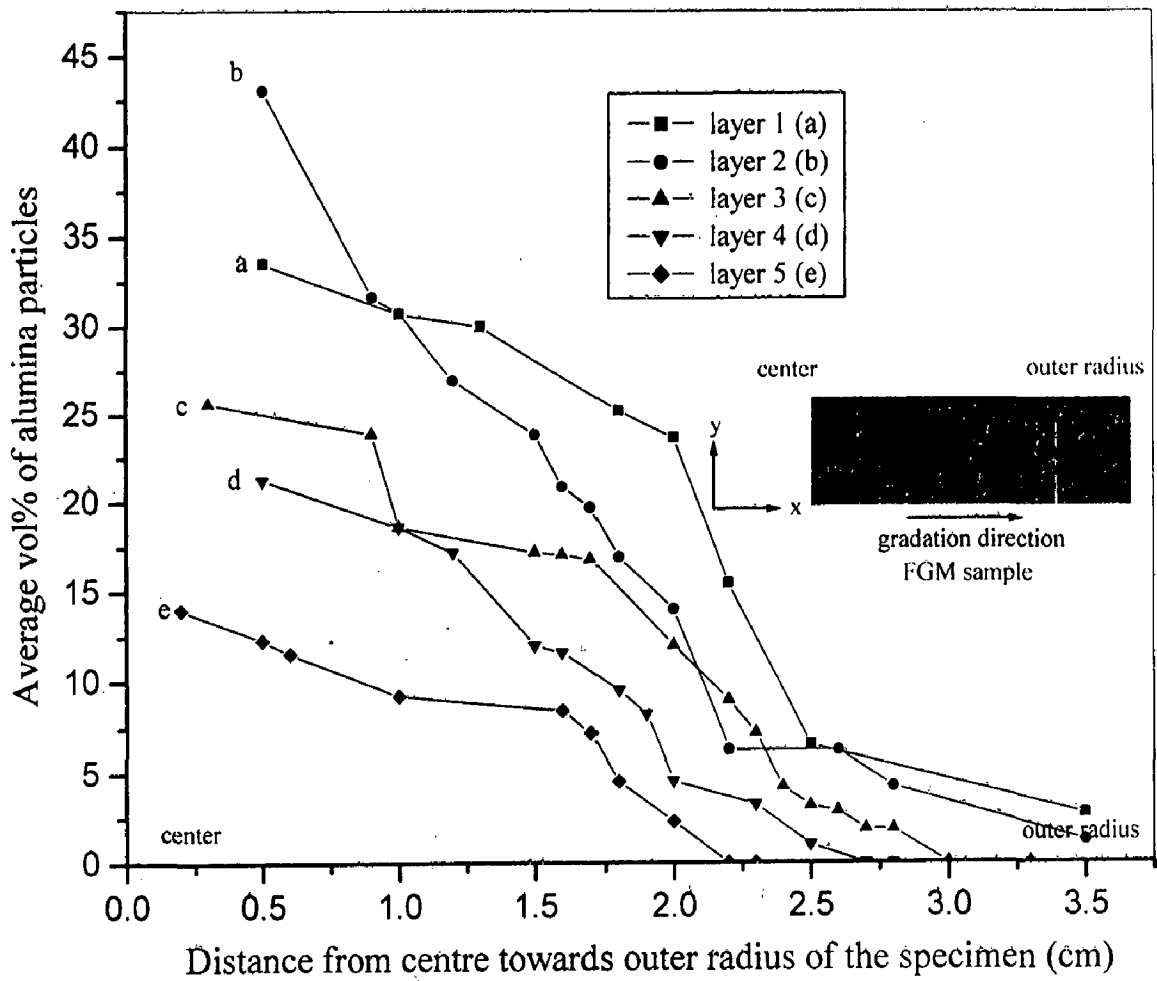
Fig. 6.45 The variation in particle content from centre to the outer radius of cast FGM ingot, $20Al/Al_2O_3$.

194
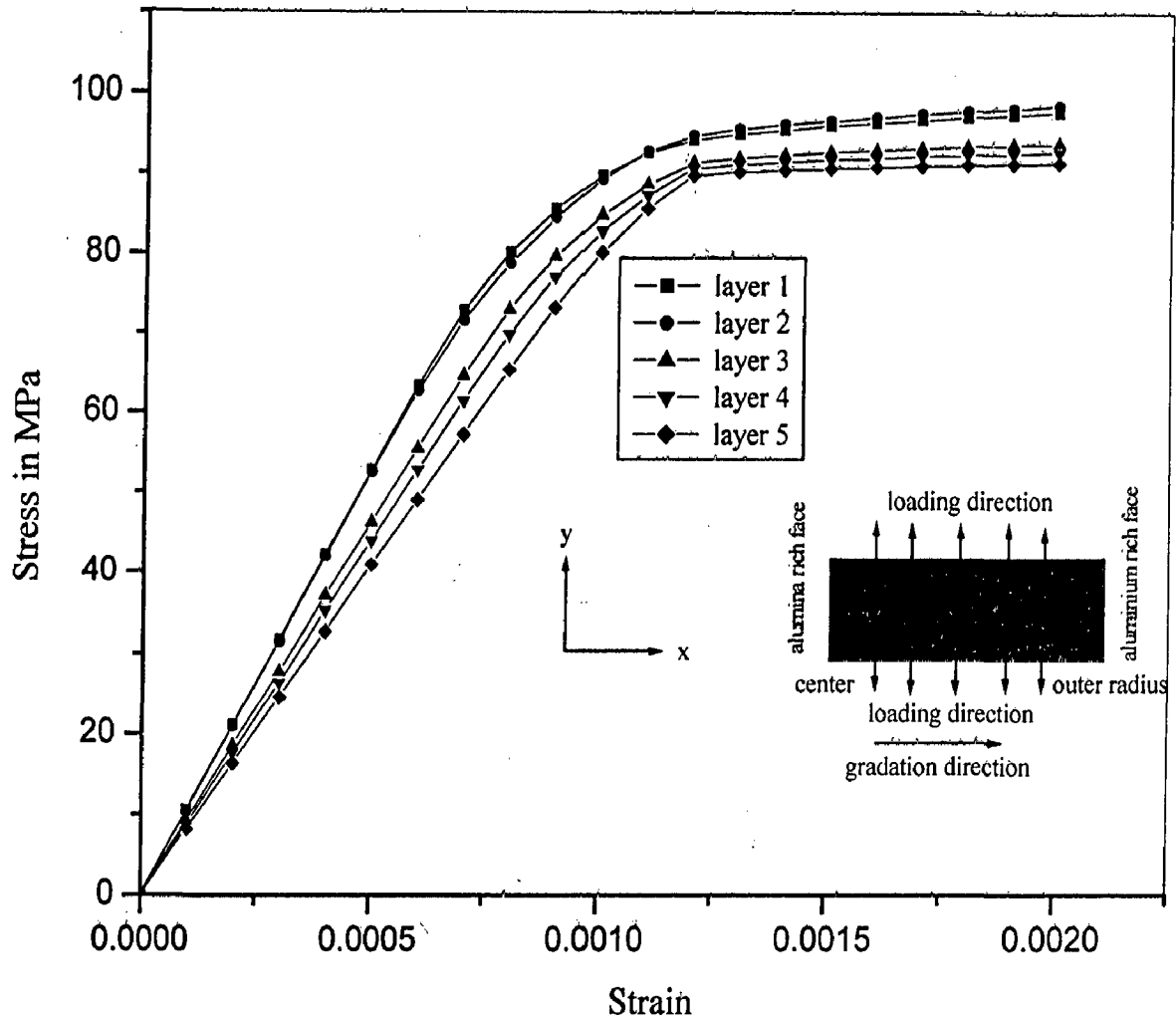
Fig. 6.46 Stress-Strain behaviour of different layers (as shown in Fig. 6.44) in the non gradation (y-axis) direction.
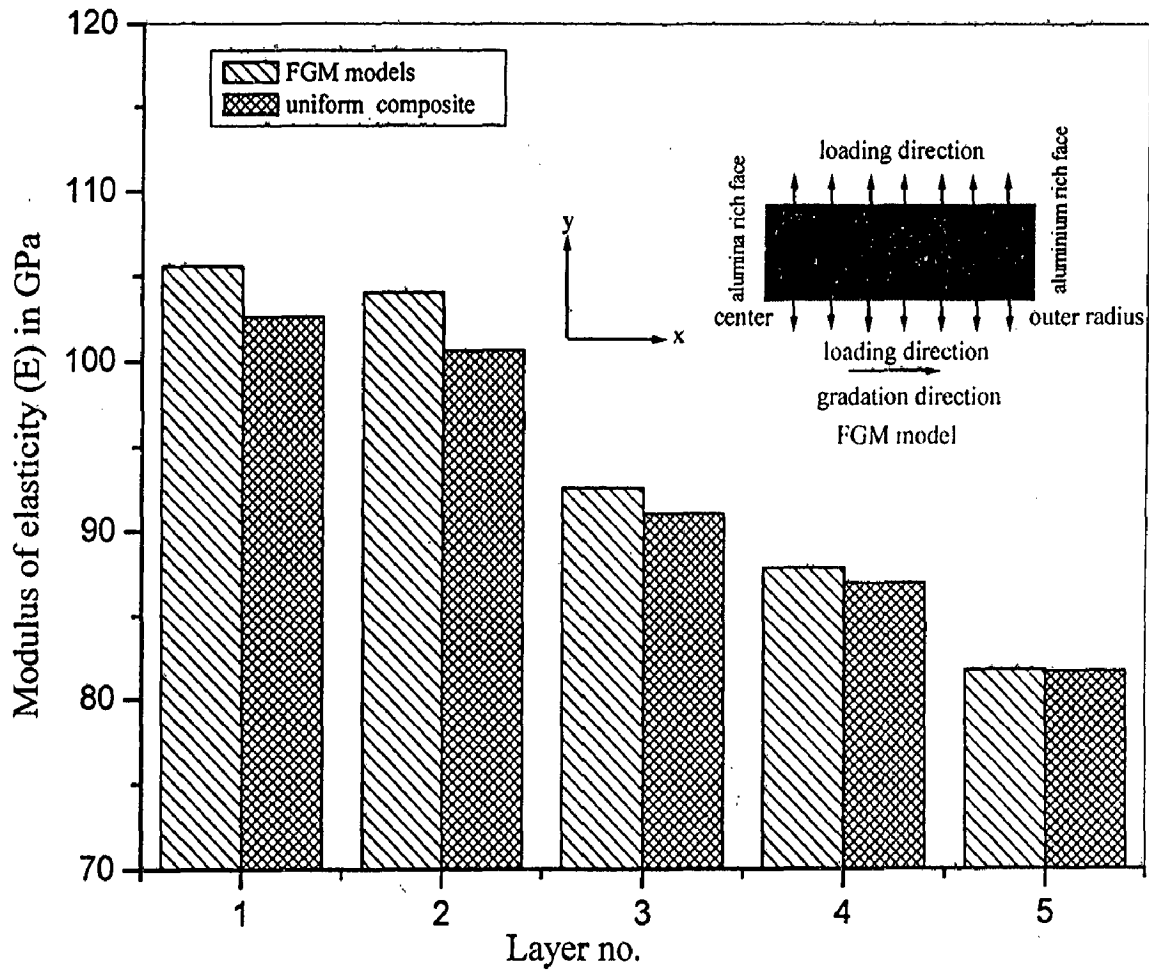
Fig. 6.47 Modulus of elasticity results for the FGM layers in the non gradation (y-axis) direction. Results for uniform composite models with the same average particle vol% as of corresponding FGMs are also presented.

196
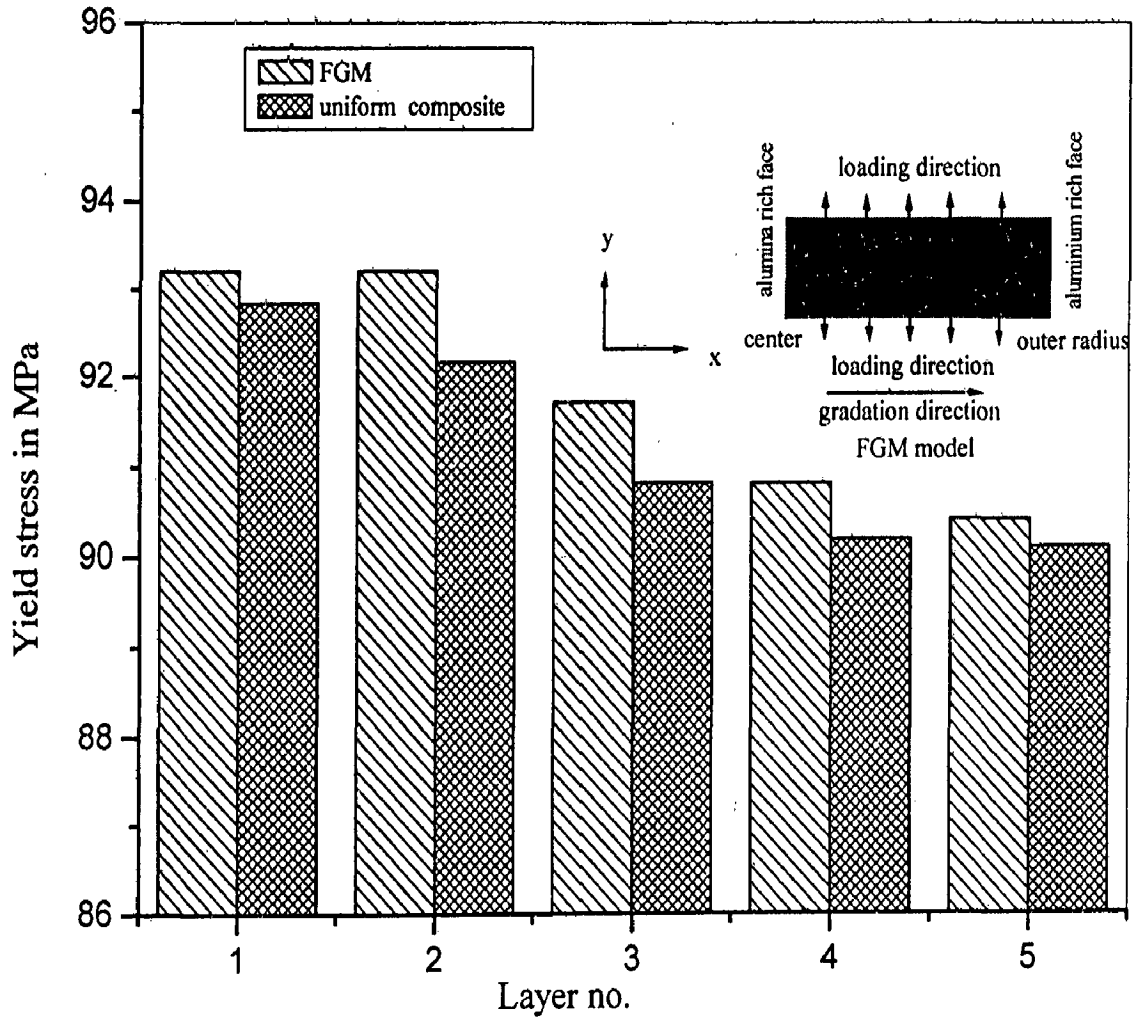
Fig. 6.48 Yield stress results for the FGM layers in the non gradation (y-axis) direction. Results for uniform composite models with the same average particle vol% as of corresponding FGMs are also presented.
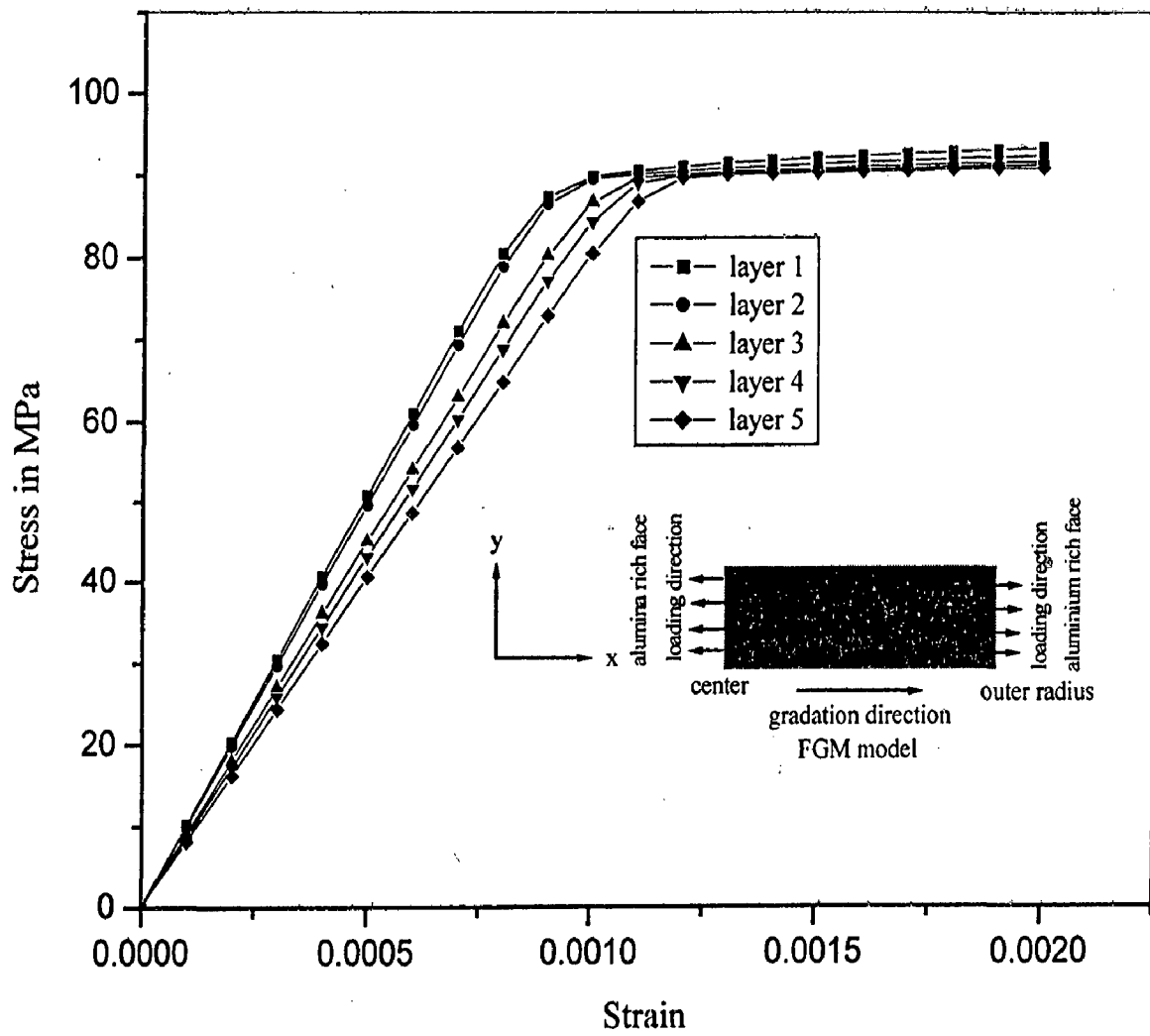
Fig. 6.49 Stress-Strain behaviour of different layers (as shown in Fig. 6.44) in the gradation (x-axis) direction.
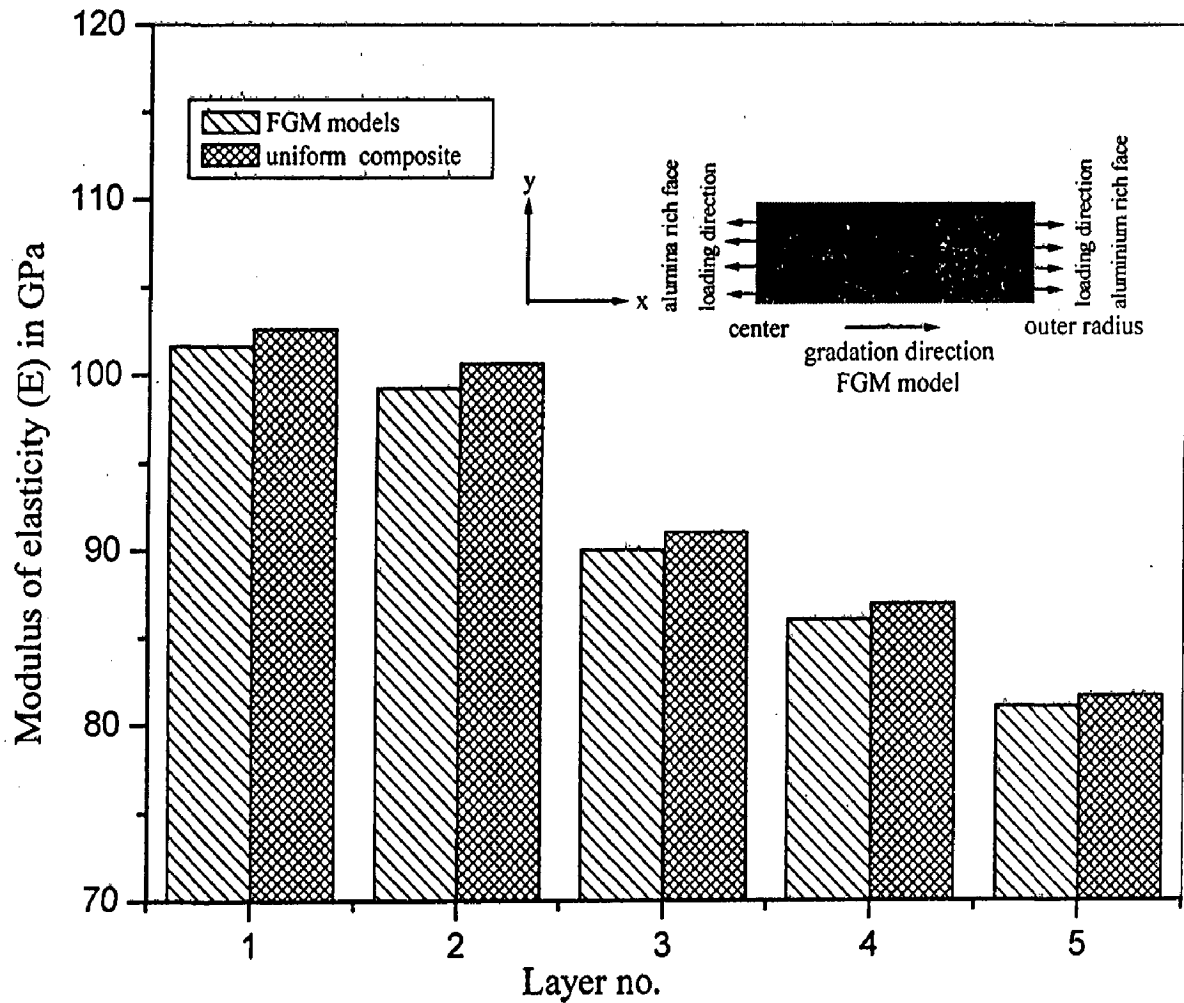
Fig. 6.50 Modulus of elasticity results for the FGM layers in the gradation direction (x-axis). Results for uniform composite models with the same average particle vol% as of corresponding FGMs are also presented.
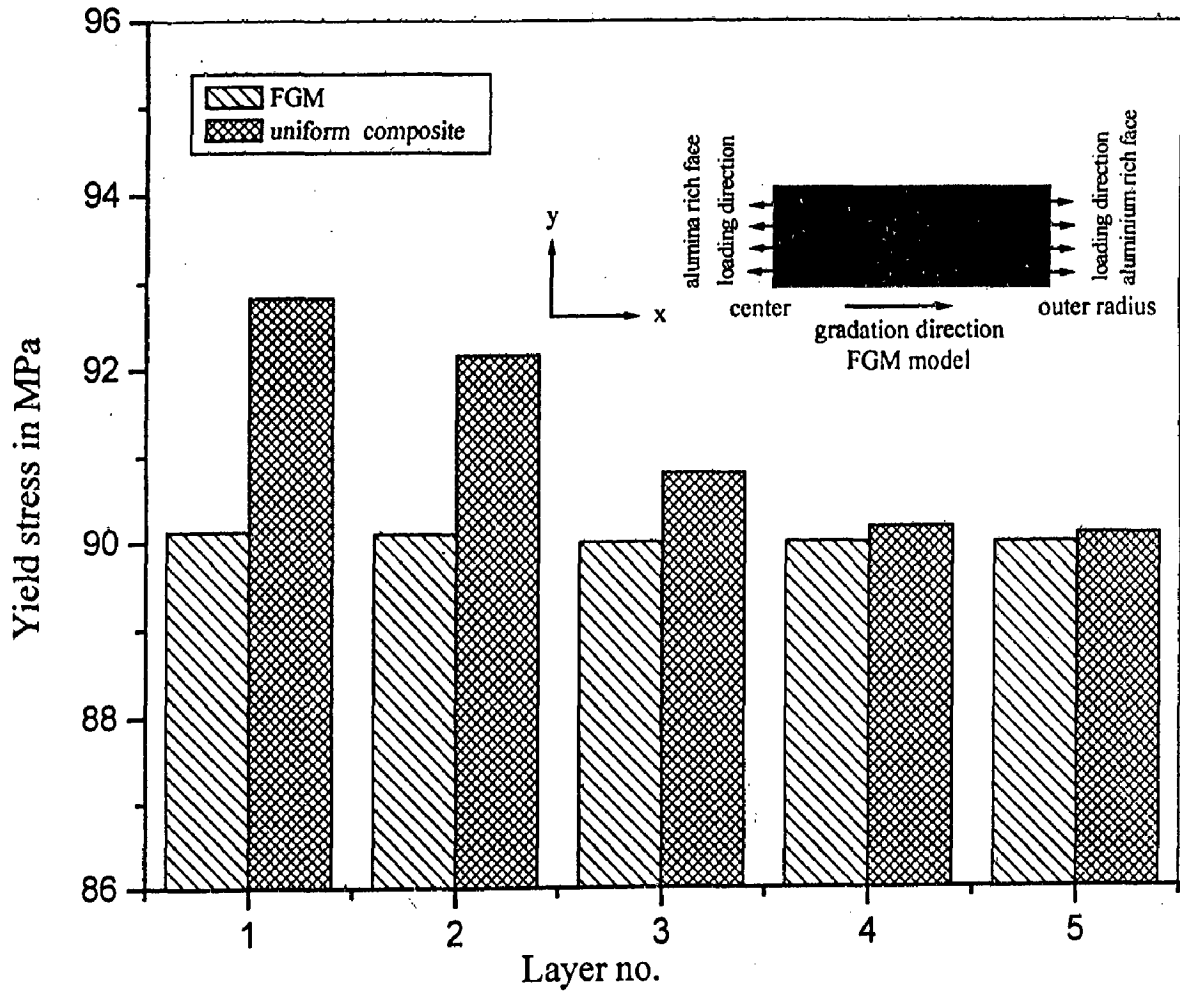
Fig. 6.51 Yield stress results for FGM layers in the gradation direction (x-axis). Results for uniform composites with the same average particle vol% as of corresponding FGMs are also presented.
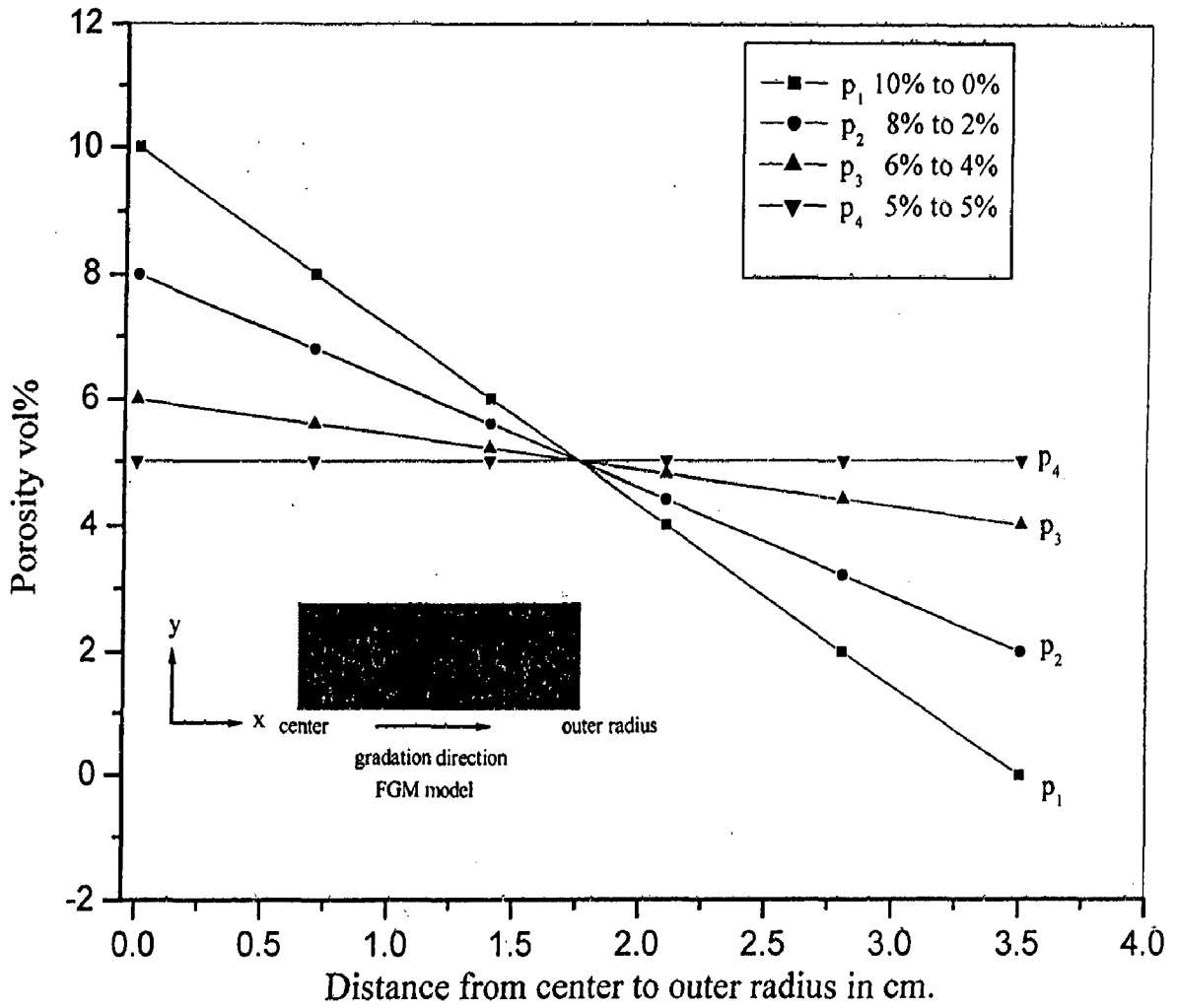
Fig. 6.52 Different linear variations for porosity investigated for layer 1.
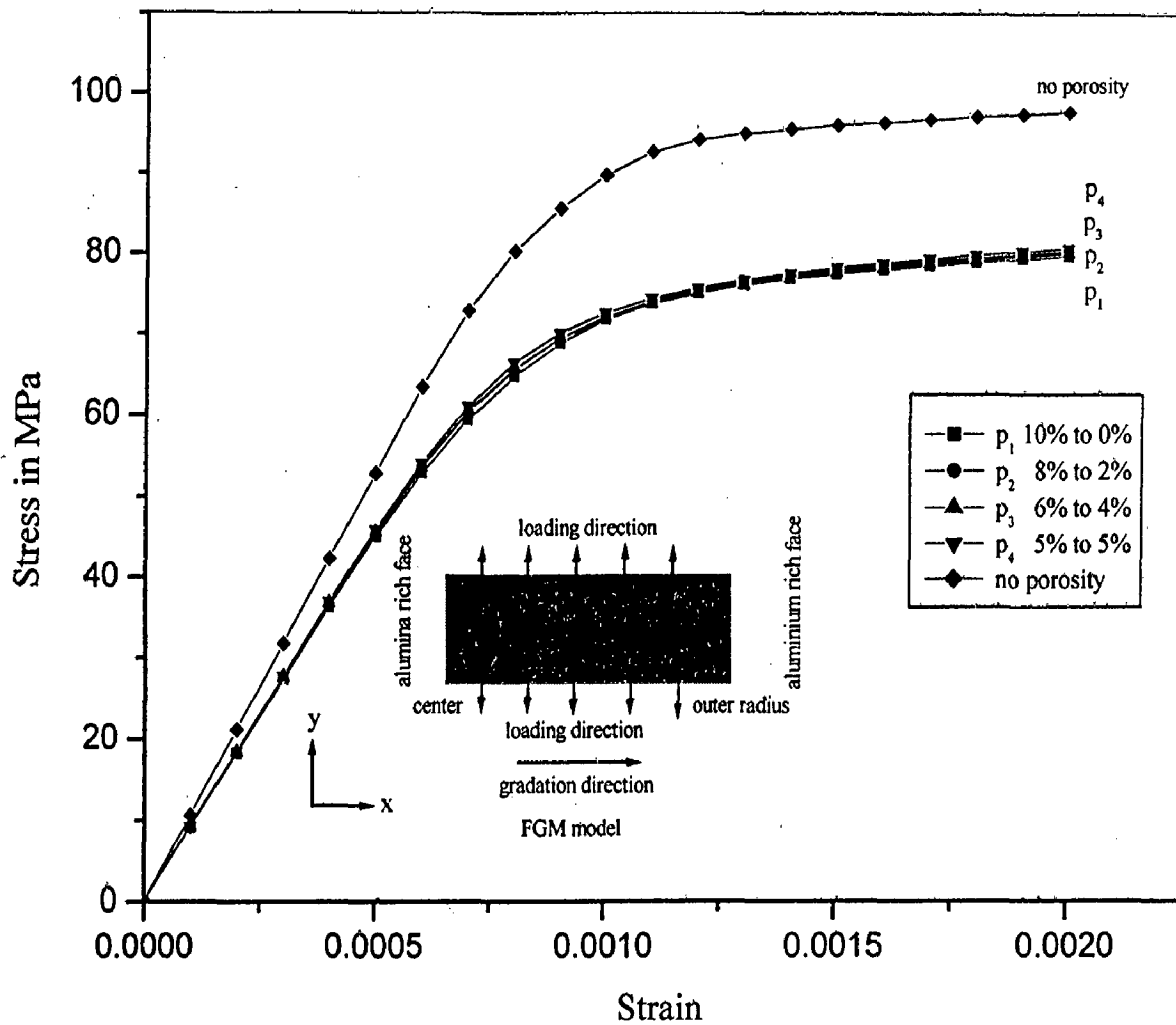
Fig. 6.53 Nonlinear behaviour in the non gradation (y-axis) direction of layer 1 with 5 vol% of porosity having different linear variations (shown in Fig. 6.52). Pores are of particle size.

The variation in yield stress along the radial direction from centre to the outer radius in layer 1 (top layer) and layer 5 (bottom layer) is also investigated by dividing the layer into seven strips of size 5 mm x 5 mm. The yield stress of each strip is assumed to be the local yield stress at the location corresponding to the mid-point of the strip. Results for yield stress in all these seven strips are obtained after imposing a uniform displacement load on the x-y section of layers along the non gradation direction. Figures 6.54 and 6.55 show the variation in yield stress along the radial direction of layer 1 and layer 5 respectively. The variations in hardness and particle content obtained from experimental investigation are also included in the same figure. The broad trend in variation of yield stress follows those of particle concentration and hardness observed experimentally. However, there is difference in local trend at places which may be due to exclusion of porosity in this model. In a monolithic material, slip line field theory has shown that hardness is proportional to yield stress and experiments have confirmed it although proportionality constant varies slightly from material to material. Figure 6.56 shows the variation of the ratio of yield stress and Vickers hardness along the radial distance in layers 1 and 5 with the expectation that it will be the same but porosity may have acted as the spoilsport by changing the ratio towards the centre where there are more particles. Although it has not been possible to match the calculated properties because of problems of direct measurement of yield stress or porosity locally but the similarity in broad trends gives the necessary confidence in the model about its ability to represent the reality.
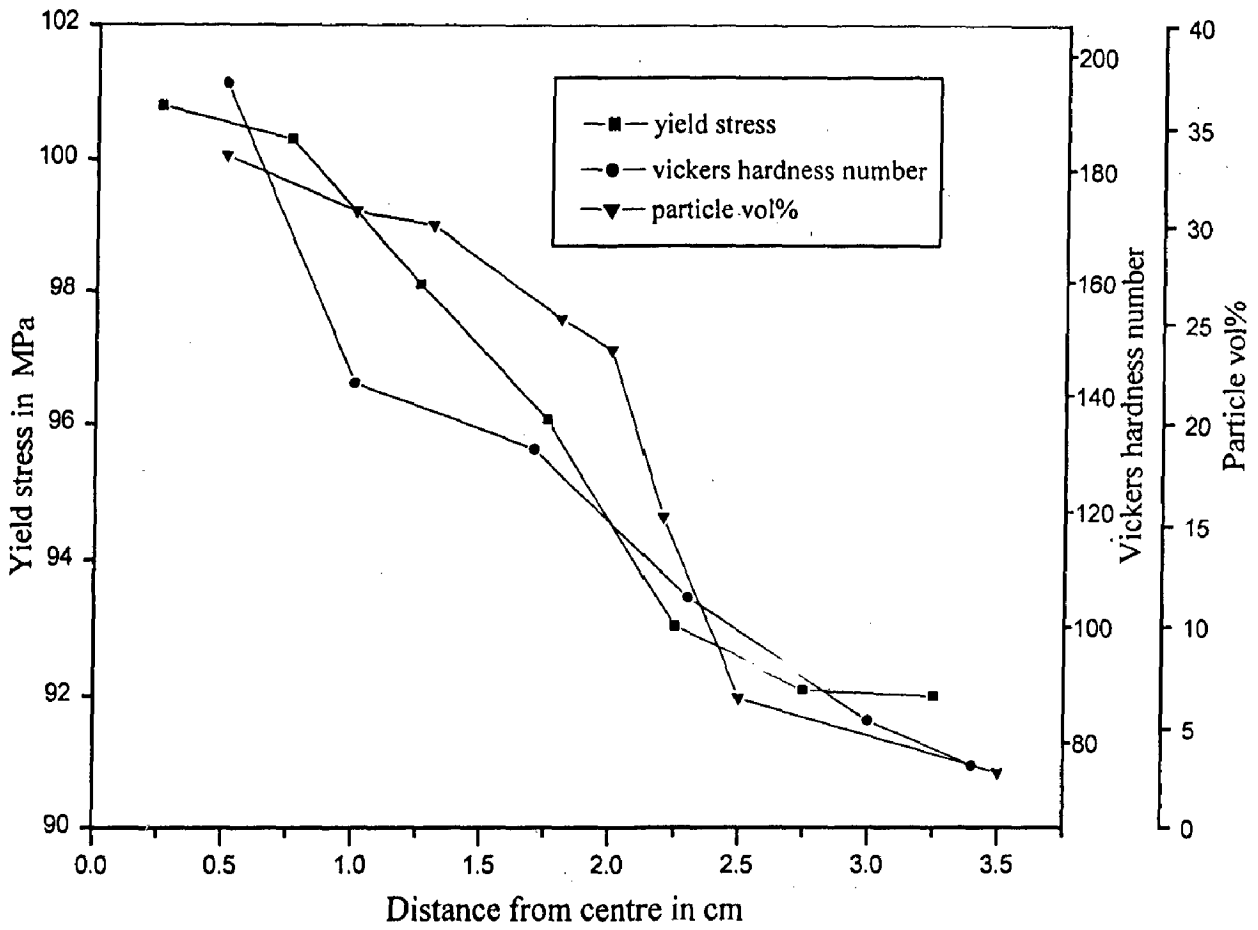
Fig. 6.54 The variation in yield stress in layer 1 (top layer) from centre to the outer radius. The experimental results for variation in particle vol% and hardness are also presented.
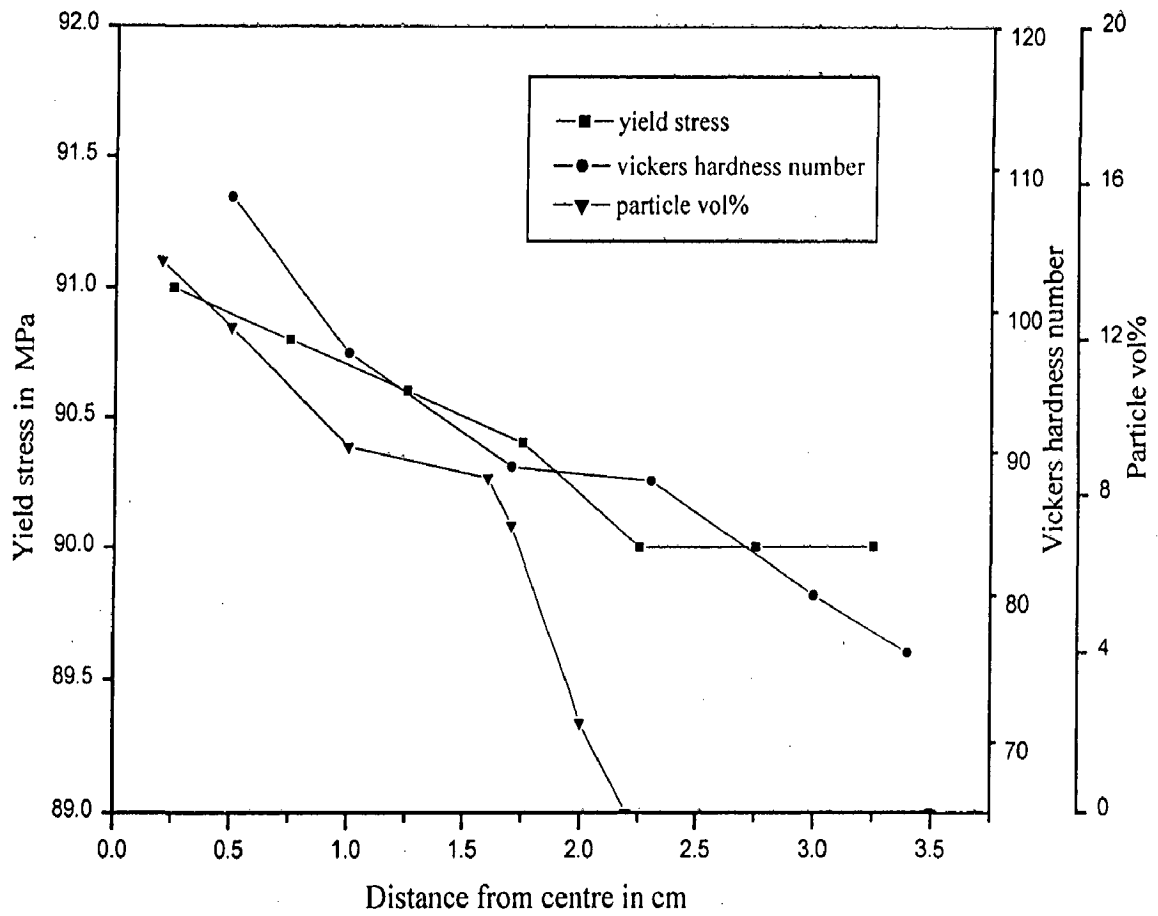
Fig. 6.55 The variation in yield stress in layer 5 (bottom layer) from centre to the outer radius. The experimental results for variation in particle vol% and hardness are also presented.
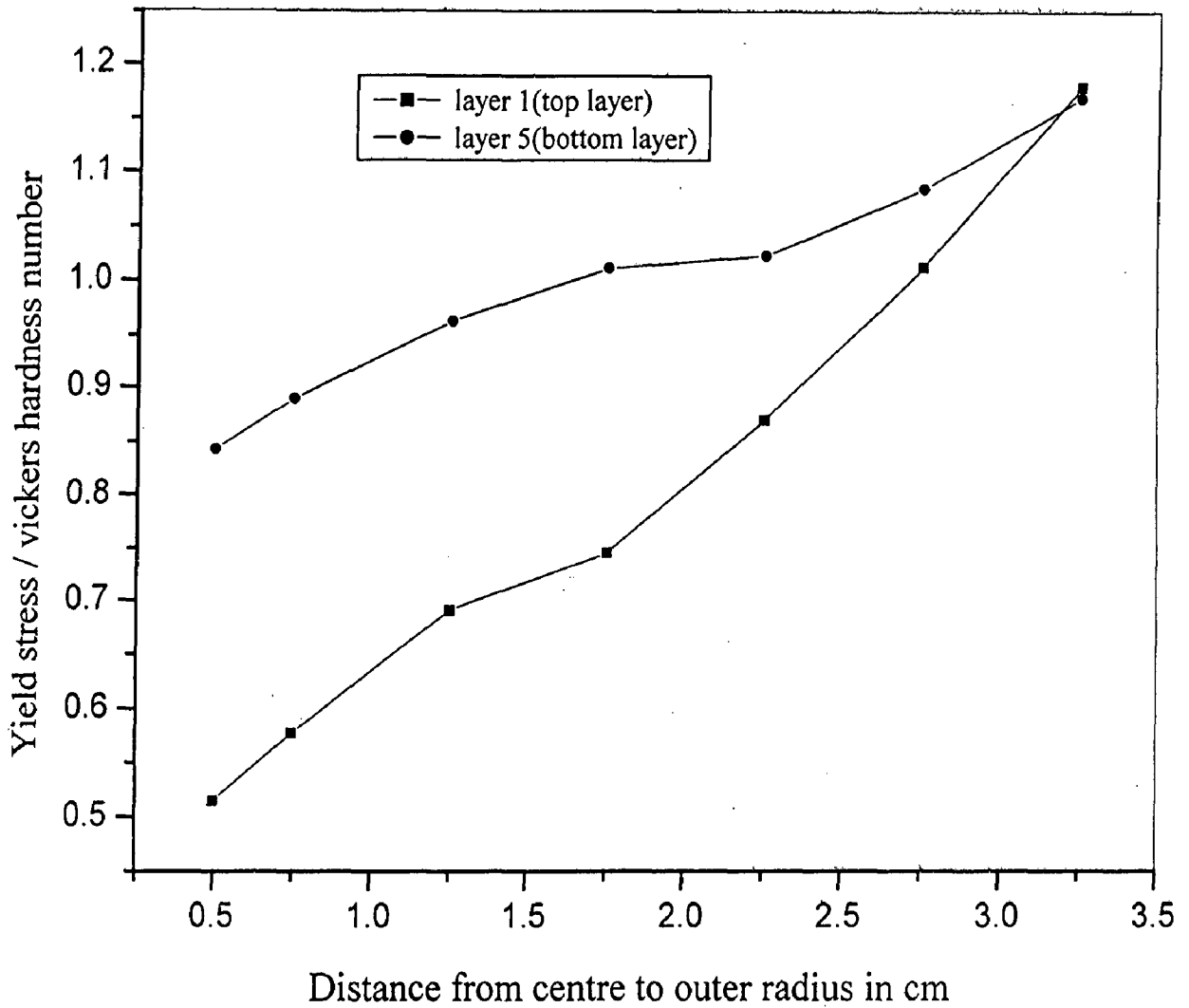
Fig. 6.56 The variation in ratio of yield stress and Vickers hardness number in the top and bottom layers from centre to the outer radius.

CONCLUSIONS

The present study on the modelling of deformation behaviour of uniform Al-Al$_2$O$_3$ composite and FGM based on it has led to the following important conclusions in different segments of the study including the influence of porosity and validation of results by experimental studies.

7.1 MODELLING OF UNIFORM COMPOSITES

1. Uniform composite models with randomly distributed particles containing different amounts of particles from 10 to 90 vol% in a step of 10% show an important difference with the unit cell models in respect of particle clustering, particularly at higher particle contents, as obtained in a 2-D square having an edge length of 5 mm, divided into grids of 50 μm, which is the size of the particle.

2. The elastic behaviour as determined by the modulus of elasticity under application of uniaxial load on the two opposite side of the square representing the uniform composite has been investigated by distributing the same amount of particles randomly and the global property like modulus of elasticity is found to be insensitive to micro level of difference in various random distribution of particles.

3. The results for modulus of elasticity of the present modelling technique for uniform composites are compared with the bounds predicted by the well established rule of mixture (ROM) and inverse rule of mixture (IROM), giving the most conservative upper and lower bounds for the modulus of elasticity respectively and the results of the present modelling technique are well within these bounds.

4. The results predicted by the present model for modulus of elasticity when compared with the well known Hashim-Shtrikman (1963) bounds, are found to be well within these bounds as well.

5.	The present model results for modulus of elasticity are in good agreement with those obtained by Halpin–Tsai (1968) equation with the parameter $\zeta = 2$.

6.	The present model results for modulus of elasticity when compared with the experimental results given by Aradhya and Surappa (1991) for aluminium matrix composite reinforced with SiC particles, show good agreement but their results for modulus of elasticity obtained from FEM model based on unit cell approach are slightly lower.

7.	On the basis of the results of the present modelling technique an empirical equation for estimating modulus of elasticity of uniform composite having a given particle content distributed randomly has been proposed.

8.	The results for modulus of rigidity for the uniform composite with different average particle contents distributed randomly are well within the bounds of rule of mixture and inverse rule of mixture and also, within the bounds given by Hashim-Shtrikman (1963).

9.	The stress distribution within the uniform composite is fairly inhomogeneous and the extent of inhomogeneity increases with increase in strain and the particle content in the composite.

10.	Non linear analysis has been carried out with the present model to predict nonlinear behaviour of the uniform composites with different average particle contents. It has been concluded that the strain required for a composite to undergo transition from elastic to plastic behaviour decreases with increasing particle reinforcement. These results are similar to those obtained by Bao and coworkers (1991) with their unit cell model.

11.	On the basis of results on yield stress as estimated by the crossover method for composites having different average particle contents up to 70 vol% distributed randomly, a linear empirical relation showing the dependence of yield stress on the particle content has been obtained.

12.	The variation of the ratio of flow stress of a composite (σ_{oc}) to that of the matrix (σ_o) with increasing particle contents obtained under the plane strain conditions compares quite well at lower particle content with those obtained by Bao and coworkers (1991) for their unit cell model for particles of different shapes and orientation but for the composites with higher particle contents, the result of the

208

present model gives higher value for the flow stress ratio, which could be attributed to clustering of particles.

13. Uniform composite models with an average particle content of 20 vol% but clustered in grids to give different shapes and sizes of particles, distributed randomly over the whole matrix show that the shape of particle affects both the modulus of elasticity and the yield stress, which decrease significantly if the particles are elongated in the direction normal to that of loading but their orientation in the direction of loading results in higher modulus of elasticity and yield strength as in aligned short fiber reinforced composite.

14. Numerical results have been obtained for the variation of modulus of elasticity of uniform composites with increasing particle vol% from 0 to 100, with three different porosity contents of 2.5, 5.0 and 7.5 vol%. It is concluded that porosity lowers the Young's modulus of the composites. The results of the present model for modulus of elasticity have been compared with Sprigg's equation.

15. The elastic modulus of uniform composite containing four different types of pores represented by $1*1$, $1*4$, $2*2$ and $4*1$ as determined by non-linear analysis, indicates that there is 33% reduction in the elastic modulus in y-axis direction of a composite containing 30 vol% of particle and 7.5 vol% of porosity when the porosity type changes from $1*4$, extended in y-axis direction, to $4*1$, extended in the x-axis direction. These results also show that for the same porosity type (type $1*4$) the reduction in the modulus of elasticity is only 5.3% when the porosity content increases from 2.5 to 5 vol%.

16. The yield strength of uniform composite containing four different types of pores represented by $1*1$, $1*4$, $2*2$ and $4*1$, as determined by non-linear analysis, indicates that the yield strength in y-axis direction of a composite containing 30 vol% of particle and 7.5 vol% of porosity, decreases from 77 MPa to 47.8 MPa when the pore type changes from 1*4, extended in y-axis direction, to $4*1$, extended in x-axis direction, which are respectively the least and most damaging pore types considered in the present work. Thus, there could be 38% reduction in the yield strength depending on the shape, size and orientation of pores for the same porosity content of 7.5 vol%. Also the results for yield strength show that

there is only 9% reduction in the yield stress for the same porosity type of *1*4* when the porosity content increases from 2.5 to 5 vol%.

17.   It has been observed that the ratio of yield stresses with and without porosity decreases with the level of reinforcement and the results of the present model compares fairly well with the experimental results and those given by Tekmen and coworkers (2003) and Ghosh (1986).

18.   The average porosity content is not a reliable parameter to predict the mechanical properties as the shape and orientation of pores are important in determining the damage. The existence of large pores perpendicular to the loading direction is more damaging because of high stress concentration as known already.

7.2   FUNCTIONALLY GRADED MATERIALS

19.   Al-Al$_2$O$_3$ based FGM ingots with average weight percentage of alumina particles of 10%, 20 % and 30% has been successfully synthesized by using centrifugal casting method and alumina content decreases gradually in the radial direction from the centre towards the outer radius. The decrease in alumina content from the centre towards the outer wall is contrary to expectation as alumina is denser but associated porosity with particle may be responsible for the observed behaviour.

20.   Alumina content in the cast ingot decreases gradually also in the axial direction from the top below the shrinkage cavity to the bottom of the cast ingots. The decreasing alumina content from the top to the bottom of cast ingots is also surprising in view of higher density of alumina particles relative to the melt but it is often observed in cast composite ingots due to pores surrounding poorly wetting ceramic particles.

21.   Vickers hardness distribution of the cast ingot follows the particle distribution but there are sometimes abrupt changes locally in the hardness distribution, which has been attributed to inhomogeneous cast structure of the cast FGM ingot. Annealing of the cast FGM ingot results in the elimination of cast structure and the radial hardness distributions become relatively smooth.

22.   FGM models with variation of particle concentration in the direction of x-axis from 0 vol% at one end and 100 vol% at the other end following a polynomial

distribution show that the global average values of modulus of elasticity under loading in the gradation direction of x-axis are lower than that in the uniform composite for the same average particle content. But for loading in the y-axis direction (normal to the gradation direction) the modulus of elasticity values are higher than that in the corresponding uniform composite.

23. FGM models with gradation in both x-axis and y-axis directions results in the global average values of modulus of elasticity almost equal to that obtained for uniform composites with the same average particle content.

24. Nonlinear analysis of FGM models with gradation in x-axis direction exhibit better yield properties when loaded in y-direction, in comparison to those in uniform composite with the same average particle content but exhibit relatively poor yield properties, when loaded in x-axis direction. It is further observed that FGM models show the same yield stress as that of the matrix up to almost 70 vol% of particle content under loading in x-axis direction. The modulus of elasticity of the FGMs is also lower when loaded in the x-axis direction, than that of the uniform composite for the same average particle content.

25. Variation in local values of modulus of elasticity for the FGM models having gradation in x-axis direction for different average particle contents follows closely the variation in particle concentration.

26. FGM models with average particle content of 30 vol% but following different types of polynomial and linear gradation have demonstrated that the global values of modulus of elasticity and yield stress of FGMs are affected by the type of the gradation in particle concentration to a great extent.

27. The FGM samples synthesized experimentally in the present study have also been modelled on the basis of particle distribution obtained experimentally and the results for global modulus of elasticity and yield stress have been obtained at different layers below the shrinkage cavity for loading in the gradation direction and normal to it and FGMs show better elastic as well as yield properties in comparison to the uniform composites with equal average particle contents when loaded in the direction normal to that of gradation. In the gradation direction FGMs

211

show poor elastic and yield properties than that of uniform composites with the same average particle content.

28. In the cast composites particles are generally associated with porosity and the linear gradation of an average of 5 vol% of porosity along with that of particles in the FGM samples does not affect the properties of elastic modulus and yield stress significantly.

29. The variation in yield stress obtained by the present modelling technique has been compared with the hardness observed experimentally and both follow a similar trend.

7.3 TEMPERATURE DISTRIBUTION AND THERMAL STRESSES

30. From the thermal analysis performed on uniform composite, FGM and layered metal-ceramic combination, it has been found that steep change in the thermal stresses at the metal ceramic interface of the layered combination could be avoided by replacing it with either FGM or uniform composite but the latter may result in relatively higher heat flux compared to FGM.

Aboudi, J., Pindera, M.J. and Arnold, S.M., (1999), "Higher-Order Theory for Functionally Graded Materials", Composites: Part B, vol. 30, pp.777–832.

Agarwal, B.D. and Bansal, R.K., (1977), "Plastic Analysis of Fibre Interactions in Discontinuous Fibre Composites", Fibre Science and Technology, vol. 10, pp. 281-297.

Agarwal, B.D. and Broutman, L.J., (1974), "Three-Dimensional Finite Element Analysis of Spherical Particle Composites", Fibre Science and Technology, vol. 7, pp. 63-77.

Agarwal, B.D., Lifshitz, J.M. and Broutman, L.J., (1974), "Elastic-Plastic Finite Element Analysis of Short Fibre Composites", Fibre Science and Technology, vol. 7, pp. 45-62.

Agarwal, B.D. and Narang, J.N., (1977), "Strength and Failure Mechanism of Anisotropic Composites", Fibre science and Technology, vol.10, pp. 37-52.

Aradhya, K.S.S. and Surappa, M.K., (1991), "Estimation of Mechanical Properties of 6061 Al-SiC$_p$ Composites Using Finite Element Method", Scripta Metallurgica et. Materialia, vol. 25, pp. 817-822.

Asthana, R., (1998), "Dynamic Wetting Effects During Infiltration of Metals", Scripta Materialia, vol. 38, No. 8, pp. 1203-1210.

Bao, G., Hutchinson, J.W. and Mcmeeking, R.M., (1991), "Particle Reinforcement of Ductile Matrices against Plastic Flow and Creep", Acta. Metall. Mater. , vol. 39, No. 8, pp. 1871-1882.

Benveniste, Y., (1987), "A New Approach to the Application of Mori-Tanka Theory in Composite Materials", Mechanics of Materials, vol. 6, pp. 147-157.

Broutman, L. J. and Krock, R.H., (1967), "Modern Composite Materials", Addison Wesley Publishing Co.

Butcher, R.J., Rousseau, C.E. and Tippur, H.V., (1999), "A Functionally Graded Particulate Composite: Preparation, Measurements and Failure Analysis", Acta. Mater., vol. 47, No. 1, pp. 259-268.

Carpenter, R. D., Liang, W. W., Paulino, G. H., Gibeling J. C. and Munir, Z. A., (1999), "Fracture Testing and Analysis of a Layered Functionally Graded Ti/TiB Beam in 3-Point Bending", Mater. Sci. Forum, vols. 308–311, pp. 837–842.

Castro, R.R., Wetherhold, R.C. and Kelestemur, M.H., (2002), "Microstructure and Mechanical Behavior of Functionally Graded Al(A359)/SiC$_p$ Composite", Materials Science and Engineering: A, vol.323, pp. 445-456.

Chakraborti, N., Kumar, R. and Jain, D., (2001), "A Study of the Continuous Casting Mold using a Pareto-Converging Genetic Algorithm", Applied Mathematical Modelling, vol. 25, pp.287-297.

Chandrupatla, T.R. and Belegundu, A.D., (2000), "Introduction to Finite Elements in Engineering, second edition", Prentice Hall of India Private Limited, New Delhi.

Cho, J.R. and Ha, D.Y., (2001), "Averaging and Finite-Element Discretization Approaches in the Numerical Analysis of Functionally Graded Materials", Materials Science and Engineering A, vol. 302, pp.187–196.

Dong M., and Schmauder, S., (1996), "Modeling of Metal Matrix Composites by a Self-Consistent Embedded Cell Model", Acta mater, vol. 44, No. 6, pp. 2465-2478.

Dorey, R.A., Yeomans, J.A. and Smith, P.A., (2002), "Effect of Pore Clustering on the Mechanical Properties of Ceramics", Journal of the European Ceramic Society, vol. 22, pp. 403-409.

Duckworth, W., (1953), "Discussion of Ryshkewitch Paper by Winston Duckworth", J.Am. Cerem. Soc., vol. 36, p. 68.

Dvorak, G. J. and Zuiker, J., (1994), "The Effective Properties of Functionally Graded Composites I. Extension of Mori–Tanaka Method to Linearly Varying Fields", Composite Eng., vol. 4, pp. 19–35.

Fuchiyama, T. and Noda, N., (1995), "Analysis of Thermal Stresses in a Plate of Functionally Gradient Material", JSAE Review, vol. 16, pp.263-268.

Gao, J.W. and Wang, C.Y., (2000), "Modeling the Solidification of Functionally Graded Materials by Centrifugal Casting", Materials Science and Engineering A, vol. 292, pp. 207-215.

Gasik, M.M., (2003), "Industrial Applications of FGM Solutions", Materials Science Forum, Trans Tech Publications, Switzerland, vols. 423-425, pp. 17-22.

Ghosh, P.K., Doctoral Thesis, (1986), "Mixing Characteristics and Mechanical Properties of Casting Al (Mg)-Al_2O_3 Composites", Indian Institute of Technology Roorkee, India.

Ghosh, P.K., Ray, S., (1986), "Effect of Porosity and Alumina Content on the Mechanical Properties of Compocast Aluminium Alloy- Alumina Particulate Composite", J Mater. Sci., vol.21, No.5, pp.1667-1674.

Giannakopoulos, A. E., Suresh, S., Finot, M. and Olsson, M., (1995), "Elastoplastic Analysis of Thermal Cycling: Layered Materials with Compositional Gradients", Acta. Metall. Mater., vol. 43, pp. 1335–1354.

Gupta, A.K., (1995), "Processing of Materials–Monolithic to Composites", Bull. Mater. Sci. vol. 18, No. 6, pp. 773-810.

214

Gupta, A.K. and Krishnadas Nair, C.G., (1989), "Proceeding of Science and Technology of Aluminium Lithium Alloys", Banglore: Aluminium Association of India, pp. 137-143.

Gupta, M. and Loke, C.Y., (2000), "Synthesis of Free Standing, One Dimensional, Al-SiC Based Functionally Gradient Materials Using Gradient Slurry Disintegration and Deposition", Materials Science and Engineering: A, vol.276, pp.210–217.

Grujicic, M. and Zhang, Y., (1998) "Determination of Effective Elastic Properties of Functionally Graded Materials Using Voronoi Cell Finite Element Method", Materials Science and Engineering: A, vol.251, pp.64–76.

Halpin, J.C. and Tsai, S.W., (1969), "Effect of Environmental Factors on Composite Materials", Report AFML- TR 67-423, U.S.A., Air Force Materials Laboratory, Dayton, Ohio.

Hasim, Z. and Shtrikman, S., (1963), "A Variational Approach to the Theory of the Elastic Behaviour of Multiphase Materials", J. Mech. Phys. Solids, vol.11, pp.127-140.

Hill, R., (1965), "A Self Consistent Mechanics of Composite Materials", J. Mech. Phys. Solids, vol.13, pp.213-222.

Hirai, T., (1996), "Functionally Gradient Materials", Materials Science and Technology, vol. 17B, pp. 292–341.

Johannesson, B., Ogin, S.L., Surappa, M.K., Tsakiropoulos, P., Brynjolfsson, S. and Thorbjornsson, I.O., (2001), "Effect of Reinforcement Geometry on Matrix Stresses in Three Aluminium Metal Matrix Composite Systems", Scripta Materialia, vol. 45, pp. 993-1000.

Kenesei, P., Borbely, A. and Biermann, H., (2004), "Microstructure Based Three Dimensional Finite Element Modeling of Particulate Reinforced Metal–Matrix Composites", Materials Science and Engineering A, vol. 387-389, pp. 852-856.

Kieback, B. Neubrand, A. and Riedel, H., (2003), "Processing Techniques for Functionally Graded Materials", Materials Science and Engineering A, vol. 362, pp. 81-105.

Koizumi, M., (1997), "FGM Activities in Japan", Composites part B, vol. 28B, pp. 1-4.

Kuruvilla, A. K., Prasad, K. S., Bhanuprasad, V. V. and Mahajan Y. R., (1990), "Microstructure-Property Correlation in Al/TiB$_2$ (XD) Composites", Scripta Metallurgica et. Materialia, vol. 24, pp. 873-878.

Leggoe, J. W., Mammoli, A. A., Bush, M. B. and Hu, X. Z., (1998), "Finite Element Modeling of Deformation in Particulate Reinforced Metal Matrix Composites with Random Local Microstructure Variation", Acta mater. vol. 46, No. 17, pp. 6075-6088.

Lin, J. S., Miyamoto, Y., Tanihata, K., Yamamoto, M. and Tanaka, R., (1998) "Toughening Effects of WC/Co Particles and Compressive Surface Stress on (Al_2O_3-WC/Co)/TiC/Ni Graded Materials", J. Mater. Sci. vol.33, pp.869-76

Majumdar, B.S., Yegneswaran, A.H. and Rohatgi, P.K., (1984), "Strength and Fracture Behaviour of Metal Matrix Particulate Composites", Materials Science and Engineering, vol. 68, pp. 85-96.

Marur, P.R., (2004), "An Engineering Approach for Evaluating Effective Elastic Moduli of Particulate Composites", Materials Letters, vol. 58, pp. 3971-3975.

Mori, T. and Tanaka, K., (1973), "Average Stress in Matrix and Average E Elastic Energy of Materials with Misfitting Inclusions", Acta. Mater., vol. 21, pp.571–574.

Mukherjee, S.K. and Bandyopadhyay, S., (1995), "A Novel Way to Make Fe_3Al/Al_2O_3 Composite", Materials Science and Engineering: A, vol.202, pp.123-127.

Mukherjee, S.K and Bandyopadhyay, S., (1997), "Mechanical and Interfacial Characterization of Fe_3Al and Fe_3Al-Al_2O_3 Intermetallic Composite Made By Mechanical Smearing and Hot Isostatic Pressing", Composites Part B, vol. 28B, pp. 45-48.

Nai, S.M.L. and Gupta, M., (2002), "Influence of Stirring Speed on the Synthesis of Al/SiC Based Functionally Graded Materials", Composites Structures, vol. 57, pp. 227-233.

Nai, S.M.L. and Gupta, M., (2003), "Synthesis and Characterization of Free Standing, Bulk Al/SiCp Functionally Gradient Materials: Effects of Different Stirrer Geometries", Materials Research Bulletin, vol. 38, pp.1573–1589.

Nemat-Alla, M., (2003), "Reduction of Thermal Stresses by Developing Two-Dimensional Functionally Graded Materials", International Journal of Solids and Structures, vol. 40, pp.7339-7356.

Nemat-Nasser, S. and Hori, M., (1993), "Micromechanics: Overall Properties of Heterogeneous Materials," North-Holland, Amsterdam, The Netherlands.

Neubrand, A., (2001), "Functionally Graded Materials", Encyclopedia of Materials: Science and Technology, pp. 3407-3413.

Pai, B.C., Ray, S., Prabhakar, K.V. and Rohatgi, P.K., (1976), "Fabrication of Aluminium–Alumina (Magnesia) Particulate Composites in Foundries Using Magnesium Additions to the Melts", Materials Science and Engineering, vol. 24, pp. 31-44.

Pal, R., (2005), "New Models for Effective Young's Modulus of Particulate Composites", Composites: Part B, vol. 36, pp. 513-523.

Paulino, G.H., Jin, Z.H. and Dodds, R.H., (2003), "Failure of Functionally Graded Materials", Comprehensive Structural Integrity, vol. 2, pp. 607-644.

Pettermann, H.E. and Suresh, S., (2000), "A Comprehensive Unit Cell Model: A Study of Coupled Effects in Piezoelectric 1-3 Composites", International journal of Solids and Structures, vol. 37, pp. 5447-5464.

Pillai, U.T.S., Pandey, R.K. and Rohatgi, P.K., (1987), "Effect of Volume Fraction and Size of Graphite Particulates on Fracture Behaviour of Al- Graphite Composites", Engineering Fracture Mechanics, vol. 28, No. 4, pp. 461-477.

Ravichandran, K.S., (1995), "Thermal Residual Stresses in a Functionally Graded Material System", Materials Science and Engineering A, vol. 201, pp.269-276.

Ray, S., (1993), "Synthesis of Cast Metal Matrix Composites", J. Mat. Sc., vol. 28, pp. 5397-5415.

Reiter, T., Dvorak, G. J. and Tvergaard, V., (1997), "Micromechanical Models for Graded Composite Materials: I", J. Mech. Phys. Solids., vol. 45, No. 8, pp. 1281-1302.

Reiter, T. and Dvorak, G. J., (1998), "Micromechanical Models for Graded Composite Materials: II. Thermomechanical loading", J. Mech. Phys. Solids, vol. 45, pp. 1655–1673.

Rohatgi, P.K., Yarandi, F.M., Liu, Y. and Asthana, R., (1991), "Segregation of Silicon Carbide by Settling and Particle Pushing in Cast Aluminium-Silicon-Carbide Particle Composites", Materials Science and Engineering: A, vol.147, pp. L1-L6.

Rooney, F. and Ferrari, M., (2001), "Tension, Bending, and Flexure of Functionally Graded Cylinders", International Journal of Solids and Structures, vol. 38, pp. 413-421.

Ryshkewitch, E., (1953), "Compression Strength of Porous Sintered Alumina and Zirconia", J.Am. Cerem. Soc., vol.36, pp. 65-68.

Sankar, B.V., (2001), "An Elasticity Solution for Functionally Graded Beams", Composites Science and Technology, vol. 61, pp.689-696.

Sivakumar, R., Nishikawa, T., Honda, S., Awaji, H. and Gnanam, F.D., (2003), "Processing of Mullite–Molybdenum Graded Hollow Cylinders by Centrifugal Molding Technique", Journal of the European Ceramic Society, vol. 23, pp.765–772.

Sohda, Y., Kude, Y., Uemura, S., Saitoh, T., Wakamatsu, Y. and Niino, M., (1993) "Carbon/Carbon Composites Graded with SiC/C Functionally Gradient Compositions", American Ceramic Society, pp. 125-32.

Spriggs, R.M., (1961), "Expression for Effect of Porosity on Elastic Modulus of Polycrystalline Refractory Materials", J. Amer. Cerem. Soc., vol. 44, pp.628-629.

Stefanescu, D.M., Dhindaw, B.K., (1988), "Behaviour of Ceramic Particles at the Solid-Liquid Metal Interface in Metal Matrix Composites", Principles of solidification, Metals handbook, ASM International, vol. 15, pp. 142-147.

Stefanescu, D.M., Dhindaw, B.K., Kacar, S.A. and Moitra, (1988), "Behaviour of Ceramic Particles at the Solid-Liquid Metal Interface in Metal Matrix Composites", Metal. Trans. A, vol. 19A, pp. 2847-2855.

Suresh, S. and Mortensen, A., (1998), "Fundamentals of Functionally Graded Materials: Processing and Thermomechanical Behaviour of Graded Metals and Metal-Ceramic Composites", IOM Communications, London.

Tamura, I., Tomota, Y. and Ozawa, H., (1973), "Proceedings of the 3rd International Conference on Strength of Metals and Alloys", Institute of Metals, Cambridge, vol. 1, p. 611.

Tekmen, C., Ozdemir, I., Cocen, U. and Onel, K., (2003), "The Mechanical Response of Al- Si- Mg/SiC$_p$ Composite: Influence of Porosity", Materials Science and Engineering A, vol. 360, pp. 365-371.

Thakur, S.K., Dhindaw, B.K. Hort, N. and Kainor, K.U., (2004), "Some Studies of the Thermal Expansion Behaviour of C-Fibre, SiCp and In-Situ Mg$_2$Si- Reinforced AZ31 Mg Alloy Based Hybrid Composites", Metall. Maters. Trans A, Vol. 35A, pp.1167-1179.

Wakashima, K., Tsukamoto, H., (1991), "Mean-field Micromechanics Model and its Application to the Analysis of Thermomechanical Behaviour of Composite Materials", Materials Science and Engineering A, vol.146, pp.291-316.

Westwood, A. R. C. and Winzer, S.R., (1987), Edited by: Psaras, P.A., Langford, H.D., in: Advanced Materials Research, National Academy Press, Washington, DC, pp. 225-226.

Williamson, R. L., Rabin, B. H. and Drake, J. T., (1993), "Finite Element Analysis of Thermal Residual Stresses at Graded Ceramic-Metal Interfaces: Part I, Model Description and Geometrical Effects", J. Appl. Phy., vol. 74, pp. 1310–1320.

Yang, C., Huh, H. and Hahn, T.H., (2003), "Evaluation of Effective Material Properties of Composite Materials Using Special FEM", Journal of materials processing Technology, vol. 140, pp. 185-190.

Yin, H.M., Sun, L.Z. and Paulino, G.H., (2004), "Micromechanics-Based Elastic Model for Functionally Graded Materials with Particle Interactions", Acta Materialia, vol.52, pp.3535-3543.

Zhang, J., Wang, Y.Q. and Zhou, B.L., (1999), "Microstructure and Tensile Properties of Graded Al-Mg2Si In-Situ Composites Fabricated by Centrifugal Casting", Materials Science and Technology, vol.15, pp. 1236-1240.